Chaos, Solitons and Fractals 207 (2026) 117942

Contents lists available at ScienceDirect

Chaos, Solitons and Fractals

journal homepage: www.elsevier.com/locate/chaos

Head-on nonlinear excitation of tilted linear modes in photorefractive medium

Dejan V. Timotijević [a], Aleksandra Ž. Piper [a], Jadranka M. Vasiljević [b,*], Damir V. Mitić [b], Dragana M. Jović Savić [b]

[a] University of Belgrade - Institute for Multidisciplinary Research, National Institute of the Serbia, Kneza Višeslava 1, 11030, Belgrade, Serbia
[b] Institute of Physics, University of Belgrade, Pregrevica 118, 11080, Belgrade, Serbia

ARTICLE INFO

Keywords:
Tilted beams
Non-diffracting beams
Waveguiding

ABSTRACT

We present hypothesis intending to explain the mechanism of localized tilted modes formation during the nonlinear propagation of aperiodic non-diffracting beams, considering only aperiodic discrete structures that support linear modes. Such modes are experimentally realized head-on in a single experimental configuration, through optical induction in a photorefractive medium. Our findings suggest that appropriate nonlinearity with localized symmetry deviation leads to excitation of tilted mode without a tilted probe beam and guiding potential, but we confirm that such potentials arise through nonlinear evolution.

1. Introduction

Due to their unique spatial structures and interference properties, non-diffracting beams exhibit self-healing and resilience to perturbations, including moderate nonlinearity [1]. They have attracted significant interest for applications in optical trapping, imaging, nonlinear and quantum optics [2–9]. Weber and Mathieu beams [10,11] are a type of non-diffracting optical wave characterized by aperiodic transverse profiles that exhibit essentially one-dimensional (1D) structural features within their respective families. These beams can be generated through spatial light modulation techniques that imprint the required phase structure onto an input wavefront [12]. They have significant potential for a new type of optical lattice-writing light [13,14] in the range of their stability, but they still attract considerable attention in nonlinear photonics [15–18].

Discrete diffraction occurs when light propagates through a waveguide array, resulting from evanescent coupling between adjacent waveguides [19–25]. It provides a versatile platform for exploring both linear and nonlinear wave phenomena in engineered optical media [21]. In the examination of how the tilted wide probe beam refracts and diffracts depending upon the incident angle [19,20], it was noticed that there are discrete and periodic angles where diffraction is suppressed, depending on the lattice scale (period in wavelength units). Under these conditions, the tilted beam suppressed by diffraction becomes the dominant propagating mode.

Tilted beams can be generated in discrete media by exciting linear modes with a probe beam incident at an appropriate angle. In this paper, we claim that an analogous nonlinear mode can be generated head-on in a homogeneous medium. Our hypothesis, intending to explain the mechanism of nonlinear modes generation, links these two phenomena. We present discrete strand structures that are invariant along the propagation direction and commonly used to write waveguides, forming a photonic lattice in photorefractive materials. We introduce a procedure in which a single head-on beam both writes a discrete structure and excites a tilted mode. Using a non-diffracting beam with linear invariance, we show that when the nonlinearity becomes strong

* Corresponding author.
E-mail address: jadranka@ipb.ac.rs (J.M. Vasiljević).

https://doi.org/10.1016/j.chaos.2026.117942
Received 10 October 2025; Received in revised form 10 December 2025; Accepted 16 January 2026
Available online 30 January 2026

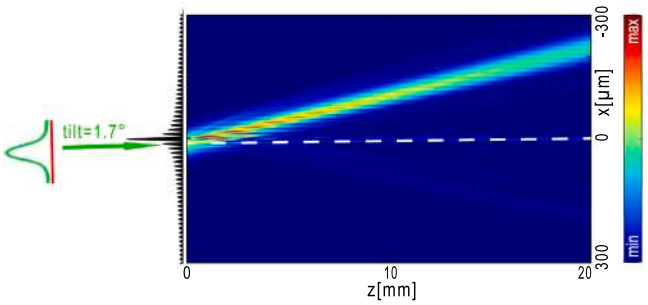

Fig. 1. Linear tilted modes in Weber WGA. (left) Weber WGA with the input Gaussian and its incident angle marked with the arrow. (right) The numerically obtained intensity distributions of tilted mode along the propagation distance. The white dashed line shows the Gaussian beam path in the bulk crystal. Parameters are: $\Delta n = 0.0002$ a.u., probe Gaussian waist 70 μm and intensity = 0.81.

enough to break this invariance, a tilted mode forms: first, the beam writes the lattice, then the tilted mode emerges. The resulting aperiodic energy distribution breaks the symmetry sufficiently to individual strands start to bend, thus enabling angles captured by linear modes.

We clarify the mechanism of localized tilted modes formation by the nonlinear propagation of a non-diffracting beam in normal incidence on the photorefractive crystal, in settings of discrete aperiodic structures that support linear modes. These phenomena are obtained through single-pass experiments in a photorefractive crystal, using the Weber beam of zero parabolicity as a representative case in 1D geometry. A similar effect was observed in our previous investigation of the Mathieu beam [26]. The effort to clarify the mechanism of nonlinear localized tilted modes excitation and find a connection with the excitation of linear modes allowed us to demonstrate the same effects in different geometries and dimensionality, which will be reported separately.

2. Nonlinear excitation of localized tilted modes: Clarification of underlying mechanism

As a representative non-diffracting beam in 1D geometry, we use the Weber beam of zero parabolicity, generated using even zero-order Weber beam [10], $A = U_e(\eta, \xi; a) = \frac{1}{\pi\sqrt{2}}|\Gamma_1|^2 P_e(\sigma\xi; a)P_e(\sigma\eta; -a)$, where P_e is the even parabolic cylinder function, Γ is Gamma functions, $\Gamma_1 = \Gamma[(1/4) + (1/2)ia]$, $\sigma = (4\pi/\lambda)^{1/2}$, (ξ, η) are the parabolic cylinder coordinates, and the parameter $a = 0$ determines the curvature of the Weber beam lobes and acts as an indicator of *parabolicity*. In the linear regime, a non-diffracting Weber beam can be used to induce a nearly 1D aperiodic waveguide array (WGA) in a photorefractive medium (Fig. 1). However, as the power is gradually increased, the beam begins to diffract, and within a narrow power range, nonlinearly localized tilted modes are formed (Fig. 3). With further increases in power, unstable structures appear (Fig. 5(a)). The observation of self-induced localized tilted modes in the nonlinear regime (Fig. 3) (similar to the linear tilted modes obtained with a tilted probe in a pre-inscribed WGA (Fig. 1)) motivated us to clarify the mechanism responsible for their formation. We hypothesize that beams with suppressed diffraction can explain the formation of localized tilted modes during the nonlinear propagation of Weber beams in a bulk medium, i.e., without a pre-inscribed WGA. In other words, localized tilted modes are nonlinear excitations of a linear mode observed in periodic WGA [20]. Here, the tilt is taken relative to the refracted angle of the beam's direction of propagation. Our results suggest that appropriate nonlinearity with localized symmetry deviation induces excitation of localized tilted modes and does not necessarily occur using the tilted probe beam in an appropriate potential. Furthermore, we found that such potentials naturally emerge during the nonlinear formation of tilted beams. In the following, we will present several steps that helped us clarify the mechanism.

2.1. Permanent lattice with oblique incidence of a wide Gaussian

First, we verify numerically that, similar to periodic WGA, linear modes can be excited in immutable inscribed aperiodic Weber WGA by broad Gaussian beams with suitable power and incident angle. As Weber WGA is not periodic, excitation also depends on the transverse position of incidence. Varying parameters such as the Weber beam scale (illustrated with the parameter in Fig. 4, here $b = 12$ μm), the position and incident angle of the Gaussian beam (tilt in Fig. 1), we observe the formation of tilted modes within a narrow range of conditions: an example is presented in Fig. 1. Furthermore, we have precise control over the refractive index modulation depth (Δn) and the angle α of the resulting tilted modes. Using the opposite probe incident tilt angle and position, it is possible to observe the mirror-symmetric beam. Fig. 1 presents the excitation of the dominant mode; in addition, other modes are observed by varying the input parameters. The numerical data are obtained using a linear isotropic model [27].

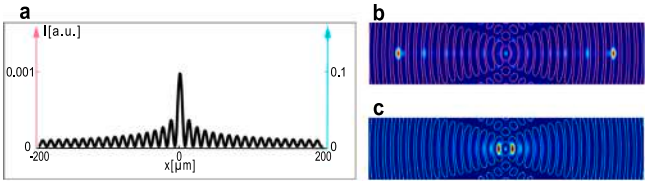

Fig. 2. Tilted localized modes in Weber WGA observed with Weber probe beam. (a) Weber WGA. The numerically obtained intensity distributions of the Weber probe beam at the 20 mm propagation distance for: (b) lattice intensity = 0.001, probe intensity = 1.5, and (c) lattice intensity = 0.1, probe intensity = 0.5. Blue and magenta contours represent the underlying structure of the permanent Weber WGA. (For interpretation of the references to color in this figure legend, the reader is referred to the web version of this article.)

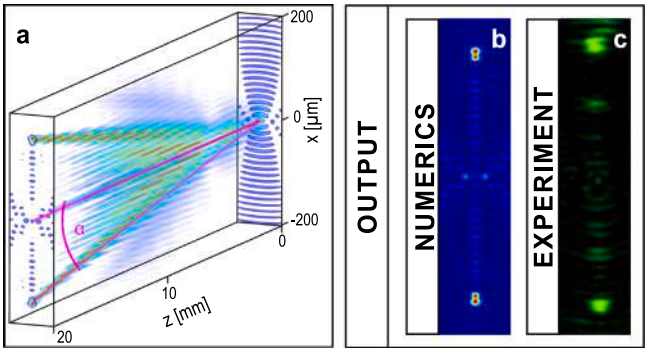

Fig. 3. Localized tilted modes observed in nonlinear propagation of Weber beam. (a) The 3D intensity volume visualizes the formation of localized tilted modes through the crystal. The angle of tilted modes relative to the z-axis is marked with α. (b) Numerically and (c) experimentally observed intensity distribution of the Weber beam at the crystal back face. Parameters are intensity = 0.8 a.u., power = 11.5 μW.

2.2. Permanent lattice with normal incidence of the nonlinear Weber beam

Next, we show that there is a range of Weber WGA depths enabling nonlinear excitations of tilted modes with normal incidence of the Weber beam of the same structure as the one inscribing the lattice. With a large depth outside this range, excitation is suppressed. Within a certain parameter region, one can observe a tilted localized modes, presented at the crystal exit in Fig. 2(b). Increasing the lattice intensity and decreasing the probe beam intensity, suppression of excitation occurs (Fig. 2(c)). For this investigation, we used an anisotropic model [28] consisting of the nonlinear paraxial propagation equation and an anisotropic potential equation describing the spatial evolution of the electrostatic potential [9].

2.3. Bulk nonlinear propagation of Weber beam

We show that nonlinear propagation of the Weber beam in bulk material forms structures with localized tilted modes, which we hypothesize are caused by the accumulation of energy in directions corresponding to linear modes presented in Fig. 1. We study zero-order Weber beams of different scales and orientations to investigate how their propagation is affected by the beam power increase. At lower beam powers, propagation remains stable along the crystal length. However, as the power increases, the symmetry is broken, leading to diffracting phenomena, but at higher beam powers, localized tilted modes can be observed (Fig. 3).

The numerical results are obtained using an anisotropic model [26,29]. For experimental realization, the optical induction technique is used, which allows refractive index changes of the photorefractive material, a birefringent cerium-doped strontium barium niobate crystal (SBN61:Ce). The experimental setup is shown in Fig. 4. As a light source, we use a continuous frequency-doubled Nd:YVO_4 laser with a wavelength of $\lambda = 532$ nm. A linearly polarized laser beam is spatially modulated via the spatial light modulator (SLM) to produce the desired structure, inducing a corresponding refractive index modulation in the biased photosensitive crystals. Then, a spatially modulated input laser beam from SLM passes through several optical elements, including lenses, a beamsplitter, a half-wave plate, and a Fourier filter, before it illuminates the crystal. The SBN61:Ce crystal, with dimensions of $5\times5\times20\,\mathrm{mm}^3$, is biased to an external electric field (E_{ext}), applied along the optical $c = x$-axis. This electric field is perpendicular to the wave propagation direction (the z-axis). As a result, the extraordinarily polarized structure light field with power (P) propagates through the crystal. We used an imaging system with a microscope objective (MO x10) and a camera to observe the transverse intensity distribution on the exit face of the crystal. A detailed description of the experimental procedure is described in our previous work [30]. Numerics provide insight into the propagation along our crystal.

Fig. 5(a) provides a detailed analysis of how changes in the Weber beam scale b and intensity (power) influence the formation of localized tilted modes. At lower values of either or both parameters, the Weber beams remain stable during propagation. As these

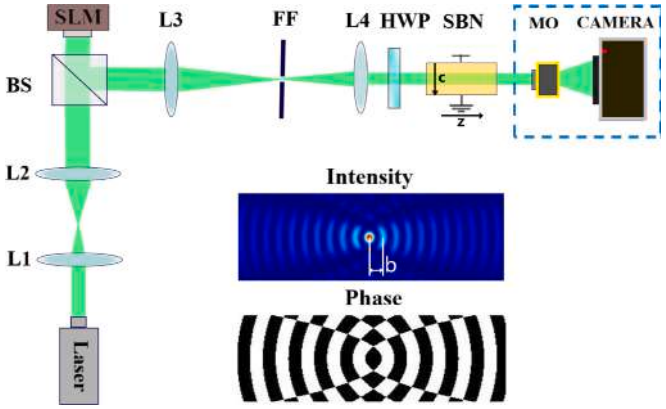

Fig. 4. Experimental setup for investigating the nonlinear propagation of Weber beams with insets presenting the input intensity and phase distributions. L — lens, BS — nonpolarized beam splitter (50:50), SLM – spatial light modulator, FF - Fourier filter, SBN — photorefractive medium, HWP — half-wave plate, MO — microscope objective.

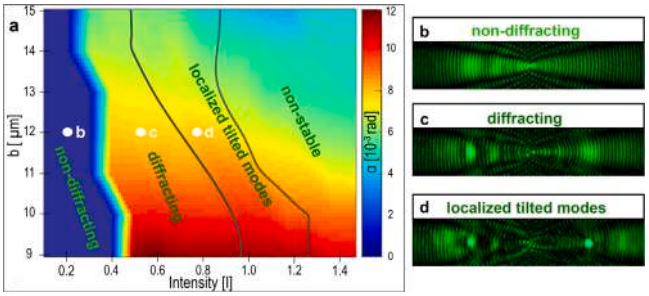

Fig. 5. (a) Parameter space diagram with different regimes of the zero-order Weber beam propagation in the nonlinear regime. The color bar indicates the angles of localized tilted modes relative to the z-axis. (b)–(d) Experimentally observed intensity distributions at the crystal exit, during the time corresponding to various regimes in the phase diagram (a) labeled with white dots (b–d). (For interpretation of the references to color in this figure legend, the reader is referred to the web version of this article.)

parameters are increased, there is a region of diffraction, but further increase in both parameters leads to the formation of localized tilted modes. At the highest values of the control parameters, instabilities can be observed. The angles of localized tilted modes (α) relative to the z-axis (Fig. 3(a)) are measured and shown as color bar values in Fig. 5(a). By adjusting the beam's parameters, the tilted angles of such modes can be precisely controlled and fine-tuned.

2.4. Time section of nonlinear propagation dynamics

We show that in the dynamics of the nonlinear interaction process of light with the photorefractive crystal, there are phases where non-diffracting Weber WGA is formed, and that in subsequent phases (Fig. 5(b)–(d)) we can identify structures presented in Fig. 2. Our understanding of the time evolution of the nonlinear propagation dynamics (verified by Fig. 5) is that the residual cylindrical lattice is formed, thus enabling the mechanism described in the paragraph with permanent lattice and normal incidence of the nonlinear Weber beam. Fig. 5(b)–(d) present experimentally obtained intensity distributions during the time, corresponding to various regimes in the phase diagram (Fig. 5(a)). Investigating the temporal dynamics observed in the experiment has motivated us to further validate the accurate dynamical model.

Linear modes of tilted beams are light traps that propagate in their direction. Once in a trap, diffraction is suppressed, and conditions for formation of localized tilted modes are satisfied. By examining the propagation of light with normal incidence through a permanent periodic lattice, we see that there is not enough energy traveling in the direction of dominant linear modes. In an aperiodic lattice, due to the balance of influences, there is no cause for bending [31]. In our simulation, we did not detect spontaneous breaking of the symmetry. If externally localized symmetry is deviated, such as by truncation, balance would be disturbed, and nonlinear light could bend together. In our study, Mathieu and Weber beams are structures where periodicity deviates not as much in the waveguide distribution but with waveguide depth, whose profile shows a pronounced maximum. Shallow enough, WGA would support linear mode, but does not suppress light from bending nonlinearly. Such a nonlinear bending enables light to steer into a nonlinear trap.

A key aspect of our mechanism is that, in the early stage of the propagation, the Weber beam remains non-diffracting over a short distance. It is necessary to point out that a temporal cusp occurs during the nonlinear destruction of the non-diffracting beam, where one part of the energy is used for writing the lattice and the other part for self-focusing. Understanding of that mechanism allows us to generalize tilted modes with other structures that can produce photonic lattice in the linear regime. This understanding enables us to propose a new approach for *predicting* the initial structures required to generate localized tilted modes with specific numbers and properties, and in various *geometries* and *dimensionalities*. Clarifying the mechanism allows us to predict how structured light can be fragmented, which tilted modes will form, and how to control their angles. Our approach can be viewed as a controlled fragmentation process that produces well-defined tilted modes, with predictable tilts. These tilted modes may be regarded as soliton-like, except for the criterion of long-distance stability, which is outside the focus of this work. Clarification of the mechanism for localized tilted mode formation is also crucial for improving the dynamical model. Our reliance on the memory effect is strongly supported by the observed temporal behavior of the output. This does not necessarily invalidate the possibility that the Kerr-like medium (whose response is instantaneous and ephemeral) could produce similar behavior by supporting linear modes in which part of the energy is engaged for the lattice and part of the energy for the tilted mode.

3. Conclusion

In conclusion, we recognized the capability of structured light to form tilted modes that can be experimentally realized head-on in a single experimental configuration. The experiment is performed with a single beam, not as a two-stage experiment, separately creating a lattice and a tilted probe of different polarizations. This advantage arises from the fact that we have nonlinear system exhibiting memory effects. Clarifying the mechanism of localized tilted modes formation within the nonlinear propagation of non-diffracting beams, we suggest that appropriate nonlinearity with localized symmetry deviation induces excitation of a localized tilted modes, without requiring a tilted probe beam in an appropriate potential. In addition, we found that such potentials naturally emerge during the nonlinear formation of localized tilted modes. We confirm that the Weber beam partially inscribes a residual lattice during nonlinear propagation, leading to beam localization and splitting. This process relies on mode excitation enabled by the non-periodic structure of the beam and a balanced residual lattice depth. These findings provide new possibilities for the design of unique beam structures and shapes with novel topologies.

CRediT authorship contribution statement

Dejan V. Timotijević: Writing – original draft, Software, Methodology, Conceptualization. **Aleksandra Ž. Piper:** Writing – original draft, Software, Methodology, Conceptualization. **Jadranka M. Vasiljević:** Writing – review & editing, Visualization, Validation, Investigation, Formal analysis. **Damir V. Mitić:** Writing – review & editing, Visualization, Data curation. **Dragana M. Jović Savić:** Writing – review & editing, Supervision, Funding acquisition, Conceptualization.

Declaration of competing interest

The authors declare no potential conflict of interests.

Acknowledgments

The authors acknowledge funding provided by the Institute of Physics Belgrade and Institute for Multidisciplinary Research (IMSI), through the grants by the Ministry of Science, Technological Development and Innovations of the Republic of Serbia (IMSI contract no. 451-03-66/2024-03/200053) and by the Science Fund of the Republic of Serbia, **GRANT No 7714356, IDEAS - CompsLight**.

Data availability

The results presented in this paper are not publicly available at this time but may be obtained from the authors upon reasonable request.

References

[1] Bouchal Z. Nondiffracting optical beams: Physical properties, experiments, and applications. Czech J Phys 2003;53:537–78. http://dx.doi.org/10.1023/A:1024802801048.
[2] Woerdemann M, Alpmann C, Esseling M, Denz C. Advanced optical trapping by complex beam shaping. Laser Photon Rev 2013;7:839–54. http://dx.doi.org/10.1002/lpor.201200058.
[3] Garcés-Chávez V, McGloin D, Melville H, Sibbett W, Dholakia K. Simultaneous micromanipulation in multiple planes using a self-reconstructing light beam. Nature 2002;419:145–7. http://dx.doi.org/10.1038/nature01007.
[4] Baumgartl J, Mazilu M, Dholakia K. Optically mediated particle clearing using airy wavepackets. Nat Photonics 2008;2:675–8. http://dx.doi.org/10.1038/nphoton.2008.201.
[5] Bloch I. Ultracold quantum gases in optical lattices. Nat Phys 2005;1:23–30. http://dx.doi.org/10.1038/nphys138.
[6] Fleischer JW, Segev M, Efremidis NK, Christodoulides DN. Observation of two-dimensional discrete solitons in optically induced nonlinear photonic lattices. Nature 2003;422:147–50. http://dx.doi.org/10.1038/nature01452.

[7] Martin H, Eugenieva ED, Chen Z, Christodoulides DN. Discrete solitons and soliton-induced dislocations in partially coherent photonic lattices. Phys Rev Lett 2004;92:123902. http://dx.doi.org/10.1103/PhysRevLett.92.123902.
[8] Vasiljević JM, Zannotti A, Timotijević DV, Denz C, Savić DMJ. Light transport and localization in disordered aperiodic Mathieu lattices. Opt Lett 2022;47(3):702–5. http://dx.doi.org/10.1364/OL.445779.
[9] Vasiljević JM, Jovanović VP, Tomović AŽ, Timotijević DV, Žikic R, Belić MR, Savić DMJ. Interdimensional radial discrete diffraction in Mathieu photonic lattices. Opt Express 2023;31(18):28946–53. http://dx.doi.org/10.1364/OE.497795.
[10] Bandres MA, Gutiérrez-Vega JC, Chávez-Cerda S. Parabolic nondiffracting optical wave fields. Opt Lett 2004;29:44–6. http://dx.doi.org/10.1364/OL.29.000044.
[11] Gutiérrez-Vega JC, Iturbe-Castillo MD, Chávez-Cerda S. Alternative formulation for invariant optical fields: Mathieu beams. Opt Lett 2000;25:1493–5. http://dx.doi.org/10.1364/OL.25.001493.
[12] Davis JA, Cottrell DM, Campos J, Yzuel MJ, Moreno I. Encoding amplitude information onto phase-only filters. Appl Opt 1999;38:5004–13. http://dx.doi.org/10.1364/AO.38.005004.
[13] Rose P, Boguslawski M, Denz C. Nonlinear lattice structures based on families of complex nondiffracting beams. New J Phys 2012;14:033018. http://dx.doi.org/10.1088/1367-2630/14/3/033018.
[14] Tomović AŽ, Vlaović Mitić IJ, Jovanović VP, Timotijević DV, Jović Savić DM. Assembling of truncated deterministic aperiodic lattices with defects using Weber beams. Opt Mater 2024;157:116334. http://dx.doi.org/10.1016/j.optmat.2024.116334.
[15] Freedman B, Bartal G, Segev M, Lifshitz R, Christodoulides DN, Fleisher J. Wave and defect dynamics in nonlinear photonic quasicrystals. Nature 2006;440:1166–9. http://dx.doi.org/10.1038/nature04722.
[16] Quan Q, Lian S, Liu Z, Chen H, Yan B, Deng D. Observation of off-axis solitary waves propagating along a specific trajectory in photorefractive crystals. Opt Lett 2024;49(16):4585–8. http://dx.doi.org/10.1364/OL.532244.
[17] Chen H, Liu Z, Lian S, Quan Q, Malomed BA, Li S, Zhang Y, Li H, Deng D. Tunable beam splitting via photorefractive nonlinearity and its applications in chiral waveguide induction and vortex generation. Chaos Solitons Fractals 2024;183:114936. http://dx.doi.org/10.1016/j.chaos.2024.114936.
[18] Lian S, Quan Q, Liu Z, Chen H, Yan B, Li Y, Lin W, Deng D. Dynamics of stable solitons of circular pearcey Gaussian beams in a photorefractive strontium barium niobate crystal. Opt Lett 2025;50(3):856–9. http://dx.doi.org/10.1364/OL.547236.
[19] Eisenberg HS, Silberberg Y, Morandotti R, Aitchison JS. Diffraction management. Phys Rev Lett 2000;85:1863–6. http://dx.doi.org/10.1103/PhysRevLett.85.1863.
[20] Pertsch T, Zentgraf T, Peschel U, Bräuer A, Lederer F. Anomalous refraction and diffraction in discrete optical systems. Phys Rev Lett 2002;88:093901. http://dx.doi.org/10.1103/PhysRevLett.88.093901.
[21] Hudock J, Efremidis NK, Christodoulides DN. Anisotropic diffraction and elliptic discrete solitons in two-dimensional waveguide arrays. Opt Lett 2004;29(3):268–70. http://dx.doi.org/10.1364/OL.29.000268.
[22] Pertsch T, Peschel U, Lederer F, Burghoff J, Will M, Nolte S, Tünnermann A. Discrete diffraction in two-dimensional arrays of coupled waveguides in silica. Opt Lett 2004;29(5):468–70. http://dx.doi.org/10.1364/OL.29.000468.
[23] Lederer F, Stegeman GI, Christodoulides D, Assanto G, Segev M, Silberberg Y. Discrete solitons in optics. Phys Rep 2008;463:1–126. http://dx.doi.org/10.1016/j.physrep.2008.04.004.
[24] Fleischer JW, Segev M, Efremidis NK, Christodoulides DN. Observation of two-dimensional discrete solitons in optically induced nonlinear photonic lattices. Nature 2003;422:147–50. http://dx.doi.org/10.1038/nature01452.
[25] Christodoulides DN, Lederer F, Silberberg Y. Discretizing light behaviour in linear and nonlinear waveguide lattices. Nature 2003;424:817–23. http://dx.doi.org/10.1038/nature01936.
[26] Zannotti A, Vasiljević JM, Timotijević DV, Jović Savić DM, Denz C. Morphing discrete diffraction in nonlinear Mathieu lattices. Opt Lett 2019;44(7):1592–5. http://dx.doi.org/10.1364/OL.44.001592.
[27] Kivshar Y, Agrawal G. Optical solitons: From fibers to photonic crystals. Academic Press; 2003, URL https://books.google.rs/books?id=zzWgibj4ypsC.
[28] Zozulya AA, Anderson DZ. Propagation of an optical beam in a photorefractive medium in the presence of a photogalvanic nonlinearity or an externally applied electric field. Phys Rev A 1995;51:1520–31. http://dx.doi.org/10.1103/PhysRevA.51.1520.
[29] Zannotti A, Vasiljević JM, Timotijević DV, Jović Savić DM, Denz C. Visualizing the energy flow of tailored light. Adv Opt Mater 2018;6(8):1701355. http://dx.doi.org/10.1002/adom.201701355.
[30] Mitić DV, Vasiljević JM, Timotijević DV, Jović Savić DM. Self-induced parabolic surface states. Opt Mater 2025;167:117249. http://dx.doi.org/10.1016/j.optmat.2025.117249.
[31] Stegeman GI, Segev M. Optical spatial solitons and their interactions: Universality and diversity. Science 1999;286(5444):1518–23. http://dx.doi.org/10.1126/science.286.5444.1518.

ACS APPLIED OPTICAL MATERIALS

pubs.acs.org/acsaom Article

Surface-Distributed Twisted Beams Nonlinearly Induced by Nondiffracting Beams

Jadranka M. Vasiljević,* Miroslav M. Petroski, Dejan V. Timotijević, and Dragana M. Jović Savić

Cite This: ACS Appl. Opt. Mater. 2026, 4, 352−359 Read Online

ACCESS | Metrics & More | Article Recommendations | Supporting Information

ABSTRACT: We developed an experimental method for generating light-induced microstructures in the form of twisted beam bundles arranged across curved surfaces. These structures arise during the nonlinear propagation of aperiodically modulated nondiffracting beams and are formed without the need for a prefabricated lattice or a tilted probe beam. Anisotropic refractive index patterns are optically induced in a single-pass experiment using a photorefractive medium. Our observations reveal the simultaneous formation of discrete soliton and helicoidal beam bundles. Discrete solitons follow trajectories conforming to a hyperboloidal surface, whereas the inner moving components trace cylindrical paths, resulting in the formation of helicoidal waveguides. The number of beams and their spatial arrangement can be precisely controlled by tuning the order, scale, and modulation parameters of the input beam. Although the initial light field is confined to a single surface, nonlinear self-interactions enable the transition of light across one or more curved surfaces. Furthermore, variation in the input beam power offers an additional degree of control over the shape and geometry of these surfaces, allowing for the fine adjustment of the propagation dynamics and structure of the beam bundles.

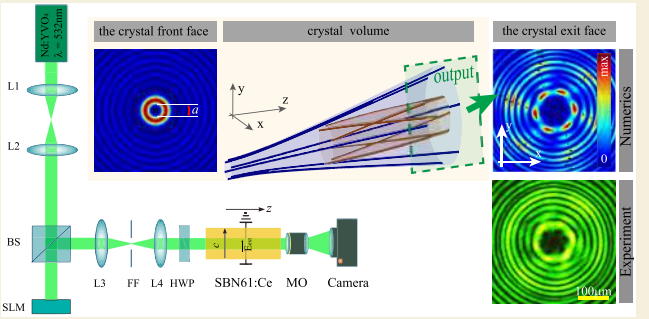

KEYWORDS: *curved light, tilted solitons, modulated Bessel beams, nonlinear optical induction, light-induced microstructure*

INTRODUCTION

Nondiffracting beams are of significant interest as structured light fields[1−3] that have wide applicability across multiple disciplines, especially in the fields of optical micromanipulation, medical, biological, and physical research,[4] optical tweezing,[5,6] quantum optics,[7] and nonlinear optical phenomena.[8−10] Bessel beams are formed as solutions of the Helmholtz equation in cylindrical coordinates[11,12] and are described by a Jinc function, which combines the Bessel function of the first kind and a Gaussian envelope. Due to their unique properties, such as self-healing, resistance to diffraction, and the presence of a central dark core, Bessel beams have found applications in various fields, including optical trapping, imaging, and material processing.[13−16] These beams also serve as important tools in nonlinear optics and optical lattice writing light[17] that are observed in specific regimes but remain unexplored in nonlinear regimes, especially with additional modulation.

Light-manipulating microstructures, i.e., engineered materials or geometries that control light properties such as intensity, phase, polarization, and direction, use effects such as interference, diffraction, plasmonic resonances, and nonlinear interactions to achieve tailored light−matter interactions.[18] They are fundamental components in applications ranging from metasurfaces and photonic crystals to optical waveguides, sensors, and quantum photonic devices.[8,19−21] By engineering light−matter interactions, the spectral components of optical waves can be discretized,[22,23] which is essential for the development of discrete optical components. Periodic photonic structures provide an ideal platform for investigating discrete optical phenomena, enabling precise control of light through photonic band structures.[24−26] The formation of tilted discrete solitons is demonstrated in the nonlinear propagation of fragmented Bessel beams, extending the concept beyond previous studies based on preinscribed lattices and tilted probes in the linear regime and providing a clarification of the mechanism of their formation.[27] The study of light propagation on curved surfaces such as spherical, cylindrical, hyperbolic, or arbitrary surfaces has received growing attention in the past decade due to its relevance in areas including transformation optics, topological photonics, and the design of structured light fields,[28−31] but their experimental realization remains highly challenging. Parabolic surface states that are

Received: September 29, 2025
Revised: January 12, 2026
Accepted: January 16, 2026
Published: February 10, 2026

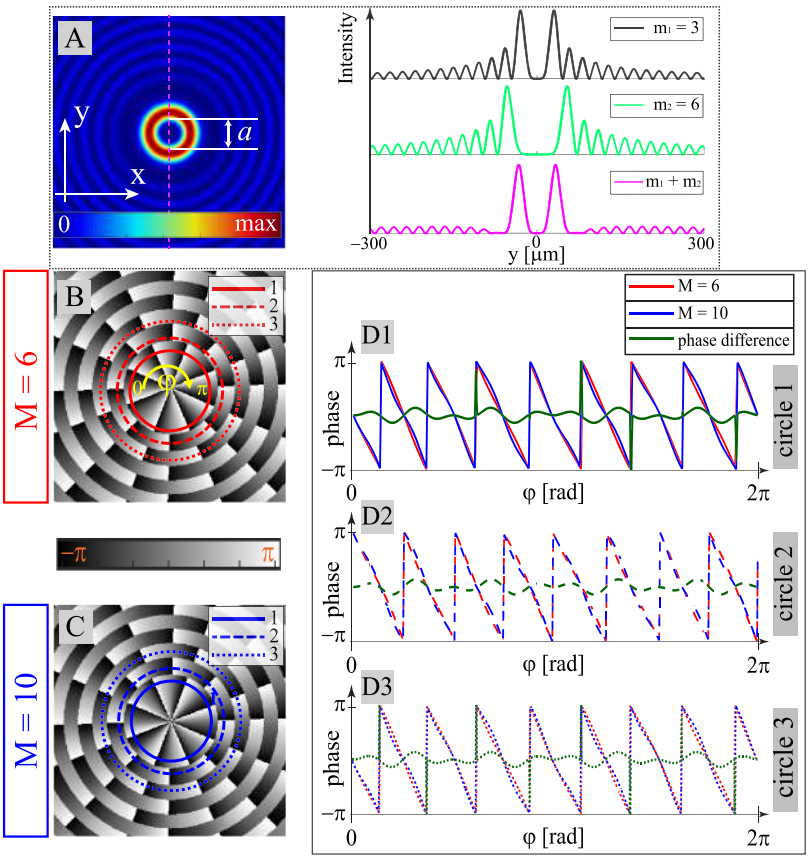

Figure 1. Characterization of modulated Bessel beams: (A) intensity distribution with the illustration of amplitude modulation; (B, C) phase distributions at the crystal input face; and (D) azimuthal phase profiles for $M = 6$, 10, and their phase difference. Other parameters are $m_1 = 3$, $m_2 = 6$, $a = 45$ μm, $p = 8$, and $\eta = 0.23$.

confined to a single surface or propagate from one to a neighboring surface are observed without any preinscribed lattice in the material using optical induction.[10]

In this paper, we introduce an experimental framework for generating light-induced microstructures, specifically twisted bundles of beams occurring simultaneously on various curved surfaces. These bundles emerge through the nonlinear propagation of modulated nondiffracting beams during a single-pass optical induction process in an anisotropic photorefractive crystal. Crucially, these structures do not require prefabricated waveguides or tilted beam incidence as in earlier approaches.[22] As a representative structured input field, we employ amplitude- and phase-modulated Bessel beams that feature aperiodic transverse intensity and phase profiles composed of concentric rings with tunable spacing, intensity contrast, and embedded orbital angular momentum. By varying the beam scale, order, modulation, and input power (beyond the thresholds for both modulation and nonlinearity), we induce twisted bundles of discrete solitons. In addition to a discrete soliton bundle, we observed the simultaneous formation of helicoidal solitary beams. Remarkably, although the input beam is initially confined to a single surface, nonlinear self-action enables energy transfer to other curved surfaces, leading to single- or multisurface microstructure formation. The outer solitons follow hyperboloidal trajectories, while the inner structures trace cylindrical paths, forming helicoidal waveguide architectures. We further demonstrate precise control over the number of generated beams, the geometry of their induced surfaces, and the direction of their twisting. This nonlinear approach provides a powerful method for predictable, tunable, and surface-confined beam shaping, advancing the capabilities of structured light control and enabling the creation of complex light-induced microstructures that are fundamentally inaccessible in linear optics. Surface states are one of the stages in the clarification of the underlying mechanism for nonlinear tilted solitons generation, considering aperiodic discrete structures that support linear modes, which is a topic of our current research.[10,27] Waveguides on such surfaces essentially produce one-dimensional (1D) lattices, not arranged in a plane but along curved surfaces. With such an approach, we can consider surfaces as 1D guiding entities.

RESULTS AND DISCUSSION

Modeling-Modulated Bessel Beam Propagation in Photorefractive Media

To enable the controlled generation of complex light-induced microstructures, we first developed a method for designing tailored input light fields with amplitude and phase modulation. Specifically, we construct a paraxial scalar field $A(x, y)$ with an aperiodic transverse intensity and phase profile, consisting of multiple concentric rings with tunable spacing and an embedded spiral orbital angular momentum. These structured input beams serve as the foundation for initiating nonlinear self-action in the medium, allowing us to influence the geometry and dynamics of the resulting microstructures precisely. Our exemplary field, named the modulated Bessel beam, is obtained by superimposing two Bessel beams of different orders m_1 and m_2, with the same phase modulation ψ

https://doi.org/10.1021/acsaom.5c00466
ACS Appl. Opt. Mater. 2026, 4, 352−359

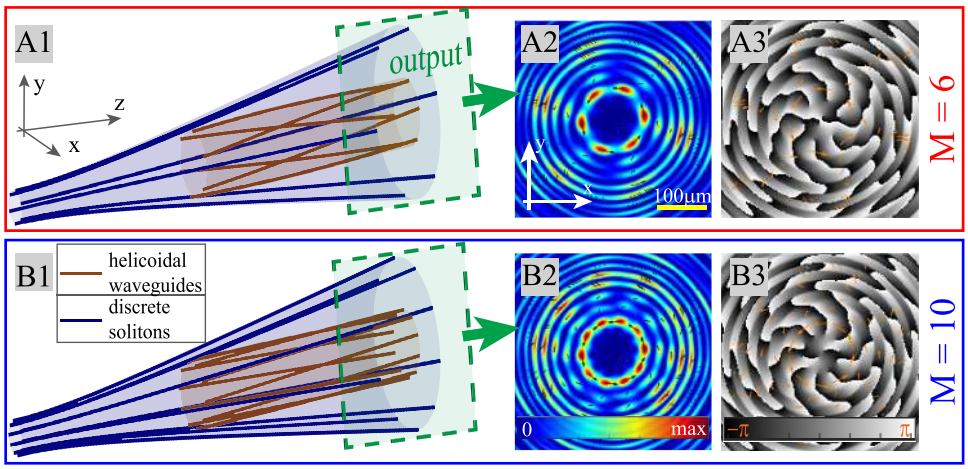

Figure 2. Light-induced microstructures of twisted bundles. (A1, B1) Schematic representation of multiple discrete solitons (dark blue) and helicoidal beams (brown) along different curved surfaces. Numerically observed intensity and phase distributions at the output crystal face for (A2, A3) $M = 6$ and (B2, B3) $M = 10$. Visualization 1 and Visualization 2 contain the numerical intensity distributions of the modulated Bessel beams along the propagation, corresponding to cases presented in panels (A2) and (B2). Visualization 3 and Visualization 4 contain the numerical phase distributions of the modulated Bessel beams along the propagation, corresponding to cases presented in panels (A3) and (B3). The energy flow, characterized by the Poynting vector, is indicated by black/orange arrows. Input beam intensity $I_0 = 0.1$. Other parameters are as shown in Figure 1.

$$A(x, y) = (J_{m_1}(k_\perp \rho) + J_{m_2}(k_\perp \rho))e^{i\psi(\varphi)\varphi} \quad (1)$$

J_m is the first kind of Bessel function of order m, and $k_\perp = 2\pi/a$ is the transverse wave vector defined by the beam scale a (Figure 1A), which controls the spatial size of the beam and simultaneously affects the size of its Fourier transform. The cylindrical coordinates (radial distance ρ and azimuth φ) and Cartesian coordinates are related via $\rho = \sqrt{x^2 + y^2}$, $\varphi = \tan^{-1}\left(\frac{y}{x}\right)$, $\rho \in (-\infty, +\infty)$, $\varphi \in (0, 2\pi)$. In this way, phase modulation is introduced through the azimuthal term

$$\psi(\varphi) = p + \eta \cdot \cos(M\varphi) \quad (2)$$

where the parameters p, η, and M control the level of modulation, i.e., p is the topological charge, while η and M are the depth and frequency of modulation, respectively. The interplay of different Bessel beam orders controls the intensity distribution by adjusting the spacing of the concentric rings and their modulation depth (Figure 1A). This approach enables simultaneous control over both the amplitude and phase of the structured beam $A(x, y)$, which exhibits complex aperiodic transverse profiles.

Figure 1 presents the intensity and phase distributions of two modulated Bessel beams with $M = 6$ and 10, obtained from eq 2, while all other parameters remain the same. They share the same intensity distribution (Figure 1A) observed using amplitude modulation (eq 1), but differ in the phase distribution (Figure 1B,C). Therefore, in Figure 1D1−D3, we present a comparison of azimuthal phase profiles along three exemplary circles (marked in Figure 1B,C) for these two cases (red and blue lines) and their phase difference (green line). The phase difference between these two cases is more pronounced along the first and third circles. Here, we employ such tailored beams to investigate the influence of nonlinearity on their structural evolution during propagation through a photorefractive crystal.

Numerically, we modeled the nonlinear propagation of structured light in the birefringent cerium-doped strontium barium niobate crystal, CeO_2-doped at 0.002 wt % (SBN61:Ce), by solving the nonlinear Schrödinger equation

$$i\partial_z A(\mathbf{r}) + \frac{1}{2k_z}[\Delta_\perp + G(I)]A(\mathbf{r}) = 0 \quad (3)$$

using the spectral split-step method.[9,32,33] A is the paraxial propagational scalar light field with a longitudinal wave vector k_z. The nonlinear potential given by $G(I) = -k_z^2 n_e^2 r_{33} E(I)$ is calculated as the nonlinear light−matter interaction by assuming a light-induced refractive index modulation as presented in ref 34. $n_e = 2.35$ and $r_{33} = 267$ pm/V are the refractive index and the corresponding electro-optic coefficient of the crystal for extraordinary polarized light. The wavenumber $k = 2\pi/\lambda = \sqrt{(k_\perp^2 + k_z^2)}$ is determined by the wavelength of the laser $\lambda = 532$ nm. The total electric field that builds up inside the crystal $E(I) = E_{ext} + E_{sc}(I)$ consists of an external bias field $E_{ext} = 2000$ V/cm applied aligned with the optical axis $c = y$ (normal to the propagation direction z) to induce the photorefractive effect in the crystal and an internal electric space-charge field E_{sc} induced by the light intensity $I = |A(\mathbf{r})|^2$ within the potential equation. The intensity-dependent, saturable, nonlocal, and anisotropic refractive index modulation[35] is obtained through the space-charge field $E_{sc} = \partial_y \phi_{sc}$ and the electrostatic potential ϕ_{sc}, by numerically solving the anisotropic potential equation

$$\Delta_\perp \phi_{sc} + \nabla_\perp \ln(1 + I) \cdot \nabla_\perp \phi_{sc} = E_{ext} \partial_y \ln(1 + I) \quad (4)$$

$I = |A(\mathbf{r})|^2$ is obtained from eq 3, and the calculated space-charge field $E_{sc} = \partial_y \phi_{sc}$ is obtained by solving eq 4 which updates eq 3. This numerical procedure is iterated along the propagation direction z.

Self-Induced Twisted Bundles on Various Curved Surfaces

We start our investigation by analyzing modulated Bessel beams at different spatial scales and modulation parameters to understand how their propagation behavior changes as the input power increases. At low powers, the concentric rings undergo fragmentation. During the nonlinear propagation of modulated Bessel beams, twisted segments are maintained but

https://doi.org/10.1021/acsaom.5c00466
ACS Appl. Opt. Mater. 2026, 4, 352−359

migrate to outer rings. Figure 2 shows two representative examples. After fragmentation along the most intense ring, individual beam fragments begin to diffract into neighboring rings, forming multiple discrete solitons (i.e., soliton pairs) during propagation. At a certain propagation distance, part of the energy is transferred to the central ring, reconstructing a pattern similar to the initial fragmented structure, which subsequently begins to move along a circular trajectory (see Visualization 1 and Visualization 2). For both discrete solitons and helicoidal beams, we observe that they are formed in pairs aligned along the same direction because of the anisotropy of the crystal. We assume that the trajectories of the discrete solitons follow geodesics on a hyperboloid surface (dark blue in Figure 2A1,B1). During the same time, the fragments evolve along cylindrical paths, giving rise to helicoidal solitary waves (brown in Figure 2A1,B1).

The initial phase has a topological charge of 8, but it undergoes radial modulation that changes as the beam propagates. When ring filaments begin to form, the phase develops localized distortions that correspond to the appearance of local vortices. The number of these vortices is determined by the modulation parameter M. As the filaments start to move, these phase variations are more pronounced, revealing the underlying twisting dynamics of the beam (see Visualization 3 and Visualization 4).

The parameter M influences only the phase modulation of the input beam without affecting its initial spatial intensity distribution. However, nonlinear propagation in the photorefractive crystal changes significantly with different values of M, resulting in clear differences in the number and size of the resulting twisted bundles. We systematically analyzed examples with various M values and observed that a well-defined formation of twisted bundles emerges only when M exceeds a certain threshold (specifically, $M > 4$). Increasing M beyond the threshold results in a larger number of constituents in each bundle, while the spatial size of the constituents decreases. Although the three phase modulation parameters p, η, and M influence the behavior of the beam, the number of resulting fragments is most strongly affected by M. Additionally, changing the sign of parameter p directly reverses the twisting direction of the beam.

To quantitatively characterize the energy dynamics of the beams, we calculate the transverse Poynting vector (the time-averaged directional energy flux of the electromagnetic field).[9,36,37] For a monochromatic, linearly polarized, and paraxial optical field with envelope $A(\mathbf{r})$, the transverse Poynting vector is

$$\langle \mathbf{S}_\perp \rangle = \frac{i\varepsilon_0 \omega}{2}(A\nabla_\perp A^* - A^*\nabla_\perp A) \tag{5}$$

where $\omega = ck$ is the angular frequency, ε_0 is the vacuum permittivity, and k is the wavenumber. The transverse Poynting vector provides insight into the spatial distribution of transverse energy flow in structured light fields, particularly in modulated Bessel beams, where phase discontinuities and nonlinearity give rise to a nontrivial dynamical behavior. In Figure 2(A2)/(A3) and (B2)/(B3), the black/orange arrows indicate the direction of the energy flow, as described by the Poynting vector (eq 5). Supporting Visualizations 1−4 provide energy flow along the propagation distance. At the input crystal face, energy is transferred circularly along every ring. During propagation along each tilted beam, energy is transferred from the inner rings to the outer rings. In contrast, when helicoidal structures begin to form, part of the energy is directed along the direction of their twisting, circulating azimuthally along the ring. In Figure 2, the energy flows counterclockwise, but the direction can be reversed by changing the sign of parameter p. This behavior remains consistent over distances up to 5 cm (not shown), demonstrating the robustness of such structures in nonlinear regimes. The nonlinear evolution of modulated Bessel beams leads to a transition from an initially circular energy flow to a regime with both azimuthal and radial components.

For a more detailed analysis of the resulting light-induced microstructures, we compare the examples from Figure 2. We consider the angles of pairs of discrete solitons (ϕ_s) and pairs of helicoidal waveguides (ϕ_w) relative to the optical c-axis (Figure 3A1). In addition, we measure the diffraction angles θ_w

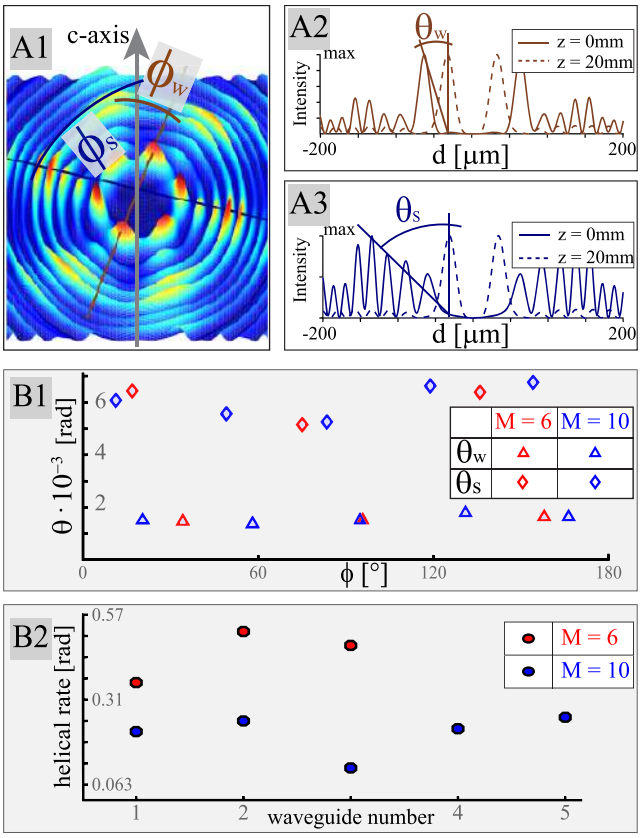

Figure 3. Diffraction angles and helicity analysis of twisted bundles. (A1) Output intensity distribution for $M = 6$ with marked angles relative to the optical c-axis, illustrating one example of a discrete soliton (ϕ_s) and one helicoidal waveguide (ϕ_w) pair. Input and output intensity profiles along the (A2) ϕ_w and (A3) ϕ_s directions, with diffraction angles θ_w for the helicoidal waveguide and θ_s for the discrete soliton pairs, marked at the corresponding profiles. (B1) Diffraction angle θ versus the angle relative to the optical axis ϕ for $M = 6$ and 10. (B2) Corresponding helical rate as a function of the helicoidal waveguide number for $M = 6$ and 10.

for helicoidal solitary beam pairs (waveguide pairs) and θ_s for discrete soliton pairs as marked in input and output intensty profiles in Figure 3A2,A3. Figure 3B1 presents the phase diagram of these two parameters for two examples. Despite the differing number of beams in the bundles, the phase diagram shows that the propagation paths on the curved surfaces are nearly identical for the two representative cases. But twisted

https://doi.org/10.1021/acsaom.5c00466
ACS Appl. Opt. Mater. 2026, 4, 352−359

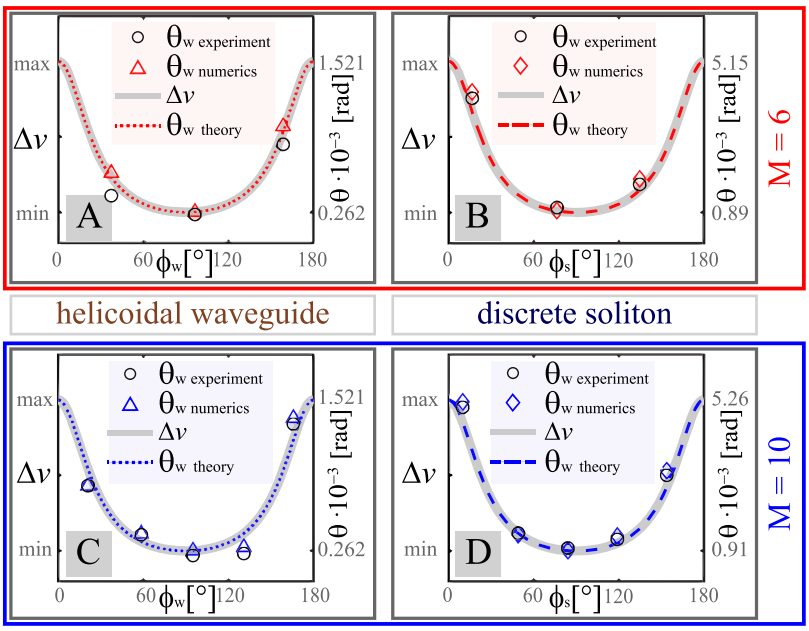

Figure 4. Influence of crystal anisotropy on the bundles of beams. Propagation velocity and diffraction angle as a function of the angle relative to the *c*-axis, for (A, B) $M = 6$ and (C, D) $M = 10$. Other parameters are as shown in Figure 1.

bundles on different surfaces can be observed by varying parameters such as beam scale a and beam orders m_1 and m_2. We also calculate the helical rate of the helicoidal beams in bundles, presenting the phase diagram of the helical rate versus the waveguide number (Figure 3B2). Since the helicoidal waveguides appear in pairs with the same helical rate, the helical rate is shown per pair, and it is more pronounced for $M = 6$ compared to $M = 10$.

Our crystal is anisotropic, as indicated by the anisotropy term (∂_y) in eq 2, and the external electric field is aligned along the optical axis of the crystal ($c = y$). This anisotropy causes differences in the intensity distributions (Figure 2A2,B2) and the diffraction angles along the various directions. We examine how this affects the numerical results, focusing on the diffraction angles (Figure 3B1). The refractive index change, Δn, is highest along the *c*-axis, decreases with deviation, and is minimal in the perpendicular direction, following a periodic pattern. As a result, the effective refractive index ($n_{eff} = n_e - \Delta n$) is the lowest along the *c*-axis and the highest perpendicular to it. This causes stronger light localization along the *x*-axis. Since the propagation velocity (Δv) is inversely related to n_{eff}, diffraction is enhanced along the *c*-axis (Figure 4). The angular distribution of the light velocity determines the diffraction angles. Theoretical predictions are based on scaling the diffraction angles of the discrete soliton (θ_s) and the helicoidal waveguide (θ_w) by using this distribution. They are compared with the numerical results in Figure 4 for two modulated Bessel beams, showing good agreement.

Figure 5 shows the influence of the nonlinearity strength on the twisted bundle of discrete beams. Three representative examples of various nonlinearities are presented as intensity distributions through the crystal volume. Figure 2A corresponds to the schematic representation shown in Figure 5A1. As the beam intensity increases, the energy along the helicoidal geodesics on the inner cylindrical surface disappears. This energy is transferred to rectilinear geodesics on the outer curved surface; a higher intensity enhances the formation of discrete solitons while suppressing the appearance of helicoidal

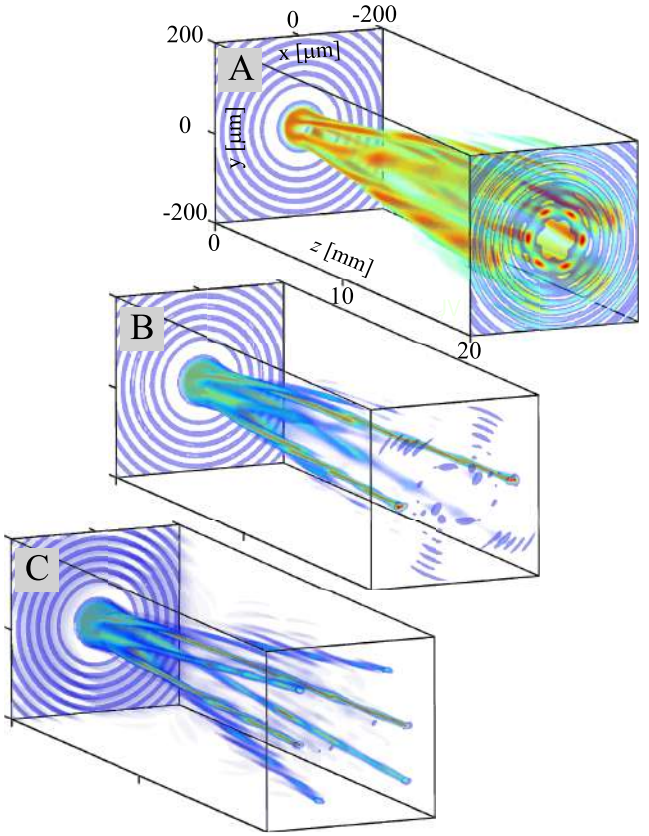

Figure 5. Surface-distributed discrete solitons. Influence of nonlinearity on the twisted bundles of discrete solitons: (A) $I_0 = 0.1$, (B) $I_0 = 0.2$, and (C) $I_0 = 0.3$. Other parameters are as shown in Figure 2A1.

beams. With increasing nonlinearity, the positions of the beams remain unchanged, with slight modulations along the propagation. The influence of crystal anisotropy is evident through the asymmetry of the intensity distributions along

https://doi.org/10.1021/acsaom.5c00466
ACS Appl. Opt. Mater. 2026, 4, 352−359

different directions relative to the optical axis for the variations of modulations and input beam intensity. At very high nonlinearities, the discrete solitons lie on hyperboloids that are deformed due to the effects of anisotropy.

Experimental Method for Surface-Confined Bundle Realization

To experimentally examine and describe the effects of the nonlinear propagation of modulated Bessel beams in the cerium-doped strontium barium niobate crystal, CeO_2 doped at 0.002 wt % (SBN61:Ce) crystal of dimensions ($5 \times 5 \times 20$ mm^3), we utilize the experimental setup shown in Figure 6. As

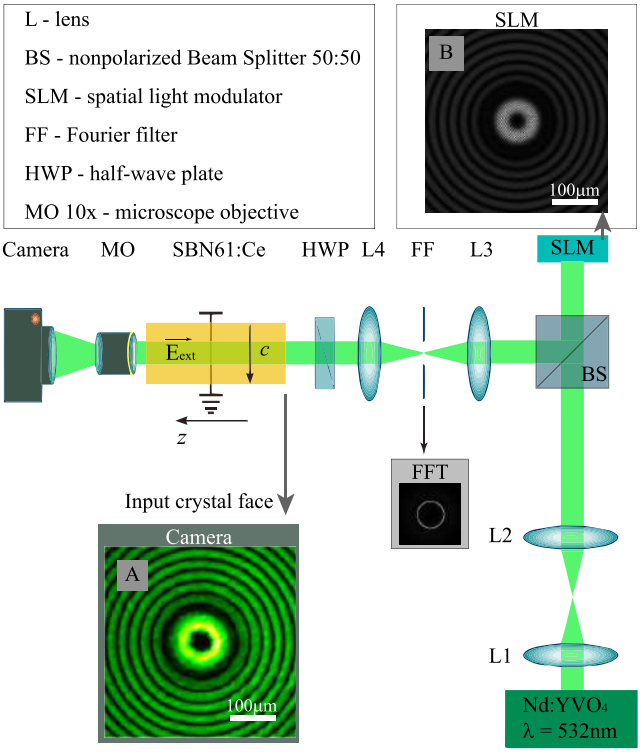

Figure 6. Experimental setup for investigating the nonlinear propagation of modulated Bessel beams. (A) Experimentally observed intensity distributions at the input crystal face for (B) a numerically precalculated hologram.

a light source, a continuous frequency-doubled Nd:YVO_4 laser (λ = 532 nm) provides a linearly polarized beam, which is expanded and collimated through a telescope (L1−L2) to form a plane wave incident on a spatial light modulator (SLM). The reflected full HD-HOLOEYE-PLUTO-2.1 SLM (pixel size = 8 μm) modulates both the amplitude and phase of the reflected light field (example shown in Figure 1A,B), which is achived by addressing a numerically precalculated hologram (Figure 6B) to the SLM containing information on the complex light field of a modulated Bessel beam (structured beam), encoded with an additional blazed grating.[38] The second telescope (L3−L4) adjusts the transverse size of the structured beam so that the experimental input intensity distribution (Figure 6A) has the same spatial beam scale a as in numerics (Figure 1A). The Fourier transform of the beam appears in the focal plane of L3, where a Fourier filter performs band-pass filtering. A half-wave plate aligns the linear polarization of the beam with the optical crystal axis, thereby enhancing the nonlinear response owing to a larger electro-optic coefficient. The extraordinarily polarized structured beam propagates through an externally biased crystal with an external electric field (E_{ext}), applied along the optical $c = y$ axis, perpendicular to the propagation direction (the z-axis). The crystal exhibits strong nonlinearity at comparatively low power levels. The beam power per unit area P serves as a control parameter for the nonlinearity strength, corresponding to the intensity I_0 used in numerical simulations. Here, we use the most intensive inner ring for the unit area. The transverse intensity distributions at the output crystal face are recorded using an imaging system (a 10× microscope objective and a Thorlabs CS126CU camera) and subsequently compared with the simulation results.

First, we examine the linear propagation of the ordinary polarized structured beam without an external electric field and at a sufficiently low input power (P = 3.6 mW/cm^2). The corresponding intensity distributions at the crystal exit face are presented for three representative cases for M = 6, 8, and 10 (Figure 7A1−C1). Beam fragmentation is visible along the inner rings.

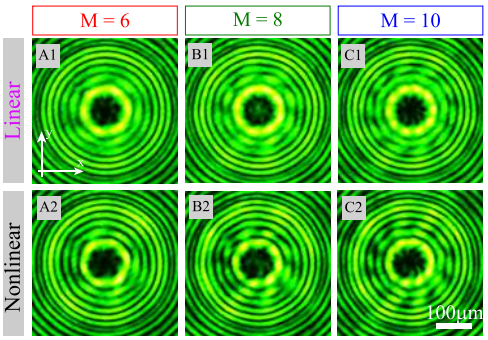

Figure 7. Experimentally observed intensity distributions at the output crystal face in linear (the first row) and nonlinear (the second row) regimes for (A) M = 6, (B) M = 8, and (C) M = 10. Visualizations 5, 6, and 7 show the experimental temporal evolution of the nonlinear self-action process at the output crystal face for the cases presented in panels (A2), (B2), and (C2). Parameters: P = 3.6 mW/cm^2, E_{ext} = 0 V/cm (the first row), P = 18.5 mW/cm^2, E_{ext} = 2000 V/cm, exposure time: 50 s (the second row). Other parameters are as shown in Figure 1.

In the nonlinear regime, with an external electric field E_{ext} and an input power P = 18.5 mW/cm^2, light-induced microstructures of the twisted bundles are observed and presented as intensity distributions on the output face of the crystal (Figure 7A2−C2). The corresponding output crystal face dynamics during nonlinear self-action are presented as Supporting Visualizations 5−7. Two examples (A2) and (C2) correspond to the numerical results of Figure 2A2,B2, showing good agreement between the experiment and the numerics. Experimentally observed diffraction angles of the discrete soliton (θ_s) and the helicoidal waveguide (θ_w) in dependence of the angles of pairs of discrete solitons (ϕ_s) and pairs of helicoidal waveguides (ϕ_w) are also presented in Figure 4, validating the good agreement between the numerical simulations and the experimental results. Compared with the linear case, twisted segments are maintained in the nonlinear case, but they migrate to outer rings; Figure 2 shows two representative examples.

Our findings provide precise control over the light-induced microstructures of twisted bundles of beams, including the number, spatial positioning, and individual characteristics of

https://doi.org/10.1021/acsaom.5c00466
ACS Appl. Opt. Mater. 2026, 4, 352−359

the constituent beams. Moreover, this approach enables the precise manipulation of light propagation paths across curved surfaces and control over the direction of their twisting or moving. In addition, it improves the predictability and tunability of structured light propagation, supporting advanced beam shaping in complex optical systems.

CONCLUSION

In summary, we have introduced a method for creating light-induced microstructures composed of twisted beam bundles distributed across various surfaces. As a demonstration, modulated Bessel beams were used in a single-pass optical induction experiment within a uniaxial anisotropic photorefractive crystal. The nonlinear propagation behavior of these beams is investigated by varying their scale, modulation level, and input power. We demonstrate the formation of multiple discrete solitons on the surfaces without the need for an inscribed photonic lattice or tilted probe beam incidence. Helicoidal solitary beams are observed simultaneously with discrete solitons confined on cylindrical and hyperboloidal surfaces, respectively. Our method can also be applied to other types of nondiffracting beams and enables precise control over beam bundles, including the number of individual beams, their twisting direction, and the shape of their propagation surfaces. This flexibility offers significant potential for the advancement of research in areas such as optical communication, information processing, particle manipulation, and biophotonics.

ASSOCIATED CONTENT

Supporting Information

The Supporting Information is available free of charge at https://pubs.acs.org/doi/10.1021/acsaom.5c00466.

Visualization 1: numerical intensity distributions of the modulated Bessel beams along the propagation, corresponding to cases presented in Figure 2A2, with the corresponding energy flow, characterized by the Poynting vector, indicated by black arrows (AVI)

Visualization 2: numerical intensity distributions of the modulated Bessel beams along the propagation, corresponding to cases presented in Figure 2B2, with the corresponding energy flow, characterized by the Poynting vector, indicated by black arrows (AVI)

Visualization 3: numerical phase distributions of the modulated Bessel beams along the propagation, corresponding to cases presented in Figure 2A3, with the corresponding energy flow, characterized by the Poynting vector, indicated by orange arrows (AVI)

Visualization 4: numerical phase distributions of the modulated Bessel beams along the propagation, corresponding to cases presented in Figure 2B3, with the corresponding energy flow, characterized by the Poynting vector, indicated by orange arrows (AVI)

Visualization 5: experimental temporal evolution during the nonlinear self-action process from the output crystal face, for the example presented in Figure 7A2; the video was recorded at 4 frames per second (4 fps) and shows the transverse area of 1966 μm × 1440 μm (AVI)

Visualization 6: experimental temporal evolution during the nonlinear self-action process from the output crystal face, for the example presented in Figure 7B2; the video was recorded at 4 frames per second (4 fps) and shows the transverse area of 1966 μm × 1440 μm (AVI)

Visualization 7: experimental temporal evolution during the nonlinear self-action process from the output crystal face, for the example presented in Figure 7C2; the video was recorded at 4 frames per second (4 fps) and shows the transverse area of 1966 μm × 1440 μm (AVI)

AUTHOR INFORMATION

Corresponding Author

Jadranka M. Vasiljević − *Institute of Physics, University of Belgrade, 11080 Belgrade, Serbia*; Email: jadranka@ipb.ac.rs

Authors

Miroslav M. Petroski − *Institute of Physics, University of Belgrade, 11080 Belgrade, Serbia*

Dejan V. Timotijević − *University of Belgrade - Institute for Multidisciplinary Research, National Institute of the Republic of Serbia, National Institute of the Republic of Serbia, 11030 Belgrade, Serbia*

Dragana M. Jović Savić − *Institute of Physics, University of Belgrade, 11080 Belgrade, Serbia*

Complete contact information is available at: https://pubs.acs.org/10.1021/acsaom.5c00466

Author Contributions

J.M.V. performed the formal analysis, investigation, and result validation, prepared all figures and visualizations, and wrote the original draft of the manuscript. M.M.P. contributed to the investigation, data curation, and participated in the review and editing of the manuscript. D.V.T. was responsible for the conceptualization, methodology, and software development and contributed to the review and editing of the manuscript. D.M.J.S. was responsible for conceptualization, funding acquisition, supervision, and manuscript review and editing. All authors reviewed and approved the final manuscript.

Notes

The authors declare no competing financial interest.

ACKNOWLEDGMENTS

The authors acknowledge funding provided by the Institute of Physics Belgrade and Institute for Multidisciplinary Research (IMSI) through the grants by the Ministry of Science, Technological Development and Innovations of the Republic of Serbia (IMSI contract no. 451-03-66/2024-03/200053) and by the Science Fund of the Republic of Serbia (grant no. 7714356, IDEAS—CompsLight).

REFERENCES

(1) Bouchal, Z. Nondiffracting Optical Beams: Physical Properties, Experiments, and Applications. *Czech. J. Phys.* **2003**, *53*, 537−578.

(2) Bandres, M. A.; Gutiérrez-Vega, J. C.; Chávez-Cerda, S. Parabolic nondiffracting optical wave fields. *Opt. Lett.* **2004**, *29*, 44−46.

(3) Tomović, A. Ž.; Vlaović Mitić, I. J.; Jovanović, V. P.; Timotijević, D. V.; Jović Savić, D. M. Assembling of truncated deterministic aperiodic lattices with defects using Weber beams. *Opt. Mater.* **2024**, *157*, No. 116334.

(4) Woerdemann, M.; Alpmann, C.; Esseling, M.; Denz, C. Advanced optical trapping by complex beam shaping. *Laser Photonics Rev.* **2013**, *7*, 839−854.

(5) Garcés-Chávez, V.; McGloin, D.; Melville, H.; Sibbett, W.; Dholakia, K. Simultaneous micromanipulation in multiple planes using a self-reconstructing light beam. *Nature* **2002**, *419*, 145−147.
(6) Baumgartl, J.; Mazilu, M.; Dholakia, K. Optically mediated particle clearing using Airy wavepackets. *Nat. Photonics* **2008**, *2*, 675−678.
(7) Bloch, I. Ultracold quantum gases in optical lattices. *Nat. Phys.* **2005**, *1*, 23−30.
(8) Lederer, F.; Stegeman, G. I.; Christodoulides, D.; Assanto, G.; Segev, M.; Silberberg, Y. Discrete solitons in optics. *Phys. Rep.* **2008**, *463*, 1−126.
(9) Zannotti, A.; Vasiljević, J. M.; Timotijević, D. V.; Jović Savić, D. M.; Denz, C. Visualizing the Energy Flow of Tailored Light. *Adv. Opt. Mater.* **2018**, *6*, No. 1701355.
(10) Mitić, D. V.; Vasiljević, J. M.; Timotijević, D. V.; Jović Savić, D. M. Self-induced parabolic surface states. *Opt. Mater.* **2025**, *167*, No. 117249.
(11) Durnin, J.; Miceli, J. J.; Eberly, J. H. Diffraction-free beams. *Phys. Rev. Lett.* **1987**, *58*, 1499−1501.
(12) McGloin, D.; Dholakia, K. Bessel beams: Diffraction in a new light. *Contemp. Phys.* **2005**, *46*, 15−28.
(13) Garcés-Chávez, V.; Volke-Sepulveda, K.; Chávez-Cerda, S.; Sibbett, W.; Dholakia, K. Transfer of orbital angular momentum to an optically trapped low-index particle. *Phys. Rev. A* **2002**, *66*, No. 063402.
(14) Planchon, T. A.; Gao, L.; Milkie, D. E.; Davidson, M. W.; Galbraith, J. A.; Galbraith, C. G.; Betzig, E. Rapid three-dimensional isotropic imaging of living cells using Bessel beam plane illumination. *Nat. Methods* **2011**, *8*, 417−426.
(15) Schulze, C.; Roux, F. S.; Dudley, A.; Rop, R.; Duparré, M.; Forbes, A. Accelerated rotation with orbital angular momentum modes. *Phys. Rev. A* **2015**, *91*, No. 043821.
(16) Duocastella, M.; Arnold, C. Bessel and annular beams for materials processing. *Laser Photonics Rev.* **2012**, *6*, 607−621.
(17) Rose, P.; Boguslawski, M.; Denz, C. Nonlinear lattice structures based on families of complex nondiffracting beams. *New J. Phys.* **2012**, *14*, No. 033018.
(18) Lonergan, A.; O'Dwyer, C. Many Facets of Photonic Crystals: From Optics and Sensors to Energy Storage and Photocatalysis. *Adv. Mater. Technol.* **2023**, *8*, No. 2201410.
(19) Joannopoulos, J. D.; Johnson, S. G.; Winn, J. N.; Meade, R. D. *Fotonic Crystals: Molding the Flow of Light*, 2nd ed.; Princeton University, 1995.
(20) Chang, S.; Guo, X.; Ni, X. Optical Metasurfaces: Progress and Applications. *Annu. Rev. Mater. Res.* **2018**, *48*, 279−302.
(21) Wang, P.; Krasavin, A. V.; Liu, L.; Jiang, Y.; Li, Z.; Guo, X.; Tong, L.; Zayats, A. V. Molecular Plasmonics with Metamaterials. *Chem. Rev.* **2022**, *122*, 15031−15081.
(22) Pertsch, T.; Zentgraf, T.; Peschel, U.; Bräuer, A.; Lederer, F. Anomalous Refraction and Diffraction in Discrete Optical Systems. *Phys. Rev. Lett.* **2002**, *88*, No. 093901.
(23) Eisenberg, H. S.; Silberberg, Y.; Morandotti, R.; Aitchison, J. S. Diffraction Management. *Phys. Rev. Lett.* **2000**, *85*, 1863−1866.
(24) Christodoulides, D. N.; Lederer, F.; Silberberg, Y. Discretizing light behaviour in linear and nonlinear waveguide lattices. *Nature* **2003**, *424*, 817−823.
(25) Fleischer, J. W.; Segev, M.; Efremidis, N. K.; Christodoulides, D. N. Observation of two-dimensional discrete solitons in optically induced nonlinear photonic lattices. *Nature* **2003**, *422*, 147−150.
(26) Hudock, J.; Efremidis, N. K.; Christodoulides, D. N. Anisotropic diffraction and elliptic discrete solitons in two-dimensional waveguide arrays. *Opt. Lett.* **2004**, *29*, 268−270.
(27) Petroski, M. M.; Timotijević, D. V.; Jović Savić, D. M.; Vasiljević, J. M. Head-on excitation of tilted solitons by fragmented Bessel beams. *Chaos, Solitons Fractals* **2026**, *202*, No. 117434.
(28) Batz, S.; Peschel, U. Linear and nonlinear optics in curved space. *Phys. Rev. A* **2008**, *78*, No. 043821.
(29) Schultheiss, V. H.; Batz, S.; Szameit, A.; Dreisow, F.; Nolte, S.; Tünnermann, A.; Longhi, S.; Peschel, U. Optics in Curved Space. *Phys. Rev. Lett.* **2010**, *105*, No. 143901.
(30) Xu, C.; Wang, L.-G. Theory of light propagation in arbitrary two-dimensional curved space. *Photonics Res.* **2021**, *9*, 2486.
(31) Schultheiss, V. H.; Batz, S.; Peschel, U. Light in curved two-dimensional space. *Adv. Phys.: X* **2020**, *5*, No. 1759451.
(32) Agrawal, G. *Nonlinear Fiber Optics*, 5th ed.; Academic Press, 2012.
(33) Zannotti, A.; Vasiljević, J. M.; Timotijević, D. V.; Jović Savić, D. M.; Denz, C. Morphing discrete diffraction in nonlinear Mathieu lattices. *Opt. Lett.* **2019**, *44*, 1592−1595.
(34) Kukhtarev, N. V.; Markov, V. B.; Odulov, S. G.; Soskin, M. S.; Vinetskii, V. L. Holographic storage in electrooptic crystals. i. steady state. *Ferroelectrics* **1978**, *22*, 949−960.
(35) Zozulya, A. A.; Anderson, D. Z. Propagation of an optical beam in a photorefractive medium in the presence of a photogalvanic nonlinearity or an externally applied electric field. *Phys. Rev. A* **1995**, *51*, 1520−1531.
(36) Born, M.; Wolf, E. *Principles of Optics*, 7th ed.; Cambridge University Press, 1999.
(37) Sztul, H. I.; Alfano, R. The Poynting vector and angular momentum of Airy beams. *Opt. Express* **2008**, *16*, 9411−9416.
(38) Davis, J. A.; Cottrell, D. M.; Campos, J.; Yzuel, M. J.; Moreno, I. Encoding amplitude information onto phase-only filters. *Appl. Opt.* **1999**, *38*, 5004−5013.

https://doi.org/10.1021/acsaom.5c00466
ACS Appl. Opt. Mater. 2026, 4, 352−359

Chaos, Solitons and Fractals 202 (2026) 117434

Contents lists available at ScienceDirect

Chaos, Solitons and Fractals

journal homepage: www.elsevier.com/locate/chaos

Head-on excitation of tilted solitons by fragmented Bessel beams

Miroslav M. Petroski [a], Dejan V. Timotijević [b], Dragana M. Jović Savić [a], Jadranka M. Vasiljević [a,*]

[a] Institute of Physics, University of Belgrade, Pregrevica 118, 11080, Belgrade, Serbia
[b] Institute for Multidisciplinary Research, University of Belgrade, Kneza Višeslava 1, 11030, Belgrade, Serbia

ARTICLE INFO

Keywords:
Discrete solitons
Tilted solitons
Non-diffracting beams
Waveguiding

ABSTRACT

This work demonstrates the formation of tilted discrete solitons via the nonlinear self-action of non-diffracting fragmented Bessel beams in photorefractive media, using a single-pass optical induction scheme that induces anisotropic refractive index modulation experimentally. Unlike typical methods for the generation of tilted solitons based on preinscribed periodic structures and tilted probe beam excitation, our approach enables soliton formation under normal (head-on) incidence of an aperiodic structure and without any prefabricated lattice. Particularly, we suggest a clarification of the mechanism underlying their formation. Appropriate localized symmetry deviations with nonlinearity lead to the formation of tilted discrete solitons. Multiple tilted soliton pairs are generated along distinct directions, determined by the number and arrangement of the Bessel beam fragments. The system exhibits high tunability: by adjusting the Bessel beam's order, scale, phase, and input power, we gain precise control over the number, orientation, and position of the resulting solitons. This work advances the understanding of structured light propagation, offering a versatile platform for soliton generation, beam shaping, and diffraction control.

1. Introduction

Non-diffracting beams [1] have attracted considerable attention as light structures due to their evident potential for diverse applications such as optical micromanipulation technologies as a useful tool in medical, biological, and physics research [2], optical tweezing [3,4], quantum optics [5], and nonlinear optics [6–8]. These light beams represent exact solutions of the Helmholtz equation in different coordinate systems: plane waves in Cartesian, Bessel beams in cylindrical [9], Mathieu beams in elliptical cylindrical [10], and parabolic beams in parabolic cylindrical coordinates [11]. They have significant potential in nonlinear photonics [12–15], and for a new type of optical lattice-writing light [16–18]. Such lattices, produced using non-diffracting beams, are primarily observed in specific linear regimes. Due to their distinctive characteristics, self-healing ability, diffraction resistance, and a central dark core, Bessel beams have been utilized in a wide range of applications, such as optical trapping, high-resolution imaging, and laser-based material processing [19–24]. However, the nonlinear dynamics of non-diffracting beams continue to attract considerable research attention.

Tailoring the spatial and spectral structure of electromagnetic fields enables deeper insight into nonlinear wave dynamics and the intricacies of light-matter interaction, offering broad utility across various fields, including imaging, spectroscopy, optical communications, and bioscience [25]. Nonlinear interaction can suppress the self-acceleration of swallowtail beams, resulting in stable off-axis solitons guided by the initial beam trajectory [26]. The self-splitting of nondiffracting beams via photorefractive

* Corresponding author.
E-mail address: jadranka@ipb.ac.rs (J.M. Vasiljević).

https://doi.org/10.1016/j.chaos.2025.117434
Received 28 July 2025; Received in revised form 10 October 2025; Accepted 16 October 2025
Available online 22 October 2025

nonlinearity has been demonstrated, enabling the realization of chiral waveguides and the generation of vortices [27]. The discretization of light as the main idea for the development of discrete optical components can be achieved by manipulating light through its interaction with functional materials, allowing for the discretization of the spectral components of the wave [28,29]. The propagation of light in periodically structured media shows dynamics that cannot be realized in homogeneous media, leading to light control by band structures. Dielectric media with a periodically modulated refractive index serve as an example for controlling and investigating discrete light propagation [28,30]. In such periodic systems, tilted beams are observed using a wide probe at the incident angle [28,29]. It was noticed that there are discrete and periodic angles where tilted solitons occur, depending on the lattice scale (period in wavelength units). The investigation of tilted solitons in other physical systems remains an open and largely unexplored field, particularly in the nonlinear regime [31,32].

In this paper, using the non-linear propagation of fragmented Bessel beams in photorefractive media, we demonstrate the formation of tilted solitons without a tilted incidence of the probe beam in the lattice and such extending the concept of tilted discrete soliton generation. Clarifying the excitation mechanism of nonlinear tilted solitons, their connection to linear modes, and the residual lattice allows us to predict the initial structures needed to generate solitons with specific numbers and properties. This understanding enables us to propose a new approach for designing the initial structures, using controlled beam fragmentation of azimuthally and phase-modulated Bessel beams, with the aim of generating tilted solitons. We explore the behavior of various fragmented Bessel beams during propagation in different nonlinear regimes. Increasing nonlinearity, the non-diffracting nature of fragmented Bessel beams breaks down during propagation through the crystal, and tilted discrete solitons are formed. Unlike *periodic* waveguide arrays, where similar phenomena have been observed [29], we show that these tilted discrete solitons can be excited in *normal* incidence and *without* preinscribed waveguides, arising from *aperiodic* refractive index modulations. Our results suggest that appropriate nonlinearity and localized symmetry deviation are responsible for the generation of tilted discrete solitons. By clarifying the excitation mechanism of nonlinear tilted solitons and their link to linear modes, we have demonstrated similar effects in other geometries with various dimensionalities of guiding structures, considering only aperiodic discrete structures that support linear modes, which will be reported separately for the 1D geometry.

The properties of tilted discrete solitons are highly sensitive to and can be effectively tuned by adjusting the Bessel beam order, scale, phase, and input power. These effects are experimentally demonstrated in a single-pass configuration using optical induction in a photorefractive crystal. Numerical simulations predicting multiple pairs of tilted discrete solitons agree well with their experimental realization. We observe different effects along the separate directions (along the spikes) that are caused by crystal anisotropy. The ability to fine-tune these solitons opens new opportunities for advanced control of light in nonlinear media and holds significant potential for applications in optical engineering, communications, and information processing.

2. Numerical modeling and experimental realization of nonlinear propagation of the fragmented bessel beams in photorefractive media

We numerically model the nonlinear propagation of structured light in the photorefractive birefringent cerium-doped strontium barium niobate (SBN61:Ce) crystal, by solving the nonlinear Schrödinger equation

$$\mathrm{i}\partial_z A(\mathbf{r}) + \frac{1}{2k_z}\left[\Delta_\perp + G(I)\right] A(\mathbf{r}) = 0, \tag{1}$$

using the spectral split-step method [13,14,33]. $A(\mathbf{r})$ is the paraxial propagational scalar light field, with the longitudinal wave number k_z. The nonlinear potential is given by $G(I) = -k_z^2 n_e^2 r_{33} E(I)$ where $n_e = 2.35$ and $r_{33} = 267\,\mathrm{pm/V}$ are the extraordinary refractive index and the corresponding electro-optic coefficient of the SBN61:Ce crystal for extraordinary polarized light, and $k = 2\pi/\lambda = \sqrt{(k_\perp^2 + k_z^2)}$ is the wave number determined by the laser wavelength $\lambda = 532\,\mathrm{nm}$. The SBN61:Ce crystal provides strong nonlinearity at comparatively low power levels. The nonlinear light-matter interaction is calculated by assuming a light-induced refractive index modulation as presented in [34]. The total electric field $E(I) = E_{\mathrm{ext}} + E_{\mathrm{sc}}(I)$ that builds up inside the crystal consists of an external bias field $E_{\mathrm{ext}} = 2000\,\mathrm{V/cm}$ applied aligned with the optical $c = y$ axis (perpendicular to the z–axis) to induce the photorefractive effect in the crystal and an internal electric space charge field E_{sc} induced by the light intensity $I = |A(\mathbf{r})|^2$ within the potential equation. The intensity-dependent, nonlocal, saturable, and anisotropic refractive index modulation [35] is obtained through the space-charge field $E_{\mathrm{sc}} = \partial_y \phi_{sc}$, where ϕ_{sc} is the electrostatic potential, by numerically solving the anisotropic potential equation

$$\Delta_\perp \phi_{\mathrm{sc}} + \nabla_\perp \ln(1+I) \cdot \nabla_\perp \phi_{\mathrm{sc}} = E_{\mathrm{ext}} \partial_y \ln(1+I). \tag{2}$$

$I = |A(\mathbf{r})|^2$ is obtained from Eq. (1), the calculated space-charge field $E_{sc} = \partial_y \phi_{sc}$, obtained by solving Eq. (2) updates Eq. (1), and this procedure is iterated along the propagation direction z.

In our study, the structured light field A is defined as a sum of modulated Bessel beams $U_{m,p,a}$ of order m, given by

$$U_{m,p,a}(x,y) = J_m(k_\perp \rho) e^{ip\varphi}, \tag{3}$$

where J_m is the first kind Bessel function of order m, p denotes the modulation, and $k_\perp = 2\pi/a$ is the transverse wave number defined by the beam scale a (denoted in Fig. 1), which controls the spatial size of the beam and affects the size of its Fourier transform. The cylindrical (radial distance ρ and azimuth φ) and Cartesian coordinates are related via $x = \rho\cos\varphi$, $y = \rho\sin\varphi$.

To experimentally investigate the nonlinear propagation of fragmented Bessel beams, we employ the experimental setup shown in Fig. 1. A continuous frequency-doubled Nd:YVO_4 laser ($\lambda = 532\,\mathrm{nm}$) provides a linearly polarized beam, which is expanded and

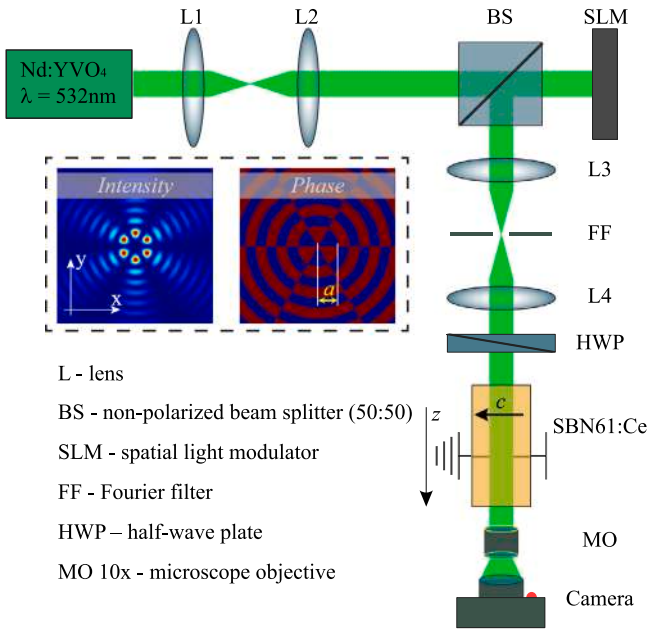

Fig. 1. Experimental setup for investigation of nonlinear propagation of fragmented Bessel beams. The insert shows intensity and phase at the crystal input face.

collimated through a telescope (L1–L2) to form a plane wave incident on a spatial light modulator (SLM). The full HD - HOLOEYE - PLUTO - 2.1 LCOS SLM, with a pixel pitch of 8 μm, modulates both the amplitude and phase of the reflected light field (example shown in the insert of Fig. 1), by displaying a precomputed hologram of a fragmented Bessel beam (structured beam), overlaid with a blaze grating [36]. A second telescope (L3–L4) adjusts the beam to the appropriate size and illuminates the SBN61:Ce crystal. The Fourier transform of the beam appears in the focal plane of L3, where a Fourier filter (FF) performs bandpass filtering. A half-wave plate aligns the linear polarization of the beam with the optical axis of the crystal, amplifying the nonlinear optical response as a result of the larger electro-optic coefficient. The extraordinarily polarized structured beam propagates through an externally biased SBN61:Ce crystal ($5 \times 5 \times 20\,\mathrm{mm}^3$) with the external electric field (E_{ext}) applied along the optical $c = y$ axis, perpendicular to the propagation direction (the z- axis). The variable beam power P adjusts the nonlinearity strength, corresponding to the intensity I in the numerical simulations. The transverse intensity distributions at the crystal exit face are recorded using an imaging system (10x microscope objective + camera (THORLABS CS126CU)) and compared with the numerical results.

3. Self-induced multiple pairs of tilted solitons

We start our study by presenting an approach to obtain discrete structures with a controlled number of fragments. First, we modulate the Bessel beams so that the beam's amplitude corresponds to the first kind of Bessel function of order m, while the phase is independently defined through a parameter p as shown in Eq. (3). We superpose two modulated Bessel beams of the same order m but with opposite modulations $p_2 = -p_1$, $A = U_{m,p_1,a} + U_{m,-p_1,a}$, and obtain a simplified expression for paraxial light field distribution in the transverse plane:

$$A(x, y) = 2J_m(k_\perp \rho)\cos(p\varphi). \tag{4}$$

Unlike individual Bessel beams, which form continuous concentric rings, the resulting fragmented structure A is divided into discrete fragments (insert in Fig. 1 for $p = 3$). This approach enables precise control over the number of fragments, $f = |p_1| + |p_2|$, in each concentric ring. By superimposing two oppositely modulated Bessel beams and varying the parameter p, we systematically shape the spatial structure and control its fragmentation. In the following, we will call such structures *fragmented Bessel beams*. Increasing the parameter p produces more fragments while reducing their individual size. We analytically confirm that these fragmented Bessel beams remain non-diffracting in the linear regime.

Next, we study the nonlinear propagation of fragmented Bessel beams with different numbers of fragments. For low nonlinearity (low intensity/power), the beam maintains its non-diffracting nature along the length of the SBN61:Ce crystal (both numerically and experimentally (not shown here)). However, with increasing nonlinearity, stability is broken, and the beams lose their non-diffracting properties. Fig. 2 summarizes the nonlinear propagation of fragmented Bessel beams with an increased number of fragments in each concentric circle. With higher nonlinearity, we observe a radial spreading of the highest intensities away from the center in all directions (along the spikes), along the propagation. In a certain nonlinear regime, tilted discrete solitons are observed along the

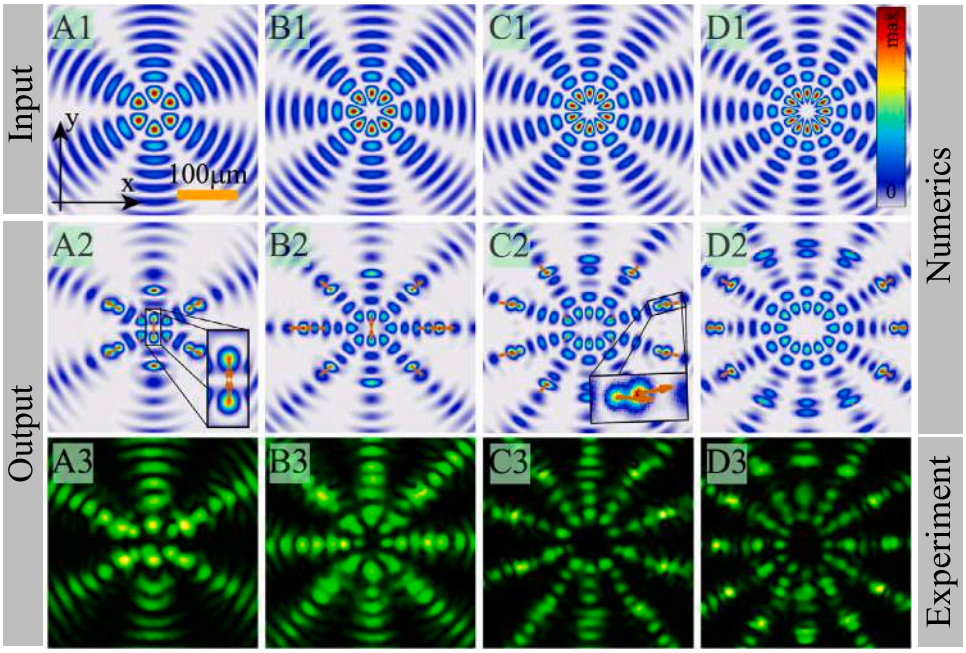

Fig. 2. Self-induced tilted discrete solitons. Intensity distributions of fragmented Bessel beams at the input (the first row) and after $z = 20\,\text{mm}$ propagation distance with the corresponding transverse Poynting vectors indicated by orange arrows (the second row), obtained numerically. The third row: experimentally observed intensity distribution at the crystal exit face. Parameters are: (A) $p = 3$, input beam intensity $I_0 = 0.3$, input power $P = (16.3 \pm 0.49)\mu\text{W}$, (B) $p = 4$, $I_0 = 0.4$, $P = (14.6 \pm 0.44)\mu\text{W}$, (C) $p = 5$, $I_0 = 0.5$, $P = (15.7 \pm 0.47)\mu\text{W}$, (D) $p = 6$, $I_0 = 0.5$, $P = (16 \pm 0.48)\mu W$. Other parameters: $m = 3$, $a = 45\,\mu\text{m}$.

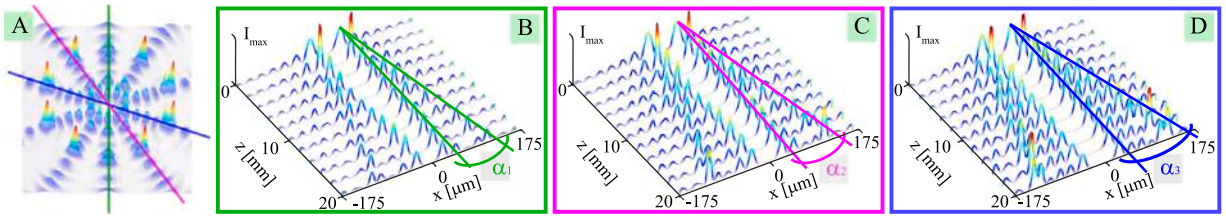

Fig. 3. Tilted soliton pairs along various directions. Projections of intensity distributions of fragmented Bessel beam along propagation for different spikes marked with lines in (A): green (B), pink (C), and red (D) with corresponding soliton tilted angles $\alpha_1 = 0.0042\,\text{rad}$, $\alpha_2 = 0.0044\,\text{rad}$, $\alpha_3 = 0.0052\,\text{rad}$, respectively. Parameters are as in Fig. 2(C).

propagation distance (movies Fig2A2.avi, Fig2B2.avi, Fig2C2.avi, and Fig2D2.avi in Supporting Information). The number of tilted solitons is proportional to the number of fragments (along the circle) of the fragmented Bessel beams. The tilt angle of the observed solitons increases with the number of fragments. For each example, there are soliton pairs with the same tilted angles of separate solitons: the tilted angles are different for various radial directions, owing to the crystal anisotropy.

We investigate the influence of crystal anisotropy on the discrete tilted soliton pairs along various spikes (with various angles relative to the optical axis). Fig. 3 presents an example of Fig. 2(C). Three main projections along representative spikes are presented as intensity distributions along the propagation distance (Fig. 3(B), (C), (D)). The angle between pairs of tilted solitons is the smallest along the optical axis and increases with the angular deviation from this axis.

We also examine how crystal anisotropy affects the formation of discrete tilted solitons by comparing different configurations of fragmented Bessel beams. Fig. 4 shows the results for two cases: Bessel beams fragmented into 8 and 12 parts along each circle. Regardless of the number of fragments, the angle of tilted solitons is larger in the direction perpendicular to the optical axis. However, the number of fragments also influences the tilt angle. Changes in beam modulation affect both the number of fragments and their orientation relative to the optical axis, thereby allowing precise control over the tilt angle of the solitons in different directions.

The tilted discrete solitons formation during the nonlinear propagation of a nondiffracting beam motivated us to consider their excitation mechanism and explore their connection to linear mode excitation in preinscribed refractive index potentials. The linear modes associated with tilted beams act as optical traps that guide light along their propagation direction and suppress diffraction, thereby creating favorable conditions for soliton formation. When light is normally launched into a permanent periodic lattice, only

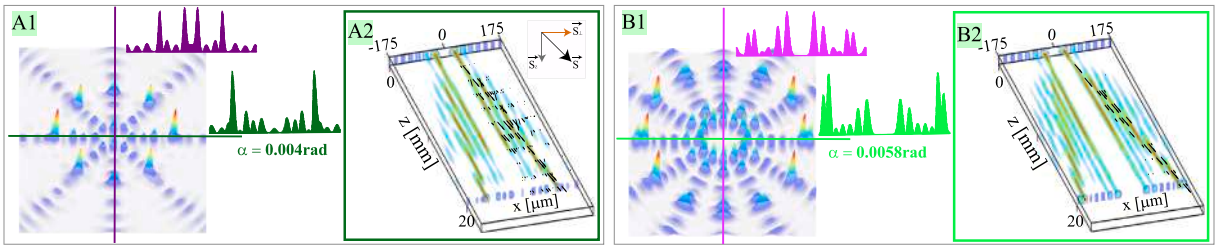

Fig. 4. Tilted solitons observed with various fragmented Bessel beams. Comparison of soliton pairs along y-axis (optical axis) and x-axis: (A) p = 4, (B) p = 6. (A2), (B2) Appropriate pairs of tilted solitons in the x direction, along the propagation distance. The black arrows in (A2) and (B2) indicate the direction of energy flow (i.e., the Poynting vector) along the propagation direction (same for the left-tilted soliton, not shown here). Other parameters: $m = 3$, $a = 45\,\mu m$, $I_0 = 0.5$.

a limited portion of the optical energy couples into the dominant linear modes. In our simulations, when periodicity is externally disrupted, this balance is disturbed, enabling nonlinear light to bend collectively. In the case of fragmented Bessel beams, the overall periodicity of the waveguide distribution remains preserved, while the modulation depth of the refractive index is broken, as a consequence of phase modulation. If the modulation remains sufficiently shallow, the waveguide array may still support a linear mode, but it does not prevent the beam from bending under nonlinear conditions. This nonlinear bending allows the light to be steered into a self-induced nonlinear trap. Moreover, our analysis shows that guiding potentials can spontaneously emerge during the nonlinear formation of tilted solitons.

4. Nonlinear propagation of modulated fragmented Bessel beams

To further control the nonlinear propagation of fragmented Bessel beams, we applied additional modulation to such beams according to the relation

$$A = 2J_m(k_\perp \rho)\cos(p\varphi)e^{i\theta}, \tag{5}$$

where $\theta = \eta cos(M\varphi)$ results in a weak phase modulation controlled by the parameters η and M. Fig. 5 shows the intensity distributions of the nonlinear propagation of two modulated fragmented Bessel beams after $z = 20\,mm$. Each intensity distribution along the spike exhibits different modulation, which becomes evident when compared to the corresponding unmodulated fragmented Bessel beams (Figs. 2(C), (D)). With additional modulation, oscillations are also observed along the propagation distances (movies

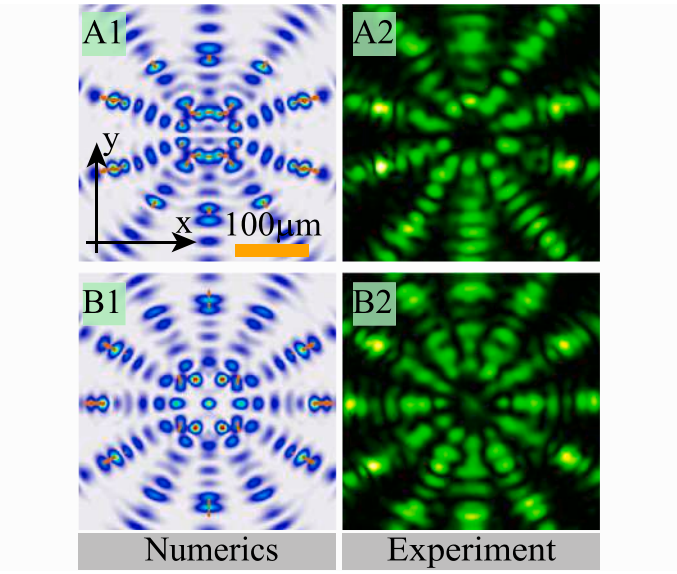

Fig. 5. Self-induced discrete solitons obtained by modulated fragmented Bessel beams. Intensity distributions after $z = 20\,mm$ propagation distance obtained numerically with the corresponding transverse Poynting vectors indicated by orange arrows (the first column), and experimentally (the second column). Parameters are: (A) $p = 5$, $P = (16.86 \pm 0.51)\mu W$, (B) $p = 6$, $P = (16.94 \pm 0.51)\mu W$. Other parameters are as in Fig. 4 and $\eta = 0.23$, $M = 6$.

Fig5A1.avi and Fig5B1.avi in the Supporting Information). The influence of crystal anisotropy produces a similar effect on the beam structure. The central parts of the observed structures have various distributions, depending on whether there is attraction or repulsion of appropriate fragments owing to various phase modulations.

5. Energy flow during the nonlinear propagation of fragmented bessel beams

To quantitatively describe the energy flow in fragmented Bessel beams, we calculate the transverse and longitudinal Poynting vector. For a monochromatic, linearly polarized, and paraxial optical field with envelope $A(\mathbf{r})$, the *transverse* component of the time-averaged Poynting vector is given by [14]:

$$\langle \mathbf{S}_\perp \rangle = \frac{i\varepsilon_0 \omega}{2} \left(A \nabla_\perp A^* - A^* \nabla_\perp A \right), \tag{6}$$

where ε_0 is the vacuum permittivity, $\omega = ck$ is the angular frequency, $k = 2\pi/\lambda$ is the wavenumber. Eq. (6) provides insight into the spatial distribution of transverse energy flow in structured light fields, particularly in fragmented Bessel beams, where phase discontinuities and nonlinear evolution give rise to nontrivial dynamical behavior. The *longitudinal* component of the Poynting vector, which corresponds to the energy flow in the direction of propagation (the z- axis), is often approximated under the paraxial assumption by:

$$S_z \approx \frac{1}{2} \varepsilon_0 c |A|^2, \tag{7}$$

where $|A|^2$ is the local intensity distribution of the field.

At the initial plane ($z = 0\,\mathrm{mm}$), fragmented Bessel beams exhibit real-valued field distributions and, therefore, do not carry orbital angular momentum (OAM), due to the symmetric interference of oppositely charged angular momentum components. In nonlinear media such as photorefractive crystals, transverse energy flow is no longer conserved, and the Poynting vector can develop complex dynamics with non-zero transverse components. As a result, fragmented Bessel beams acquire transverse energy flow, enabling the transfer of OAM while also continuing to transport energy along the propagation direction. The second row of Fig. 2 shows the transverse intensity distributions at $z = 20\,\mathrm{mm}$ with their respective transverse Poynting vectors (orange arrows) (movies Fig2A2.avi, Fig2B2.avi, Fig2C2.avi, and Fig2D2.avi in the Supporting information during the propagation direction). The transverse Poynting vector reveals that the energy is predominantly directed radially in fragmented Bessel beams. The zoomed-in regions in Figs. 2(A2) and (C2) emphasize distinct features. In (A2), neighboring points along specific radial directions exhibit oppositely oriented transverse Poynting vectors, while in (C2), two adjacent fragments show Poynting vectors aligned along different radial directions. Next, we analyze the transverse and longitudinal components of the Poynting vector, which are orthogonal to each other, together with the resultant Poynting vector describing the overall energy flow (presented as an inset in Fig. 4(A2)). Figs. 4(A2) and (B2) show the numerically obtained intensity distribution along the propagation direction, where the black arrows represent the resultant Poynting vectors. For clarity, the visualization is shown only for the right-tilted soliton along the direction normal to the optical axis; the left one exhibits identical behavior. Hence, the resulting Poynting vectors indicate that the light propagates along the direction defined by the tilted solitons.

Figs. 5(A1)–(B1) show the transverse intensity distributions of modulated fragmented Bessel beams at $z = 20\,\mathrm{mm}$ with their respective transverse Poynting vectors (orange arrows) (movies Fig5A1.avi and Fig5B1.avi in the Supporting Information during the propagation direction). Notably, modulated fragmented Bessel beams exhibit distinct energy flow characteristics already at the input plane, in contrast to their unmodulated counterparts. Furthermore, a comparison of the corresponding Poynting vectors for the unmodulated and modulated fragmented Bessel beams reveals notable differences during propagation. These findings underscore the importance of phase and amplitude structuring in controlling both the local and global energy dynamics of nonlinear optical fields, thereby enabling precise light manipulation, with potential applications in integrated optics and optical communication.

6. Conclusion

In summary, we have introduced and experimentally demonstrated a way for generating tilted discrete solitons via the nonlinear self-action of head-on fragmented Bessel beams in the photorefractive SBN61:Ce crystal, without requiring tilted beam incidence or prefabricated lattices. Our findings indicate that appropriate localized symmetry deviation and nonlinearity can induce tilted soliton excitation without a tilted probe beam. By employing tunable azimuthal and phase modulation of Bessel beams, we achieve controlled beam fragmentation and observe the spontaneous formation of multiple pairs of tilted solitons through symmetry breaking above a nonlinearity threshold. The number, direction, and angular tilt of the resulting solitons are highly sensitive to the order, spatial scale, phase, and input power of the Bessel beam and can be precisely tuned by them. This process represents a form of nonlinear self-organization in an aperiodically modulated refractive index landscape, offering new insights into localized wave dynamics in non-integrable systems. The strong agreement between experimental observations and numerical simulations confirms the robustness of the approach and establishes a flexible, reconfigurable platform for controlling structured light in nonlinear media. These findings open up new possibilities for diffraction control, beam shaping, and soliton-based applications in nonlinear optics or a toolbox for engineering structured light in complex nonlinear systems, with potential relevance for optical communications, photonic devices, and information processing technologies.

CRediT authorship contribution statement

Miroslav M. Petroski: Writing – review & editing, Investigation, Data curation. **Dejan V. Timotijević:** Writing – review & editing, Software, Methodology, Conceptualization. **Dragana M. Jović Savić:** Writing – review & editing, Supervision, Funding acquisition, Conceptualization. **Jadranka M. Vasiljević:** Writing – original draft, Visualization, Validation, Investigation, Formal analysis.

Declaration of competing interest

The authors declare no potential conflict of interests.

Acknowledgments

The authors acknowledge funding provided by the Institute of Physics Belgrade and Institute for Multidisciplinary Research (IMSI), through the grants by the Ministry of Science, Technological Development and Innovations of the Republic of Serbia (IMSI contract no. 451-03-66/2024-03/200053) and by the Science Fund of the Republic of Serbia, GRANT No 7714356, IDEAS - CompsLight.

Appendix A. Supplementary data

The supplementary videos, Fig2A2, Fig2B2, Fig2C2, and Fig2D2, show the nonlinear propagation dynamics of a fragmented Bessel beam along the 20 mm long photorefractive SBN61:Ce crystal, corresponding to the conditions presented in Figures 2(A2), 2(B2), 2(C2), and 2(D2), respectively, in the main text, which depicts intensity distribution at the crystal output face at $z = 20$ mm. Each video frame shows the intensity distribution with the corresponding transverse Poynting vectors indicated by orange arrows.

The supplementary videos, Fig5A1 and Fig5B1, show the nonlinear propagation dynamics of the modulated fragmented Bessel beam along the 20 mm long photorefractive SBN61:Ce crystal, corresponding to the conditions presented in Figures 5(A1) and 5(B1), respectively, in the main text, which depicts intensity distribution at the crystal output face at $z = 20$ mm. Each video frame shows the intensity distribution with the corresponding transverse Poynting vectors indicated by orange arrows.

Supplementary material related to this article can be found online at https://doi.org/10.1016/j.chaos.2025.117434.

Data availability

Data will be made available on request.

References

[1] Bouchal Z. Nondiffracting optical beams: Physical properties, experiments, and applications. Czech J Phys 2003;53:537–78. http://dx.doi.org/10.1023/A:1024802801048.
[2] Woerdemann M, Alpmann C, Esseling M, Denz C. Advanced optical trapping by complex beam shaping. Laser Photon. Rev 2013;7:839–54. http://dx.doi.org/10.1002/lpor.201200058.
[3] Garcés-Chávez V, McGloin D, Melville H, Sibbett W, Dholakia K. Simultaneous micromanipulation in multiple planes using a self-reconstructing light beam. Nature 2002;419:145–7. http://dx.doi.org/10.1038/nature01007.
[4] Baumgartl J, Mazilu M, Dholakia K. Optically mediated particle clearing using airy wavepackets. Nat Photonics 2008;2:675–8. http://dx.doi.org/10.1038/nphoton.2008.201.
[5] Bloch I. Ultracold quantum gases in optical lattices. Nat Phys 2005;1:23–30. http://dx.doi.org/10.1038/nphys138.
[6] Fleischer JW, Segev M, Efremidis NK, Christodoulides DN. Observation of two-dimensional discrete solitons in optically induced nonlinear photonic lattices. Nature 2003;422:147–50. http://dx.doi.org/10.1038/nature01452.
[7] Martin H, Eugenieva ED, Chen Z, Christodoulides DN. Discrete solitons and soliton-induced dislocations in partially coherent photonic lattices. Phys Rev Lett 2004;92:123902. http://dx.doi.org/10.1103/PhysRevLett.92.123902.
[8] Lederer F, Stegeman GI, Christodoulides D, Assanto G, Segev M, Silberberg Y. Discrete solitons in optics. Phys Rep 2008;463:1–126. http://dx.doi.org/10.1016/j.physrep.2008.04.004.
[9] Durnin J, Miceli JJ, Eberly JH. Diffraction-free beams. Phys Rev Lett 1987;58:1499–501. http://dx.doi.org/10.1103/PhysRevLett.58.1499.
[10] Gutiérrez-Vega JC, Iturbe-Castillo MD, Chávez-Cerda S. Alternative formulation for invariant optical fields: Mathieu beams. Opt Lett 2000;25:1493–5. http://dx.doi.org/10.1364/OL.25.001493.
[11] Bandres MA, Gutiérrez-Vega JC, Chávez-Cerda S. Parabolic nondiffracting optical wave fields. Opt Lett 2004;29:44–6. http://dx.doi.org/10.1364/OL.29.000044.
[12] Freedman B, Bartal G, Segev M, Lifshitz R, Christodoulides DN, Fleisher J. Wave and defect dynamics in nonlinear photonic quasicrystals. Nature 2006;440:1166–9. http://dx.doi.org/10.1038/nature04722.
[13] Zannotti A, Vasiljević JM, Timotijević DV, Jović Savić DM, Denz C. Morphing discrete diffraction in nonlinear mathieu lattices. Opt Lett 2019;44(7):1592–5. http://dx.doi.org/10.1364/OL.44.001592.
[14] Zannotti A, Vasiljević JV, Zannotti A, Timotijević DV, Jović Savić DM, Denz C. Visualizing the energy flow of tailored light. Adv Opt Mater 2018;6(8):1701355. http://dx.doi.org/10.1002/adom.201701355.
[15] Mitić DV, Vasiljević JM, Timotijević DV, Jović Savić DM. Self-induced parabolic surface states. Opt Mater 2025;167:117249. http://dx.doi.org/10.1016/j.optmat.2025.117249.
[16] Vasiljević JV, Zannotti A, Timotijević DV, Denz C, Jović Savić DM. Creating aperiodic photonic structures by synthesized mathieu-Gauss beams. Phys Rev A 2017;96:023840. http://dx.doi.org/10.1103/PhysRevA.96.023840.

[17] Vasiljević JV, Zannotti A, Timotijević DV, Denz C, Jović Savić DM. Elliptical vortex necklaces in mathieu lattices. Phys Rev A 2018;97:033848. http://dx.doi.org/10.1103/PhysRevA.97.033848.
[18] Tomović AŽ, Vlaović Mitić IJ, Jovanović VP, Timotijević DV, Jović Savić DM. Assembling of truncated deterministic aperiodic lattices with defects using Weber beams. Opt Mater 2024;157:116334. http://dx.doi.org/10.1016/j.optmat.2024.116334.
[19] Garcés-Chávez V, Volke-Sepulveda K, Chávez-Cerda S, Sibbett W, Dholakia K. Transfer of orbital angular momentum to an optically trapped low-index particle. Phys Rev A 2002;66:063402. http://dx.doi.org/10.1103/PhysRevA.66.063402.
[20] Planchon TA, Gao L, Milkie DE, Davidson MW, Galbraith JA, Galbraith CG, Betzig E. Rapid three-dimensional isotropic imaging of living cells using bessel beam plane illumination. Nature Methods 2011;8:417–26. http://dx.doi.org/10.1038/nmeth.1586.
[21] Duocastella M, Arnold C. Bessel and annular beams for materials processing. Laser Photonics Rev 2012;6(5):607–21. http://dx.doi.org/10.1002/lpor.201100031.
[22] Schulze C, Roux FS, Dudley A, Rop R, Duparré M, Forbes A. Accelerated rotation with orbital angular momentum modes. Phys Rev A 2015;91:043821. http://dx.doi.org/10.1103/PhysRevA.91.043821.
[23] Belloni VV, Bollani M, Eaton SM, Di Trapani P, Jedrkiewicz O. Micro-hole generation by high-energy pulsed bessel beams in different transparent materials. Micromachines 2021;12:455. http://dx.doi.org/10.3390/mi12040455.
[24] Song Z, Nakajima T. Formation of filament and plasma channel by the bessel incident beam in ar gas: role of the outer part of the beam. Opt Express 2010;18(12):12923–38. http://dx.doi.org/10.1364/OE.18.012923.
[25] Yu Z, Li H, Zhong T, Park J-H, Cheng S, Woo CM, Zhao Q, Yao J, Zhou Y, Huang X, Pang W, Yoon H, Shen Y, Liu H, Zheng Y, Park Y, Wang LV, Lai P. Wavefront shaping: A versatile tool to conquer multiple scattering in multidisciplinary fields. Innov 2022;3(5):100292. http://dx.doi.org/10.1016/j.xinn.2022.100292.
[26] Quan Q, Lian S, Liu Z, Chen H, Yan B, Deng D. Observation of off-axis solitary waves propagating along a specific trajectory in photorefractive crystals. Opt Lett 2024;49(16):4585–8. http://dx.doi.org/10.1364/OL.532244.
[27] Chen H, Liu Z, Lian S, Quan Q, Malomed BA, Li S, Zhang Y, Li H, Deng D. Tunable beam splitting via photorefractive nonlinearity and its applications in chiral waveguide induction and vortex generation. Chaos Solitons Fractals 2024;183:114936. http://dx.doi.org/10.1016/j.chaos.2024.114936.
[28] Eisenberg HS, Silberberg Y, Morandotti R, Aitchison JS. Diffraction management. Phys Rev Lett 2000;85:1863–6. http://dx.doi.org/10.1103/PhysRevLett.85.1863.
[29] Pertsch T, Zentgraf T, Peschel U, Bräuer A, Lederer F. Anomalous refraction and diffraction in discrete optical systems. Phys Rev Lett 2002;88:093901. http://dx.doi.org/10.1103/PhysRevLett.88.093901.
[30] Christodoulides DN, Lederer F, Silberberg Y. Discretizing light behaviour in linear and nonlinear waveguide lattices. Nature 2003;424:817–23. http://dx.doi.org/10.1038/nature01936.
[31] Rosberg CR, Neshev DN, Sukhorukov AA, Kivshar YS, Krolikowski W. Tunable positive and negative refraction in optically induced photonic lattices. Opt Lett 2005;30(17):2293–5. http://dx.doi.org/10.1364/OL.30.002293.
[32] Neshev D, Sukhorukov AA, Hanna B, Krolikowski W, Kivshar YS. Controlled generation and steering of spatial gap solitons. Phys Rev Lett 2004;93:083905. http://dx.doi.org/10.1103/PhysRevLett.93.083905.
[33] Agrawal G. Nonlinear fiber optics. 5th ed. Academic Press; 2012, http://dx.doi.org/10.1016/C2011-0-00045-5.
[34] Kukhtarev NV, Markov VB, Odulov SG, Soskin MS, Vinetskii VL. Holographic storage in electrooptic crystals. i. steady state. Ferroelectrics 1978;22(1):949–60. http://dx.doi.org/10.1080/00150197908239450.
[35] Zozulya AA, Anderson DZ. Propagation of an optical beam in a photorefractive medium in the presence of a photogalvanic nonlinearity or an externally applied electric field. Phys Rev A 1995;51:1520–31. http://dx.doi.org/10.1103/PhysRevA.51.1520.
[36] Davis JA, Cottrell DM, Campos J, Yzuel MJ, Moreno I. Encoding amplitude information onto phase-only filters. Appl Opt 1999;38:5004–13. http://dx.doi.org/10.1364/AO.38.005004.

Optical Materials 167 (2025) 117249

Contents lists available at ScienceDirect

Optical Materials

journal homepage: www.elsevier.com/locate/optmat

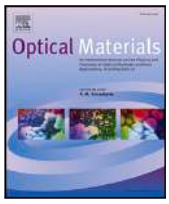

Research article

Self-induced parabolic surface states

Damir V. Mitić [a,*], Jadranka M. Vasiljević [a], Dejan V. Timotijević [b], Dragana M. Jović Savić [a]

[a] Institute of Physics Belgrade, University of Belgrade, Pregrevica 118, 11080, Belgrade, Serbia
[b] Institute for Multidisciplinary Research, University of Belgrade, Kneza Višeslava 1, 11030, Belgrade, Serbia

ARTICLE INFO

MSC:
78-05
78A60

Keywords:
Surface states
Non-diffracting beam

ABSTRACT

We observed parabolic surface states during the nonlinear propagation of a Weber beams in an SBN crystal. The refractive index is modulated anisotropically using the optical induction technique. These states appear without the need for a pre-inscribed lattice in the material. Their characteristics can be tuned by adjusting the Weber beam's scale, parabolicity, orientation, and power. We also observed oscillatory discrete surface states during the linear propagation of a probe Gaussian beam within the aperiodic Weber photonic lattice. In both cases, such specific parabolic states are observed as surface states extending across multiple adjacent parabolas, or edge parabolic states localized along the border parabola. Our approach presents the first demonstration of self-induced parabolic surface states in aperiodic systems.

1. Introduction

Non-diffracting beams, exhibiting unique spatial structures and self-healing properties [1–4], have considerable interest in applications such as imaging, optical trapping, nonlinear and quantum optics [5–12]. Among them, Weber beams [13] form a class of non-diffracting optical waves with aperiodic transverse profiles in parabolic cylindrical coordinates. These beams can be generated using spatial light modulators that imprint the necessary phase structure onto an input wavefront [14]. Within their stability range, they offer significant promise for generating novel types of optical lattice [15,16], but their potential in nonlinear photonics remains still unexplored [17].

Electromagnetic waves located near the interface between two different media, known as surface modes, have attracted considerable attention due to their unique physical properties and potential applications in all-optical switching and sensing [10,18,19]. In optics, surface waves can arise at the interface between a continuous and a periodic medium and between different waveguide arrays [10]. Truncating photonic lattices leads to the formation of localized surface states, as demonstrated in 1D waveguide arrays [20] and 2D photonic lattices [21]. Surface state effects offer an additional mechanism for light confinement and expands the possibilities for controlling light with photonic lattices. The generation of lattice edges with various shapes remains an underexplored area with significant potential in nonlinear photonics [16].

In this paper, we extend the concept of surface state generation by investigating the nonlinear propagation of non-diffracting Weber beams in photorefractive media. Specifically, we observe the formation of *parabolic* surface states induced by refractive index modulation during the nonlinear propagation of Weber beams in photorefractive media. Unlike the surface states observed in truncated photonic lattices [18–21], our approach enables the observation of surface states *with no* permanent lattice structure inscribed in the material in advance. These states are generated through single-pass experiments and are supported by numerical simulations that closely match the experimental results. Such specific states are observed in the form of surface states that extend across multiple adjacent parabolas or edge parabolic states localized along the border parabola. We demonstrate precise control over the properties of the parabolic surface states by tuning the initial parameters of the Weber beam such as its scale, parabolicity, and orientation, as well as the degree of nonlinearity, governed by the beam power. Specifically, we can control the shape and parabolically of such surface states. Furthermore, we investigate the linear propagation of a narrow Gaussian probe beam in a Weber aperiodic lattice inscribed in photorefractive crystal (SBN61:Ce) to study surface effects. Under specific parameter regimes, we observe oscillatory surface states near the lattice boundary, characterized by cyclic energy exchange between adjacent lattice sites. They are observed as surface states extending across multiple adjacent parabolas, or edge parabolic states along the border parabola. These approaches enhance the predictability and control of the parabolic surface states, enabling new ways to manage diffraction, localization, topological states, and exploring novel nonlinear optical effects. These findings not only contribute to theoretical advances in

* Corresponding author.
E-mail address: damir@ipb.ac.rs (D.V. Mitić).

https://doi.org/10.1016/j.optmat.2025.117249
Received 27 May 2025; Received in revised form 10 June 2025; Accepted 16 June 2025
Available online 28 June 2025

optics and photonics but also pave the way for a range of practical applications such as optical information processing, communications, and biophotonics.

2. Numerical model for investigation of parabolic surface states

To investigate Weber beam propagation in strontium barium niobate (SBN61:Ce) crystal we use the nonlinear Schrödinger equation

$$i\partial_z A(r) + \frac{1}{2k_z}\left[\Delta_\perp + G(I)\right] A(r) = 0, \tag{1}$$

and spectral split step propagation method [22–24]. It relates to the paraxial propagation of the scalar light field A(r) with longitudinal wave vector k_z in a nonlinear potential $G(I) = -k_z^2 n_e^2 r_{33} E(I)$ defined by photorefractive nonlinearity, where $n_e = 2.35$ is the extraordinary bulk refractive index, $r_{33} = 267\,\mathrm{pm/V}$ is the corresponding electro-optical coefficients of the SBN61:Ce crystal and the wave number $k = 2\pi/\lambda = \sqrt{(k_\perp^2 + k_z^2)}$ is defined by the laser wavelength $\lambda = 532\,\mathrm{nm}$. The total electric field $E(I) = E_{\mathrm{ext}} + E_{\mathrm{sc}}(I)$ that builds up inside the crystal is a superposition of an external electric field $E_{\mathrm{ext}} = 2000\,\mathrm{V/cm}$ applied aligned with the optical $c = y$ axis (perpendicular to the propagation direction z-axis) to induce the photorefractive effect in the crystal and an internal electric space charge field E_{sc} that results from the incident intensity distribution $I = |A(r)|^2$ within the potential equation. We calculate the resulting intensity-depended, nonlocal, saturable, and anisotropic refractive index modulation [25] via $E_{sc} = \partial_x \phi_{sc}$ by numerically solving the anisotropic potential equation for the spatial evolution of the electrostatic potential ϕ_{sc} of the optically-induced space-charge field E_{sc}

$$\Delta_\perp \phi_{\mathrm{sc}} + \nabla_\perp \ln(1+I)\cdot\nabla_\perp \phi_{\mathrm{sc}} = E_{\mathrm{ext}}\partial_x \ln(1+I), \tag{2}$$

as shown in previous works of us [23,24] where I is obtained from Eq. (1). Subsequently, Eq. (1) is updated with the optically induced space-charge field $E_{sc} = \partial_x \phi_{sc}$, obtained by solving Eq. (2). This procedure is iteratively repeated along the propagation direction z.

Anisotropic model, consisting of Eqs. (1) and (2), is appropriate for investigation of Weber beam propagation in the SBN61:Ce crystal because this crystal is inherently anisotropic. While saturation reduces effective nonlinearity at high intensities, limiting the maximum achievable index change and affecting the confinement and existence of surface states, nonlocality introduces spatial averaging, which enhances stability, but may broaden or shift surface-bound modes, reducing their localization. Together, saturation and nonlocality critically determine the shape, stability, and threshold conditions of surface states and guided modes in SBN61:Ce.

As the paraxial scalar light field A (structure beam in the experiment), we use even Weber beams [13]

$$A = U_e(\eta,\xi;a) = \frac{1}{\pi\sqrt{2}}|\Gamma_1|^2 P_e(\sigma\xi;a)P_e(\sigma\eta;-a), \tag{3}$$

where P_e is even parabolic cylinder function, Γ is Gamma functions, $\Gamma_1 = \Gamma[(1/4) + (1/2)ia]$, $\sigma = (4\pi/\lambda)^{1/2}$, ($\xi$, η) are parabolic cylinder coordinates, and the parameter a determines the curvature of the Weber beam lobes and acts as an indicator of parabolicity. The relationship between parabolic cylinder coordinates (ξ, η) and spatial Cartesian coordinates (x, y) is defined by coordinate transformations $\xi = \sqrt{x + \sqrt{x^2+y^2}}$ and $\eta = \sqrt{\sqrt{x^2+y^2} - x}$. Odd beams yield similar results.

3. Experimental method for parabolic surface states generation

The experimental optical induction technique is used that allows refractive index changes of the photorefractive material, a birefringent cerium-doped strontium barium niobate crystal (SBN61:Ce). The experimental setup is shown in Fig. 1. As a light source, we use a continuous frequency-doubled Nd:YVO_4 laser with a wavelength of $\lambda = 532\,\mathrm{nm}$. The linearly polarized laser beam is spatially modulated using a phase-only full HD HOLOEYE PLUTO-2.1 LCoS SLM, with resolution 1920 × 1080, featuring a pixel pitch of 8 μm, to generate the desired beam structure, inducing a corresponding refractive index modulation in the biased photosensitive crystals. Although inherently phase-only, the SLM enables simultaneous modulation of both the amplitude and phase of the reflected light field by displaying a precomputed hologram of a Weber beam superimposed with an additional blaze grating and Fourier filtering in the Fourier plane of lens L3 [14]. Then, a spatially modulated initiation laser beam from SLM passes through several optical elements, including lenses, a beamsplitter, and a pinhole, before it illuminates the crystal. The SBN61:Ce crystal, with dimensions of $5\times5\times20\,\mathrm{mm}^3$, is biased to an external electric field (E_{ext}), applied along the optical $c = y$ axis. This electric field is perpendicular to the wave propagation direction (the z-axis). As a result, the extraordinarily polarized structure light field with power (P_w) propagates through the crystal. Changing beam power P_w affects different nonlinearity strengths. The SBN61:Ce crystal provides strong nonlinearity at comparatively low power levels. We used powers that are reproducible for our results. Such powers are below the threshold for optical damage. This crystal is doped with cerium (Ce), a dopant known to improve resistance to optical damage. We used an imaging system with a 10x microscope objective (MO) and camera to observe the transverse intensity distribution on the exit face of the crystal.

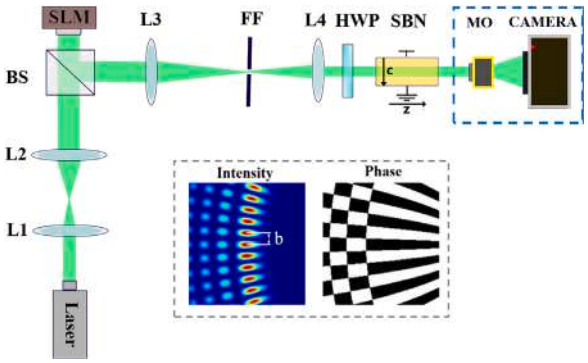

Fig. 1. Experimental setup for investigating the nonlinear propagation of Weber beams. L — lens, BS — depolarized beam splitter, SLM — spatial light modulator, FF — Fourier filter, SBN — medium, HWP — half-wave plate, MO — 10x microscope objective. Inset presents one example of Weber beam intensity and phase distributions, with typical beam scale indicated with b.

Typical examples of parabolic surface states induced by nonlinear self-action are shown in Fig. 2. Parabolic surface states can be localized on few adjacent parabolas (Fig. 2(a)). Another representative example is the edge surface state, localized along the edge parabola (Fig. 2(b)). The characteristics of these states can be effectively controlled by adjusting the Weber beam's parabolicity, scale, and intensity (power).

4. Self-induced parabolic surface states obtained during the nonlinear propagation of Weber beams

We begin our investigation with Weber beams with varying parabolicities, scales, and orientations to study how their propagation behavior changes with increasing beam power. At low beam powers, the beams propagate stable along the length of the crystal, maintaining their symmetry and non-diffracting nature. As the power increases, stability is broken, and the beams lose their non-diffracting characteristics. At these lower powers, parabolic surface states extending across multiple adjacent parabolas are observed. With further increases in power, surface states become localized along the border parabola, so we call them parabolic edge states. At the highest beam powers, we observe the migration of parabolic surface states along an adjacent parabola,

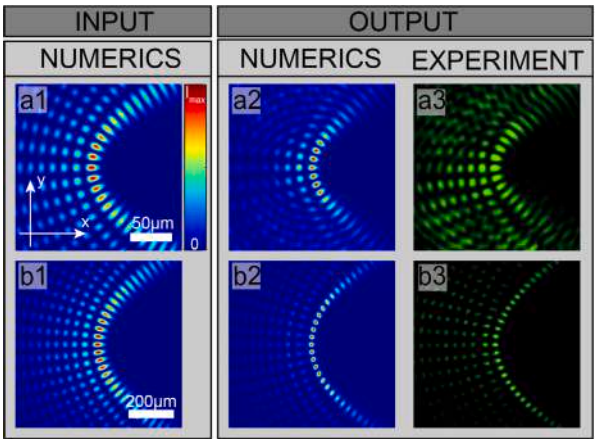

Fig. 2. Representative examples of self-induced parabolic surface states. First column: Intensity distributions of Weber beams at the input. The second and third columns: Intensity distributions at the exit face of the crystal obtained numerically (the second column) and experimentally (the third column), after 20 mm propagation distance. Parameters are: (a) $a = 6$, $b = 12$ μm, $I = 0.7$, $P_w = (34 \pm 1.02)$ μW and (b) $a = 10$, $b = 35$ μm, $I = 0.08$, $P_w = (3.4 \pm 0.102)$ μW.

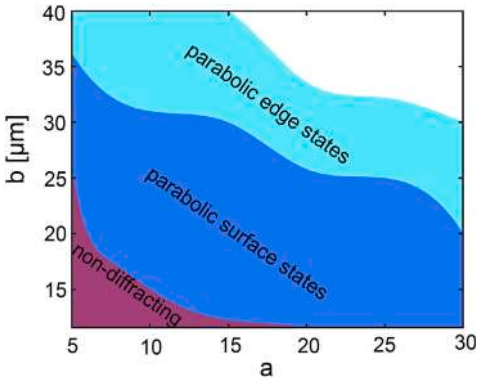

Fig. 3. (a) Parameter space diagram with different regimes of the Weber beam propagation in nonlinear regime. b is Weber beam scale, and a is parabolicity of Weber beam. Input beam intensity $I = 0.16$ [*a.u.*].

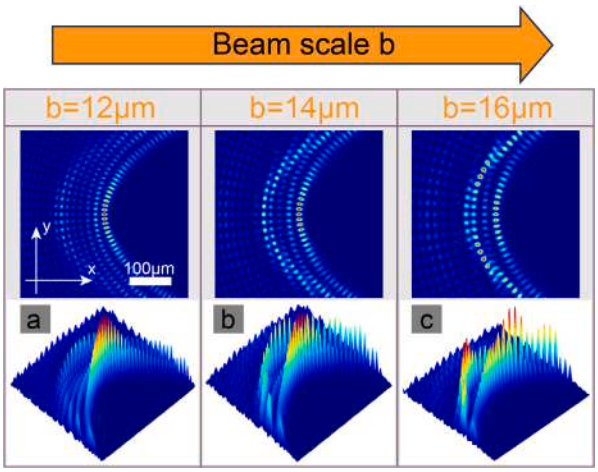

Fig. 4. Influence of Weber beam scale on the formation of the parabolic surface states. Transverse intensity distributions of Weber beam after 20 mm propagation. Parameters: Weber beam parabolicity $a = 15$, and input intensity $I = 0.3$.

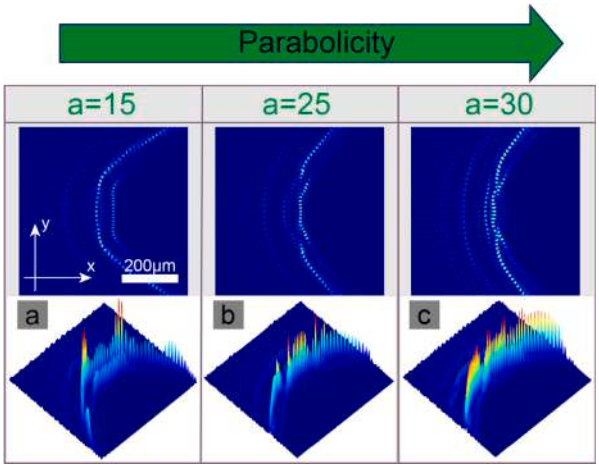

Fig. 5. Influence of Weber beam parabolicities on the formation of the parabolic surface states. Transverse intensity distributions of Weber beam after 20 mm propagation. Parameters: Weber beam structure size $b = 15$ μm, and input intensity $I = 0.8$.

indicating a dynamic transitions and modulation instabilities. Quantitative thresholds for transition between two regions depend on the Weber beam parameters such as beam scale, parabolicity, and orientation. Threshold values for intensity/power corresponding to transitions between regions can be defined only for one fixed set of these three parameters.

Fig. 3 provides a detailed phase diagram of the Weber beam scale b and parabolicity a, for the Weber beam intensity $I = 0.16$. At lower values of either or both parameters, the Weber beams remain stable during propagation, preserving their non-diffracting character. As these parameters are increased, there is a region of parabolic surface states across a few adjacent parabolas, but further increasing both parameters leads to the formation of parabolic edge states. At the highest values of the control parameters, modulation instabilities can be observed (white region in parameter space). By adjusting the beam's parameters, the shape and parabolicity of the surface state can be precisely controlled and fine-tuned.

Fig. 4 illustrates the effect of the Weber beam scale parameter b on the formation of parabolic surface states. At lower values of b, the beam structure remains almost stable, with only minimal energy transfer to neighboring parabolas. As b increases, a variety of two-dimensional surface states emerge. These results demonstrate that tuning the scale parameter b allows precise control over the shape and curvature of the surface states, enabling fine adjustments to their spatial structure.

The influence of Weber beam parabolicity a on the formation of parabolic surface states at high beam intensities I, corresponding to increased power in the experiment, is presented in Fig. 5. Under these conditions, various surface state configurations emerge, predominantly localized near the border and adjacent parabola. By varying the parabolicity of the beam, it becomes possible to independently control the curvature, shape, and spatial extent of self-induced surface states, offering a high degree of surface states tunability.

5. Oscillatory surface states obtained during linear propagation of Gaussian probe beam in Weber lattice

At the end, we investigate the effects during the *linear* propagation of a narrow Gaussian probe beam near the edge of various aperiodic Weber photonic lattices. Weber photonic lattices are naturally truncated, therefore build-up processes such as multiplexing or some kind of occlusion is avoided for their generation. First, we find parameters for the generation of photonic lattices using Weber beams of various parabolicity, scale, and orientation. The process of photonic lattice generation is modeled through the potential $I = I_{latt}$ in Eq. (1). We

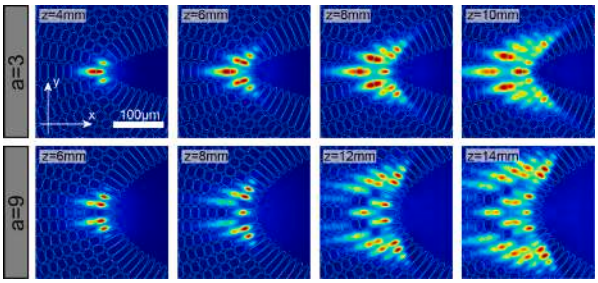

Fig. 6. Discrete surface states. Transverse intensity distributions of probe Gaussian beam in aperiodic Weber lattice with parabolicity: $a = 3$ (the first row), $a = 9$ (the second row), at various propagation distances, marked at individual figures. Contours indicate Weber lattice position. Parameters: $b = 12$ μm, and lattice intensity $I_{latt} = 0.5$.

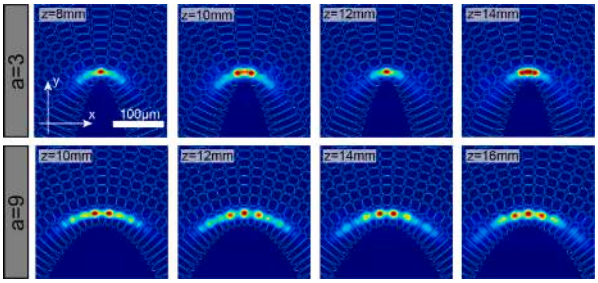

Fig. 7. Discrete edge states. Transverse intensity distributions of probe Gaussian beam in aperiodic Weber lattice with parabolicity: $a = 3$ (the first row) and $a = 9$ (the second row), at various propagation distances, marked at individual figures. Contours indicate Weber lattice position. Parameters: $b = 12$ μm, and lattice intensity $I_{latt} = 0.5$.

obtain the spatial distribution of I_{latt} through a separate numerical simulation of Eqs. (1) and (2) based on propagation of an ordinary Weber beam under weak nonlinearity, finding the fixed value of I_{latt} for the formation of the uniform lattice along the propagation distance. Then, we use such an obtained distribution as the lattice potential for the simulation of extraordinary Gaussian probe beam propagation using equations modified such that $I = I_p + I_{latt}$, where the Gaussian probe beam intensity $I_p = |A|^2$ is obtained from Eq. (1). Gaussian probe beam width is sufficient to cover one lattice site. In our probing simulations I_p is sufficiently weak so as not to cause nonlinear modification [12].

We study how the variation in the parabolicity of the Weber lattice a influences the discrete diffraction of light and the formation of surface states. Furthermore, we consider two different orientations of the Weber lattice, as presented in Figs. 6 and 7. We perform our investigation by probing Weber lattices with various parabolicities $a = 3$ and $a = 9$. The input position of the probe beam is at the central lattice site along the edge (outer) parabola. In all figures, the white contours overlaid on the intensity distributions indicate the positions of the waveguides.

For the lattice orientation shown in Fig. 6, we observe oscillatory discrete surface states. With increasing propagation distance, the probe beam gradually spreads from the edge towards the inner lattice sites. In contrast, the lattice orientation presented in Fig. 7 supports edge surface states that remain confined to the lattice edge. This difference is attributed to the anisotropic properties of the photorefractive crystal. In both lattice orientations, oscillatory surface effects are evident, characterized by an alternating excitation of the central site and its two nearest neighbors.

Surface states observed with linear probe beam propagation in the Weber lattice could provide predictions and appropriate parameters for nonlinear self-induced surface states. The anisotropy of the SBN crystal is an additional control factor, allowing various surface states to be obtained along a different orientation. For both linear and nonlinear surface states, we have fine-tuning for various surface states covering a few parabolas or only the one (border) parabola.

6. Conclusion

We have developed a method for generation of parabolic surface states in photorefractive media using a single-pass experimental setup and optical induction. Our results demonstrate that nonlinear Weber beams can induce parabolic surface states without the need for prefabricated lattices or lattice truncation. We systematically investigated how these surface states depend on the strength of the nonlinearity, as well as on the scale, parabolicity, and orientation of the Weber beam. This approach enables precise control over the shape and curvature of the parabolic surface states, offering new opportunities to design beam structures with complex topologies and manage novel surface phenomena. Also, we have shown parabolic discrete oscillatory surface states during the linear propagation of Gaussian probe beam in aperiodic Weber photonic lattice. These findings not only advance the theoretical understanding of light–matter interactions in nonlinear photonics but also open new possibilities for applications in optical information processing, communication technologies, and biophotonics.

CRediT authorship contribution statement

Damir V. Mitić: Visualization, Methodology, Investigation. **Jadranka M. Vasiljević:** Investigation, Data curation. **Dejan V. Timotijević:** Writing – review & editing, Software, Conceptualization. **Dragana M. Jović Savić:** Writing – original draft, Supervision.

Declaration of competing interest

The authors declare the following financial interests/personal relationships which may be considered as potential competing interests: Dragana Jović Savić, Dejan Timotijević and Jadranka Vasiljević reports financial support was provided by Fund of the Republic of Serbia, GRANT No 7714356, IDEAS - CompsLight. If there are other authors, they declare that they have no known competing financial interests or personal relationships that could have appeared to influence the work reported in this paper.

Acknowledgments

The authors acknowledge funding provided by the Institute of Physics Belgrade and Institute for Multidisciplinary Research (IMSI), through the grants by the Ministry of Science, Technological Development and Innovations of the Republic of Serbia (IMSI contract no. 451-03-66/2024-03/200053) and by the Science Fund of the Republic of Serbia, GRANT No 7714356, IDEAS - CompsLight.

Data availability

Data will be made available on request.

References

[1] J. Durnin, Exact solutions for nondiffracting beams. I. The scalar theory, J. Opt. Soc. Amer. A 4 (1987) 651–654.
[2] J. Durnin, J.J. Miceli, J.H. Eberly, Diffraction-free beams, Phys. Rev. Lett. 58 (1987) 1499–1501.
[3] E.G. Kalnins, J. W. Miller, Lie theory and separation of variables. 9. Orthogonal R-separable coordinate systems for the wave equation $\Psi_{tt} - \Delta_2 \Psi = 0$, J. Math. Phys. 17 (1976) 331–355.
[4] J.C. Gutiérrez-Vega, M.D. Iturbe-Castillo, S. Chávez-Cerda, Alternative formulation for invariant optical fields: Mathieu beams, Opt. Lett. 25 (2000) 1493–1495.
[5] M. Woerdemann, C. Alpmann, M. Esseling, C. Denz, Advanced optical trapping by complex beam shaping, Laser Photon. Rev. 7 (2013) 839–854.

[6] V. Garcés-Chávez, D. McGloin, H. Melville, W. Sibbett, K. Dholakia, Simultaneous micromanipulation in multiple planes using a self-reconstructing light beam, Nature 419 (2022) 145–147.
[7] J. Baumgartl, M. Mazilu, K. Dholakia, Optically mediated particle clearing using airy wavepackets, Nat. Photonics 2 (2008) 675–678.
[8] J.W. Fleischer, M. Segev, N.K. Efremidis, D.N. Christodoulides, Observation of two-dimensional discrete solitons in optically induced nonlinear photonic lattices, Nature 422 (2003) 147–150.
[9] H. Martin, E.D. Eugenieva, Z. Chen, D.N. Christodoulides, Discrete solitons and soliton-induced dislocations in partially coherent photonic lattices, Phys. Rev. Lett. 92 (2004) 123902.
[10] F. Lederer, G.I. Stegeman, D. Christodoulides, G. Assanto, M. Segev, Y. Silberberg, Discrete solitons in optics, Phys. Rep. 463 (2008) 1–126.
[11] J.M. Vasiljević, A. Zannotti, D.V. Timotijević, C. Denz, D.M.J. Savić, Light transport and localization in disordered aperiodic Mathieu lattices, Opt. Lett. 47 (3) (2022) 702–705.
[12] J.M. Vasiljević, V.P. Jovanović, A.Ž. Tomović, D.V. Timotijević, R. Žikic, M.R. Belić, D.M.J. Savić, Interdimensional radial discrete diffraction in mathieu photonic lattices, Opt. Express 31 (18) (2023) 28946–28953.
[13] M.A. Bandres, J.C. Gutiérrez-Vega, S. Chávez-Cerda, Parabolic nondiffracting optical wave fields, Opt. Lett. 29 (2004) 44–46.
[14] J.A. Davis, D.M. Cottrell, J. Campos, M.J. Yzuel, I. Moreno, Encoding amplitude information onto phase-only filters, Appl. Opt. 38 (1999) 5004–5013.
[15] P. Rose, M. Boguslawski, C. Denz, Nonlinear lattice structures based on families of complex nondiffracting beams, New J. Phys. 14 (2012) 033018.
[16] A.Ž. Tomović, I.J.V. Mitić, V.P. Jovanović, D.V. Timotijević, D.M.J. Savić, Assembling of truncated deterministic aperiodic lattices with defects using Weber beams, Opt. Mater. 157 (2024) 116334.
[17] B. Freedman, G. Bartal, M. Segev, R. Lifshitz, D.N. Christodoulides, J. Fleisher, Wave and defect dynamics in nonlinear photonic quasicrystals, Nature 440 (2006) 1166–1169.
[18] S. Suntsov, K.G. Makris, G.A. Siviloglou, R. Iwanovw, R. Schiek, D.N. Christodoulides, G.I. Stegeman, R. Morandotti, H. Yang, G. Salamo, M. Volatier, V. Aimez, R. Arès, M. Sorel, Y. Min, W. Sohler, X. Wang, A. Bezryadina, Z. Chen, Observation of one and two-dimensional discrete surface spatial solitons, J. Nonlinear Opt. Phys. Mater. 16 (04) (2007) 401–426.
[19] Y.S. Kivshar, Nonlinear tamm states and surface effects in periodic photonic structures, Laser Phys. Lett. 5 (10) (2008) 703.
[20] C.R. Rosberg, D.N. Neshev, W. Krolikowski, A. Mitchell, R.A. Vicencio, M.I. Molina, Y.S. Kivshar, Observation of surface gap solitons in semi-infinite waveguide arrays, Phys. Rev. Lett. 97 (2006) 083901.
[21] X. Wang, A. Bezryadina, Z. Chen, K.G. Makris, D.N. Christodoulides, G.I. Stegeman, Observation of two-dimensional surface solitons, Phys. Rev. Lett. 98 (2007) 123903.
[22] G. Agrawal, Nonlinear Fiber Optics, fifth ed., Academic Press, 2012.
[23] A. Zannotti, J.M. Vasiljević, D.V. Timotijević, D.M.J. Savić, C. Denz, Morphing discrete diffraction in nonlinear mathieu lattices, Opt. Lett. 44 (7) (2019) 1592–1595.
[24] A. Zannotti, J.M. Vasiljević, D.V. Timotijević, D.M. Jović Savić, C. Denz, Visualizing the energy flow of tailored light, Adv. Opt. Mater. 6 (8) (2018) 1701355.
[25] A.A. Zozulya, D.Z. Anderson, Propagation of an optical beam in a photorefractive medium in the presence of a photogalvanic nonlinearity or an externally applied electric field, Phys. Rev. A 51 (1995) 1520–1531.

Research Article | Vol. 31, No. 18 / 28 Aug 2023 / Optics Express 28946
Optics EXPRESS

Interdimensional radial discrete diffraction in Mathieu photonic lattices

JADRANKA M. VASILJEVIĆ,[1,*] VLADIMIR P. JOVANOVIĆ,[2] ALEKSANDAR Ž. TOMOVIĆ,[2] DEJAN V. TIMOTIJEVIĆ,[2] RADOMIR ŽIKIC,[2] MILIVOJ R. BELIĆ,[3] AND DRAGANA M. JOVIĆ SAVIĆ[1]

[1] *Institute of Physics, University of Belgrade, P.O. Box 68, 11001 Belgrade, Serbia*
[2] *Institute for Multidisciplinary Research, University of Belgrade, Kneza Višeslava 1, 11030, Belgrade, Serbia*
[3] *Division of Arts and Sciences, Texas A & M University at Qatar, 23874, Doha, Qatar*
[*] *jadranka@ipb.ac.rs*

Abstract: We demonstrate transitional dimensionality of discrete diffraction in radial-elliptical photonic lattices. Varying the order, characteristic structure size, and ellipticity of the Mathieu beams used for the photonic lattices generation, we control the shape of discrete diffraction distribution over the combination of the radial direction with the circular, elliptic, or hyperbolic. We also investigate the transition from one-dimensional to two-dimensional discrete diffraction by varying the input probe beam position. The most pronounced discrete diffraction is observed along the crystal anisotropy direction.

1. Introduction

The ability to tailor and manipulate light in photonic lattices is an important topic of scientific investigations and practical applications in optics [1]. Photonic lattices or arrays of evanescently coupled waveguides are typical examples of structures where discrete effects and dynamics can be investigated. Light focused into one waveguide that linearly propagates along the waveguide array will tunnel to neighboring sites, exhibiting a characteristic diffraction pattern with the intensity mainly focused in the outer lobes. This phenomenon, called the discrete diffraction of light [2] was theoretically and experimentally observed in one-dimensional (1D) waveguide arrays [3] and two-dimensional (2D) photonic lattices [4]. It is also investigated in aperiodic photonic lattices [5–8] as well as in other systems, such as atomic photonic lattices [9–11].

The truncation of periodic photonic lattice causes an additional distortion in the periodicity and results in the formation of optical surface states that are analogous to the surface states in the electronic theory of periodic systems [12,13]. Optical self-trapped discrete surface waves - surface solitons - have been demonstrated in 1D waveguide arrays [14,15] and in 2D photonic lattices [16]. Physical systems with dimensionality crossover have attracted huge attention, for example, the continuous transformation of photonic lattice from one dimension to two dimensions [17]. In such systems, intermediate states can occur that do not exist in either 1D or 2D geometries. For these structures, there are still open questions: How, when and why does a system cross over from one to two dimensions?

Nondiffracting beams are convenient for the generation of 2D photonic lattices, since they can retain propagation-invariant structure even under weak nonlinearity [18]. There are four major nondiffracting beam families that are exact solutions of the Helmholtz equation in different coordinate systems [19,20]: plane waves in Cartesian, Bessel beams in circular cylindrical [21], Mathieu beams in elliptic cylindrical [22], and parabolic beams in parabolic cylindrical coordinates [23]. We opt for Mathieu beams, since they are used for optical lattice-writing that allows solitons or even elliptically shaped vortex solitons [24]. They are also used for the creation

#497795 https://doi.org/10.1364/OE.497795
Journal © 2023 Received 12 Jun 2023; revised 30 Jul 2023; accepted 30 Jul 2023; published 14 Aug 2023

Optics EXPRESS

of different aperiodic photonic lattices by the optical induction technique in photorefractive crystals [8,25], as well as for particle manipulation [26].

In this paper, we investigate the conditions for discrete diffraction occurrence and its properties in the aperiodic Mathieu photonic lattices, both experimentally and theoretically. Owing to their shape, Mathieu beams enable one-pass experimental realization of naturally *truncated aperiodic* photonic lattices, supporting *surface states* as well as discrete diffraction on the surface. We focus on the aperiodic photonic structures in elliptical-radial geometries, since they offer a broad range of shapes, including ellipticity as an additional degree of freedom. They also allow to raise the question on the dimensionality of discrete diffraction. For difference, in periodic photonic lattices there are only two parameters affecting discrete diffraction: the lattice period and the refractive index modulation depth, and they are uniform over the whole lattice. However, the lattice period and the refractive index modulation of Mathieu lattices are not independent parameters; they are connected via Mathieu beam parameters (the beam order, characteristic structural size, and the ellipticity of the beam). Due to the aperiodicity of Mathieu lattice, there are various probing local environments supporting discrete diffraction influenced by the nearest neighbors. During the propagation, diffracting probe can pass through changed local enviroments, unlike in the periodic lattice, causing additional variations in the discrete diffraction effects.

Here, we demonstrate elliptical-radial discrete diffraction in photonic lattices realized by a single Mathieu beam. By changing the order, characteristic structure size, and ellipticity of the Mathieu beam, we are able to control discrete diffraction in the radial direction, as well as the shape of their distributions in the perpendicular directions: circular, elliptic, or hyperbolic. By changing the input probe beam position, we observe switching from the 1D to the 2D discrete diffraction. In our medium - the photorefractive birefringent cerium-doped strontium barium niobate (SBN61:Ce) - the crystal anisotropy plays an important role in the discrete diffraction phenomenon: we observe the most pronounced 2D discrete diffraction along the crystal anisotropy direction.

2. Numerical modeling and experimental realization of light propagation in Mathieu photonic lattices

We investigate the light propagation in Mathieu photonic lattices in the photorefractive medium and study the conditions for the discrete diffraction of light in such lattices. We model linear light propagation in a photonic lattice by solving the coupled system of two equations: the nonlinear Schrödinger equation for the scalar electric field, as the propagation equation, and the diffusion equation for the electrostatic potential as the potential equation [27,28]. We solve both equations numerically, by employing a spectral split-step beam propagation method [29]. The propagation equation of the scalar electric field A with longitudinal wave vector k_z is given by:

$$\mathrm{i}\partial_z A + \frac{1}{2k_z}\Delta_\perp A + \frac{k_z}{2n_{\mathrm{o,e}}^2}\delta n^2 A = 0, \tag{1}$$

where the wave number $k = 2\pi/\lambda = \sqrt{\left(k_\perp^2 + k_z^2\right)}$ is defined by the laser wavelength $\lambda = 532\mathrm{nm}$. The potential in the propagation equation is specified by $\delta n^2 = -n_{\mathrm{o,e}}^4 r_{13,33} E$, where $n_\mathrm{e} = 2.325$ and $n_\mathrm{o} = 2.358$ are the extraordinary and ordinary indices, and $r_{13} = 47\mathrm{pm/V}$ and $r_{33} = 237\mathrm{pm/V}$ are the corresponding electro-optic coefficients of the birefringent SBN61:Ce crystal. The total electric field $E = E_\mathrm{ext} + E_\mathrm{sc}$ that builds up inside the crystal is a superposition of an external electric field $E_\mathrm{ext} = 2000\mathrm{V/cm}$ aligned with the optical $c = x$ axis and an internal space charge field E_sc that results from the incident intensity distribution within the potential equation.

In order to take the electric bias of the crystal into account and the photorefractive material response, we implement an anisotropic potential equation for the spatial evolution of the

Optics EXPRESS

electrostatic potential ϕ_{sc} of the optically-induced space-charge field $E_{\rm sc}$

$$\Delta_\perp \phi_{\rm sc} + \nabla_\perp \ln(1+I) \cdot \nabla_\perp \phi_{\rm sc} = E_{\rm ext} \partial_x \ln(1+I), \tag{2}$$

where $I = |A|^2$ is obtained from Eq. 1. Subsequently, Eq. 1 is updated with the optically induced space-charge field

$$E_{\rm sc} = \partial_x \phi_{sc}, \tag{3}$$

obtained by solving Eq. 2. This procedure is iteratively repeated along the propagation direction.

The process of generation of the propagation-invariant Mathieu photonic lattice is modeled through the distribution $I = I_{latt}$ from Eq. (2), which we refer to as the writing lattice pattern in the experiment [25]. Thus, we obtain first the spatial distribution of I_{latt} in a separate numerical simulation of Eqs. (1) and (2), by propagating an ordinary Mathieu beam in the weak nonlinear case. Then we use such a nearly diffractionless lattice distribution as a lattice potential, to simulate an extraordinary Gaussian probe beam propagation. For this, we use the same equations but with the modified total intensity distribution $I = I_p + I_{latt}$, where the Gaussian probe beam intensity $I_p = |A|^2$ is obtained from Eq. 1. In our simulations with the probe beam, I_p is kept sufficiently weak, so as not to cause an excessive nonlinear modification.

To experimentally investigate the linear light propagation of narrow probe Gaussian beam in Mathieu photonic lattices, we use the experimental setup shown in Fig. 1. As a light source, we use a frequency-doubled Nd:YVO_4 laser that emits continuous wave laser light at a wavelength of $\lambda = 532$nm. The expanded and collimated laser beam (telescope L1-L2) illuminates as a plane wave the phase-only spatial light modulator (SLM). Both the amplitude and phase of the reflected light field are modulated. This is accomplished by addressing to the SLM a precalculated hologram containing the information on the complex light field of the Mathieu lattice, encoded with an additional blazed grating [25,30]. In this way, an ordinary polarized beam is spatially modulated and we use it as the writing beam. We demagnify it by a telescope (L3-L4), to illuminate a crystal. The diffraction pattern of the Mathieu lattice is bandpass filtered in Fourier space (FF) [30]. The SBN61:Ce crystal with dimensions of $5 \times 5 \times 20\text{mm}^3$ is externally biased with an electric field of $E_{\rm ext}$ aligned with the optical $c = x$ axis, perpendicular to the direction of propagation, z axis, and parallel to the long axis of the crystal. As a result, the ordinary polarized beam optically induces a refractive index modulation, using the lattice writing beam power P, corresponding to the numerically calculated Mathieu lattice. After the fabrication of the Mathieu lattice, the writing beam and the external electric field are switched off. Then an extraordinary polarized narrow Gaussian probe beam illuminates the specified lattice position and we observe linear light propagation in the Mathieu photonic lattice. A half-wave plate rotates the probe beam's linear polarization by 90° relative to the writing beam's polarization, addressing the

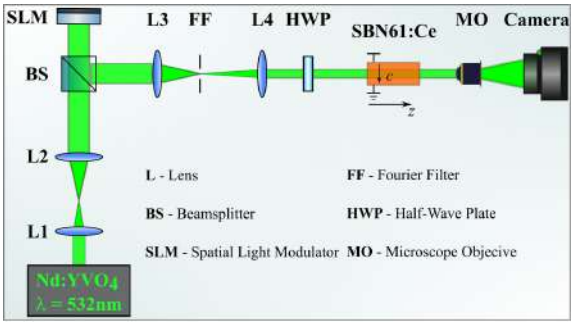

Fig. 1. Experimental setup for the light beam propagation investigation in the two-dimensional Mathieu photonic lattice.

Optics EXPRESS

stronger electro-optic coefficient. We use an imaging system formed by a microscope objective (MO) with the camera to detect the transverse intensity distribution of the writing and/or probing beam at the back face of the crystal. A low probe beam's power keeps the propagation in a linear regime, and the lattice refractive index modulation remains unmodified (until erased by white light). The probe beam of full-width-at-half-maximum of 8μm is directly positioned in front of the crystal and its transverse position defines the input center. We determine the beam size to be adequate to illuminate one lattice site.

3. Transition from 1D to 2D discrete diffraction

Mathieu beams are a class of nondiffracting beams suitable for the realization of photonic lattices. We base our study on even Mathieu beams $M_m(\xi, \eta)$ of order m, which are mathematically described as a product of the radial c_{em} and angular J_{em} Mathieu functions of order m: $M_m(\xi, \eta) = C_m(q)J_{em}(\xi; q)c_{em}(\eta; q)$. Here, $C_m(q)$ is a weighting constant that depends on the ellipticity parameter $q = f^2k_t^2/4$ that is related to the positions of the two foci f and the transverse wave number $k_t = 2\pi/a$, where a is the characteristic structure size. Elliptical coordinates (ξ, η) are related to the Cartesian coordinates (x, y) by $x + iy = fcosh(\xi + i\eta)$. Mathieu beams M_m are used for generating lattice intensity distribution I_{latt} by numerical simulation of Eq. 1 and Eq. 2. By changing some of the main characteristics of Mathieu beams, defined by the parameters: beam order m, ellipticity q, and characteristic structure size a, we are capable of managing various spatial intensity distributions of Mathieu lattices [25]. The refractive index change and the lattice period of such a lattice are not independent parameters, but are connected via Mathieu beam parameters m, q, and a. Various probing local environments in Mathieu lattices support the formation of different discrete diffraction patterns. By changing the ellipticity of the Mathieu lattice, one changes the curvature of the lines connecting nearest neighbour sites (which is zero in the periodic lattice), thus influencing discrete diffraction patterns. Similarly, the anisotropy of our medium (SBN61:Ce crystal) enables the conditions for supporting discrete diffraction in certain directions.

We start by using Mathieu lattice with zero ellipticity ($q = 0$), where the waveguide arrays are distributed along the circles, as well as along the radial spikes. Three input probe beam positions are chosen, shown in Fig. 2(a1), (1, 2, and 3) marked with yellow arrows for the sites at the first, second, and fourth circle waveguide arrays, respectively. All 3 positions belong to the same radial spike, while positions 4 and 5 (the green arrows) belong to the most intense first circular waveguide. We compare the numerical and experimental results of the probe beam intensity distributions at the crystal back face after 2 *cm* propagation. For the first input probe beam position on the lattice edge (marked as position 1 in Fig. 2(a1)), we observe behavior similar to the 2D discrete diffraction. We will refer to it as the radial 2D discrete diffraction in the truncated elliptical-radial lattice (Fig. 2(b1),(b2)). On the same circular waveguide array, but on the opposite side of the input probe beam position, we notice out-of-order appearance of intensive spots collecting evanescent leakage of the waveguides from the opposite side.

Following the geometrical distribution of the lattice, we show the projection of the probe beam intensity distributions on the circle and spike waveguide arrays (the corresponding circles and spikes are marked in Fig. 3(a)) along the propagation distance. In the circular direction, we cut the first four circles opposite to the excitation position and show flattened probe intensity distributions in Fig. 3(b), presenting discrete diffraction along circles. On the edges of Fig. 3(b) distribution, corresponding to the cut point, we can follow the dynamics of the previously mentioned opposite intensive spot. In the radial direction, we notice discrete edge diffraction along some of the truncated spike waveguide arrays (Fig. 3(c)). When we shift the probe beam input position away from the lattice edge (position 2 in Fig. 2(a1)), the two-dimensionality of discrete diffraction is less pronounced, but at the expense of separate circular and radial 1D discrete diffractions. For the third probe beam position (position 3 in Fig. 2(a1)), we notice separate circular and radial

Optics EXPRESS

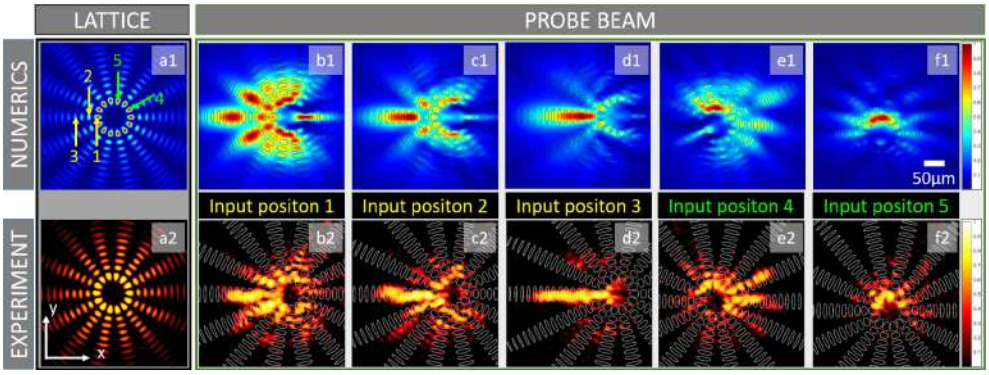

Fig. 2. Influence of various probe beam input positions on the discrete diffraction in Mathieu lattice. The intensity distribution of the Mathieu lattice at the exit crystal face observed numerically (a1) and experimentally (a2), with yellow arrows in (a1) indicating various input probe beam positions. Intensity distributions of the probe beam at the exit crystal face obtained numerically (the first row) for the input probe beam positions: 1 (b1), 2 (c1), 3 (d1), 4 (e1), and 5 (f1), taken from Visualization 1, Visualization 2, Visualization 3, Visualization 4 and Visualization 5, respectively, representing the numerical intensity distributions of the probe beam along the propagation direction. Experimentally obtained intensity distributions at the crystal exit face (the second row) for input probe beam positions: 1 (b2), 2 (c2), 3 (d2), 4 (e2), and 5 (f2). Parameters are: Mathieu lattice order m = 7, ellipticity $q = 0$, and characteristic structure size $a = 30\mu m$, $I_{latt} = 1$, experimental lattice writing beam power $P = 0.5mW$.

discrete diffractions. Hence, we observe the switching from 2D to 1D discrete diffraction in truncated elliptical-radial lattice, by changing the input probe beam position.

Additionally, we investigate the influence of crystal anisotropy on light diffraction in such a lattice (Fig. 2). We consider various input probe beam positions, depicted as positions 1, 4, and 5 in Fig. 2(a1): All input beam positions are on the same circular waveguide array and would be equivalent, apart from the relative orientation to the crystal anisotropy. As one can see, in such lattices 2D discrete diffraction is possible to observe *only* for input probe beam positions along the crystal anisotropy direction (c-axis) (Fig. 2(b)).

With increasing Mathieu lattice order m, the number of spike waveguide arrays is increased, favoring 2D discrete diffraction (Fig. 4(a-c)). We study the probe beam propagation for three

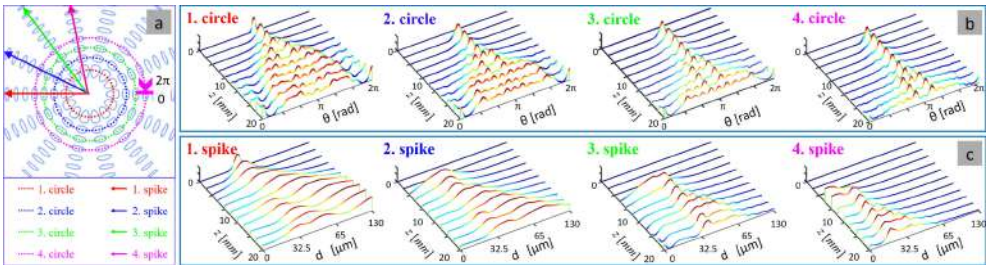

Fig. 3. Discrete diffraction along the circular and spike waveguide arrays. Projections of intensity distributions along circles (b), and spikes (c) corresponding to (a). For each circle, the circumference is measured in the angular coordinate θ starting from the cut point, and the radial coordinate d from the common center of the circles. The parameters are as in Fig. 2(b1).

Optics EXPRESS

lattice orders: $m = 7, 9$, and 12, and obtain more pronounced 2D discrete diffraction for higher lattice order. Also, we study how the variation of the Mathieu lattice characteristic structure size a influences the propagation of the probe beam: Increasing the characteristic structure size a uniformly increases the distance between neighboring sites (Fig. 4(c-e)). We are able to control optimal conditions for 2D or more 1D discrete diffractions in certain regions, and with the variation of structure size a, we are able to move those regions. We investigate Mathieu lattices for three characteristic structure sizes: $a = 30, 35$, and $40\mu m$. 2D discrete diffraction becomes less pronounced with the increase of a, which is caused by the increasing order separation in each concentric elliptical waveguide array.

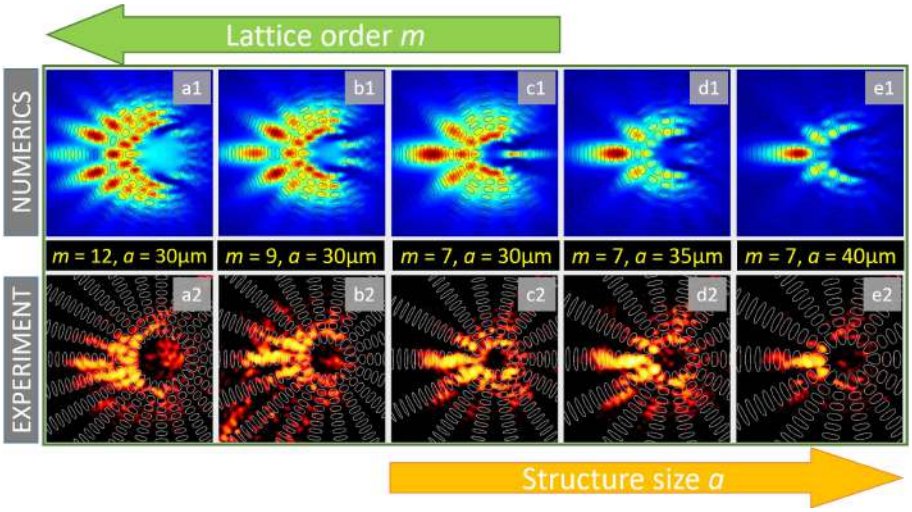

Fig. 4. Influence of Mathieu lattices order m and structural size a on the discrete diffraction patterns. (a1-e1) Numerically observed intensity distributions of the probe beam at the exit crystal face for different parameters m, a, marked in each panel, and $q = 5$, taken from Visualization 6, Visualization 7, Visualization 8, Visualization 9, Visualization 10, respectively. The second row presents the corresponding experimental exit face intensity distributions (a2-e2). Other parameters are as in Fig. 2.

At the end, we study how the variation of Mathieu lattice ellipticity q influences the discrete diffraction of light (Fig. 5). We perform our investigation by probing Mathieu lattices with various ellipticities: $q = 0, 10, 125$, and 625. Probe beam input positions are marked with the yellow arrows depicted in Fig. 5 (the first row). For ellipticity $q = 0$, we notice 2D radial discrete diffraction, in contrast to the ellipticity of $q = 10$, where one notices the splitting to 1D radial discrete diffractions along the inner ellipse and the left spike waveguide array. With further increasing q, due to modulation depth distributions - i.e., nonuniform distributions, favorable conditions for discrete diffraction appear for high q, where we have hyperbolic lattices. For ellipticity $q = 125$, we obtain 2D discrete diffraction across hyperbolas, while for $q = 625$, we observe more 1D discrete diffraction along the edge hyperbola, mostly due to the sharp decrease of array intensity distribution away from the edge hyperbola. As stated, the distribution is rapidly decaying away from the edge row, which in the absence of anisotropy would result in dominantly 1D discrete diffraction (not shown).

Optics EXPRESS

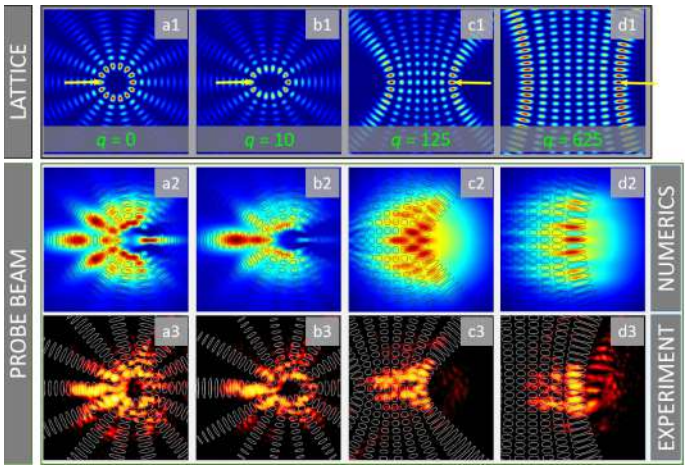

Fig. 5. Lattice ellipticity q influence on the discrete diffraction of light. First row: Intensity distributions of Mathieu lattice. Second row: probe beam intensity distributions at the exit face of the crystal, obtained numerically (a2- d2), taken from the corresponding numerical intensity distributions of the probe beam along the propagation direction: Visualization 1, Visualization 11, Visualization 12, Visualization 13, respectively. The third row: Experimental intensity distributions of the probe beam at the crystal exit face (a3-d3). Other parameters are as in Fig. 2.

4. Conclusion

In summary, we have presented a method for radial and angular discrete diffraction generation in various Mathieu lattices, experimentally and numerically. Such photonic lattices are optically induced in a photorefractive crystal, using one-pass creation in the experiment. They are also a kind of truncated lattices that could support surface states. Mathieu photonic structures offer an extensive variation of shapes as well as ellipticity, as the additional degree of freedom, with the waveguides deployed along circles, ellipses, and hyperbolas, as well as radial spikes. We have controlled radial discrete diffraction by changing the order, characteristic structure size, and ellipticity of Mathieu beams used for the optical induction of photonic lattices. Shifting the input probe beam position, we have observed a transition from 1D to 2D discrete diffraction. We have found the most pronounced 2D discrete diffraction along the crystal anisotropy direction. Note that the discrete diffraction created by our approach exhibits branching 1D discrete diffraction along circle/ellipse and spike waveguide arrays, while predominantly 1D discrete diffraction occurs in hyperbolic lattices. Our results pave the way for exploiting light propagation in a novel class of optical lattices, but they are not limited to these particular lattices: They can readily be generalized in other kinds of optically induced lattices. Adaptivity and reconfigurability of the light-guiding structures play an important role in enabling functionality, displaying a significant advance in modern photonics and providing an important step towards novel innovative wave-guiding applications and light routing approaches. They will hopefully find useful applications in the capacity-enhanced optical information processing.

Funding. Ministry of Science, Technological Development and Innovations of the Republic of Serbia; Science Fund of the Republic of Serbia (GRANT No 7714356, IDEAS - CompsLight).

Acknowledgments. The authors acknowledge funding provided by the Institute of Physics Belgrade and Institute for Multidisciplinary Research, through the grants by the Ministry of Science, Technological Development and Innovations of the Republic of Serbia and by the Science Fund of the Republic of Serbia, **GRANT No 7714356, IDEAS - CompsLight**.

Disclosures. The authors declare no conflicts of interest.

Optics EXPRESS

Data availability. Data underlying the results presented in this paper are not publicly available at this time but may be obtained from the authors upon reasonable request.

References

1. F. Lederer, G. I. Stegeman, D. N. Christodoulides, G. Assanto, and M. S. Y. Silberberg, "Discrete solitons in optics," Phys. Rep. **463**(1-3), 1–126 (2008).
2. D. N. Christodoulides, F. Lederer, and Y. Silberberg, "Discretizing light behaviour in linear and nonlinear waveguide lattices," Nature **424**(6950), 817–823 (2003).
3. T. Pertsch, T. Zentgraf, U. Peschel, A. Bräuer, and F. Lederer, "Anomalous refraction and diffraction in discrete optical systems," Phys. Rev. Lett. **88**(9), 093901 (2002).
4. J. W. Fleischer, M. Segev, N. K. Efremidis, and D. N. Christodoulides, "Observation of two-dimensional discrete solitons in optically induced nonlinear photonic lattices," Nature **422**(6928), 147–150 (2003).
5. Z. Vardeny, A. Nahata, and A. Agrawal, "Optics of photonic quasicrystals," Nat. Photonics **7**(3), 177–187 (2013).
6. L. Negro and S. Boriskina, "Deterministic aperiodic nanostructures for photonics and plasmonics applications," Laser Photonics Rev. **6**(2), 178–218 (2012).
7. M. Boguslawski, N. M. Lučić, F. Diebel, D. V. Timotijević, C. Denz, and D. M. J. Savić, "Light localization in optically induced deterministic aperiodic fibonacci lattices," Optica **3**(7), 711–717 (2016).
8. J. M. Vasiljević, A. Zannotti, D. V. Timotijević, C. Denz, and D. M. J. Savić, "Light propagation in aperiodic photonic lattices created by synthesized mathieu–gauss beams," Appl. Phys. Lett. **117**(4), 041102 (2020).
9. J. Yuan, H. Zhang, C. Wu, G. Chen, L. X. Lirong Wang, and S. Jia, "Creation and control of vortex-beam arrays in atomic vapor," Laser Photonics Rev. **17**, 2200667 (2023).
10. H. Zhang, J. Yuan, L. Xiao, S. Jia, and L. Wang, "Geometric pattern evolution of photonic graphene in coherent atomic medium," Opt. Express **31**(7), 11335–11343 (2023).
11. J. Yuan, C. Wu, L. Wang, G. Chen, and S. Jia, "Observation of diffraction pattern in two-dimensional optically induced atomic lattice," Opt. Lett. **44**(17), 4123–4126 (2019).
12. Y. S. Kivshar, "Nonlinear tamm states and surface effects in periodic photonic structures," Laser Phys. Lett. **10**, 703–713 (2008).
13. S. Suntsov, K. G. Makris, G. A. Siviloglou, R. Iwanow, R. Schiek, D. N. Christodoulides, G. I. Stegeman, R. Morandotti, H. Yang, G. Salamo, M. Volatier, V. Aimez, R. Arès, M. Sorel, Y. Min, W. Sohler, X. Wang, A. Bezryadina, and Z. Chen, "Observation of one- and two-dimensional discrete surface spatial solitons," J. Nonlinear Optic. Phys. Mat. **16**(04), 401–426 (2007).
14. K. G. Makris, S. Suntsov, D. N. Christodoulides, G. I. Stegeman, and A. Hache, "Discrete surface solitons," Opt. Lett. **30**(18), 2466–2468 (2005).
15. C. R. Rosberg, D. N. Neshev, W. Krolikowski, A. Mitchell, R. A. Vicencio, M. I. Molina, and Y. S. Kivshar, "Observation of surface gap solitons in semi-infinite waveguide arrays," Phys. Rev. Lett. **97**(8), 083901 (2006).
16. X. Wang, A. Bezryadina, Z. Chenand, K. G. Makris, D. N. Christodoulides, and G. I. Stegeman, "Observation of two-dimensional surface solitons," Phys. Rev. Lett. **98**(12), 123903 (2007).
17. A. Szameit, Y. V. Kartashov, F. Dreisow, M. Heinrich, T. Pertsch, S. Nolte, A. Tünnermann, V. A. Vysloukh, F. Lederer, and L. Torner, "Soliton excitation in waveguide arrays with an effective intermediate dimensionality," Phys. Rev. Lett. **102**(6), 063902 (2009).
18. A. Zannotti, J. M. Vasiljević, D. V. Timotijević, D. M. J. Savić, and C. Denz, "Morphing discrete diffraction in nonlinear mathieu lattices," Opt. Lett. **44**(7), 1592–1595 (2019).
19. M. V. Berry and N. L. Balazs, "Nonspreading wave packets," Am. J. Phys. **47**(3), 264–267 (1979).
20. E. G. Kalnins and J. W. Miller, "Lie theory and separation of variables. 9. orthogonal r-separable coordinate systems for the wave equation $\psi_{tt} - \triangle_2\psi = 0$," J. Math. Phys. **17**(3), 331–355 (1976).
21. J. Durnin, J. J. Miceli, and J. H. Eberly, "Diffraction-free beams," Phys. Rev. Lett. **58**(15), 1499–1501 (1987).
22. J. C. Gutiérrez-Vega, M. D. Iturbe-Castillo, and S. Chávez-Cerda, "Alternative formulation for invariant optical fields: Mathieu beams," Opt. Lett. **25**(20), 1493–1495 (2000).
23. M. A. Bandres, J. C. Gutiérrez-Vega, and S. Chávez-Cerda, "Parabolic nondiffracting optical wave fields," Opt. Lett. **29**(1), 44–46 (2004).
24. J. M. Vasiljević, A. Zannotti, D. V. Timotijević, C. Denz, and D. M. Jović Savić, "Elliptical vortex necklaces in mathieu lattices," Phys. Rev. A **97**(3), 033848 (2018).
25. J. V. Vasiljević, A. Zannotti, D. V. Timotijević, C. Denz, and D. M. J. Savić, "Creating aperiodic photonic structures by synthesized mathieu-gauss beams," Phys. Rev. A **96**(2), 023840 (2017).
26. K. Dholakia and T. Čižmár, "Shaping the future of manipulation," Nat. Photonics **5**(6), 335–342 (2011).
27. A. A. Zozulya and D. Z. Anderson, "Propagation of an optical beam in a photorefractive medium in the presence of a photogalvanic nonlinearity or an externally applied electric field," Phys. Rev. A **51**(2), 1520–1531 (1995).
28. D. V. Timotijević, J. M. Vasiljević, and D. M. J. Savić, "Numerical methods for generation and characterization of disordered aperiodic photonic lattices," Opt. Express **30**(5), 7210–7224 (2022).
29. G. Agrawal, *Nonlinear Fiber Optics*, 5th ed (Academic Press, 2012).
30. J. A. Davis, D. M. Cottrell, J. Campos, M. J. Yzuel, and I. Moreno, "Encoding amplitude information onto phase-only filters," Appl. Opt. **38**(23), 5004–5013 (1999).

Research Article | Vol. 30, No. 5 / 28 Feb 2022 / Optics Express 7210
Optics EXPRESS

Numerical methods for generation and characterization of disordered aperiodic photonic lattices

DEJAN V. TIMOTIJEVIĆ,[1] JADRANKA M. VASILJEVIĆ,[2,*] AND DRAGANA M. JOVIĆ SAVIĆ[2]

[1] *Institute for Multidisciplinary Research, University of Belgrade, Kneza Višeslava 1, 11030, Belgrade, Serbia*
[2] *Institute of Physics, University of Belgrade, P.O. Box 68, 11001 Belgrade, Serbia*
[*] *jadranka@ipb.ac.rs*

Abstract: We introduce numerical modeling of two different methods for the deterministic randomization of two-dimensional aperiodic photonic lattices based on Mathieu beams, optically induced in a photorefractive media. For both methods we compare light transport and localization in such lattices along the propagation, for various disorder strengths. A disorder-enhanced light transport is observed for all disorder strengths. With increasing disorder strength light transport becomes diffusive-like and with further increase of disorder strength the Anderson localization is observed. This trend is more noticeable for longer propagation distances. The influence of input lattice intensity on the localization effects is studied. The difference in light transport between two randomization methods is attributed to various levels of input lattice intensity. We observe more pronounced localization for one of the methods. Localization lengths differ along different directions, due to the crystal and lattice anisotropy. We analyze localization effects comparing uniform and on-site probe beam excitation positions and different probe beam widths.

1. Introduction

The phenomenon of Anderson localization (AL) originally discovered a few decades ago is one of the basic prominent phenomena in solid-state physics [1,2]. Originally introduced to explain the localization of electronic wave functions in disordered crystals, it has found growing applications in a variety of classical and quantum systems [3–5], including light waves in different materials [6–8]. AL of light has achieved renewed interest due to the potential for the realization of localization of optical waves in random media, especially in discrete systems [9], laser-written waveguide arrays [10–13], and/or optically induced randomized potential [14]. It is in the focus of investigations, especially in nonlinear optics and photonics, due to the development of new optical technologies and media, such as disordered photonic crystals and photonic lattices, in which the presence of AL appreciably changes the propagation of light [15–17]. Owing to the analogy of paraxial photonic systems to solid-state systems, where the wave function evolution corresponds to propagation of light and thanks to the fact that longitudinally invariant disorder can be effectively realized in lattices, experimental activities in AL of light started to attract the attention of optical community [8].

Up to now, periodic photonic structures have led to light control by photonic band gaps in space and time, whereas random photonic structures give rise to localization [6,8,18]. Dynamical control and manipulation of light by deterministic aperiodic or complex photonic structures [19–21] at the intersection between periodic and random crystal structures, especially the randomization of aperiodic structures, have not yet been fully understood nor exploited for applications. Two-dimensional aperiodic photonic lattices were experimentally realized by the optical induction technique in photorefractive crystal by different combinations of nondiffracting

#447572 https://doi.org/10.1364/OE.447572
Journal © 2022 Received 7 Nov 2021; revised 20 Jan 2022; accepted 2 Feb 2022; published 17 Feb 2022

Optics EXPRESS

Mathieu beams [22], combining them in metastructures by splicing in both transverse dimensions with different offsets, thus allowing for the tunable optical response. Nondiffracting beams are convenient for the generation of photonic lattices by optical induction technique since they have propagation invariant property that is retained under the condition of week nonlinearity [23]. There are four nondiffracting beam families that are exact solutions of the Helmholtz equation in different coordinate systems [24,25]: plane waves in Cartesian, Bessel beams in circular cylindrical [26], Mathieu beams in elliptic cylindrical [27], and parabolic beams in parabolic cylindrical coordinates [28].

Aperiodic lattices in contrast to periodic lattices contain non-uniform distances between the lattice sites with non-homogeneous intensity depths distributions, therefore light propagation strongly depends on the probe beam excitation position local environments [29–31]. Such lattices including quasiperiodic Penrose and Fibonacci, and aperiodic Mathieu lattice, are shown to hamper diffraction of linear light [30,31] which can be explained by excitation of highly localized linear modes [32]. Such lattices also support nonlinear light localization [29,31]. Disordering periodic lattices can lead to AL [7,8] or its suppression [33], referred therein as inverse Anderson transition. AL is enhanced by self-focusing nonlinearity in disordered periodic lattice [7,8]. Disordered quasiperiodic Penrose lattice can support AL and disorder-enhanced transport (DET) which is associated with broadening of eigenfunctions with the disorder. Instead of a singular pattern of quasiperiodic structures such as Penrose or Fibonacci with limited variation in probing local environments, we are proposing consideration of a whole class of aperiodic structures based on Mathieu beams [22] with the adjustable spatial and intensity distribution, thus providing different probing local environments, as well as introducing structure anisotropy variability. A further step is randomization of such class of aperiodic structures in order to create an appropriate platform for investigation of light propagation effects and study their possible transition to AL or DET, which is still an unexplored topic. Exhaustive theoretical or experimental analysis of light propagation in such a large class of aperiodic structures is difficult to implement, therefore, in this paper, we focused on one exemplary aperiodic Mathieu structure and numerically model their possible randomizations and probing of resulting disordered lattices.

In this article, we introduce the modeling of two different methods for the generation of two-dimensional propagation invariant disordered aperiodic Mathieu lattices, corresponding to two different experimental realizations using optical induction technique in a photorefractive crystal. One of the methods corresponds to the already known randomization method [32] with potentially simpler experimental realization such as we use in our previous studies. But for the first time, we suggest a substantially different randomization method and compare them with the previous method, with additional improvement. We present a comprehensive numerical study of transverse light localization in such waveguides arrays. We aim at elucidating the effect of disorder on light propagation considering localization effects along propagation. The influence of lattice intensity on the diffraction rate is also analyzed; specifically differences in the localization while varying a nominal lattice intensity, as well as investigating the averaged lattice intensity. We discuss the effect of different choices for input excitation sites on the disorder-induced localization in such a system. Finally, the effect of the probe beam width on the localization effects is studied.

By gradually adding disorder to the lattice we demonstrate enhanced light transport of the probe beams for all disorder strengths, as well as show the transition from diffusive-like transport to the AL for higher disorder levels. More pronounced localization is observed for longer propagation distances even for lower disorder levels. We attribute effective beam width difference between two randomization methods to varying levels of lattice intensities. We observe more pronounced localization for one of the methods; shorter localization length decreases indicating more pronounced localization. It is shown that localization length differs along different directions, which we attribute to the lattice and crystal anisotropy. There is no noticeable difference in

Optics EXPRESS

localization effects when probe beam excitation positions are distributed only on-site instead of uniformly. For broad Gaussian probe beams localization is not observed in such lattices.

2. Numerical modeling of light propagation in disordered lattices

By solving the coupled nonlocal system of two equations: the nonlinear Schrödinger equation, as propagation equation and a potential equation [34], we numerically simulate the weak nonlinear propagation of probe beam in the photorefractive cerium-doped strontium barium niobate (SBN) crystal with disordered aperiodic Mathieu lattices modeled as propagation invariant potential. Both propagation and potential equations are initial values problems with absorbing boundaries numerically solved by the symmetrized spectral split-step beam propagation method [35]. The propagation equation for an initial extraordinary polarized scalar electric field A (probe beam) with longitudinal wave vector k_z is

$$\mathrm{i}\partial_z A + \frac{1}{2k_z}\Delta_\perp A + \frac{k_z}{2n_{\mathrm{o,e}}^2}\delta n^2\left(|A|^2\right)A = 0. \tag{1}$$

The wave number $k = 2\pi/\lambda = \sqrt{\left(k_\perp^2 + k_z^2\right)}$ is defined by the wavelength $\lambda = 532\,\mathrm{nm}$. The potential in this equation is given by nonlinear refractive index $\delta n^2\left(|A|^2\right) = -n_{\mathrm{o,e}}^4 r_{13,33}E$, where $n_\mathrm{e} = 2.325$ and $n_\mathrm{o} = 2.358$ are the extraordinary and ordinary indices, and $r_{13} = 47\,\mathrm{pm/V}$, $r_{33} = 237\,\mathrm{pm/V}$ are corresponding electro-optic coefficients of photorefractive birefringent SBN crystal, respectively. The electric field $E = E_\mathrm{ext} + E_\mathrm{sc}$ that builds up inside the SBN crystal is a superposition of an external electric field $E_\mathrm{ext} = 2000\,\mathrm{V/cm}$ and an internal space charge field E_sc that is determined by the intensity distribution $I = |A|^2$ with a potential equation. The external electric field E_ext is aligned with the optical $c = x$-axis, perpendicular to the $z-$ axis, the direction of propagation, that is parallel to the long axis of the crystal.

In order to take photorefractive material response as well as the electric bias of the SBN crystal into account, we deploy the anisotropic, diffusive potential equation for the spatial evolution of the electrostatic potential ϕ_{sc} of the optically induced space-charge field E_sc,

$$\Delta_\perp\phi_\mathrm{sc} + \nabla_\perp \ln\left(1 + I + I_{DL}\right)\cdot\nabla_\perp\phi_\mathrm{sc} = E_\mathrm{ext}\partial_x \ln\left(1 + I + I_{DL}\right), \tag{2}$$

where I is obtained from Eq. (1) and subsequently Eq. (1) is updated with $E_\mathrm{sc} = \partial_x\phi_{sc}$, iteratively. Disordered lattice intensity distribution $I_{DL} = |A_{DL}|^2$, with input lattice intensity I_in, modeling transverse intensity distribution of nondiffracting pattern homogeneous in the propagation direction, is persistent through iterations. Experimental laser power P is connected with I_{DL} via I_in. Intensity and spatial distribution of I_{DL} determine $\delta n^2\left(|A|^2\right)$ in Eq. (1) through iterations. In this way, instead of modeling refractive index modulation $\delta n^2\left(|A|^2\right)$ directly, we model its underlying cause. Potential $I_{DL} = |A_{DL}|^2$ of disordered lattices ***DL*** is formed by coherently adding the two-dimensional original structure ***L*** and disorder pattern ***D*** with same maximum structure intensity according to the relation

$$A_{DL} = (1 - p) * A_L + p * A_D, \tag{3}$$

where A stands for field amplitude. Parameter p is the relative contribution of the original structure and disorder pattern, which we identify as disorder strength (disorder level). By varying p ($0 \le p \le 1$), considering it a uniform measure of disorder strength, we gradually adjust the level of lattice disorder relative to the original, undisturbed structure.

The whole process of writing propagation invariant disordered lattice is here abstracted and modeled through potential I_{DL} in Eq. (2), which we will further refer as a writing lattice pattern.

Optics EXPRESS

Justification of substitution of the writing process with model potential I_{DL} is based on numerically simulation of writing process and the experimental realization of propagation invariant photonic lattices in SBN crystal as in our previous publication [22]. The same writing simulation is carried out as part of our preparation procedure to find a range of input lattice intensities I_{in} for which aperiodic Mathieu lattice stays stable and propagation invariant through the SBN crystal.

3. Two methods for the generation of disordered lattices

Here, we present two methods for the realization of two-dimensional propagation invariant disordered photonic lattices with adjustable disorder strength. We calculated the complex light field of disordered lattice for any disorder strength according to Eq. (3). Such calculated complex light fields of disordered lattices can be used as the writing light patterns for the generation of waveguide lattice by optical induction in the SBN crystal. Previous studies that applied the optical induction technique for realization of photonic lattices in birefringent SBN crystal, externally biased with an electric field aligned along the optical $c = x$-axis, and perpendicular to the propagation direction (z-axis), used the ordinary polarized writing beam with a laser power P, considered to be fairly linear in SBN crystal.

For each disorder strength, when the maximum lattice intensity of the resulting disordered lattice is left unscaled, we will refer to that case as the first method (*M1*), and laser power for experimental realization will vary with change disorder strength. The second method (*M2*) is characterized with scaling I_{DL} with I_{in} for each disorder strength, which effectively keeps the experimental lesser power constant. This distinction in methods results is the result of differences in potential experimental realizations.

For the proposed fabrication of the disordered lattices by the optical induction technique, which corresponds to M1 and M2 we can use our experimental setup from our previous study [22] using one spatial light modulator (SLM) which modulated writing beam, producing computer generating hologram. Another way for experimental realization of M1 based on experimental setup presented in Ref. [32] is to split the structure beam into two parts with controllable powers. The complex light field of the original structure would modify one part of the structure beam by the first SLM, while the complex light field of the disorder pattern addressed on the second SLM would modify the other part of the structure beam. Afterward, those two structure beams, which spectra in the transverse Fourier space are set to be located on the same circle with radius k to ensure the same propagation constant, coherently interfere to create propagation invariant disordered aperiodic lattice. In this way, a relative disorder strength would be indirectly deduced from structure beam powers.

In this paper, as the original undisturbed structure $\boldsymbol{L}$, we use aperiodic Mathieu structure designed by Mathieu Gauss beams, introduced in our previously paper [22]. Disorder pattern $\boldsymbol{D}$ is numerically calculated by interfering plane waves with constant amplitude and random phases, to generate the propagation invariant structure with random pattern in transverse dimension. We generate the disorder pattern whose spectrum in the transverse Fourier space is located on the same circle with radius k as the original undisturbed structure [36], to crate propagation invariant structures with the same propagation constant. The disorder pattern's mean grain size $2\pi/k$ is equal to the characteristic structure size $a = 25\mu m$ of Mathieu Gauss beams, used for the realization of the aperiodic structure. Transverse intensity distributions of the original aperiodic Mathieu structure and disorder pattern, that constitute disordered lattice $\boldsymbol{DL}$ created according to Eq. (3), are shown in Figs. 1 (A1) and (B1), respectively. By increasing disorder strength we change the geometry of the original structure until we completely substitute the original structure with a disorder pattern. As the difference in methods causes two choices of intensity scaling, we will investigate and compare the consequences of such scaling options. For both methods, variation of disorder strength p leads to the variation of writing lattice intensity, effectively correlating disorder strength with writing lattice intensity and indirectly with optically induced

Optics EXPRESS

refractive index modulation inside the crystal. For the same disorder levels averaged lattice intensities differ for M1 and M2, causing differentiation in propagation characteristics under these method's conditions. Transverse intensity distributions of disordered aperiodic lattices with 40% disorder for these two methods are presented in Fig. 1 (C1) and Fig. 1 (D1). Their displayed area is less than 3% of the whole transversal computational space.

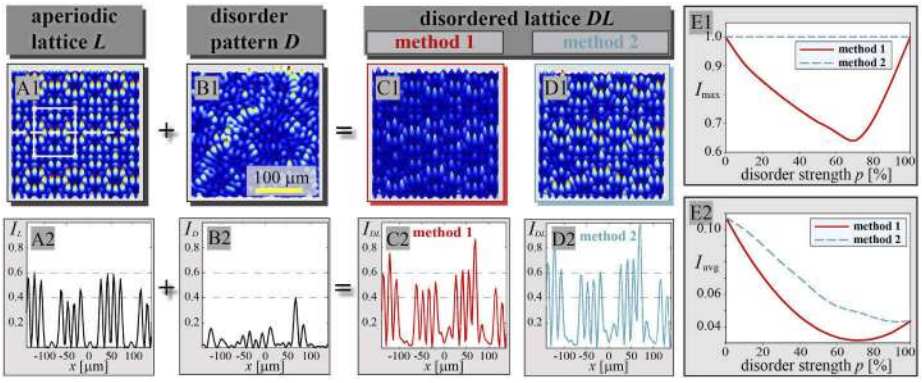

Fig. 1. Two methods of modeling disordered lattices. The transverse intensity distribution of: (A1) aperiodic lattice, with white box indicating typical pattern; (B1) disorder pattern; (C1) and (D1) disordered aperiodic lattices with 40% disorder for M1 and M2, respectively. (A2) - (D2) Corresponding representative lattice intensity cross-section taken along the x-axis marked with a white dashed line in (A1); dashed lines indicate maximum intensities of original lattice and disorder pattern. The maximum lattice intensity (E1) and the averaged lattice intensities (E2) versus disorder strength for different methods.

As an illustration of Eq. (3) in Figs. 1 (A2) - (D2) we present a single typical intensity cross-section along the x-axis (y-position indicated with a dashed line in Fig. 1 (A1)) for aperiodic lattice, disorder pattern, and resulting disordered aperiodic lattices with 40% disorder for two different methods. Levels for $p = 0.4$ and $1 - p = 0.6$ are dashed and coincide with maximum intensities of disorder and aperiodic structure, respectively. Unlike the periodic lattice, our aperiodic lattice is not uniform in the waveguide's distances and their depths vary. For M1 and M2 spatial distribution of the disordered aperiodic lattices are the same, but they differ in waveguides depths as M2 intensity values are greater than M1 intensity values (red and blue plots in Figs. 1 (C2) and (D2)).

We noted that the disorder strength p changes the lattice intensity, hence in addition to maximum lattice intensity $I_{\max}$, we calculate averaged lattice intensity $I_{\text{avg}} = \sum_r I_{DL}(\mathbf{r}) = \sum_{\mathbf{r}} |A_{DL}(\mathbf{r})|^2$, representing the level of influence of potential term in Eq. (2). The resulting differentiation of our methods in $I_{\max}$ and I_{avg} dependence on disorder strength is shown in Figs. 1 (E1) and (E2), respectively. In the first method disordered aperiodic maximum lattice intensity and the averaged lattice intensity decrease from 0% to 70% disorder, afterward increase. For 100% disorder, only maximum lattice intensity returns to an input value. In the second method, the maximum lattice intensity of disordered aperiodic lattice is equal to I_{in} for all disorder strengths, but averaged lattice intensity always decreases with increasing disorder strength. Both the maximum lattice intensity and the averaged lattice intensity for M1 are lower than for M2, except for 0% and 100% disorder. Assuming the same disorder pattern, both methods produce the same lattices for 0% and 100% disorder strengths we will exclude these two endpoints when we discuss method differences.

Optics EXPRESS

4. Quantitative description of localization phenomenon

To investigate the transverse light localization in disordered lattices, we statistically analyzed probe beam propagation for different excitation positions selected to involve various local environments. For probe beam excitation positions we use an equidistant 8×8 grid covering one complete typical pattern depicted in Fig. 1 (A1). We performed such analysis, averaging 64 various probe beam intensity distributions at the different propagation distances, for several disorder levels. For each disorder level, we have different realizations of the disordered lattice that are spatially similar due to fixed deterministic disorder pattern with statistical sampling spanning excitation probe positions only (N=64). In the preliminary investigations, we perform statistics with several different fixed disorder patterns and concluded that the statistical quantities and their dependence of disorder we want to report are not significantly influenced by the choice of disorder pattern. Due to the aperiodicity of our lattice, not each typical pattern is the same so we perform N=64 statistics on several of them, again finding no significant variation in statistical quantities of interest. Based on this preliminary analysis we did not vary the disorder pattern between different realizations of disordered lattices.

For comparison, in addition to sampling equidistant excitation positions (uniform), we also perform the statistical analysis sampling on-site positions, exciting only positions of waveguides. On-site excitation positions are chosen according to the positions of aperiodic lattice waveguides, which implies that for higher disorder strengths these positions become less accurate as waveguide's positions and depths are modified by randomization. The process of defining and numerically detecting waveguides positions modified by disorder is time-consuming and we did not pursue it, therefore we abstained from giving strong conclusions regarding on-site positioning at higher disorder levels.

In order to characterize light propagation and localization, we calculate the effective beam width along the propagation distance z according to the relation

$$W_{eff}(z) = P(z)^{-1/2}, \tag{4}$$

where $\mathrm{P}(z) = (\int |A(x,y,z)|^4 dxdy)/(\int |A(x,y,z)|^2 dxdy)^2$ is the inverse participation ratio [8]. We present scaled averaged effective beam width $\langle \omega_{\mathrm{eff}} \rangle = W_{\mathrm{eff}}(z)/(W_{\mathrm{eff}}(0)/FWHM)$ where $FWHM$ is probe beam full width at half maximum. In addition to averaged transverse output intensity distribution, we consider the log-plot profiles of such output intensity distributions to further describe light propagation. Parabolic log-plot fit indicates diffusive-like transport. The exponential decay of the transverse intensity distribution profile determines light localization, hence the linear fit of log-plots of such intensity profiles around the center demonstrates AL. In the region of disorder strength where AL occurs, we obtain localization length ξ_x along the x-axis by fitting intensity profiles $\mathrm{I}(x, y_0)$ with the exponential function

$$I(x, y_0) = \exp\left(-2\frac{|x - x_0|}{\xi_x}\right), \tag{5}$$

where x_0, y_0 denote the position of the beam center. The analogous procedure is applied along the y-direction. In some intermediate cases, when the linear fit is not obvious we compare the goodness of fit of parabolic and linear fits, where higher goodness of fit (closer to 1) indicates preferable fitting of the log plots. Hence, we use the goodness of fit to confirm a suitable fit, linear, or parabolic i.e. to discern the diffusive-like transport or AL. By shrinking the domain where we fit log-plots we notice an increase of the goodness of fit, indicating that localization occurs in a finite central domain, not in whole computation space.

5. Light transport and localization in disordered aperiodic lattices

We compare effects along light propagation in disordered aperiodic lattices generated with two different randomization methods. Figure 2 summarizes the difference between the two methods

Optics EXPRESS

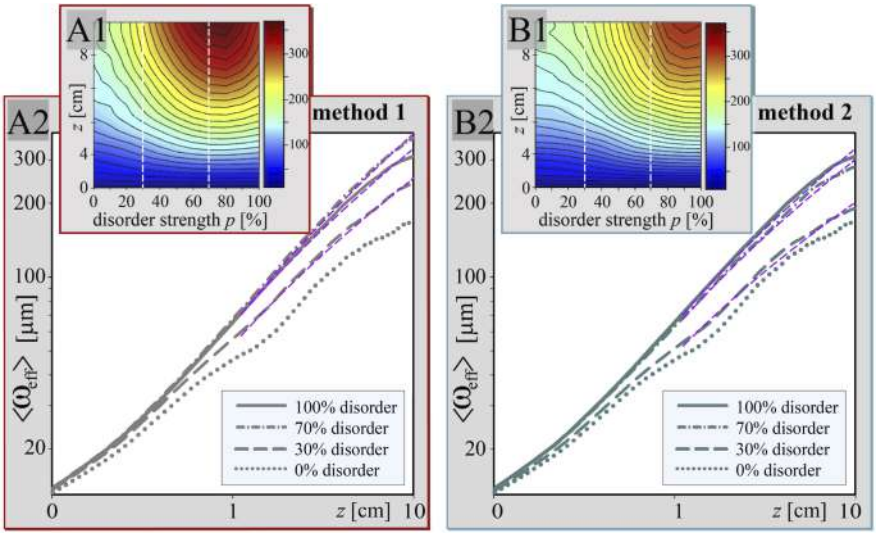

Fig. 2. Comparison of diffraction dependence on disorder strength and propagation distance for two methods. $\langle\omega_{\text{eff}}\rangle$ for various disorder strengths along the propagation distance for: (A1) M1, and (B1) M2; the colormaps display $\langle\omega_{\text{eff}}\rangle$ [μm]. $\langle\omega_{\text{eff}}\rangle$ along the propagation distance for 0%, 30%, 70%, 100% disorder strengths on a double logarithmic scale for: (A2) M1, and (B2) M2. Parameters: input Gaussian probe beam *FWHM* is 8 μm and $I_{\text{in}} = 0.7$.

considering scaled averaged effective beam width $\langle\omega_{\text{eff}}\rangle$. Figures 2 (A1), (B1) display the difference between the two methods presenting $\langle\omega_{\text{eff}}\rangle$ along the propagation distance for various disorder strengths. $\langle\omega_{\text{eff}}\rangle$ during the propagation increases for all disorder strengths. Beam expansion is maximal in the region of 60% to 80% disorder strength for M1 (Fig. 2 (A1)), and in the region of 80% to 90% disorder strength for M2 (Fig. 2 (B1)) indicated with a distribution of points where black isolines cross vertical sections. Examining the horizontal cross-sections from Figs. 2 (A1) and (B1) for each propagation length we confirm DET occurrence. For both methods during the propagation when disorder strengths deviate from that region, we observe the deceleration of $\langle\omega_{\text{eff}}\rangle$ increase. For deviation from disorder strength with maximal beam expansion toward lower disorder strengths, we observe a reduction of DET while for deviation toward higher disorder strengths reduction of DET could be attributed to AL. But, in the case of our lattice, this process is strongly mediated with variation in aggregate lattice intensity, so that we could not identify AL as the sole cause. To confirm that AL of light occurs, and for which disorder levels, we will investigate where the log-plots of the averaged intensity distributions are linearly fitted near the center.

For both methods, in Figs. 2 (A2), (B2) we present $\langle\omega_{\text{eff}}\rangle$ as a function of propagation distance z (on a double logarithmic scale), for four disorder strengths. A purple dashed lines define fits of $\langle\omega_{\text{eff}}\rangle$ by power-law $\langle\omega_{\text{eff}}\rangle(z) \propto z^{\nu}$, for M1 and M2, respectively. ν corresponds to beam expansion rate: $\nu = 1$ signifying ballistic transport and $\nu = 0.5$ characterize diffusive-like transport. For a short propagation distance (z<1 cm), beam expansion is almost linear ($\nu = 1$ i.e. ballistic transport). For a longer propagation distance (from 1 cm to 10 cm), the beam expansion rate is closest to $\nu = 0.5$ i.e. diffusive-like transport. For M1 is maximal for 70% $\nu = 0.52$ and lower $\nu = 0.48$ for both 30% and 100%. For M2 the beam expansion rate is maximal for 100% $\nu = 0.48$ and lower for 70% and 30%, $\nu = 0.47$ and $\nu = 0.45$, respectively.

For both methods in the disordered aperiodic lattice with any percent of disorder $\langle\omega_{\text{eff}}\rangle$ is greater than in the lattice without disorder indicating DET, which could be explained that disorder spreads linear modes [32] (Fig. 3 (A)). At the shorter propagation distance ($z = 2$ cm), $\langle\omega_{\text{eff}}\rangle$s

Optics EXPRESS

are increasing with increasing disorder strength. A broadening of the beam is more pronounced for longer propagation distances (z = 6 cm and 10 cm). There we notice that $\langle\omega_{\text{eff}}\rangle$s at the fixed propagation distances are increasing up to the maximum values which occur at disorder strength 80% for M1 and 90% for M2, indicating maximum of DET. With the further increase of disorder strength, $\langle\omega_{\text{eff}}\rangle$s are decreasing indicating the possibility of AL occurrence. Corresponding $\langle\omega_{\text{eff}}\rangle$s have greater values for M1 than for M2, which is easily discerned from Fig. 3 (A).

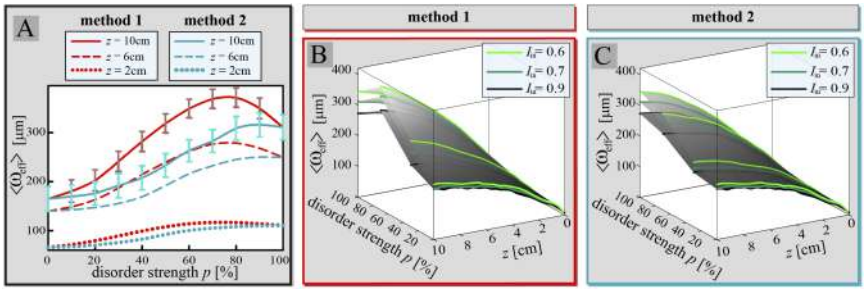

Fig. 3. Influence of disorder strength p and input lattice intensity I_{in} on the light diffraction. (A) $\langle\omega_{\text{eff}}\rangle$ versus disorder strength after 2 cm, 6 cm, and 10 cm of propagation for $I_{\text{in}} = 0.7$ for both methods. The error bars are the statistical standard deviations of $\langle\omega_{\text{eff}}\rangle$. (B) M1 and (C) M2: interpolated surfaces of $\langle\omega_{\text{eff}}\rangle$ along the propagation distance for 0%, 30%, 70%, 100% disorder strengths and for various I_{in}. Other parameters are as in Fig. 2.

The following study is the independent verification of the influence of input lattice intensity I_{in} on diffraction. We compare $\langle\omega_{\text{eff}}\rangle$s in dependence of disorder strength along propagation distance for 3 different values of the input lattice intensity I_{in}. Figures 3 (B), (C) summarize $\langle\omega_{\text{eff}}\rangle$ for two methods where we highlight lines of constant disorder strength along the propagation distance. By observing slopes of highlighted lines for each I_{in}, we illustrate the beam expansion explained in the description of Fig. 2. For all disorder strengths and propagation distances, we observe the direct influence of lattice intensity on diffraction, for both methods, where lowering I_{in} causes an increase in $\langle\omega_{\text{eff}}\rangle$. Since the explicit independent increase in lattice intensity leads to a similar effect as the inclusion of weak nonlinearity in disordered lattices, indirect change in intensity due to correlation with variation of disorder strength can also influence AL [7,8]. This effect will especially be visible in Figs. 6 and 7, where comparing log-plots of average intensity distributions for two methods for the same higher disorder strengths, observing that M1 which has lower lattice intensity than M2, produces lover central picks and higher tails, similar to Refs. [7,8].

The main difference in our methods is caused by the difference in the maximum lattice intensity I_{max}, which is varying with change of disorder strength for the first method, while it is constant for the second method, as well as different variations of the averaged lattice intensities I_{avg} with the change of disorder strength for different methods (Figs. 1 (E1), (E2)). For both methods, $\langle\omega_{\text{eff}}\rangle$ variation versus disorder strength is different for different propagation distances (Fig. 3 (A)). We notice that $\langle\omega_{\text{eff}}\rangle$s after a longer propagation distance (10 cm), have a dependence on disorder strength similar to I_{avg} (Fig. 1 (E2)). Hence, to investigate this connection, we normalize $\langle\omega_{\text{eff}}\rangle$ and reciprocal averaged lattice intensity $(I_{\text{avg}})^{-1}$ according to relation $F(p)/(F(1) - F(0)) - F(0)$, where F is $\langle\omega_{\text{eff}}\rangle$ or $(I_{\text{avg}})^{-1}$, and p is disorder strength. We present them, as well as their differences in Fig. 4 for both methods. For both methods, variations of normalized $\langle\omega_{\text{eff}}\rangle$ closely follow $(I_{\text{avg}})^{-1}$. Therefore, we conclude that $\langle\omega_{\text{eff}}\rangle$ is strongly influenced with the variation in $(I_{\text{avg}})^{-1}$ versus disorder strength for longer propagation distances, for narrow probe beam width.

Deviation of $\langle\omega_{\text{eff}}\rangle$ and $(I_{\text{avg}})^{-1}$ graphs is quantified with their difference, quantity that contains the influence of parameters not directly connected to the lattice intensity, such as lattice and beam shapes. For M2 where the dependence of $(I_{\text{avg}})^{-1}$ on p is monotonous, distributions of $\langle\omega_{\text{eff}}\rangle$ and

Optics EXPRESS

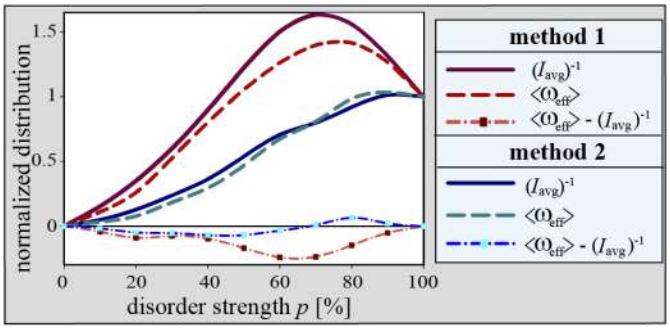

Fig. 4. Comparison of methods via $\langle\omega_{\text{eff}}\rangle$ and $(I_{\text{avg}})^{-1}$. Normalized $\langle\omega_{\text{eff}}\rangle$, $(I_{\text{avg}})^{-1}$ and their differences for both methods as a function of disorder strength. Other parameters are as in Fig. 2.

$(I_{\text{avg}})^{-1}$ and $(I_{\text{avg}})^{-1}$ vs. p closely overlap. We associate a dip of deviation for M1 in Fig. 4 with a sharp minimum in dependence of the maximum lattice intensity I_{max} versus p (Fig. 1 (E1)) and also with a minimum in I_{avg} versus p (Fig. 1 (E2)), occurring at the same disorder level. As we demonstrate in Fig. 3, light diffraction is reverse proportional to input lattice intensity. Hence, for the minimum of the maximum lattice intensity in M1, we have the highest $\langle\omega_{\text{eff}}\rangle$ (maximal DET). The narrow probe beam for low lattice intensity diffracts the most, but at longer propagation distances $\langle\omega_{\text{eff}}\rangle$ does not reach the variation of I_{avg} as at minimal lattice intensities beam already rapidly expanded early in propagation. Further in this section, we will independently study probe beam width influence on diffraction in our lattice.

We analyze the averaged transverse intensity distributions of probe beam along the propagation distance by using the log-plot cross sections of averaged intensity distributions and localization lengths. Figures 5 (A) - (D) summarize the averaged transverse intensity distributions of probe beam for some disorder strengths and some propagation distances. Parallelly, we investigate a suitable log-plot cross section along the x-axis (gray/red/cyan plots) and y-axis (black/dark red/dark cyan plots) in Fig. 6.

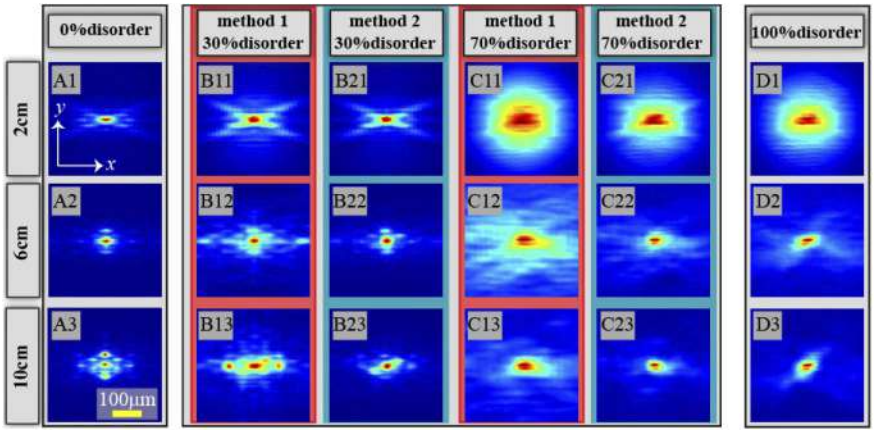

Fig. 5. Disorder-induced light transport and localization in aperiodic Mathieu lattice. Numerically averaged intensity distributions at the lattice output for different disorder strengths at different propagation distances. Other parameters are as in Fig. 2.

Optics EXPRESS

Figure 5 (A) depicts averaged intensity distribution in aperiodic lattice without the disorder, for 3 different propagation distances (2 cm, 6 cm, and 10 cm), demonstrating discrete diffraction of light, also visible in Fig. 6 (A). Figures 5 (B), (C) present averaged intensity distributions for two values of disorder strength (30% and 70%) after 3 propagation distances for both methods; suitable log-plot cross section along the x-axis (red and cyan plots) and y-axis (dark red and dark cyan plots) are presented in Figs. 6 (B), (C). For 30% disorder averaged intensity distributions and the log-plot cross sections near the center are broader for M1 than for M2. More pronounced diffraction, i.e. DET for M1 is evident (Figs. 5 (B), Fig. 6 (B)). Also, the less pronounced diffraction of light along the y-direction, for both methods, is noticeable due to the crystal ($r_{33}>>r_{13}$) and lattice anisotropy (Fig. 1 (A1)).

With further increasing disorder strength (>30%), averaged intensity distributions and the log-plot cross sections near the center are broadened, indicating DET. Additionally, the diffraction and localization effects are more noticeable along the y-transverse direction, for both methods, due to the crystal and lattice anisotropy: as visible for 70% disorder strength at $z = 2$ cm (Figs. 6 (C11), and (C21)). The interplay of lattice and crystal anisotropy influence is evident for shorter propagation distances in the log-plot cross sections near the center for M1 (Figs. 6 (C11)), where the log-plot along the x-axis is fitted with parabola, indicating diffusive-like transport, while the log-plot along the y-axis is linearly fitted indicating light localization. At the same time, as the influence of lattice anisotropy is mediated with lattice intensity, for M2 the log-plots cross sections near the center along the x- and y-axis are linearly fitted (Fig. 6 (C21)). The localization length is shorter along the y-axis, indicating that localization is still stronger in this direction. The influence of the lattice and crystal anisotropy persists for longer propagation distances (Figs. 6 (C12), (C22), (C13), (C23)), which will be illustrated with different localization lengths along the x- and y-direction in Fig. 8. Also, localization lengths in both directions for M2 are shorter than for M1, which shows that stronger localization occurs for M2.

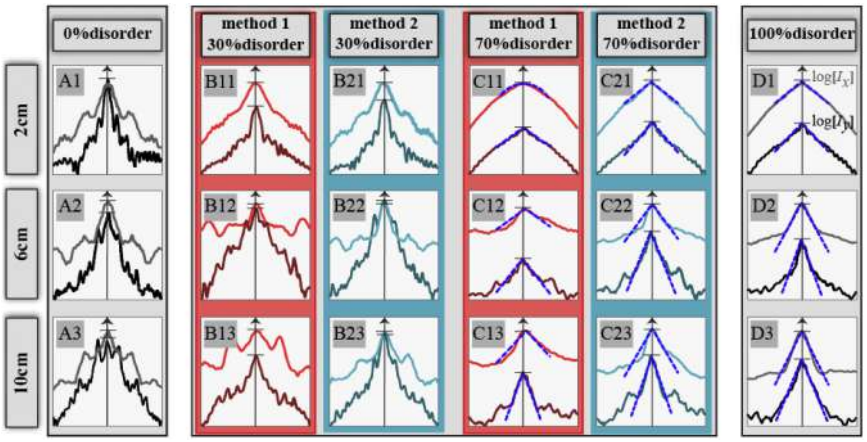

Fig. 6. Comparison of light localization along different directions. Log-plot cross sections of averaged intensity distributions along the x-axis (gray/red/cyan plots) and y-axis (black/dark red/ dark cyan plots), for different disorder strengths: (A) 0% , (B1), (B2) 30%, (C1), (C2) 70% and (D) 100%; blue dashed lines are corresponding linear fits. The horizontal axes span 400 μm in the x- and the y-direction. For each plot, there are two stacked vertical axes, where short horizontal bars are set on 1's. Other parameters are as in Fig. 2.

For 100% disorder, we notice even more pronounced localization with a longer propagation distance (Fig. 5 (D), and Fig. 6 (D)). Also, more pronounced localization is along the y-axis than the x-axis. Since, for 100% disorder, the original lattice does not contribute to anisotropy and the disorder pattern, we use in our study, does not have clear x-y anisotropy preference, we conclude

Optics EXPRESS

that the direction of crystal anisotropy is primarily cause of more pronounced localization in the y-direction. On the other hand, the asymmetry of log plots (along any axis and arbitrary disorder level) is due to the specific occurrence of the used disorder pattern. The influence of the disorder pattern anisotropy (not along x-y-direction) is noticeable at some probe beam transverse intensity distributions, as can be discerned comparing Figs. 5 (D2) - (D3) with Fig. 1 (B1).

To mitigate asymmetry of the log-plot cross-sections of averaged intensity distributions we use the average of the left and right sides of such profiles along the x-axis from the center. We fit such averaged log-plots cross sections and calculate the localization length according to Eq. (5) for disorder levels where the log-plot cross sections are linearly fitted. Figure 7 depicts a comparison of localization along the x-axis in our two methods for various disorder strengths and two propagation distances (4 cm and 8 cm). For lower disorder strengths we do not fit the log-plots (Figs. 7 (A1) and (B1)), where significant features of aperiodic lattices are remaining. However, we notice the spreading of the log-plots simultaneous with increased $\langle\omega_{\text{eff}}\rangle$, indicating that DET occurs. For both methods, at disorder strength between 50-60% at the shorter propagation distance (4 cm) light diffraction is closest to diffusive-like transport where the parabolic fits of the log-plots near the center could be attempted with low confidence (goodness of fit lower than 0.85). But, this tendency is further weakened at a longer propagation distance, so after 8 cm of propagation for 60% disorder log-plots are linearly fitted near the center indicating light localization (Fig. 7 (B2)). For higher disorder strength (80% and 100%) light localization is visible for the shorter propagation distance (4 cm, Fig. 7 (A2)), but more pronounced localization is evident for longer propagation distances also proved by linear fits of log-plots. One can see more pronounced localization for M2 than M1: log-plot fits for the same disorder level are steeper for M2, the slopes of the fits determine localization lengths.

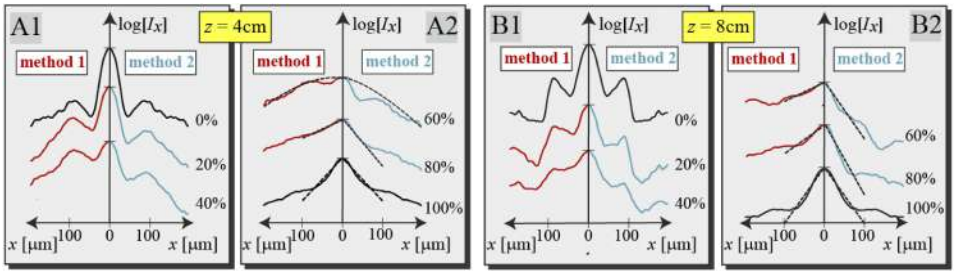

Fig. 7. Comparison of light localization in two methods for various disorder strengths and two propagation distances. Log-plot cross sections of intensity distributions symmetrized over left and right side of the x-direction, for M1 (left), M2 (right), and different disorder strengths after (A1)-(A2) 4 cm, and (B1)-(B2) 8 cm of propagation. The y-axes stacked similarly as in Fig. 6 and the other parameters are as in Fig. 2.

We characterize light localization by comparing the localization length (Eq. (5)) of linearly fitted log-plots along the x- and y-direction (Fig. 8) after 10 cm of propagation. The localization lengths in either direction are greater for M1 than for M2 indicating more pronounced localization for M2, qualitatively connecting lattice intensity with AL strength. For both methods, more pronounced localization is visible along the y-axis where the localization lengths have lower values comparing to the x-axis, due to the crystal and lattice anisotropy. One can see that differences between localization lengths are larger for lower disorder strengths, while their values converge to each other as disorder strength increases, meeting at 100% disorder strength; a similar conclusion stands for $\langle\omega_{\text{eff}}\rangle$s (Fig. 2 (A)). We notice that AL occurs at different disorder levels along different directions. Along the y-axis, localization appears for lower disorder strengths than along the x-axis. Figure 8 illustrates diffusive-like transport along the x-axis and light localization along the y-axis for the same 50%-60% disorder region.

Optics EXPRESS

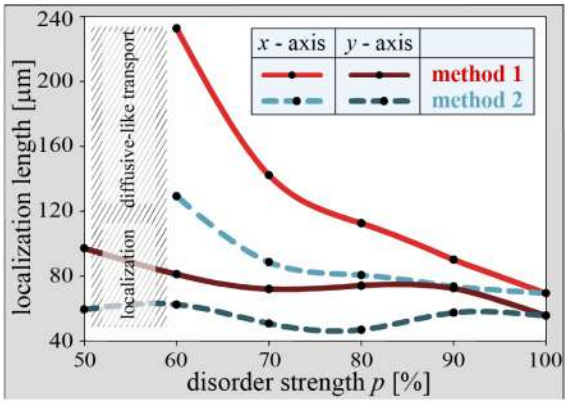

Fig. 8. Comparison of localization lengths after 10 cm of propagation distances for various disorder strengths for both methods and both the x- and y-directions. Other parameters are as in Fig. 2.

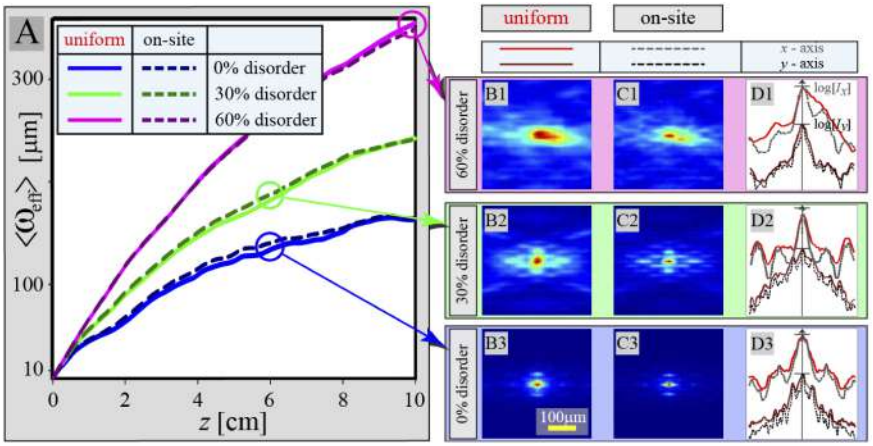

Fig. 9. Influence of probe beam excitation positions on the diffraction and localization (for M1). (A) $\langle\omega_{\text{eff}}\rangle$ versus propagation distances for uniform excitation positions and only on-site positions for different disorder strengths. (B) and (C) Appropriate averaged intensity distributions at the lattice output. (D) Log-plot cross sections of averaged intensity distributions along the x-axis (red/gray plots) and y-axis (dark red/black plots) for uniform and on-site positions for different disorder strengths. Other parameters are as in Fig. 2.

Optics EXPRESS

Moreover, we study the consequences of the choice of excitation probe beam positions distribution on the beam propagation. Statistics presented up to this point was based on the uniform distribution of probe beam excitations regardless of waveguide positions. Further, we investigate if the choice of only on-site excitation positions significantly changes the diffraction and localization characteristics. Figure 9 summarizes such results for M1. We compare $\langle\omega_{\text{eff}}\rangle$s for three disorder levels (Fig. 9 (A)) and observe slight differences between uniform and on-site excitation. Appropriate averaged intensity distributions are presented in Figs. 9 (B), (C) as well as their log-plots along the x- and y-axis (Fig. 9 (D)). We notice dissimilarity in $\langle\omega_{\text{eff}}\rangle$s for uniform one and on-site cases, at the different propagation distances for 0% and 30% disorder than for 60% disorder. $\langle\omega_{\text{eff}}\rangle$ has higher values for on-site excitation cases than for uniform, especially for lower disorder strengths (0% and 30%) after 6 cm propagation distance. However, for higher disorder strength (60%) $\langle\omega_{\text{eff}}\rangle$ is greater for uniform excitation case after 10 cm propagation distance. Such difference is caused by different computational spaces: the effective beam width is calculated for the whole computation space, with the significant contribution of tails in calculations, while the transverse intensity distributions and the log-plots are shown for the shorter (central domain), where tails contributions are discounted. Also, discrete diffraction is more pronounced for lower disorder strength for on-site excitation cases than for uniform cases, as is visible from intensity distributions and log-plots (Figs. 9 (B2) - (D2), and (B3) - (D3)). For 60% disorder, discrete diffraction is not observed for the on-site case, due to the diminished accuracy of on-site positions for higher disorder strengths. For all disorder strengths, the weaker difference is in log-plots along the y-direction. Asymmetry of log-plots is due to the specific occurrence of the used disorder pattern. However, the consequence of this choice is unsubstantial on statistical quantities.

In this research, we observe that dependence of light diffraction on various parameters is more noticeable for longer propagation. However, the question remains if the wider beams that are consequences of longer propagation distance lose their sensitivity to the local environment and thus hinder the accuracy of diffraction properties investigation. We observed different rates of increase of averaged effective beam width during propagation in our disordered lattices and consequently a variety of beam widths and shapes. Hence, we investigate the independent influence of probe beam width on light transport and localization in our disordered lattices in comparison to the free space propagation of the Gaussian beam. Figure 10 summarizes such results.

We choose three various input probe beam widths (8μm, 20μm, and 50μm). Averaged effective beam widths are considered along the propagation distance for different disorder strengths: 0%, 70%, and 100% (Fig. 10 (A)). More pronounced light transport is observed for narrower probe beam widths. Strong correlation of $\langle\omega_{\text{eff}}\rangle$ with I_{avg}^{-1} for input probe beam of 8μm presenting in Fig. 4, gradually diminish for wider probe beams. Also, wider probe beam reduces their sensitivity on disorder strength p and propagation distance, making wider beams less suitable for our investigation. Appropriate averaged intensity distributions after 4 cm propagation are presented in Figs. 10 (B), (C), (F). For 70% disorder, the log-plots along the different domains of the x-axis are shown in Fig. 10 (D) for different input probe beam widths, while Fig. 10 (E) present only their central domain along the x-axis of 400μm. We show that for all probe beam widths, along the x-axis in our disorder lattices light is spreading to the same degree as the Gaussian in free space propagation. Different domains along the x-axis represent the degree of diffraction for different probe beam widths (Fig. 10 (D)). However, a significant difference between the log-plots in our disordered lattice and the log-plots of Gaussian free space propagation is noticeable only in a limited central domain after the same propagation distance (Fig. 10 (E)). For narrow probe beam widths (8μm and 20μm), Figs. 10 (E1) (E2), localization occurs in the central domain with a size comparable to the size of the typical lattice pattern. In contrast, a wide probe beam (50μm)

Optics EXPRESS

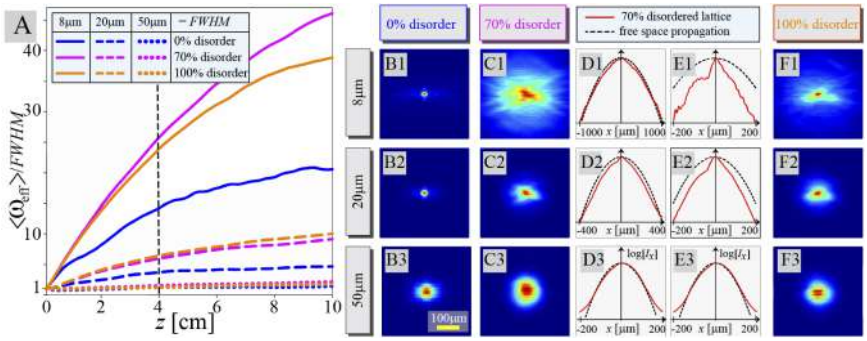

Fig. 10. Influence of probe beam width on the localization effects for M1. (A) Normalized $\langle\omega_{\text{eff}}\rangle$s versus propagation distances for three probe beam widths and different disorder strengths. Appropriate averaged intensity distributions after 4 cm (the dashed line in (A)) propagation distance for various disorder strengths: (B) 0%, (C) 70%, (F) 100%. (D) Log-plots of averaged intensity distributions along the x-axis in disordered lattice with 70% disorder strength compared with corresponding log-plots of Gaussian free space propagation. (E) The same log-plots along the x-axis as in (D) for narrow central domain from -200 to 200 μm. Other parameters are as in Fig. 2.

barely diffracts, i.e. propagates almost the same as a wide Gaussian beam in free space, limiting suitable widths of the probe beam for lattice excitation.

6. Conclusion

In this article, we presented two different theoretical methods for the realization of disordered two-dimensional photonic lattices optically induced in a photorefractive media. We numerically model light propagation in disordered aperiodic Mathieu lattices. We observed enhanced light transport for all disorder strengths but AL of light for higher disorder strengths in both methods. Localization effects are more pronounced for longer propagation distances. More pronounced localization is observed for M2 than M1: we attributed the difference between the two methods to various levels of lattice intensity. When studying the dependence of AL and DET on disorder level, to mitigate the influence of lattice intensity, we suggest further modification of our M2 in which averaged intensity levels are equalized for every disorder strength used. Localization length differs along different directions, due to the crystal and lattice anisotropy. There is no noticeable difference in localization effects if we choose only on-site probe beam excitation positions, as compared to uniform position distribution. For broad probe Gaussian beams localization is not observed in such lattices.

Funding. Ministry of Education, Science, and Technological Development of the Republic of Serbia .

Acknowledgments. The authors acknowledge funding provided by the Institute of Physics Belgrade and Institute for Multidisciplinary Research, through the grants by the Ministry of Education, Science, and Technological Development of the Republic of Serbia.

Disclosures. The authors declare no conflicts of interest.

Data availability. Data underlying the results presented in this paper are not publicly available at this time but may be obtained from the authors upon reasonable request.

References

1. P. W. Anderson, "Absence of diffusion in certain random lattices," Phys. Rev. **109**(5), 1492–1505 (1958).
2. H. De Raedt, A. Lagendijk, and P. de Vries, "Transverse localization of light," Phys. Rev. Lett. **62**(1), 47–50 (1989).
3. P. Sheng, *Scattering and Localization of Classical Waves in Random Media* (World Scientific, 1990), 2nd ed.

Optics EXPRESS

4. A. Lagendijk, B. Tiggelen, and D. S. Wiersma, "Fifty years of anderson localization," Phys. Today **62**(8), 24–29 (2009).
5. S. S. Abdullaev and F. K. Abdullaev, "On the light propagation in the system of tunnel-coupled waveguides," Sov. J. Radiofizika **23**, 766–767 (1980).
6. T. Pertsch, U. Peschel, J. Kobelke, K. Schuster, H. Bartelt, S. Nolte, A. Tünnermann, and F. Lederer, "Nonlinearity and disorder in fiber arrays," Phys. Rev. Lett. **93**(5), 053901 (2004).
7. Y. Lahini, A. Avidan, F. Pozzi, M. Sorel, R. Morandotti, D. N. Christodoulides, and Y. Silberberg, "Anderson localization and nonlinearity in one-dimensional disordered photonic lattices," Phys. Rev. Lett. **100**(1), 013906 (2008).
8. T. Schwartz, G. Bartal, S. Fishman, and M. Segev, "Transport and anderson localization in disordered two-dimensional photonic lattices," Nature **446**(7131), 52–55 (2007).
9. G. Kopidakis, S. Komineas, S. Flach, and S. Aubry, "Absence of wave packet diffusion in disordered nonlinear systems," Phys. Rev. Lett. **100**(8), 084103 (2008).
10. A. Szameit, Y. V. Kartashov, P. Zeil, F. Dreisow, M. Heinrich, R. Keil, S. Nolte, A. Tünnermann, V. Vysloukh, and L. Torner, "Wave localization at the boundary of disordered photonic lattices," Opt. Lett. **35**(8), 1172–1174 (2010).
11. L. Martin, G. D. Giuseppe, A. Perez-Leija, R. Keil, F. Dreisow, M. Heinrich, S. Nolte, A. Szameit, A. F. Abouraddy, D. N. Christodoulides, and B. E. A. Saleh, "Anderson localization in optical waveguide arrays with off-diagonal coupling disorder," Opt. Express **19**(14), 13636–13646 (2011).
12. U. Naether, Y. V. Kartashov, V. A. Vysloukh, S. Nolte, A. Tünnermann, L. Torner, and A. Szameit, "Observation of the gradual transition from one-dimensional to two-dimensional anderson localization," Opt. Lett. **37**(4), 593–595 (2012).
13. S. Stützer, Y. V. Kartashov, V. A. Vysloukh, A. Tünnermann, S. Nolte, M. Lewenstein, L. Torner, and A. Szameit, "Anderson cross-localization," Opt. Lett. **37**(10), 1715–1717 (2012).
14. M. Boguslawski, S. Brake, J. Armijo, F. Diebel, P. Rose, and C. Denz, "Analysis of transverse anderson localization in refractive index structures with customized random potential," Opt. Express **21**(26), 31713–31724 (2013).
15. D. M. Jović and M. R. Belić, "Steady-state and dynamical anderson localization of counterpropagating beams in two-dimensional photonic lattices," Phys. Rev. A **81**(2), 023813 (2010).
16. D. M. Jović, Y. S. Kivshar, C. Denz, and M. R. Belić, "Anderson localization of light near boundaries of disordered photonic lattices," Phys. Rev. A **83**(3), 033813 (2011).
17. D. M. Jović, M. R. Belić, and C. Denz, "Transverse localization of light in nonlinear photonic lattices with dimensionality crossover," Phys. Rev. A **84**(4), 043811 (2011).
18. C. Conti and A. Fratalocchi, "Dynamic light diffusion, three-dimensional anderson localization and lasing in inverted opals," Nat. Phys. **4**(10), 794–798 (2008).
19. Z. Vardeny, A. Nahata, and A. Agrawal, "Optics of photonic quasicrystals," Nat. Photonics **7**(3), 177–187 (2013).
20. L. Negro and S. Boriskina, "Deterministic aperiodic nanostructures for photonics and plasmonics applications," Laser Photonics Rev. **6**(2), 178–218 (2012).
21. E. Maciá, "The role of aperiodic order in science and technology," Rep. Prog. Phys. **69**(2), 397–441 (2006).
22. J. V. Vasiljević, A. Zannotti, D. V. Timotijević, C. Denz, and D. M. J. Savić, "Creating aperiodic photonic structures by synthesized mathieu-gauss beams," Phys. Rev. A **96**(2), 023840 (2017).
23. A. Zannotti, J. M. Vasiljević, D. V. Timotijević, D. M. J. Savić, and C. Denz, "Morphing discrete diffraction in nonlinear mathieu lattices," Opt. Lett. **44**(7), 1592–1595 (2019).
24. M. V. Berry and N. L. Balazs, "Nonspreading wave packets," Am. J. Phys. **47**(3), 264–267 (1979).
25. E. G. Kalnins and J. W. Miller, "Lie theory and separation of variables. 9. orthogonal r-separable coordinate systems for the wave equation $\psi_{tt} - \triangle_2\psi = 0$," J. Math. Phys. **17**(3), 331–355 (1976).
26. J. Durnin, J. J. Miceli, and J. H. Eberly, "Diffraction-free beams," Phys. Rev. Lett. **58**(15), 1499–1501 (1987).
27. J. C. Gutiérrez-Vega, M. D. Iturbe-Castillo, and S. Chávez-Cerda, "Alternative formulation for invariant optical fields: Mathieu beams," Opt. Lett. **25**(20), 1493–1495 (2000).
28. M. A. Bandres, J. C. Gutiérrez-Vega, and S. Chávez-Cerda, "Parabolic nondiffracting optical wave fields," Opt. Lett. **29**(1), 44–46 (2004).
29. B. Freedman, G. Bartal, M. Segev, R. Lifshitz, D. N. Christodoulides, and J. Fleisher, "Wave and defect dynamics in nonlinear photonic quasicrystals," Nature **440**(7088), 1166–1169 (2006).
30. M. Boguslawski, N. M. Lučić, F. Diebel, D. V. Timotijević, C. Denz, and D. M. J. Savić, "Light localization in optically induced deterministic aperiodic fibonacci lattices," Optica **3**(7), 711–716 (2016).
31. J. M. Vasiljević, A. Zannotti, D. V. Timotijević, C. Denz, and D. M. J. Savić, "Light propagation in aperiodic photonic lattices created by synthesized mathieu–gauss beams," Appl. Phys. Lett. **117**(4), 041102 (2020).
32. L. Levi, M. Rechtsman, B. Freedman, T. Schwartz, O. Manela, and M. Segev, "Disorder-enhanced transport in photonic quasicrystals," Science **332**(6037), 1541–1544 (2011).
33. S. Longhi, "Inverse anderson transition in photonic cages," Opt. Lett. **46**(12), 2872–2875 (2021).
34. A. Zozulya and D. Anderson, "Propagation of an optical beam in a photorefractive medium in the presence of a photogalvanic nonlinearity or an externally applied electric field," Phys. Rev. A **51**(2), 1520–1531 (1995).
35. G. Agrawal, *Nonlinear Fiber Optics* (Academic Press, 2012), 5th ed.
36. Z. Bouchal, "Nondiffracting optical beams: Physical properties, experiments, and applications," Czech. J. Phys **53**(7), 537–578 (2003).

Optics Letters

Light transport and localization in disordered aperiodic Mathieu lattices

Jadranka M. Vasiljević,[1,*] Alessandro Zannotti,[2] Dejan V. Timotijević,[3] Cornelia Denz,[2] and Dragana M. Jović Savić[1]

[1] Institute of Physics, University of Belgrade, P.O. Box 68, 11001 Belgrade, Serbia
[2] Institute of Applied Physics and Center for Nonlinear Science (CeNoS), University of Münster, 48149 Münster, Germany
[3] Institute for Multidisciplinary Research, University of Belgrade, Kneza Višeslava 1, 11030, Belgrade, Serbia
*Corresponding author: jadranka@ipb.ac.rs

Received 12 October 2021; revised 8 December 2021; accepted 8 December 2021; posted 9 December 2021; published 31 January 2022

Complex optical systems such as deterministic aperiodic Mathieu lattices are known to hinder light diffraction in a manner comparable to randomized optical systems. We systematically incorporate randomness in our complex optical system, measuring its relative contribution of randomness, to understand the relationship between randomness and complexity. We introduce an experimental method for the realization of disordered aperiodic Mathieu lattices with numerically controlled disorder degree. Added disorder always enhances light transport. For lower disorder degrees, we observe diffusive-like transport, and in the range of highest light transport, we detect Anderson localization. With further increase of disorder degree, light transport is slowly decreasing and localization length decreases indicating more pronounced Anderson localization. Numerical investigation at longer propagation distances indicates that the threshold of Anderson localization detection is shifted to lower disorder degrees.

https://doi.org/10.1364/OL.445779

Localization of light has drawn considerable attention in many areas of light–matter interaction owing to the evident potential for the realization in disordered media [1–4]. In contrast, Anderson localization (AL) is a well-known effect in condensed-matter physics, which predicts that electrons may become immobile in a disordered crystal. This concept of waves in disordered media has been subsequently transferred to many other areas, such as matter waves, ultracold atoms, and light or sound waves [2]. Realizing that AL is a wave phenomenon relying on interference, these concepts were extended to optics and photonics. The AL of light has been successfully demonstrated in various customized configurations, when the disorder degree (DD) is increased [5–10]. In optically induced disordered photonic quasicrystals with weak disorder, it is observed that weak disorder enhances light transport. When increasing disorder finite-time, diffusive-like transport appears, while a further increase of disorder leads first to coherent backscattering [11] and for the strong disorder to AL. Thereby, the spatial extent of the probe beam decreases and its central part of the log-plot intensity profile displays an exponential decay [9,12,13].

In nature, perfect periodicity, in contrast to disorder or aperiodicity, is not very often encountered. Deviation from periodicity results in higher complexity. In optics, the properties of various photonic quasicrystals and aperiodic systems have been studied [13–18]. Considering localization characteristics, such structures lie between periodic and random structures. Numerous aperiodic and quasiperiodic photonic structures have been realized artificially [19–21]. Non-diffracting beams, with propagation invariant transverse intensity distributions, are applicable in modern photonic research e.g. numerous two-dimensional aperiodic photonic lattices have been optically induced in photosensitive media using them [21–23]. Aperiodic lattices contain non-uniform distances between the lattice sites with non-homogeneous intensity depth distributions, and hence light propagation crucially depends on the nature of the local environment of the probe beam positions. In contrast that occurring in periodic systems, light diffraction is hampered owing to the aperiodicity [12,21,22,24]. Still, light localization in aperiodic lattices is an unexplored area of research, especially in randomized aperiodic lattices. In our previous studies, we introduced a method for the creation of various two-dimensional aperiodic photonic structures by the interference of Mathieu beams, experimentally realized in a single optical induction process in parallel [23]. We showed that such obtained aperiodic Mathieu photonic lattice (AML) hinders linear light expansion in comparison to periodic lattice and supports nonlinear light localization[24].

In this Letter, we introduce a numerical method for controllable randomization of AMLs to investigate if they support AL. We construct an experimental system for the realization of disordered lattices by a single optical induction process in parallel using a spatial light modulator (SLM) and numerically precalculated disordered patterns with adjustable DDs. This numerical method and experimental configuration, in comparison to the previous one [5,12], enable us direct control of the lattice DD and parallel optical induction of the corresponding light intensity in the whole volume of the photorefractive crystal.

Here, we investigate the light propagation in disordered AMLs numerically and experimentally. We study the conditions for light localization in such lattices as well as the effects of disorder during the propagation. For all DDs, we experimentally obtain and numerically confirm disorder-enhanced transport in

such lattices. For lower DDs, we observe diffusive-like transport. In contrast, for strongly disordered lattices, AL is verified. We demonstrate that the localization length differs along different transverse directions owing to the crystal and lattice anisotropy. We also confirm numerically a more pronounced localization for longer propagation distances, while for lower DDs, the AL prevails over diffusive-like transport for longer propagation distances.

To realized disordered aperiodic lattices with an adjustable DD, we generate numerically a two-dimensional disordered aperiodic Mathieu structure ***DS*** by combining the original aperiodic Mathieu structure ***S*** with disorder pattern ***D*** according to the relation:

$$A_{DS} = (1-p) * A_S + p * A_D, \quad \textbf{(1)}$$

where A stands for the field amplitude and the parameter p ($0 \le p \le 1$) denotes the DD as the relative contribution of the original structure and disorder pattern. We experimentally generate the aperiodic Mathieu structure as a combination of the spatially shifted patterns from Fig. 3(e1) of Ref. [23] with the x and y shifts of 144 and 152 μm, respectively. Such a structure has an invariant transverse intensity profile during propagation, with Fourier components located on a circle with radius $k_\perp$ [23,25]. A two-dimensional disorder pattern is numerically created by interfering plane waves with constant amplitude and random phases [9]. We generate a propagation invariant disorder pattern whose spectra are located on the same circle in the transverse Fourier space as the original aperiodic structure. The grain size of the disorder pattern plays a significant role in the propagation behavior [9], and we specify it to be equal to the characteristic structure size of the Mathieu–Gauss beams used for the realization of the original aperiodic structure.

We use the experimental configuration presented in Fig. 1 to fabricate and probe two-dimensional disordered AMLs. The laser source is a frequency-doubled Nd:YVO_4 laser that emits continuous wave laser light at a wavelength of $\lambda = 532$ nm and a maximum power of 5 W. The expanded and subsequently collimated laser beam is divided into two separate beams – the writing beam being ordinary polarized and an extraordinary polarized probe beam. The writing beam optically induces a refractive index modulation in a photorefractive birefringent cerium-doped strontium barium niobate (SBN) crystal (Altechna), addressing the weaker electro-optic coefficient $r_{13} = 47$ pm/V. Probing the artificial photonic structure with extraordinarily polarized probe beams addresses the stronger electro-optic coefficient $r_{33} = 237$ pm/V. The SBN crystal with

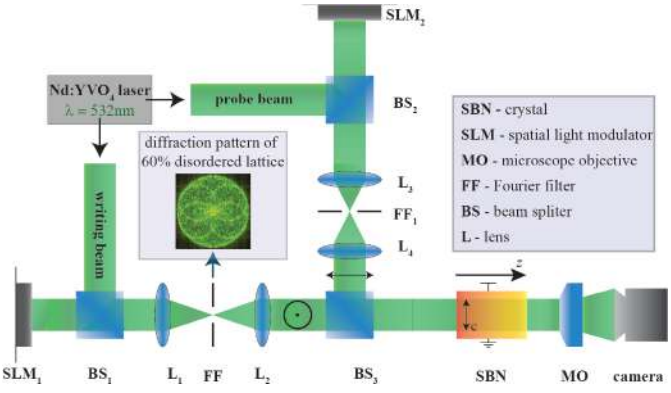

Fig. 1. Experimental configuration for investigating light propagation in two-dimensional disordered aperiodic lattices.

dimensions of $5 \times 5 \times 20\,\text{mm}^3$ has refractive indices of $n_o = 2.325$ and $n_e = 2.358$. We use an imaging system formed by a microscope objective (MO) and a 16-bit camera with 0.32 μm per pixel to detect the transverse intensity distribution of the writing and/or probing beam at the back face of the crystal.

For our experimental realization of disordered lattices, we first calculate numerically the respective complex light fields we are using as digital holograms that we image onto the optical system by a phase-only SLM [26]. The entire field information of the desired structure is encoded in elaborate diffraction gratings displayed by the SLM1. The diffraction pattern of the disordered lattice is bandpass filtered in Fourier space (FF_1) [26]. In this way, an ordinarily polarized beam is spatially modulated. We expand it to illuminate the SBN crystal. The crystal is externally biased with an electric field of $E_{ext} = 2000$ V/cm aligned along the optical $c = x$ axis, perpendicular to the direction of propagation, the z axis, and parallel to the long axis of the crystal. As a result, the ordinarily polarized beam optically induces a refractive index modulation, which corresponds to the numerically calculated disordered aperiodic structure.

We demonstrate a powerful approach for the experimental creation of two-dimensional disordered photonic lattices (periodic, quasiperiodic, or aperiodic) in a single writing process. For the experimental induction, it is sufficient to numerically precalculate the light field of desired structures with any DD according to Eq. 1, and encode by SLM, thus generating in a single step a corresponding light intensity distribution in the volume of the SBN crystal. One example of disordered AML is presented in Fig. 2.

After fabrication of the lattice, the writing beam and the external electric field are switched off, and a narrow Gaussian probe beam illuminates the lattice. Because the probe beam power of ≈ 10 μW keeps propagation in the linear regime, the modulation of the lattice refractive index stays near unmodified until active deletion. The probe beam of a full width at half maximum of 8 μm is directly positioned in front of the crystal and its transverse position defines the input center, and the beam size is adequate to illuminate one lattice site. Simulation of the light propagation along the z axis in optically induced disordered aperiodic Mathieu lattices in a photorefractive SBN crystal is numerically described by solving a system of equations as explained in Ref. [24].

To investigate the transverse localization of light in disordered lattices, we statistically analyze the probe beam propagation for different excitation positions selected to involve various local environments [12,21,24]. We performed such an analysis for each disordered lattices at various DDs using only one disorder pattern, averaging 100 different intensity distributions at the output face of the crystal, after a propagation distance of 2 cm. In addition to the averaged transverse output intensity distribution, we consider the log-plot profiles of such output intensity

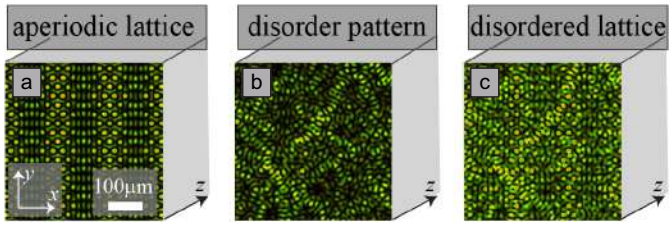

Fig. 2. Transition from aperiodic to disordered lattice: (a) original AML; (b) disorder pattern; (c) disordered AML with 60% DD.

distributions to further analyze the light propagation. To characterize the light localization, we consider the averaged effective beam widths at the output of the crystal and along the propagation distance. We calculate the effective beam width according to the relation $\omega_{\text{eff}} = \text{P}(z)^{-1/2}$, where $\text{P}(z)$ is the inverse participation ratio [5]. Considering the averaged ω_{eff}s and log-plot intensity profiles, we determine the DD range for the light localization. The parabolic fit (a Gaussian shape) of the log-plots of the averaged transverse intensity distribution profiles indicate diffusive-like transport [22]. However, the exponential decay of the transverse intensity distribution profile characterizes the light localization [22]. When the log-plots of such intensity profiles can be linearly fitted around the center, we consider AL to be confirmed. Owing to the crystal and lattice anisotropy, we obtain the localization lengths ξ along the x and y axes separately. ξ along the x axis is determined by fitting the intensity profiles $I(x)$ with the exponential function $I(x) = \exp[-2|x - x_0|/\xi]$, where x_0 denotes the position of the beam center. The same functional form applies to the y axis.

Figures 3(a1)–3(f1) represent experimental results for averaged intensity distributions at the output crystal face for six values of DD and their experimental log-plot cross-section along the x axis (white plots). Corresponding numerical log-plots (red line) are depicted in Figs. 3(a2)–3(f2). Comparing experimental and numerical log-plots and their linear and parabolic fits of the central areas (shown in black), we notice a good agreement between experimental and numerical results. Figure 3(a1) depicts the experimental averaged intensity distribution in the original AML [24], which demonstrates discrete diffraction of light. Next, we introduce disorder in this aperiodic lattice. For 10% DD, the averaged intensity distribution is broader than without disorder, as is shown in Fig. 3(b1). With further increase of DD, the averaged intensity distributions are broadened, while the log-plot cross-sections near the center can be fitted by a parabola, indicating diffusive-like transport, presented in Figs. 3(c)–3(d). However, an even stronger DD narrows the averaged intensity distributions, and the log-plot cross-sections near the center can be linearly fitted, as depicted in Figs. 3(e)–3(f), demonstrating AL in such a disordered aperiodic lattice.

To quantify the amount of beam expansion, we calculate the average ω_{eff}se of the output intensity distributions from experiment and numerics (2 cm) for different DDs; Fig. 4(a) summarizes such results with a very good agreement between numerics and experiment. Figure 4(b) presents a log-plot cross-section along the x axis of the experimental averaged intensity distributions. Comparing the ω_{eff}s and log-plots, we find regions of diffusive-like transport and light localization in our disordered aperiodic lattices. The averaged ω_{eff} in the disordered aperiodic lattice with any DD is larger than in a corresponding lattice without disorder. We notice that the averaged ω_{eff}s increase up to 60% DD indicating disorder-enhanced transport and decrease with further increase of the DD indicating light localization. Additionally, for lower DDs, log-plots are parabolically fitted near the center, characterizing diffusive-like transport [Fig. 4(b)]. AL of light is obtained for the highest DDs (80%–100%) where the log-plots are linearly fitted near the center [Fig. 4(c)]. In addition to this characterization, we also describe the light localization using ξ for DDs where linear fits of the log-plot are obtained. We notice that ξ decreases as DD increases. For 100% DD, we find the lowest $\xi = (107.3 \pm 7.2)\,\mu\text{m}$, while for 90% and 80% DD, ξs increase by 15% and 30%, respectively. Diffraction in disordered AMLs along different directions (x axis and y axis) is different owing to the crystal and lattice anisotropy, as noticeable from Fig. 3. With increasing DD, even as the log-plots along the y axis exhibit the same tendency as the log-plots along the x axis, transition to AL does not necessarily occur at the same DD. In the region of AL, ξs along the x axis are lower in comparison to ξs along the y axis. With the further increase of DD, ξs along the x direction are lower for 30% to 70% than in the y direction as noticeable from Fig. 4(c).

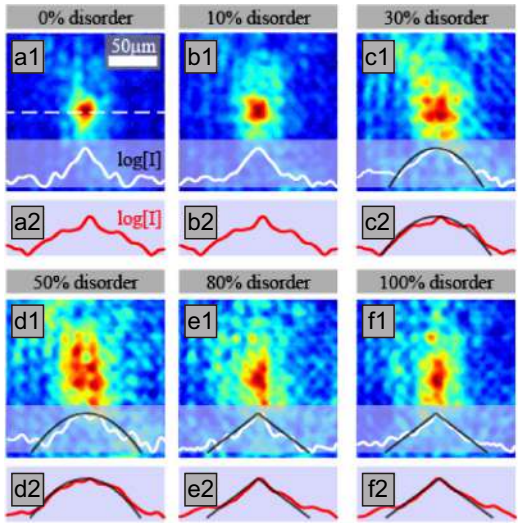

Fig. 3. Disorder-induced light transport and localization in AMLs. (a1)–(f1) Experimentally obtained averaged intensity distributions at the crystal output for different DDs, with their experimental log-plot cross-section along the x axis [marked with a white dashed line in panel (a1)]. We clean the experimental noise (caused by the rapid multiple experimental realizations of disordered lattices and subsequent probing) by removing 10% of the overall intensity for every intensity distribution. (a2)–(f2) Corresponding log-plots of numerically simulated averaged intensity distributions. Black lines represent the corresponding fits near the center. In the experiment, a laser writing beam power of 50 μW corresponds to the input maximum lattice intensity of 0.7 a.u. in simulations.

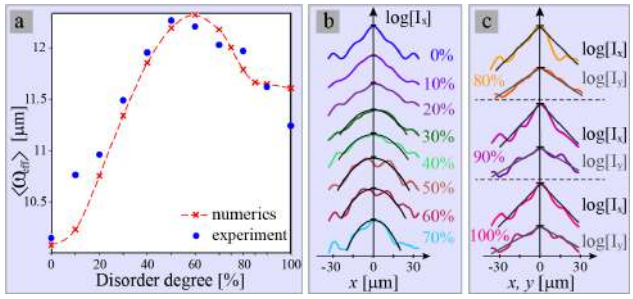

Fig. 4. Light localization dependence on DD. (a) Numerically simulated and experimentally obtained averaged ω_{eff}s at crystal back face versus DD after 2 cm of propagation. (b) Experimental log-plot cross-sections along the x axis of averaged intensity distributions from the back face of the crystal. (c) Experimental log-plots of averaged intensity distributions at the back face of the crystal along different directions (the x and y axes). Experimental log-plot cross-sections in panels (b), (c) are shown for all DDs (dots) from panel (a).

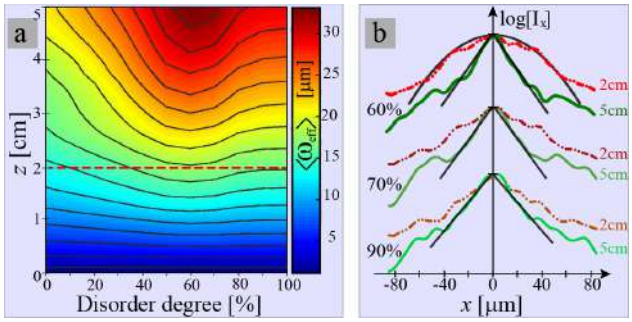

Fig. 5. Light localization dependence on the propagation distance. (a) Numerically simulated averaged ω_{eff} along with the propagation distance for different DDs. The red dashed line indicates the experimental propagation distance. (b) Numerical log-plot cross-section taken along the horizontal direction of averaged intensity distributions after propagation distances of 2 and 5 cm.

To understand if localization also occurs for lower DDs, we investigate the effects of disorder along the propagation distance. Numerically we choose a propagation length longer than the experimental crystal length. We calculate the averaged ω_{eff} along the propagation (for a 5 cm long crystal) for different DDs [Fig. 5(a)]. ω_{eff} increases during propagation for all DDs. The beam expansion is minimal for the original AML and maximal in the region of 50% to 70% DD, which is indicated by a distribution of points where black isolines cross vertical sections. For non-zero DDs up to 60%, ω_{eff} increases at a higher rate during the propagation indicating disorder-enhanced light transport. For DDs larger than 60%, ω_{eff}s increase at a lower rate during the propagation (for all propagation distances) simultaneously with the occurrence of light localization. However, AL is more evident from intensity distribution log-plots for the longer propagation distances. Figure 5(b) depicts log-plots along the x axis of the averaged intensity distributions after propagation lengths of 2 and 5 cm for different DDs. For 60% DD after 2 cm of propagation, the log-plot is fitted with a parabola near the center indicating diffusive-like transport. In contrast, after 5 cm of propagation, the log-plot is linearly fitted near the center indicating light localization. For higher DD, light localization is visible for a shorter propagation distance (2 cm), but more pronounced localization is evident for longer propagation distances also proved by the linear fits of the log-plots. Notwithstanding that we have a higher expansion at 5 cm than at 2 cm (higher ω_{eff}), we observe that the localization is more pronounced at 5 cm than at 2 cm. At longer propagation, it is easier to see that regions of AL and maximum expansion overlap. We further quantify light localization by comparing ξ of such linear fitted log-plots after propagation distances of 2 and 5 cm. ξs we obtain after 2 cm are approximately 30% larger than ξs after 5 cm, which indicates more pronounced AL as the propagation distance increases.

To conclude, we have introduced an advanced experimental approach with the numerical controllable DDs for the realization of disordered AMLs by one parallel induction process. By introducing different DDs, we have realized controllable media for the investigation of light localization effects. Experimentally and numerically, we have investigated linear propagation of the narrow Gaussian probe beam in such disordered aperiodic Mathieu lattices. For all DDs, we have demonstrated disorder-enhanced light transport. AL of light in disordered AMLs is observed for the highest DD. Localization lengths along the x axis are lower than the corresponding localization lengths along the y axis, according to crystal and lattice anisotropy. Nevertheless, for the longer propagation distances, a more pronounced AL is demonstrated. The results we obtained in disordered aperiodic Mathieu lattices are similar to those in disordered quasicrystals and in contrast to those in disordered periodic lattices. In general, our approach can be applied to other kinds of photonic lattices using the presented ideas and methods.

Funding. Ministarstvo Prosvete, Nauke i Tehnološkog Razvoja; Deutscher Akademischer Austauschdienst (57219089).

Acknowledgments. The authors acknowledge funding provided by the Institute of Physics Belgrade and Institute for Multidisciplinary Research, through the grants by the Ministry of Education, Science, and Technological Development of the Republic of Serbia and support by the German Academic Exchange Service (Project 57219089).

Disclosures. The authors declare no conflicts of interest.

Data availability. Data underlying the results presented in this Letter are not publicly available at this time but may be obtained from the authors upon reasonable request.

REFERENCES

1. D. S. Wiersma, P. Bartolini, A. Lagendijk, and R. Righini, Nature **390**, 671 (1997).
2. A. Lagendijk, B. Tiggelen, and D. S. Wiersma, Phys. Today **62**, 24 (2009).
3. B. Kumar, R. Homri, X. Priyanka, S. K. Maurya, M. Lebental, and P. Sebbah, Optica **8**, 1033 (2021).
4. M. Rashidi, H. H. Tan, and S. Mokkapati, Optica **8**, 1160 (2021).
5. T. Schwartz, G. Bartal, S. Fishman, and M. Segev, Nature **446**, 52 (2007).
6. D. M. Jović, M. R. Belić, and C. Denz, Phys. Rev. A **84**, 043811 (2011).
7. D. M. J. Savić, C. Denz, and M. R. Belić, Opt. Lett. **37**, 4455 (2012).
8. U. Naether, J. M. Meyer, S. Stützer, A. Tünnermann, S. Nolte, M. I. Molina, and A. Szameit, Opt. Lett. **37**, 485 (2012).
9. M. Boguslawski, S. Brake, J. Armijo, F. Diabel, P. Rose, and C. Denz, Opt. Express **21**, 31713 (2013).
10. D. M. Jović, Y. S. Kivshar, C. Denz, and M. R. Belić, Phys. Rev. A **83**, 033813 (2011).
11. M. Boguslawski, S. Brake, D. Leykam, A. S. Desyatnikov, and C. Denz, Sci. Rep. **7**, 10439 (2017).
12. L. Levi, M. Rechtsman, B. Freedman, T. Schwartz, O. Manela, and M. Segev, Science **332**, 1541 (2011).
13. Z. Vardeny, A. Nahata, and A. Agrawal, Nat. Photonics **7**, 177 (2013).
14. L. Negro and S. Boriskina, Laser Photonics Rev. **6**, 178 (2012).
15. E. Maciá, Rep. Prog. Phys. **69**, 397 (2006).
16. C. Huang, F. Ye, X. Chen, Y. V. Kartashov, V. V. Konotop, and L. Torner, Sci. Rep. **6**, 32546 (2016).
17. P. Wang, Y. Zheng, X. Chen, C. Huang, Y. V. Kartashov, L. Torner, V. V. Konotop, and F. Ye, Nature **577**, 42 (2020).
18. Q. Fu, P. Wang, C. Huang, Y. V. Kartashov, L. Torner, V. V. Konotop, and F. Ye, Nat. Photonics **14**, 663 (2020).
19. S. V. Boriskina, A. Gopinath, and L. D. Negro, Opt. Express **16**, 18813 (2008).
20. F. Diebel, P. Rose, M. Boguslawski, and C. Denz, Appl. Phys. Lett. **104**, 191101 (2014).
21. M. Boguslawski, N. M. Lučić, F. Diebel, D. V. Timotijević, C. Denz, and D. M. J. Savić, Optica **3**, 711 (2016).
22. B. Freedman, G. Bartal, M. Segev, R. Lifshitz, D. N. Christodoulides, and J. Fleisher, Nature **440**, 1166 (2006).
23. J. V. Vasiljević, A. Zannotti, D. V. Timotijević, C. Denz, and D. M. J. Savić, Phys. Rev. A **96**, 023840 (2017).
24. J. M. Vasiljević, A. Zannotti, D. V. Timotijević, C. Denz, and D. M. J. Savić, Appl. Phys. Lett. **117**, 041102 (2020).
25. Z. Bouchal, Czech. J. Phys. **53**, 537 (2003).
26. J. A. Davis, D. M. Cottrell, J. Campos, M. J. Yzuel, and I. Moreno, Appl. Opt. **38**, 5004 (1999).

Dimensionality crossover of radial discrete diffraction in optically induced Mathieu photonic lattices

Jadranka M. Vasiljević[a], Vladimir P. Jovanović[b], Aleksandar Ž. Tomović[b], Dejan V. Timotijević[1], Radomir Žikic[b], Milivoj R. Belić[c], and Dragana M. Jović Savić[a]

[a]Institute of Physics, University of Belgrade, P.O. Box 68, 11001 Belgrade, Serbia
[b]Institute for Multidisciplinary Research, University of Belgrade, Kneza Višeslava 1, 11030, Belgrade, Serbia
[c]Division of Arts and Sciences, Texas A & M University at Qatar, 23874, Doha, Qatar

ABSTRACT

We demonstrate transitional dimensionality crossover of radial discrete diffraction in optically induced radial-elliptical Mathieu photonic lattices. Varying the order, characteristic structure size, and ellipticity of the Mathieu beams used for the photonic lattices generation, we control the shape of discrete diffraction distribution over the combination of the radial direction with the circular or elliptic. We also investigate the transition from one-dimensional to two-dimensional discrete diffraction by varying the input probe beam position. Discrete diffraction is the most pronounced along the crystal anisotropy direction.

Keywords: Dimensionality crossover, radial discrete diffraction, photonic lattices, discrete diffraction, Mathieu beams, optical induction, strontium barium niobate crystal

1. INTRODUCTION

One of the main areas of research and applications in optics is the control and manipulation of light in photonic lattices.[1] Arrays of evanescently coupled waveguides or photonic lattices are common structures for discrete effects and dynamics studies. When light is focused into one single waveguide and propagates linearly along the array, it will tunnel to the neighboring waveguide and display a distinctive diffraction pattern, with the intensity mainly concentrated in the outer lobes. The discrete diffraction of light[2] was observed in one-dimensional (1D) waveguide arrays[3]and two-dimensional (2D) photonic lattices,[4] both theoretically and experimentally. It is also studied in other systems, like atomic[5,6] and aperiodic[7–10] photonic lattices.

An additional periodicity distortion is produced by the truncation of the periodic photonic lattice, leading to the development of optical surface states that are analogous to the surface states in the electrical theory of periodic systems.[11,12] Surface solitons (optical self-trapped discrete surface waves) have been found in 2D photonic lattices[13] and 1D waveguide arrays.[14,15] Physical systems that exhibit dimensionality crossover have gained significant interest; one such example is the continuous transformation of 1D into a 2D photonic lattice.[16] One can observe intermediate states that do not have 1D or 2D geometry in such systems. An unanswered question regarding these structures remains: How, when, and why does a system transition from one to two dimensions?

Nondiffracting beams are practical for 2D photonic lattice creation as they retain their propagation-invariant structure even with weak nonlinearity.[17] Four principal nondiffracting beam families are exact solutions of the Helmholtz equation in different coordinate systems:[18,19] plane waves in Cartesian, Bessel beams in circular cylindrical,[20] Mathieu beams in elliptic cylindrical,[21] and parabolic beams in parabolic cylindrical coordinates.[22] Mathieu beams are utilized for optical lattice writing, even allowing the development of elliptically formed vortex solitons.[23] They are additionally used for different aperiodic photonic lattices generation by the optical induction technique in photorefractive crystals[10,24] and for particle manipulation.[25]

Further author information: (Send correspondence to Jadranka M. Vasiljević)
Jadranka M. Vasiljević: E-mail: jadranka@ipb.ac.rs

Nonlinear Optics and its Applications 2024, edited by John M. Dudley, Anna C. Peacock, Birgit Stiller, Giovanna Tissoni, Proc. of SPIE Vol. 13004, 130040J
 · 0277-786X · doi: 10.1117/12.3017229

Both experimental and theoretical methods are used in this work to investigate the requirements for discrete diffraction occurrence and its properties in the aperiodic Mathieu photonic lattices. Mathieu beam shape enables the one-pass experimental realization of naturally *truncated aperiodic* photonic lattices, allowing both surface states and discrete diffraction on the surface. We focus on the aperiodic photonic structures in elliptical-radial geometries because they provide a diverse range of shapes, including ellipticity as an additional degree of freedom. They also allow us to consider the dimensionality of discrete diffraction. The lattice period and the refractive index modulation in periodic photonic lattices are uniform over the whole lattice. Contrarily, they are not independent parameters in Mathieu lattices since they are both related to beam characteristics (beam order, characteristic structural size, and beam ellipticity). Due to the aperiodicity of the Mathieu lattice, several probing local settings permit discrete diffraction impacted by the nearest neighbors. Unlike the periodic lattice, during the propagation, the diffracting probe might pass through several local environments, resulting in additional variations in the discrete diffraction effects.

Here, we demonstrate elliptical-radial discrete diffraction in photonic lattices realized by using a single Mathieu beam and a dimensionality crossover of radial discrete diffraction. We can control discrete diffraction in the radial direction and the shape of their distributions in the perpendicular directions by varying the order and characteristic structure size of the used Mathieu beam. By shifting the position of the input probe beam, we observe the transition from 1D to 2D discrete diffraction. In our medium - the photorefractive birefringent cerium-doped strontium barium niobate (SBN61:Ce) - the crystal anisotropy plays a significant role in the discrete diffraction phenomenon. Hence, we observe the most pronounced 2D discrete diffraction along the crystal anisotropy direction.

2. NUMERICAL MODELING AND EXPERIMENTAL REALIZATION OF LINEAR LIGHT PROPAGATION IN MATHIEU PHOTONIC LATTICES

We examine the conditions for discrete diffraction of light by investigating its linear propagation in Mathieu photonic lattices made in the photorefractive medium, SBN61:Ce crystal. By solving the coupled system of two equations, the nonlinear Schrödinger equation of the scalar electric field (propagation equation) and the diffusion equation for the electrostatic potential (potential equation),[26,27] we model linear light propagation in a photonic lattice. Using a spectral split-step beam propagation method,[28] we numerically solve both equations. The following is the propagation equation of the scalar electric field Ψ with longitudinal wave vector k_z:

$$\mathrm{i}\partial_z\Psi + \frac{1}{2k_z}\Delta_\perp\Psi + \frac{k_z}{2n_{\mathrm{o,e}}^2}\delta n^2\Psi = 0, \tag{1}$$

where the wave number $k = 2\pi/\lambda = \sqrt{(k_\perp^2 + k_z^2)}$ is defined by the laser wavelength $\lambda = 532\,\mathrm{nm}$. The potential in the propagation equation is specified by $\delta n^2 = -n_{\mathrm{o,e}}^4 r_{13,33} E$, where $n_\mathrm{e} = 2.325$ and $n_\mathrm{o} = 2.358$ are the extraordinary and ordinary indices, and $r_{13} = 47\,\mathrm{pm/V}$ and $r_{33} = 237\,\mathrm{pm/V}$ are the corresponding electro-optic coefficients of the crystal. The total electric field $E = E_\mathrm{ext} + E_\mathrm{sc}$ that builds up inside the crystal is a superposition of an external electric field $E_\mathrm{ext} = 2000\,\mathrm{V/cm}$ aligned with the optical $c = x$ axis (perpendicular to the propagation direction $z-$axis) and an internal space charge field E_sc that results from the incident intensity distribution within the potential equation. Taking into account the electric bias of the crystal and the photorefractive material response, we solve an anisotropic potential equation for the spatial evolution of the electrostatic potential ϕ_{sc} of the optically-induced space-charge field E_sc

$$\Delta_\perp\phi_\mathrm{sc} + \nabla_\perp \ln(1+I)\cdot\nabla_\perp\phi_\mathrm{sc} = E_\mathrm{ext}\partial_x \ln(1+I), \tag{2}$$

where $I = |\Psi|^2$ is obtained from Eq. (1). Subsequently, Eq. (1) is updated with the optically induced space-charge field

$$E_\mathrm{sc} = \partial_x\phi_{sc}, \tag{3}$$

obtained by solving Eq. (2). This procedure is iteratively repeated along the propagation direction z.

The propagation-invariant Mathieu photonic lattice is numerically generated using the distribution $I = I_{latt}$ from Eq. (1), which we reference as the writing lattice pattern in the experiment.[24] Thus, in distinct numerical

simulations of Eqs. (1) and (2), we first obtain the spatial distribution of I_{latt} by propagating an ordinary Mathieu beam in the weak nonlinear case. Then, we use such a nearly propagation-invariant lattice distribution as a lattice potential, to simulate an extraordinary Gaussian probe beam propagation. In this case, we use the same equations yet modify total intensity distribution $I = I_p + I_{latt}$, where the Gaussian probe beam intensity $I_p = |\Psi|^2$ is obtained from Eq. (1). Not to cause an excessive nonlinear modification in our simulations with the probe beam, I_p is kept sufficiently weak.

To experimentally investigate the linear light propagation of narrow probe Gaussian beam in Mathieu photonic lattices generated in photorefractive SBN61:Ce crystal, we use the experimental setup shown in Fig. 1. As a light source, we use the continuous frequency-doubled Nd:YVO_4 laser that emits at a wavelength of $\lambda = 532\,\text{nm}$. The collimated and expanded laser beam (telescope L1-L2) illuminates as a plane wave the phase-only reflected spatial light modulator (SLM). In this fashion, both the amplitude and phase of the reflected light field are modulated. That is accomplished by addressing to the SLM a precalculated hologram containing the information on the complex light field of the Mathieu lattice, additionally encoded with a blazed grating.[24,29] In this way, an ordinary polarized beam is spatially modulated, and we use it as the writing beam. The second telescope (L3-L4) demagnifies the writing beam to illuminate the crystal. The diffraction pattern of the Mathieu lattice is bandpass filtered in Fourier space (FF).[29] The SBN61:Ce crystal with dimensions of $5 \times 5 \times 20\,\text{mm}^3$ is externally biased with an electric field E_{ext}, aligned with the optical $c = x$ axis, perpendicular to the direction of propagation, z axis, and parallel to the long axis of the crystal. As a result, the ordinary polarized beam, with power P, optically induces a refractive index modulation, writing the lattice in the crystal whose nodes conform with the numerically calculated Mathieu lattice.

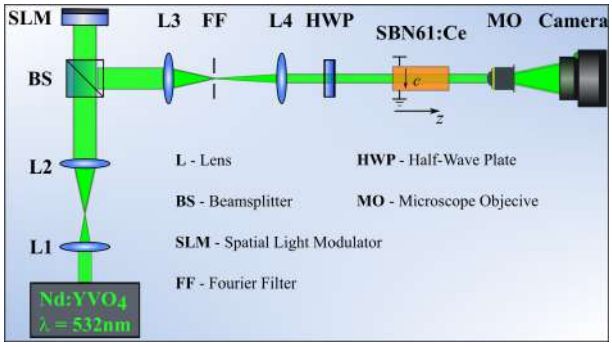

Figure 1. Experimental setup for investigating the light beam propagation in the two-dimensional Mathieu photonic lattice.

After the fabrication of the Mathieu lattice, the writing beam and the external electric field are switched off. Subsequently, an extraordinarily polarized narrow Gaussian probe beam illuminated the specified lattice position, and we observed linear light propagation in the Mathieu photonic lattice. A half-wave plate rotates the probe beam's linear polarization by 90° relative to the writing beam's polarization, addressing the higher electro-optic coefficient. We use an imaging system formed by a microscope objective (MO) with the camera to detect the transverse intensity distribution of the writing and/or probing beam at the back face of the crystal. A probe beam's low power keeps the propagation in a linear regime, and the lattice refractive index modulation remains unmodified (until erased by homogeneous white light). The probe beam, whose full-width-at-half-maximum is $8\,\mu\text{m}$, is directly positioned in front of the crystal, and its transverse position defines the input center. The probe beam size is adequate to illuminate only one lattice site.

3. DIMENSIONALITY CROSSOVER OF RADIAL DISCRETE DIFFRACTION IN MATHIEU PHOTONIC LATTICES

Mathieu beams, as a class of nondiffracting beams, are suitable for the photonic lattices generation. We base our study on even Mathieu beams $M_m(\xi, \eta)$ of order m, which are mathematically described as a product of the angular J_{em} and radial c_{em} Mathieu functions of order m: $M_m(\xi, \eta) = C_m(q) J_{em}(\xi; q) c_{em}(\eta; q)$. A weighting constant $C_m(q)$ depends on the ellipticity parameter $q = f^2 k_t^2/4$, related to the positions of the two foci f and

the transverse wave number $k_t = 2\pi/a$, where a is the characteristic structure size. Elliptical coordinates (ξ, η) are related to the Cartesian coordinates (x, y) by $x + iy = fcosh(\xi + i\eta)$. Mathieu beams M_m, whose intensity distribution I_{latt} is numerically calculated from Eqs. (1) and (2), generate lattices in photorefractive crystal. By changing Mathieu beams parameters, i.e., beam order m, characteristic structure size a, and ellipticity q, we can realize different spatial intensity distributions of Mathieu lattices.[24] The refractive index change and the period of such lattice are not independent but linked via Mathieu beam parameters m, q, and a. Various probing local environments in Mathieu lattices support the formation of different discrete diffraction patterns. By varying the Mathieu lattice ellipticity, the curvature (equal to zero in the periodic lattice) of the lines connecting nearest neighbor sites, and thus the discrete diffraction pattern, changes.

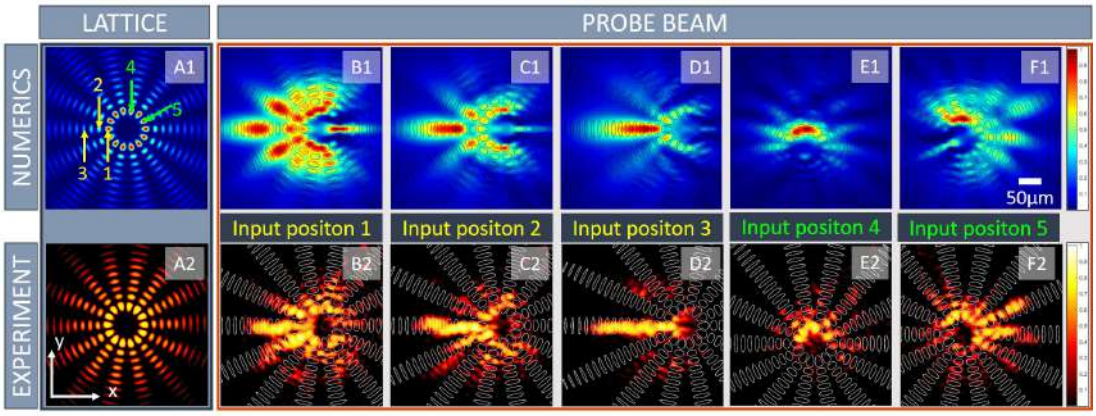

Figure 2. Discrete diffraction in Mathieu lattice for various probe beam input positions. Numerical (A1) and experimental (A2) intensity distribution of the Mathieu lattice at the exit crystal face, with arrows in (A1) indicating various input probe beam positions. The first row shows numerically observed probe beam intensity distributions at the exit crystal face for the input probe beam positions: 1 (B1), 2 (C1), 3 (D1), 4 (E1), and 5 (F1). The second row presents experimentally obtained intensity distributions at the crystal exit face for input probe beam positions: 1 (B2), 2 (C2), 3 (D2), 4 (E2), and 5 (F2). Parameters are: Mathieu lattice order m = 7, ellipticity $q = 0$, and characteristic structure size $a = 30\,\mu m$, $I_{latt} = 1$, experimental lattice writing beam power $P = 0.5mW$.

We first use the Mathieu lattice with zero ellipticity ($q = 0$), where the waveguides are distributed along the ***circles*** and the radial spikes. The input probe beam enters the lattice at the leftmost sites (positions 1, 2, and 3 in Fig. 2 (A1) marked with yellow arrows) of the first, second, and fourth circular waveguide array. All three positions belong to the same radial spike, while positions 4 and 5 (the green arrows in Fig. 2 (A1)) belong to the most intense (inner) circular waveguide array. We compare the numerical and experimental results of the probe beam intensity distributions at the crystal back face after 20 mm propagation. For the first input probe beam position on the lattice edge (marked as position 1 in Fig. 2 (A1)), we observe behavior similar to the 2D discrete diffraction. We will refer to it as the radial 2D discrete diffraction in the truncated elliptical-radial lattice (Fig. 2 (B1), (B2)). On the same circular waveguide array, at the position (right) opposing the entrance of the input probe beam, we notice the out-of-order appearance of intensive spots collecting evanescent leakage of the waveguides from the opposite, left side. When we shift the probe beam input position away from the lattice edge (position 2 in Fig. 2 (A1)), the two-dimensionality of discrete diffraction is less pronounced at the expense of separate circular and radial 1D discrete diffractions. For the third probe beam position (position 3 in Fig. 2 (A1)), one notices separated circular and radial 1D discrete diffractions.

Figure 3 displays the propagation distance dependence of the light intensity of probing beams projected to circles, following the geometry of the lattice. First, we cut the four inner circles (Fig. 3 (A)) at points opposing the excitation positions 1 and 3 (Fig. 2 (A1)) and show flattened probe intensity distributions in Figs. 3 (B) and (C), respectively, exhibiting discrete diffraction along circles. At the cut point (the right-hand side position mentioned in the previous paragraph), i.e., on the edges of distributions in Figs. 3 (B) and (C), the intensity builds up near the exit side of the crystal, an effect predominantly noticeable on the first circles for both input positions. According to probe intensity distributions, for input position 1, discrete diffraction appears along

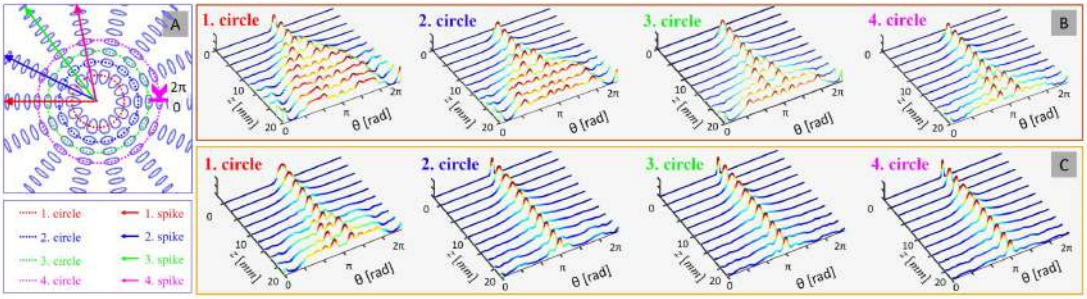

Figure 3. Discrete diffraction along the circular waveguide arrays. Propagation distance (z) dependence of intensity distributions (B) and (C), projected to four circles given in (A), for probing beams entering the lattice at positions 1 and 3 in Fig. 2 (A1), respectively. For each circle, the circumference is measured in the angular coordinate θ starting from the cut point.

the first four circles (Fig. 3 (B)). For input position 3, discrete diffraction is observed only along the first circle (Fig. 3 (C)). The discrete edge diffraction is apparent along some truncated spike waveguide arrays in the radial direction. The transition from 2D to 1D discrete diffraction happens in the truncated elliptical-radial lattice upon changing the input probe beam position.

The anisotropy of our medium (SBN61:Ce crystal) favors the discrete diffraction in some directions. Hence, to investigate the influence of crystal anisotropy on light diffraction in the Mathieu lattice, we consider different input probe beam positions, depicted as positions 1, 4, and 5 in Fig. 2 (A1). Note that all input beam positions lie on one circular waveguide array. If the crystal did not have the anisotropy, the discrete diffraction would have resulted in equal intensity distributions for all three points. However, the crystal possesses anisotropy, and the intensity distributions for the chosen input beams are not identical (Figs. 2(B), (E), and (F)). Therefore, in such lattices, 2D discrete diffraction is observable *only* when the input probe beam enters waveguides that are located at the lattice symmetry axis parallel to the crystal anisotropy direction (c-axis) (Fig. 2(B)).

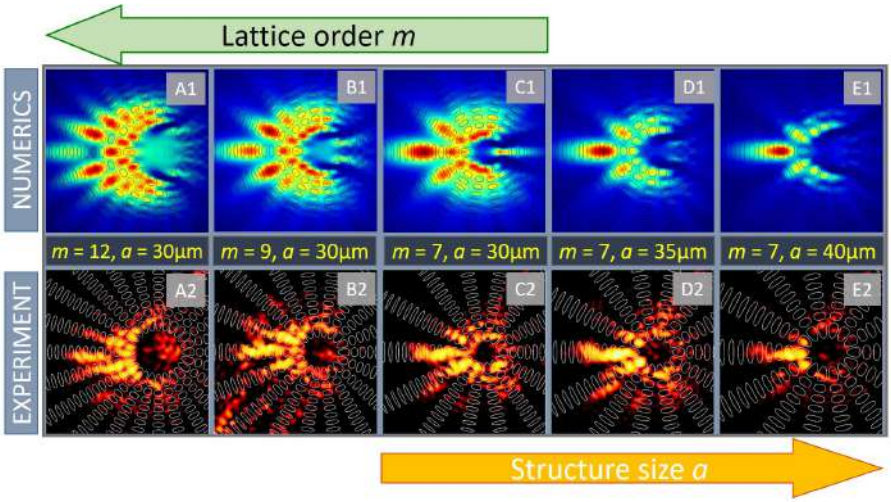

Figure 4. Influence of Mathieu lattice order m and structural size a on the discrete diffraction patterns in elliptical waveguide arrays. Numerically (A1-E1) and experimentally (A2-E2) observed intensity distributions of the probe beam at the exit crystal face for parameters m and a, marked in each panel. The ellipticity $q = 5$, and other parameters are as in Fig. 2.

Finally, we investigate how lattice order m and characteristic structure size a influence discrete diffraction patterns (Fig. 4). Mathieu lattice ellipticity q is set to 5 to observe the effects of discrete diffraction for different curvatures. Hence, the waveguide arrays are distributed along the ***ellipse***, as well as along the radial spikes. We

examined the probe beam propagation for three lattice orders, $m = 7,\ 9$, and 12 (Fig. 4 (A-C)). With increasing order m, the number of spike waveguide arrays rises, leading to more pronounced 2D discrete diffraction. The effect of tree characteristic structure sizes, $a = 30,\ 35$, and 40 μm, on descrete diffraction in Mathieu lattices was analyzed (Fig. 4 (C-E)). When characteristic structure size a increases, the distance between neighboring sites grows, lowering the order of discrete diffraction (from 2D to 1D). Controlling m and a, we can maintain optimal conditions for 1D, 2D, or intermediate discrete diffractions in certain regions, and with the structure size a variation, we can move those regions.

4. CONCLUSION

In conclusion, we presented an experimental and numerical method for obtaining radial and angular discrete diffraction in various Mathieu lattices. Mathieu photonic lattices are optically induced in a photorefractive crystal through one-pass creation in the experiment. They are also a kind of truncated lattices that could support surface states. Mathieu photonic structures have a broad spectrum of shapes and ellipticity as an additional degree of freedom, with the waveguides arranged along circles, ellipses, hyperbolas, and radial spikes. We control radial discrete diffraction by varying the order and characteristic structure size of Mathieu beams utilized for photonic lattice induction. We observed a dimensionality crossover of radial discrete diffraction from 1D to 2D discrete diffraction by shifting the position of the input probe beam. The most pronounced 2D discrete diffraction is observed along the crystal anisotropy direction. Our approach provides branching 1D discrete diffraction along circle/ellipse and spike waveguide arrays in truncated photonic lattices. The findings from this work pave the way for exploiting light propagation in novel classes of optical lattices without limitation to the ones studied here. The adaptability and reconfigurability of light-guiding structures are essential in allowing functionality, demonstrating a substantial advancement in photonics nowadays and making an important step towards novel, innovative waveguiding applications and light routing approaches. They should be of great importance in capacity-enhanced optical information processing applications.

ACKNOWLEDGMENTS

This work was supported by funding provided by the Institute of Physics Belgrade through the grants by the Ministry of Science, Technological Development and Innovations of the Republic of Serbia, by the Ministry of Science, Technological Development and Innovation of the Republic of Serbia (Contract No. 451-03-66/2024-03/200053) and by the Science Fund of the Republic of Serbia, **GRANT No 7714356, IDEAS - CompsLight**.

REFERENCES

[1] Lederer, F., Stegeman, G. I., Christodoulides, D. N., Assanto, G., and Silberberg, M. S. Y., "Discrete solitons in optics," *Physics Reports* **463**, 1–126 (2008).

[2] Christodoulides, D. N., Lederer, F., and Silberberg, Y., "Discretizing light behaviour in linear and nonlinear waveguide lattices," *Nature* **424**, 817–823 (2003).

[3] Pertsch, T., Zentgraf, T., Peschel, U., Bräuer, A., and Lederer, F., "Anomalous refraction and diffraction in discrete optical systems," *Phys. Rev. Lett.* **88**, 093901 (Feb 2002).

[4] Fleischer, J. W., Segev, M., Efremidis, N. K., and Christodoulides, D. N., "Observation of two-dimensional discrete solitons in optically induced nonlinear photonic lattices," *Nature* **422**, 147–150 (2003).

[5] Yuan, J., Zhang, H., Wu, C., Chen, G., Lirong Wang, L. X., and Jia, S., "Creation and control of vortex-beam arrays in atomic vapor," *Laser and Photonics Rev.* **5**(17), 2200667 (2023).

[6] Yuan, J., Wu, C., Wang, L., Chen, G., and Jia, S., "Observation of diffraction pattern in two-dimensional optically induced atomic lattice," *Opt. Lett.* **44**, 4123–4126 (Sep 2019).

[7] Negro, L. and Boriskina, S., "Deterministic aperiodic nanostructures for photonics and plasmonics applications," *Laser and Photonics Rev.* **6**, 178–218 (2012).

[8] Vardeny, Z., Nahata, A., and Agrawal, A., "Optics of photonic quasicrystals," *Nature Photonics* **7**, 177 – 187 (2013).

[9] Boguslawski, M., Lučić, N. M., Diebel, F., Timotijević, D. V., Denz, C., and Savić, D. M. J., "Light localization in optically induced deterministic aperiodic fibonacci lattices," *Optica* **3**, 711–717 (Jul 2016).

[10] Vasiljević, J. M., Zannotti, A., Timotijević, D. V., Denz, C., and Savić, D. M. J., "Light propagation in aperiodic photonic lattices created by synthesized mathieu–gauss beams," *Appl. Phys. Lett.* **117**, 041102 (2020).

[11] Suntsov, S., Makris, K. G., Siviloglou, G. A., Iwanow, R., Schiek, R., Christodoulides, D. N., Stegeman, G. I., Morandotti, R., Yang, H., Salamo, G., Volatier, M., Aimez, V., Arès, R., Sorel, M., Min, Y., Sohler, W., Wang, X., Bezryadina, A., and Chen, Z., "Observation of one- and two-dimensional discrete surface spatial solitons," *Journal of Nonlinear Optical Physics & Materials* **16**(04), 401–426 (2007).

[12] Kivshar, Y. S., "Nonlinear tamm states and surface effects in periodic photonic structures," *Laser Phys. Lett.* **10**, 703–713 (2008).

[13] Wang, X., Bezryadina, A., Chenand, Z., Makris, K. G., Christodoulides, D. N., and Stegeman, G. I., "Observation of two-dimensional surface solitons," *Phys. Rev. Lett.* **98**, 123903 (Mar 2007).

[14] Makris, K. G., Suntsov, S., Christodoulides, D. N., Stegeman, G. I., and Hache, A., "Discrete surface solitons," *Opt. Lett.* **30**, 2466–2468 (Sep 2005).

[15] Rosberg, C. R., Neshev, D. N., Krolikowski, W., Mitchell, A., Vicencio, R. A., Molina, M. I., and Kivshar, Y. S., "Observation of surface gap solitons in semi-infinite waveguide arrays," *Phys. Rev. Lett.* **97**, 083901 (Aug 2006).

[16] Szameit, A., Kartashov, Y. V., Dreisow, F., Heinrich, M., Pertsch, T., Nolte, S., Tünnermann, A., Vysloukh, V. A., Lederer, F., and Torner, L., "Soliton excitation in waveguide arrays with an effective intermediate dimensionality," *Phys. Rev. Lett.* **102**, 063902 (Feb 2009).

[17] Zannotti, A., Vasiljević, J. M., Timotijević, D. V., Savić, D. M. J., and Denz, C., "Morphing discrete diffraction in nonlinear mathieu lattices," *Opt. Lett.* **44**, 1592–1595 (Apr 2019).

[18] Berry, M. V. and Balazs, N. L., "Nonspreading wave packets," *Am. J. Phys.* **47**, 264 – 267 (1979).

[19] Kalnins, E. G. and W. Miller, J., "Lie theory and separation of variables. 9. orthogonal r-separable coordinate systems for the wave equation $\psi_{\rm tt} - \triangle_2 \psi = 0$," *J. Math. Phys.* **17**, 331 – 355 (1976).

[20] Durnin, J., Miceli, J. J., and Eberly, J. H., "Diffraction-free beams," *Phys. Rev. Lett.* **58**, 1499 – 1501 (1987).

[21] Gutiérrez-Vega, J. C., Iturbe-Castillo, M. D., and Chávez-Cerda, S., "Alternative formulation for invariant optical fields: Mathieu beams," *Opt. Lett.* **25**, 1493 – 1495 (2000).

[22] Bandres, M. A., Gutiérrez-Vega, J. C., and Chávez-Cerda, S., "Parabolic nondiffracting optical wave fields," *Opt. Lett.* **29**, 44–46 (2004).

[23] Vasiljević, J. M., Zannotti, A., Timotijević, D. V., Denz, C., and Jović Savić, D. M., "Elliptical vortex necklaces in mathieu lattices," *Phys. Rev. A* **97**, 033848 (Mar 2018).

[24] Vasiljević, J. V., Zannotti, A., Timotijević, D. V., Denz, C., and Savić, D. M. J., "Creating aperiodic photonic structures by synthesized mathieu-gauss beams," *Phys. Rev. A* **96**, 023840 (2017).

[25] Dholakia, K. and Čižmár, T., "Shaping the future of manipulation," *Nature Photonics* **5**, 335 – 342 (2011).

[26] Zozulya, A. A. and Anderson, D. Z., "Propagation of an optical beam in a photorefractive medium in the presence of a photogalvanic nonlinearity or an externally applied electric field," *Phys. Rev. A* **51**, 1520–1531 (Feb 1995).

[27] Timotijević, D. V., Vasiljević, J. M., and Savić, D. M. J., "Numerical methods for generation and characterization of disordered aperiodic photonic lattices," *Opt. Express* **30**, 7210–7224 (Feb 2022).

[28] Agrawal, G., [*Nonlinear Fiber Optics*], Academic Press, 5th ed. (2012).

[29] Davis, J. A., Cottrell, D. M., Campos, J., Yzuel, M. J., and Moreno, I., "Encoding amplitude information onto phase-only filters," *Appl. Opt.* **38**, 5004 – 5013 (1999).

Light propagation in disordered aperiodic Mathieu photonic lattices

Jadranka M. Vasiljević[1,*], *Dejan V.* Timotijević[2], and *Dragana M.* Jović Savić[1]

[1]Institute of Physics, University of Belgrade, P.O. Box 68, 11001 Belgrade, Serbia
[2]Institute for Multidisciplinary Research, University of Belgrade, Kneza Višeslava 1, 11030, Belgrade, Serbia

Abstract. We present the numerical modeling of two different randomization methods of photonic lattices. We compare the results of light propagation in disordered aperiodic and disordered periodic lattices. In disordered aperiodic lattice disorder always enhances light transport for both methods, contrary to the disordered periodic lattice. For the highest disorder levels, we detect Anderson localization for both methods and both disordered lattices. More pronounced localization is observed for disordered aperiodic lattice.

1 Introduction

Anderson localization (AL), a well-known phenomenon in solid-state physics [1] is transferred to other fields like ultracold atoms, matter, light or sound waves [2], and demonstrated in various customized configurations [3–6]. The physics of periodic photonic systems has fundamental importance. Still, deviations from periodicity are significant as they may result in higher complexity, like the realization of photonic quasicrystals, the structures that are between periodic and disordered ones. Heretofore, light propagation properties have been studied in periodic photonic lattices [7, 8], as well as in disordered ones [3, 9, 10]. However, the quasiperiodic and aperiodic photonic lattices are merged as a further attractive research field for light propagation.

In our previous studies, we introduced aperiodic Mathieu structures with controllable complexity [11] and we studied light localization in them [12]. In such lattice, light expansion is hindered in comparison to periodic lattice and nonlinear light localization is demonstrated [12]. Randomization of periodic lattices can lead to AL [3, 9] or its suppression [13], while disordered quasiperiodic Penrose lattice can support AL and disorder-enhanced transport (DET) [14].

In this paper, we present two numerical methods for controllable randomization of photonic lattices and study disorder level (DL) influence on light propagation. For both methods, we numerically investigate the linear light propagation in disordered aperiodic Mathieu (DA) and disordered periodic (DP) lattices. For all DLs, we observe DET and AL is verified for higher DLs in DA lattices, for both methods. In contrast, in DP lattices disorder suppress diffraction and AL is observed for higher DLs. Localization length differs along different transverse directions owing to the crystal and lattice anisotropy. We confirm a more pronounced localization for DA lattices in both directions and both methods.

*e-mail: jadranka@ipb.ac.rs

2 Light propagation in DA and DP lattics

Two-dimensional disordered structures ***DS***, with an adjustable DL, are numerically realized by combining an original structure ***S*** with a disorder pattern ***D*** according to the relation $A_{DS} = (1-p) * A_S + p * A_D$, where A is the field amplitude, and parameter p is the relative contribution of the original structure and disorder pattern, i.e. DL. To ensure propagation invariant structures with the same propagation constant, we preset the Fourier spectrum of the disorder pattern, numerically calculated by interfering plane waves with constant amplitude and random phases, to be located on the same circle with radius k as the original structure [15]. As the original structure we use an aperiodic Mathieu structure created as in our paper [11], or square lattice with period d equal to the characteristic structure size $a = 25\,\mu$m of Mathieu beams used for the creation of the aperiodic structure. Disorder pattern's mean grain size $2\pi/k$ is equal to a of Mathieu beams. A case when the maximum lattice intensity I_{m} of the disordered lattice $I_{DL} = |A_{DS}|^2$ for each DL is unscaled, we will refer as M1, and M2 is the case when I_{DL} is scaled with I_{in} for each DL. For both methods, an increase of DL modifies the transverse intensity distribution of the original structure until completely substitutes it with the disorder pattern. For the same DL, the spatial intensity distributions of the disordered lattices are the same for both methods, but they differ in waveguides depths. For both methods, I_{m} dependencies of DL for DA and DP lattices are almost the same (Fig. 1 (A)). Opposite to the periodic lattice, our aperiodic lattice is not uniform in waveguide's distances, and their depths vary. We calculate averaged lattice intensity $I_{\mathrm{avg}} = \sum_{\mathbf{r}} I_{DL}(\mathbf{r})$ of DA and DP lattices for both methods (Fig. 1 (B)). For both methods, I_{avg}s are lower for DA than for DP lattices. For M1, I_{m} and I_{avg} are lower than for M2.

We study the difference in light propagation in DA and DP lattices realized with these methods. We use intensity distributions of disordered structures I_{DL} in numerical simulation of the light propagation along the z-axis in disordered lattices in a photorefractive crystal, numerically

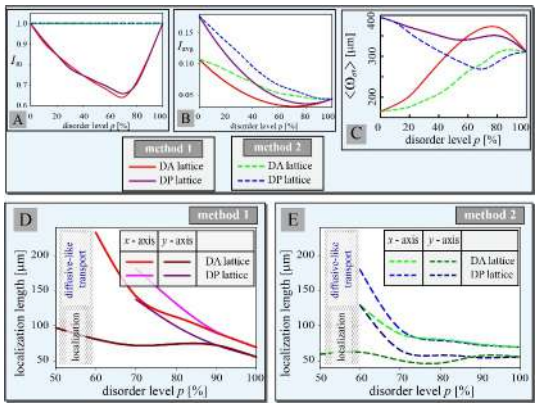

Figure 1. Methods differences of realization and light propagation in DA and DP lattices. (A) I_m, (B) I_{avg} of DA and DP lattices versus DL for different methods. (C) $\langle\omega_{eff}\rangle$ and (D)-(E) localization lengths along the x- and y-axis for M1 and M2, respectively versus DLs after 10 cm of propagation.

described by solving a system of equations as explained in Ref. [12]. We statistically analyze the propagation of a narrow Gaussian probe beam, of an FWHM of 8 μm, for different excitation positions selected to involve various local environments of the disordered lattice [14]. We realize such analysis for various DLs, using only one disorder pattern, averaging 64 different intensity distributions after 10 cm propagation distance.

According to relation $W_{eff} = \sqrt{\mathrm{IPR}(z)}$, where $\mathrm{IPR}(z)$ is the inverse participation ratio [3], we calculate the effective beam width W_{eff} and determine a range of DL where DET and light localization are obtained. In Fig. 1 (C) we show scaled averaged effective beam widths $\langle\omega_{eff}\rangle = W_{eff}(z)/(W_{eff}(0)/FWHM)$. In the DA lattice with any percent of disorder, $\langle\omega_{eff}\rangle$ is greater than in the lattice without disorder, specifying DET for both methods. A maximum DET is indicated with $\langle\omega_{eff}\rangle$ highest value noticed at 80% for M1 and 90% for M2. Further increase of DL decreases $\langle\omega_{eff}\rangle$, indicating the possibility of AL occurrence. $\langle\omega_{eff}\rangle$ has a greater value for M1 than for M2, denoting a more pronounced DET for M1. Opposite in the DP lattice, $\langle\omega_{eff}\rangle$ decreases up to the minimum values which occur at 60% for M1 and 70% for M2. With the further increase of DL, $\langle\omega_{eff}\rangle$ increases for M2, while for M1 fluctuates. We examine the averaged transverse intensity distributions and corresponding log-plots of such averaged intensity distributions (not shown here). When the log-plots intensity profiles are linearly fitted around the center, we consider AL is confirmed [10]. In the region of DL where AL occurs, we obtain localization length by fitting intensity profiles with the exponential function [10], along the x and y-axis. For DA and DP lattices, in Figs. 1 (D)-(E) we show localization lengths for M1 and M2, respectively. For both methods, more pronounced localization is visible along the y-axis where localization lengths have lower values compared to the x-axis, due to the crystal and lattice anisotropy. AL occurs at different DLs along different directions, along the y-axis appears for lower DL than along the x-axis.

3 Conclusion

We presented two different methods for the creation of disordered photonic lattices with adjustable DL. We numerically studied light propagation in DA and DP lattices. For both methods, we observed enhanced light transport for all DLs but AL of light for higher DLs in DA lattice, contrary in DP lattice, we only observed AL for higher DLs. More pronounced localization is demonstrated in DA lattices for both methods and for M2 in both DA and DP lattices. Due to the crystal and lattice anisotropy, localization lengths differ in different directions.

Acknowledgements

This paper is supported by the Institute of Physics Belgrade and Institute for Multidisciplinary Research through the grants by the Ministry of Education, Science and Technological Development of the Republic of Serbia and by the Science Fund of the Republic of Serbia, Grant No 7714356, IDEAS - CompsLight.

References

[1] P. W. Anderson, Phys. Rev. **109**, 1492 (1958).
[2] A. Lagendijk, B. Tiggelen, D. S. Wiersma, Phys. Today **62**, 24 (2009).
[3] T. Schwartz, G. Bartal, S. Fishman, M. Segev, Nature **446**, 52 (2007).
[4] D. M. Jović, Y. S. Kivshar, C. Denz, M. R. Belić, Phys. Rev. A **83**, 033813 (2011).
[5] D. U. Naether, J.M. Meyer, S. Stützer, A. Tünnermann, S. Nolte, M. I. Molina, A. Szameit, Opt. Latt. **37**, 485 (2012).
[6] D. M. Jović, C. Denz, M. R. Belić, Opt. Lett. **37**, 4455 (2012).
[7] H. S. Eisenberg, Y. Silberberg, R. Morandotti, J. S. Aitchison, Phys. Rev. Lett. **85**, 1863 (2000).
[8] J. W. Fleischer, M. Segev, N. K. Efremidis, D. N. Christodoulides, Nature **422**, 147 (2003).
[9] Y. Lahini, A. Avidan, F. Pozzi, M. Sorel, R. Morandotti, D. N. Christodoulides, Y. Silberberg, Phys. Rev. Lett. **100**, 013906 (2008).
[10] M. Boguslawski, S. Brake, J. Armijo, F. Diabel, P. Rose, C. Denz, Opt. Express **21**, 31713 (2013).
[11] J. V. Vasiljević, A. Zannotti, D. V. Timotijević, C. Denz, D. M. Jović Savić, Phys. Rev. A **96**, 023840 (2017).
[12] J. V. Vasiljević, A. Zannotti, D. V. Timotijević, C. Denz, D. M. Jović Savić, Appl. Phys. Lett. **117**, 041102 (2020).
[13] S. Longhi, Opt. Lett. **46**, 2872 (2021).
[14] L. Levi, M. Rechtsman, B. Freedman, T. Schwartz, O. Manela, M. Segev, Science **332**, 1541 (2011).
[15] Z. Bouchal, Czech. J. Phys. **53**, 537 (2003).

Light propagation in disordered aperiodic Mathieu lattices generated with two different randomization methods

Jadranka M. Vasiljević[a], Dejan V. Timotijević[b], and Dragana M. Jović Savić[a]

[a]Institute of Physics, University of Belgrade, P.O. Box 68, 11001 Belgrade, Serbia
[b]Institute for Multidisciplinary Research, University of Belgrade, Kneza Višeslava 1, 11030, Belgrade, Serbia

ABSTRACT

We present the numerical modeling of two different randomization methods of two-dimensional aperiodic photonic lattices based on Mathieu beams, optically induced in a photorefractive media. We numerically study light propagation in such lattices. For both methods, we compare light transport and localization in such lattices along the propagation and for various disorder strengths. For all disorder strengths, a disorder-enhanced light transport is observed. With increasing disorder strength light transport becomes diffusive-like while with further increase of disorder strength, the Anderson localization is observed. For longer propagation distances this transition is more pronounced. The influence of input lattice intensity on the localization effects is studied. We observe more pronounced localization for one of the methods, and different diffraction and localization along different directions, due to the crystal and lattice anisotropy. The difference in light transport and localization between two randomization methods is attributed to various levels of input lattice intensity.

Keywords: light propagation, disordered lattices, Mathieu beams, Anderson localization, disorder-enhanced light transport, diffusive-like transport

1. INTRODUCTION

Some of the fascinating effects observed when light propagation through different types of periodic photonic structures was studied are light discrete diffraction or discrete spatial solitons.[1–3] It was demonstrated that periodic lattices have essential characteristics of photonic crystal structures (Brillouin zones, band structure, etc.) leading to light control by photonic band gaps in space and time. Also, light localization in disordered media was investiagted.[4,5] Anderson localization (AL), a basic phenomenon from solid-state physics has found applications for light waves in different materials,[6–8] Bose-Einstein condensates,[9] and sound waves.[10] It was demonstrated an appreciable change of light propagation in the presence of disorder, the transition from the diffraction of light to spatial AL is observed by increasing disorder strength in different customized configurations.[8,11–14]

Deterministic aperiodic structures are at the intersection between periodic and disorder crystal structures. Various aperiodic and quasiperiodic photonic structures were realized artificially,[15,16] their properties have been studied for light control and manipulation.[17,18] Aperiodic lattices contain non-uniform distances between the lattice waveguides with unequal waveguides intensity depths. Therefore in such lattices in contrast to periodic, light propagation strongly depends on local environments of the probe beam excitation position,[15,19] and linear light diffraction is hampered owing to the aperiodicity.[15,19] Also, aperiodic lattices support nonlinear light localization.[19,20] Still, numerous aperiodic structures exist and have not yet been fully explained or exploited for applications. For instance, Penrose or Fibonacci structures have limited variation in probing local environments, however aperiodic Mathieu lattices[21] with the adjustable spatial and intensity distribution allow the tunable optical response which is provided with numerous different probing local environments, as well as introducing structure anisotropy variability. For the experimental realization of photonic lattices by optical induction technique in general, nondiffracting beams are convenient since they are propagation invariant for weak nonlinearity.[22] Two-dimensional aperiodic photonic lattices based on multiplexing of nondiffracting beams were experimentally realized by the optical induction technique in photorefractive crystal.[21,23]

Author to whom correspondence should be addressed. Electronic mail: jadranka@ipb.ac.rs

Nonlinear Optics and its Applications 2022, edited by Neil G. R. Broderick, John M. Dudley, Anna C. Peacock, Proc. of SPIE Vol. 12143, 121430A · © 2022 SPIE
0277-786X · doi: 10.1117/12.2621228

Besides nonlinear localization, an additional step of light control was the randomization of periodic or quasiperiodic photonic lattices.[7,8,24] Disordering periodic lattices can lead to AL[7,8] or its suppression, referred to as inverse Anderson transition.[25] Disordered quasiperiodic Penrose lattice can support AL and disorder-enhanced transport (DET) which is related to the broadening of eigenfunctions with the disorder.[24] However, an unexplored topic is the control and manipulation of light in other disordered aperiodic lattices. In order to create an appropriate platform for investigation of light propagation effects in disordered aperiodic lattices and study their possible transition to AL or DET, we propose considering randomization of a whole class of aperiodic structures based on Mathieu beams.[21] Since in such a large class of aperiodic structures is difficult to implement an exhaustive theoretical or experimental analysis of light propagation, in this paper, we are focusing on one aperiodic Mathieu structure and numerically model their possible randomizations and probing of resulting disordered lattices.

In this contribution, we introduce the modeling of two different methods for the generation of two-dimensional propagation invariant disordered aperiodic Mathieu lattices with adjustable disorder strength, corresponding to two different experimental realizations using optical induction technique in a photorefractive crystal.[26] We numerically investigate a transverse light localization in such lattices and compare the effects of disorder on light propagation considering two different randomization methods. We examine the influence of propagation distance, for both methods, as well as the lattice intensity influence on the diffraction rate. We demonstrate disorder-enhanced light transport of the probe beams, for all disorder strengths, by gradually adding disorder to the aperiodic Mathieu lattice. Also, we show the conversion from diffusive-like transport to AL for higher disorder strengths. More pronounced localization is demonstrated for longer propagation distances even for lower disorder strengths. We attribute the difference of effective beam width for two randomization methods to varying levels of lattice intensities. We observe more pronounced localization for one of the methods, which is related to shorter localization length for one of the methods. Also, it is shown that localization length differs along different directions, which we attribute to the lattice and crystal anisotropy.

2. TWO NUMERICAL METHODS FOR FORMATION OF DISORDERED APERIODIC LATTICES

Here, we present two methods for the generation of two-dimensional propagation invariant disordered aperiodic photonic lattices with adjustable disorder strength. We formed complex light filed of disordered lattices $\boldsymbol{DL}$ by coherently adding the two-dimensional original structure $\boldsymbol{L}$ and disorder pattern $\boldsymbol{D}$ with same maximum structure intensity according to the relation

$$\varphi_{DL} = (1-p) * \ \varphi_L + p * \ \varphi_D, \tag{1}$$

where φ stands for field amplitude, while intensity distribution of such complex light field display transverse intensity distribution of disordered aperiodic lattice $I_{DL} = |\varphi_{DL}|^2$ with input intensity I_{in}. Parameter p is the relative contribution of the original structure and disorder pattern, which we identify as disorder strength. By varying disorder strength ($0 \leq p \leq 1$) we gradually adjust the level of lattice disorder relative to the original structure. Calculated complex light fields of disordered lattices can be used as the writing light patterns for the generation of two-dimensional photonic lattice by optical induction in the cerium-doped strontium barium niobate (SBN) crystal.[21] Previous studies that applied the optical induction technique for realization of photonic lattices in birefringent SBN crystal, externally biased with an electric field aligned along the optical $c = x$-axis, and perpendicular to the propagation direction (z-axis), used the ordinary polarized writing beam with a laser power P, considered to be fairly linear in SBN crystal.

When the maximum lattice intensity of the resulting disordered lattice for each disorder strength is unscaled, we will refer to that case as the first method (*M1*). The second method (*M2*) is characterized by scaling I_{DL} with I_{in} for each disorder strength. A consequence of distinction in methods accompanies differences in potential experimental realizations. For the proposed fabrication of the disordered aperiodic lattices by the optical induction technique, which corresponds to both methods we can use experimental setup from our previous study[21] using a spatial light modulator to modulated writing beam, producing computer generating hologram. For prospective experimental realization of such disordered aperiodic lattice according to our suggest M1, laser

power of an ordinary polarized writing beam will vary with change of disorder strength, while for M2 it will be constant for each disorder strength.

As the original undisturbed structure $\boldsymbol{L}$ in this paper, we use an aperiodic Mathieu structure designed with combinations of Mathieu-Gauss beams spliced in both transverse dimensions with different offsets, as introduced in our previous paper.[21] Numerically by interfering plane waves with constant amplitude and random phases, we calculated propagation invariant structure with random pattern in transverse dimension, disorder pattern $\boldsymbol{D}$. Also, we adjusted his spectrum in the transverse Fourier space to be located on the same circle with radius k as the original structure,[27] to provide propagation invariant structures with the same propagation constant. The disorder pattern's mean grain size $2\pi/k$ is equal to the characteristic structure size $a = 25\mu m$ of Mathieu Gauss beams, used for the realization of the aperiodic structure.[21]

For both methods, by increasing disorder strength we change the geometry of the original structure shown in Fig. 1 (A) until we completely substitute the original structure with a disorder pattern display in Fig. 1 (B). Transverse intensity distributions of disordered aperiodic lattices with 40% disorder for these two methods are presented in Figs. 1 (C) and (D). As an illustration of Eq. (1) in Fig. 1 (E) we present a single typical intensity cross-section along the x-axis (y-position indicated with a dashed line in Fig. 1 (D)) for disordered aperiodic lattices with 40% disorder for two different methods. In contrast to the periodic lattice, our aperiodic lattice is not uniform in the waveguide's distances and their depths vary. For M1 and M2 spatial intensity distribution of the disordered aperiodic lattices are the same, but they differ in waveguides depths as M2 intensity values are greater than M1 intensity values, as noticeable from red and green plots in Fig. 1 (E).

The difference in methods is caused by choices of intensity scaling, hence, we will investigate and compare the consequences of such scaling options. For both methods, variation of disorder strength p leads to the variation of lattice intensity, effectively correlating disorder strength with lattice intensity and indirectly with optically induced refractive index modulation inside the crystal. For the same disorder strength, lattice intensities differ for M1 and M2, causing a distinction in light propagation characteristics in such disordered lattices. As we mentioned, the disorder strength p changes the lattice intensity, hence in addition to maximum lattice intensity $I_{\max}$, we calculate averaged lattice intensity $I_{\text{avg}} = \sum_{\mathbf{r}} I_{DL}(\mathbf{r}) = \sum_{\mathbf{r}} |\varphi_{DL}(\mathbf{r})|^2$. The resulting differentiation of our methods in $I_{\max}$ and I_{avg} dependence on disorder strength is shown in Figs. 1 (F) and (G), respectively. For M1, the maximum lattice intensity and the averaged lattice intensity of disordered aperiodic decrease from 0% to 70% disorder, afterward increase. For 100% disorder, only the maximum lattice intensity returns to an input value. For M2, the maximum lattice intensity of disordered aperiodic lattice is constant and equal to I_{in} for all disorder strengths, but the averaged lattice intensity always decreases with increasing disorder strength. Both the maximum lattice intensity and the averaged lattice intensity for M1 are lower than for M2, except for 0% and 100% disorder. Assuming the same disorder pattern, both methods produce the same lattices for 0% and 100% disorder strengths we will exclude these two endpoints when we discuss method differences.

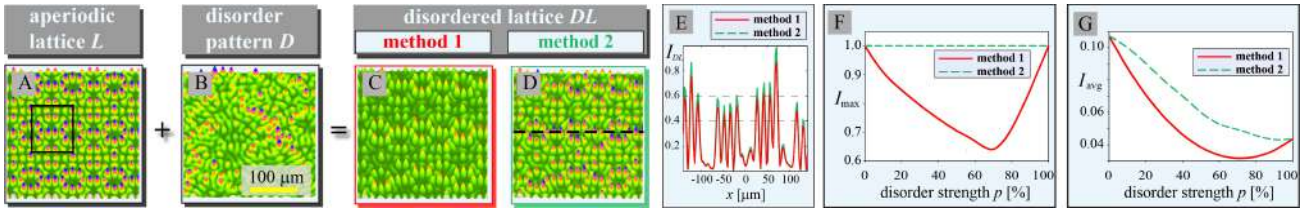

Figure 1. Two methods for generation of disordered aperiodic lattices. The transverse intensity distribution of: (A) aperiodic lattice, an typical pattern marked with black rectangle; (B) disorder pattern; (C) and (D) disordered aperiodic lattices with 40% disorder for M1 and M2, respectively. The displayed area is less than 3% of the whole transverse computational space. (E) Intensity cross-section taken along the x-axis marked with a black dashed line in (D) for disordered aperiodic lattices with 40% disorder for M1 and M2; dashed lines indicate maximum intensities of original lattice and disorder pattern. (F) The maximum lattice intensity and (G) the averaged lattice intensities versus disorder strength p for different methods.

3. NUMERICAL MODELING OF LIGHT PROPAGATION IN OPTICALLY INDUCED DISORDERED APERIODIC MATHIEU LATTICES

In this paper we consider numerically simulations of the weak nonlinear propagation of probe beam in the nolinear photorefractive SBN crystal with disordered aperiodic Mathieu lattices modeled as propagation invariant potential by solving the coupled nonlocal system of two equations: the nonlinear Schrödinger equation as propagation equation and a potential equation,[28] using a spectral split-step beam propagation method.[29] The propagation equation for an initial extraordinary polarized scalar monochromatic electric field ψ (probe beam) with longitudinal wave vector k_z is

$$\mathrm{i}\partial_z\psi + \frac{1}{2k_z}\Delta_\perp\psi + \frac{k_z}{2n_{\mathrm{o,e}}^2}\delta n^2\left(|\psi|^2\right)\psi = 0. \tag{2}$$

The wave number is defined by the wavelength $\lambda = 532\,\mathrm{nm}$ as $k = 2\pi/\lambda = \sqrt{(k_\perp^2 + k_z^2)}$. The potential in propagation equation is given by nonlinear refractive index $\delta n^2\left(|\psi|^2\right) = -n_{\mathrm{o,e}}^4 r_{13,33} E$, where $n_\mathrm{e} = 2.325$ and $n_\mathrm{o} = 2.358$ are the extraordinary and ordinary refractive indices, and $r_{13} = 47\,\mathrm{pm/V}$, $r_{33} = 237\,\mathrm{pm/V}$ are corresponding electro-optic coefficients of photorefractive birefringent SBN crystal, respectively. The electric field $E = E_\mathrm{ext} + E_\mathrm{sc}$ that builds up inside the crystal is a superposition of an external electric field E_ext and an internal space charge field E_sc. The external electric field $E_\mathrm{ext} = 2000\,\mathrm{V/cm}$ is aligned with the optical $c = x$-axis, perpendicular to the $z-$axis, the direction of propagation, that is parallel to the long axis of the crystal while the internal space charge field E_sc is determine by the intensity distribution $I = |\psi|^2$ with a potential equation.

Photorefractive material response, as well as the electric bias of the SBN crystal, are taken into account by deploying the anisotropic, diffusive potential equation for the spatial evolution of the electrostatic potential ϕ_{sc} of the optically induced space-charge field E_sc,

$$\Delta_\perp\phi_\mathrm{sc} + \nabla_\perp \ln\left(1 + I + I_{DL}\right)\cdot\nabla_\perp\phi_\mathrm{sc} = E_\mathrm{ext}\partial_x \ln\left(1 + I + I_{DL}\right), \tag{3}$$

where I is obtained from Eq. (2) and subsequently Eq. (2) is updated with $E_\mathrm{sc} = \partial_x\phi_{sc}$, iteratively. Disordered aperiodic lattice intensity distribution I_{DL}, with input lattice intensity I_in, modeling transverse intensity distribution of nondiffracting pattern homogeneous in the propagation direction, is persistent through iterations. Intensity and spatial distribution of I_{DL} determine $\delta n^2\left(|\psi|^2\right)$ in Eq. (2) through iterations. Potential I_{DL} of disordered lattices ***DL*** is formed according to Eq. (1). Here we abstracted and modeled the whole process of writing propagation invariant disordered lattice through potential I_{DL} in Eq. (3), based on numerical simulation of the writing process and the experimental realization of propagation invariant photonic lattices as in our previous publication.[21] We applied such numerical simulation to find a range of input lattice intensities I_in for which aperiodic Mathieu lattice stays stable and propagation invariant through the SBN crystal.

4. DISORDER-ENHANCED LIGHT TRANSPORT AND LOCALIZATION IN APERIODIC MATHIEU LATTICES

Here, we compare effects along light propagation in disordered aperiodic lattices with adjustable disorder strength generated with two different randomization methods. In order to study the transverse light localization in such lattices we statistically analyzed the propagation of narrow probe beam for different excitation positions, selected to involve various local environments. The probe beam excitation positions are selected from an equidistant 8×8 grid within one complete typical pattern depicted in Fig. 1 (A1). For several disorder strengths, we study averaged transverse intensity distributions, which we averaged over 64 various probe beam intensity distributions and at different propagation distances. We use the same disorder pattern for both methods and all disorder strengths. Hence, we produce the same lattices for 0% and 100% disorder strengths, consequently, we will exclude these two endpoints when we discuss method differences. To further describe light propagation we consider the log-plot profiles of such averaged intensity distributions. The parabolic log-plot fit of the log-plot profiles of averaged intensity distributions indicates diffusive-like transport. The exponential decay determines light localization, or in another word the linear fit of log-plots of such averaged transverse intensity distribution around the center demonstrates AL. In the region of disorder strength where AL occurs, we obtain localization length ξ_x along

the x-axis by fitting intensity profiles $\mathrm{I}(x, y_0)$ with the exponential function $\mathrm{I}(x, y_0) = \exp\left[-2|x - x_0|/\xi_x\right]$, where x_0, y_0 denote the beam center position. The analogous procedure is applied along the y-direction. Furthermore, in order to characterize light propagation and localization, we calculate the effective beam width along the propagation distance z according to the relation $W_{\mathrm{eff}}(z) = \mathrm{P}(z)^{-1/2}$, where $\mathrm{P}(z)$ is the inverse participation ratio.[8] We present scaled averaged effective beam width $\langle\omega_{\mathrm{eff}}\rangle = W_{\mathrm{eff}}(z)/(W_{\mathrm{eff}}(0)/FWHM)$ where $FWHM$ is probe beam full width at half maximum.

First, we study the influence of disorder strength p on light diffraction after various propagation distances. For both methods in the disordered aperiodic lattice with any percent of disorder, scaled averaged effective beam widths $\langle\omega_{\mathrm{eff}}\rangle$ is greater than in the lattice without disorder indicating DET (Fig. 2 (A)). At the shorter propagation distance ($z = 2\,\mathrm{cm}$), $\langle\omega_{\mathrm{eff}}\rangle$s are increasing with increasing disorder strength for both methods. However, a broadening of the beam is more pronounced for longer propagation distances ($z = 10\,\mathrm{cm}$). Hence, we notice that $\langle\omega_{\mathrm{eff}}\rangle$s at the fixed propagation distances are increasing up to the maximum values which occur at disorder strength 80% for M1 and 90% for M2, indicating maximum of DET. With the further increase of disorder strength, $\langle\omega_{\mathrm{eff}}\rangle$s are decreasing indicating the possibility of AL occurrence. Corresponding $\langle\omega_{\mathrm{eff}}\rangle$s have greater values for M1 than for M2, signifying more pronounced DET for M1, which is easily discerned from Fig. 2 (A).

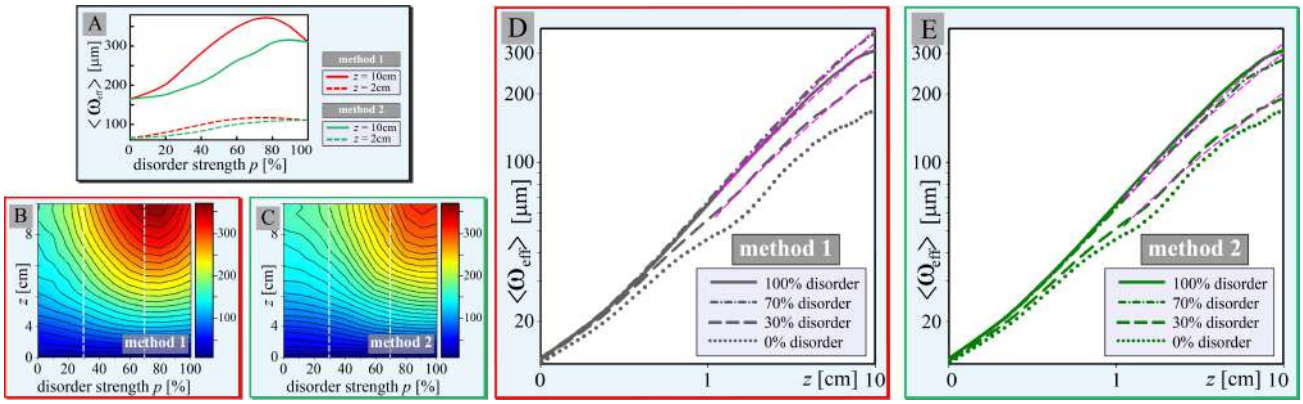

Figure 2. Diffraction dependence on disorder strength and propagation distance for two methods. (A) $\langle\omega_{\mathrm{eff}}\rangle$ versus disorder strength p, for both methods, after 2 cm and 10 cm of propagation. (B)-(C) $\langle\omega_{\mathrm{eff}}\rangle$ for various disorder strengths along the propagation distance for M1 and M2, respectively; the colormaps display $\langle\omega_{\mathrm{eff}}\rangle$ in µm. $\langle\omega_{\mathrm{eff}}\rangle$ along the propagation distance for 0%, 30%, 70%, 100% disorder strengths on a double logarithmic scale for: (D) M1, and (E) M2. Parameters: input Gaussian probe beam $FWHM$ is 8 µm and $I_{\mathrm{in}} = 0.7$.

In order to compare distinction of light propagation between methods we present $\langle\omega_{\mathrm{eff}}\rangle$ along the propagation distance for various disorder strengths for M1 and M2 in Figs. 2 (B), (C) respectively. Maximal beam expansion, noticeable from the distribution of points where black isolines cross vertical sections, is in different regions for different methods. For M1 it is in the region of 60% to 80% disorder strength (Fig. 2 (B)), and in the region of 80% to 90% disorder strength for M2 (Fig. 2 (C)). For both methods, during the propagation $\langle\omega_{\mathrm{eff}}\rangle$ increases for all disorder strengths. To quantify beam expansion rate ν, we examine $\langle\omega_{\mathrm{eff}}\rangle$ as a function of propagation distance z (on a double logarithmic scale) for 4 disorder strengths, display in Figs. 2 (D), (E) for M1 and M2, respectively. We fit $\langle\omega_{\mathrm{eff}}\rangle$ for some disorder strengths by power-law $\langle\omega_{\mathrm{eff}}\rangle(z) \propto z^{\nu}$ (indicated with a pink dashed lines in Figs. 2 (D), (E)). Only for a short propagation distance ($z < 1\,\mathrm{cm}$), beam expansion is almost linear i.e. ballistic transport, designate with $\nu = 1$. For a longer propagation distance (from 1 cm to 10 cm), the beam expansion rate is closest to $\nu = 0.5$ indicating to diffusive-like transport. For M1 the beam expansion rate is maximal for 70% $\nu = 0.52$ and lower $\nu = 0.48$ for both 30% and 100%, while for M2 is maximal for 100% $\nu = 0.48$ and lower for 70% and 30%, $\nu = 0.47$ and $\nu = 0.45$, respectively.

Next, for some disorder strengths and some propagation distances (2 cm and 10 cm), we analyze the averaged transverse intensity distributions and corresponding log-plot cross section along the x-axis (gray/red/green plots) and y-axis (black/dark red/dark green plots) summarized in Fig. 3. For aperiodic lattice without disorder, discrete diffraction of light is demonstrated, also visible from log-plot cross sections. Then we increase disorder

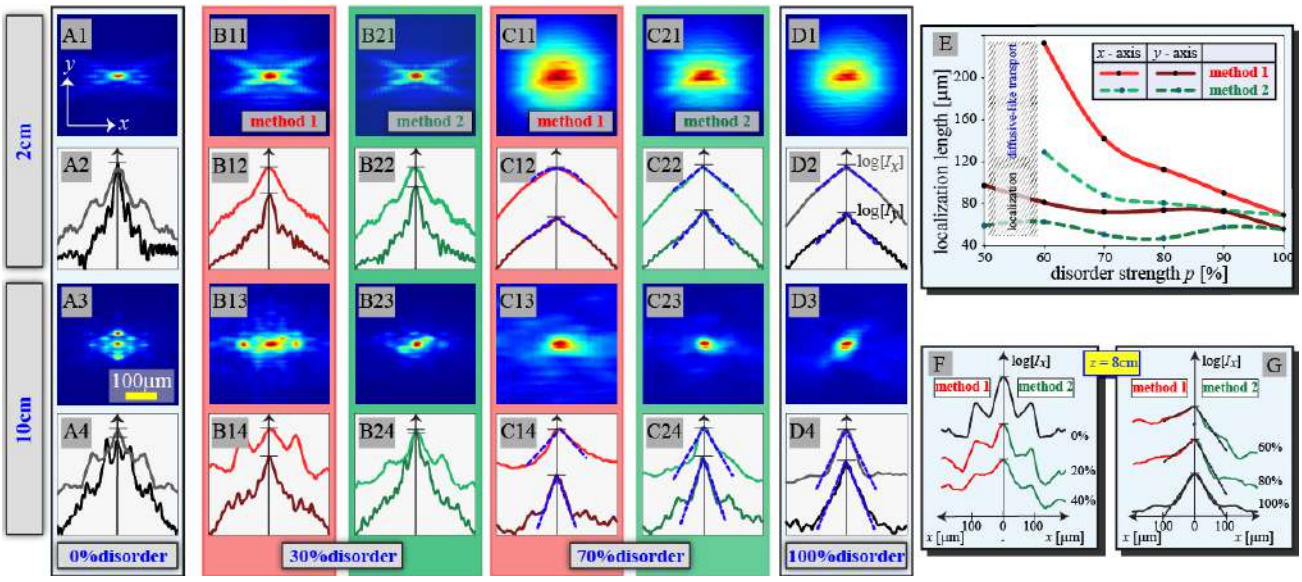

Figure 3. Light transport and localization in disorder aperiodic Mathieu lattice. Numerically averaged intensity distributions at the lattice output and corresponding log-plot cross sections of averaged intensity distributions along the x-axis (gray/red/green plots) and y-axis (black/dark red/dark green plots) (A1) - (D1) and (A2) - (D2), after 2 cm propagation distance and (A3) - (D3) and (A4) - (D24) after 10 cm propagation distance, for different disorder strengths. Blue dashed lines are corresponding linear fits. The horizontal axes span 400 μm in the x- and the y-direction. For each plot, there are two stacked vertical axes, where short horizontal bars are set on 1's. (E) Localization lengths after 10 cm of propagation distances for various disorder strengths along the x- and y-directions. Log-plot cross sections of intensity distributions symmetrical over left and right side of the x-direction, for M1 (left), M2 (right) at different disorder strengths: (F) 0%, 20% and 40% and (G) 60%, 80% and 100% disorder. Other parameters are as in Fig. 2.

strength. For 30% disorder for both methods, more pronounced diffraction i.e. DET, is noticeable from averaged intensity distributions and the log-plot cross sections Figs. 3 (B). More pronounced DET is evident for M1 than for M2. With further increasing disorder strength ($> 30\%$), averaged intensity distributions and the log-plot cross sections are more broadened, still showing DET. Also, for 70% disorder we notice DET for both methods, and at the same time, for longer propagation distance 10 cm, the log-plots cross sections are linearly fitted (Figs. 3 (C14), (C24)), demonstrating AL. The slopes of the fits determine localization lengths ξ. Since they are sharper for M2 than for M1, we conclude we have stronger localization for M2 at 70% disorder. For 100% disorder for all propagation distances (Figs. 3 (D)), we notice even more pronounced localization than for 70% disorder, mark with sharper slope of linear fits.

For both methods we examine light diffraction and localization along the x- and y- directions. For all disorder strengths, the less pronounced light diffraction along the y-direction is noticeable due to the crystal ($r_{33} >> r_{13}$) and lattice anisotropy (Fig. 1 (A)). The interplay of lattice and crystal anisotropy influence is evident for 70% disorder for shorter propagation distances from the log-plot cross sections for M1 (Fig. 3 (C12)). The log-plot along the x-axis is fitted with parabola, showing diffusive-like transport, while the log-plot along the y-axis is linearly fitted, indicating light AL. However, for M2 the log-plots along both directions are linearly fitted, therefore, AL is observed along both directions (Fig. 3 (C22)). For 70% disorder at longer propagation distances for both methods (Figs. 3 (C14), (C24)), and for 100% disorder for all propagation distances (Figs. 3 (D)) we notice liner fits of log plots along the both directions, with sharper slope of linear fits along the y-axis, indicating that AL is stronger in this direction. Since, for 100% disorder, the original lattice does not contribute to anisotropy and the disorder pattern, we use in our study, does not have clear x-y anisotropy preference, we conclude that the direction of crystal anisotropy is primarily cause of more pronounced localization in the y-direction.

For disorder strengths where we observed localization (linearly fitts of log-plot cross sections) we characterize light localization by comparing the localization length along the x- and y-direction. Such localization lengths

after 10 cm of propagation are depicted in Fig. 3 (E). For both methods, more pronounced localization is visible along the y-axis where the localization lengths have lower values compared to the x-axis, due to the crystal and lattice anisotropy. Also, it is noticeable that localization lengths are larger for lower disorder strengths, while their values converge to each other as disorder strength increases, meeting at 100% disorder strength; a similar conclusion stands for $\langle\omega_{\text{eff}}\rangle$s (Fig. 2 (C)). Even more, we notice that AL occurs at different disorder strengths along different directions. Along the y-axis, localization appears for lower disorder strengths than along the x-axis. Figure 3 (E) illustrates diffusive-like transport along the x-axis and light localization along the y-axis for the same 50%-60% disorder region.

The asymmetry of log plots cross-sections of averaged intensity distributions, along any axis and arbitrary disorder strength, is due to the specific occurrence of the used disorder pattern. The influence of the disorder pattern anisotropy (not along x-y-direction) is visible at some probe beam averaged transverse intensity distributions, as can be discerned comparing Figs. 3 (D3) with Fig. 1 (B). To mitigate asymmetry of the log-plot cross-sections we average the left and right sides of such profiles along the x-axis from the center, and we fit them with parabola or linearly. Figures 3 (F) - (G) depict a comparison of localization along the x-axis in our two methods for various disorder strengths after 8 cm) propagation distance. Since for lower disorder strengths significant features of original aperiodic lattices are remaining, the log-plots are not fitted (Fig. 3 (F)). Still, we notice the spreading of the log-plots simultaneous with increased $\langle\omega_{\text{eff}}\rangle$ along the propagation, shown in Figs. 2, indicating DET. For both methods, at disorder strength between 50-60% light diffraction is closest to diffusive-like transport, however the parabolic fits of the log-plots could be attempted with low confidence (goodness of fit < 0.85). After 8 cm of propagation for 60% disorder log-plots are linearly fitted near the center indicating light localization (Fig. 3 (G)). For higher disorder strength (80% and 100%) light localization is noticed also confirmed by linear fits of log-plots. Since the slopes of the fits determine localization lengths, one can see that log-plot fits for the same disorder strength are steeper for M2 showing more pronounced localization for M2 than M1.

In the following, we are studying the independent input lattice intensity I_{in} influence on light diffraction for both methods. We compare $\langle\omega_{\text{eff}}\rangle$s in dependence of disorder strength along propagation distance for 3 different values of I_{in}. Figures 4 (A), (B) summarize $\langle\omega_{\text{eff}}\rangle$ for M1 and M2, respectively. By observing slopes of highlighted lines for constant disorder strength along the propagation distance for each I_{in}, we emphasize the beam expansion. For all disorder strengths and propagation distances, we observe the direct influence of lattice intensity on diffraction, for both methods, where lowering I_{in} causes an increase in $\langle\omega_{\text{eff}}\rangle$.

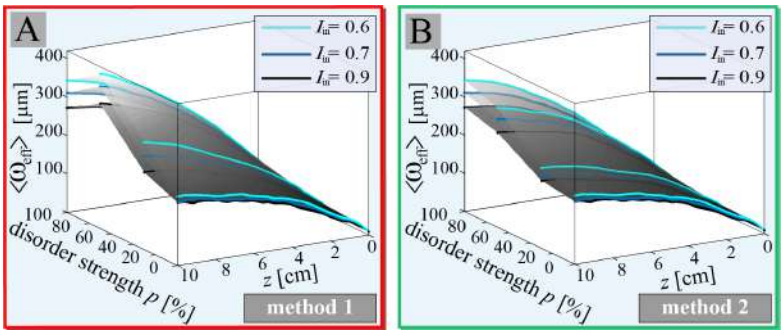

Figure 4. Input lattice intensity I_{in} influence on the light diffraction. (B) M1 and (C) M2: interpolated surfaces of $\langle\omega_{\text{eff}}\rangle$ along the propagation distance for 0%, 30%, 70%, 100% disorder strengths and for various I_{in}. Other parameters are as in Fig. 2.

In previous examinations, we notice differences in methods comparing corresponding averaged transverse intensity distributions, the log-plot cross section along the x-axis and y-axis or quantities $\langle\omega_{\text{eff}}\rangle(z,p)$ and localization lengths. As we describe in Section 2, the main difference in our methods is caused by the difference in the maximum lattice intensity I_{max} with the change of disorder strength p (Fig. 1 (F)). As a consequence, a different variation of the averaged lattice intensities I_{avg} with p for different methods is noticeable from Fig. 1 (G). For both methods, we observed that influence of disorder strength p to $\langle\omega_{\text{eff}}\rangle$ variate with increases of propagation distances (Fig. 4 (A)). After a longer propagation distance (10 cm) we noticed that $\langle\omega_{\text{eff}}\rangle$s dependence on disorder strength p is similar to reciprocal I_{avg}.

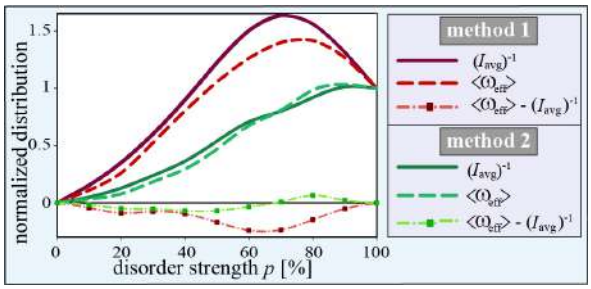

Figure 5. Methods differentiation via $\langle\omega_{\text{eff}}\rangle$ and $(I_{\text{avg}})^{-1}$. Normalized $\langle\omega_{\text{eff}}\rangle$, $(I_{\text{avg}})^{-1}$ and their differences for both methods as a function of disorder strength. Other parameters are as in Fig. 2.

To investigate $\langle\omega_{\text{eff}}\rangle$ and reciprocal averaged lattice intensity $(I_{\text{avg}})^{-1}$ connection we normalize them according to relation $F(p)/(F(1)-F(0))-F(0)$, where F is $\langle\omega_{\text{eff}}\rangle$ or $(I_{\text{avg}})^{-1}$. For both methods, we display such normalized values, as well as their differences in Fig. 5. We conclude that $\langle\omega_{\text{eff}}\rangle$ is strongly influenced with the variation of $(I_{\text{avg}})^{-1}$ with disorder strength for longer propagation distances and for narrow probe beam width, since variations of normalized $\langle\omega_{\text{eff}}\rangle$ closely follow $(I_{\text{avg}})^{-1}$ for both methods. M2 has a minor deviation of $\langle\omega_{\text{eff}}\rangle$ from $(I_{\text{avg}})^{-1}$ versus p, while for M1 a slightly more prominent deviation is visible. Also, for M2 we noticed more pronounced localization in both directions in comparison to M1, hence, we can connect lattice intensity with AL strength. Additionally for M1, a dip of deviation of $\langle\omega_{\text{eff}}\rangle$ from $(I_{\text{avg}})^{-1}$ versus p we can associate with a sharp minimum of $I_{\max}$ and I_{avg} versus p (Figs. 1 (F) - (G)) which occur at the same disorder strength. As we prove in Fig. 4, light diffraction is reverse proportional to input lattice intensity. Hence, for the minimum of the maximum lattice intensity in M1, we have the highest $\langle\omega_{\text{eff}}\rangle$ (maximal DET). The narrow probe beam for low lattice intensity diffracts the most, but at longer propagation distances $\langle\omega_{\text{eff}}\rangle$ does not reach the variation of I_{avg} as at minimal lattice intensities beam already rapidly expanded early in propagation. By a difference of $\langle\omega_{\text{eff}}\rangle$ and $(I_{\text{avg}})^{-1}$ a deviation of these two quantities that contain the influence of parameters not directly connected to the lattice intensity, such as lattice and beam shapes, can be quantified.

5. CONCLUSION

In summary, we presented two different theoretical methods for the realization of two-dimensional disordered aperiodic photonic lattices with adjustable disorder strength optically induced in a photorefractive media. We numerically investigate light propagation in disordered aperiodic Mathieu lattices. Comparing the effective beam width along the propagation distance for various disorder strengths, averaged transverse intensity distributions, the log-plot profiles of such averaged intensity distributions, and localization lengths along different directions we characterize light transport and localization for two methods. For both methods, we observed enhanced light transport for all disorder strengths but AL of light for higher disorder strengths. Localization effects are more pronounced for longer propagation distances. More pronounced localization is observed for M2 than M1, and we attributed the difference between the two methods to various levels of lattice intensity. We observe that localization length differs along different directions, due to the crystal and lattice anisotropy. According to the investigation we present in this study we suggest diminishing the influence of lattice intensity for studying the dependence of AL and DET on disorder strength. We propose a further modification of our M2 in which averaged intensity levels would be equalized for every disorder strength used.

ACKNOWLEDGMENTS

The authors acknowledge funding provided by the Institute of Physics Belgrade and Institute for Multidisciplinary Research, through the grants by the Ministry of Education, Science, and Technological Development of the Republic of Serbia and by the Science Fund of the Republic of Serbia, GRANT No 7714356, IDEAS - CompsLight.

REFERENCES

[1] Joannopoulos, J. D., Johnson, S. G., Winn, J. N., and Meade, R. D., [*Photonic Crystals: Molding the Flow of Light (Second Edition)*], Princeton University Press (2008).

[2] Pertsch, T., Zentgraf, T., Peschel, U., Bräuer, A., and Lederer, F. *Phys. Rev. Lett.* **88**, 093901 (2002).
[3] Lederer, F., Stegeman, G. I., Christodoulides, D. N., Assanto, G., Segev, M., and Silberberg, Y. *Physics Reports* **463**(1), 1–126 (2008).
[4] Wiersma, D. S., Bartolini, P., Lagendijk, A., and Righini, R. *Nature* **390**, 671 – 673 (1997).
[5] Lagendijk, A., Tiggelen, B., and Wiersma, D. S. *Phys. Today* **62**, 24–29 (2009).
[6] Pertsch, T., Peschel, U., Kobelke, J., Schuster, K., Bartelt, H., Nolte, S., Tünnermann, A., and Lederer, F. *Phys. Rev. Lett.* **93**, 053901 (2004).
[7] Lahini, Y., Avidan, A., Pozzi, F., Sorel, M., Morandotti, R., Christodoulides, D. N., and Silberberg, Y. *Phys. Rev. Lett.* **100**, 013906 (2008).
[8] Schwartz, T., Bartal, G., Fishman, S., and Segev, M. *Nature* **446**, 52–55 (2007).
[9] Roati, G., D'Errico, C., Fallani, L., Fattori, M., Fort, C., Zaccanti, M., Modugno, G., Modugno, M., and Inguscio, M. *Nature* **453**, 895 (2008).
[10] Maynard, J. D. *Rev. Mod. Phys.* **73**, 401 (2001).
[11] Szameit, A., Kartashov, Y. V., Zeil, P., Dreisow, F., Heinrich, M., Keil, R., Nolte, S., Tünnermann, A., Vysloukh, V., and Torner, L. *Opt. Lett.* **35**(8), 1172–1174 (2010).
[12] Martin, L., Giuseppe, G. D., Perez-Leija, A., Keil, R., Dreisow, F., Heinrich, M., Nolte, S., Szameit, A., Abouraddy, A. F., Christodoulides, D. N., and Saleh, B. E. A. *Opt. Express* **19**(14), 13636–13646 (2011).
[13] Jović, D. M., Belić, M. R., and Denz, C. *Phys. Rev. A* **84**, 043811 (2011).
[14] Jović, D. M., Kivshar, Y. S., Denz, C., and Belić, M. R. *Phys. Rev. A* **83**, 033813 (2011).
[15] Boguslawski, M., Lučić, N. M., Diebel, F., Timotijević, D. V., Denz, C., and Savić, D. M. J. *Optica* **3**, 711 – 716 (2016).
[16] Lučić, N. M., Savić, D. M. J., Piper, A., Ž. Grujić, D., Vasiljević, J. M., Pantelić, D. V., Jelenković, B. M., and Timotijević, D. V. *J. Opt. Soc. Am. B* **32**(7), 1510–1513 (2015).
[17] Negro, L. and Boriskina, S. *Laser Photonics Rev.* **6**, 178–218 (2012).
[18] Vardeny, Z., Nahata, A., and Agrawal, A. *Nature Photonics* **7**, 177 –187 (2013).
[19] Vasiljević, J. M., Zannotti, A., Timotijević, D. V., Denz, C., and Savić, D. M. J. *Appl. Phys. Lett.* **117**, 041102 (2020).
[20] Freedman, B., Bartal, G., Segev, M., Lifshitz, R., Christodoulides, D. N., and Fleisher, J. *Nature* **440**, 1166 – 1169 (2006).
[21] Vasiljević, J. V., Zannotti, A., Timotijević, D. V., Denz, C., and Savić, D. M. J. *Phys. Rev. A* **96**, 023840 (2017).
[22] Zannotti, A., Vasiljević, J. M., Timotijević, D. V., Savić, D. M. J., and Denz, C. *Opt. Lett.* **44**(7), 1592–1595 (2019).
[23] Diebel, F., Rose, P., Boguslawski, M., and Denz, C. *Appl. Phys. Lett.* **104**, 191101 (2014).
[24] Levi, L., Rechtsman, M., Freedman, B., Schwartz, T., Manela, O., and Segev, M. *Science* **332**, 1541 – 1544 (2011).
[25] Longhi, S. *Opt. Lett.* **46**(12), 2872–2875 (2021).
[26] Timotijević, D. V., Vasiljević, J. M., and Savić, D. M. J. *Opt. Express* **30**(5), 7210–7224 (2022).
[27] Bouchal, Z. *Czech. J. Phys* **53**, 537 – 578 (2003).
[28] Zozulya, A. and Anderson, D. *Phys. Rev. A* **51**, 1520–1531 (1995).
[29] Agrawal, G., [*Nonlinear Fiber Optics*], Academic Press, 5th ed. (2012).

Book of abstracts

PHOTONICA 2025

X International School and Conference on Photonics

25 - 29 August 2025

Belgrade, Serbia

Editors

Mihailo Rabasović, Uroš Ralević, Marina Lekić, Aleksandar Krmpot
Institute of Physics Belgrade, Serbia

Belgrade, 2025

Excitation of self-induced surface states in parabolic geometry

D. V. Mitić[1], J. M. Vasiljević[1], D. V. Timotijević[2], and D. M. Jović Savić[1]
[1]*Institute of Physics, University of Belgrade, P.O. Box 68, 11001 Belgrade, Serbia*
[2]*Institute for Multidisciplinary Research, University of Belgrade, Kneza Višeslava 1, 11030, Belgrade, Serbia*
e-mail: damir@ipb.ac.rs

Non-diffracting beams are a class of optical waves that maintain their transverse intensity profile over long propagation distances, exhibiting self-healing properties [1-5]. These beams have found applications in the field of optical trapping, high-resolution imaging, and laser material processing, where precise beam control and long-depth focusing are essential [6]. They are a significant promise for a new class of optical lattice-writing light within their stability range [7], but their potential in nonlinear photonics remains unexplored [8]. Truncating photonic lattices leads to the formation of localized surface states demonstrated in 1D waveguide arrays and 2D photonic lattices [9]. The geometrical characteristics of Weber beams offer a specific level of control over the topology of lattice surface.

We achieve the progress of these fields extending the concept of surface state generation by investigating the nonlinear propagation of non-diffracting Weber beams in photorefractive media. We present an approach for generating self-induced parabolic surface states in a photorefractive SBN crystal, utilizing a single-pass experimental setup with the optical induction technique. We systematically examined how these surface states characteristics depend on the beam parameters, orientation, and the strength of the nonlinearity. The formation of these surface states was observed without a pre-inscribed photonic lattice. This approach enhances the predictability and control of parabolic surface states, enabling new ways to manage diffraction, localization, and exploring novel nonlinear optical effects. Also, we investigate the linear propagation of a narrow Gaussian probe beam in a Weber aperiodic lattice inscribed in an SBN crystal to study surface effects. Such photonic lattices are naturally truncated, therefore build-up processes such as multiplexing or some kind of occlusion is avoided for their generation. Under specific parameter regimes, we observe oscillatory surface states near the lattice boundary, characterized by cyclic energy exchange between adjacent lattice sites. In both cases, such specific parabolic states are observed in the form of surface states extending across multiple adjacent parabolas, or edge parabolic states localized along the border parabola.

REFERENCES

[1] J. Durnin, J. Opt. Soc. Am. A 4, 651 (1987).
[2] J. Durnin, J. J. Miceli, and J. H. Eberly, Phys. Rev. Lett. 58, 1499 (1987).
[3] E. G. Kalnins and J. W. Miller, J. Math. Phys. 17, 331 (1976).
[4] J. C. Gutiérrez-Vega, M. D. Iturbe-Castillo, and S. Chávez-Cerda, Opt. Lett. 25, 1493 (2000).
[5] M. A. Bandres, J. C. Gutiérrez-Vega, and S. Chávez-Cerda, Opt. Lett. 29, 44 (2004).
[6] M. Woerdemann, C. Alpmann, M. Esseling, and C. Denz, Laser Photon. Rev. 7, 839 (2013).
[7] P. Rose, M. Boguslawski, and C. Denz, New Journal of Physics14, 033018 (2012).
[8] B. Freedman, G. Bartal, M. Segev, R. Lifshitz, D. N. Christodoulides, and J. Fleisher, Nature 440, 1166 (2006).
[9] S. Suntsov, at. al, Journal of Nonlinear Optical Physics & Materials 16, 401 (2007).
[10] D.V. Mitić, J. M. Vasiljević, D. V. Timotijević, and D. M. Jović Savić, *Self-induced parabolic surface states* Submitted in Optical Materials.

ORCID: D.M. 0009-0003-0085-9448, J.V. 0000-0001-9092-5223, D.T. 0000-0003-4538-3140, D.J.S, 0000-0002-1081-0141

2022 TECHNICAL PROGRAMME AND EXHIBITION GUIDE

SPIE. PHOTONICS EUROPE

3–7 APRIL 2022 | PALAIS DE LA MUSIQUE ET DES CONGRÈS | STRASBOURG, FRANCE

SESSION 5

LOCATION: SALON 9, NIVEAU/LEVEL 0 . . . . . TUE 10:50 TO 12:30

Multimode Dynamics I

Session Chair: **Peter Horak,** Optoelectronics Research Ctr. (United Kingdom)

10:50: **Spatiotemporal complexity: multimode fiber light sources and their applications** *(Invited Paper)*, Katarzyna Krupa, Institute of Physical Chemistry PAS (Poland) . . . . . [12143-19]

11:20: **Towards a new understanding of optical poling efficiency in multimode fibers**, Maxime Jonard, XLIM Institut de Recherche (France); Maggy Colas, Institut de Recherche sur les Céramiques, Univ. de Limoges (France); Yann Leventoux, Tigran Mansuryan, XLIM Institut de Recherche (France); Julie Cornette, Institut de Recherche sur les Céramiques (France); Alessandro Tonello, XLIM Institut de Recherche (France); Stefan Wabnitz, Mario Zitelli, Sapienza Univ. di Roma (Italy); Fabio Mangini, Univ. degli Studi di Brescia (Italy); Mario Ferraaro, Yifan Sun, Sapienza Univ. di Roma (Italy); Vincent Couderc, Claire Lefort, XLIM Institut de Recherche (France) . [12143-21]

11:40: **Dissipative solitons and frequency combs in a ring quantum cascade laser** *(Invited Paper)*, Lorenzo Luigi L. Columbo, Dipartimento di Elettronica e Telecomunicazioni, Politecnico di Torino (Italy); Marco Piccardo, Harvard John A. Paulson School of Engineering and Applied Sciences, Harvard University, Cambridge (USA) and Center for Nano Science, Fondazione Istituto Italiano di Tecnologia and Technology, Milano (Italy); Franco Prati, Luigi Lugiato, Dipartimento di Scienza e Alta Tecnologia, Università dell'Insubria, Como (Italy); Massimo Brambilla, Dipartimento di Fisica Interateneo and CNR-IFN, Università e Politecnico di Bari (Italy); Alessandra Gatti, Dipartimento di Scienza e Alta Tecnologia, Università dell'Insubria, Como (Italy) and Istituto di Fotonica e Nanotecnologie IFN-CNR (Italy); Carlo Silvestri, Mariangela Gioannini, Dipartimento di Elettronica e Telecomunicazioni,Politecnico di Torino (Italy); Nikola Opacak, Institute of Solid State Electronics, TU Wien (Austria); Benedikt Schwarz, Institute of Solid State Electronics (Austria); Federico Capasso, Harvard John A. Paulson School of Engineering and Applied Sciences, Cambridge (USA). . . . . [12143-8]

12:10: **Discretized X-wave in a multimode optical fiber**, Karolina Stefanska, Lab. Interdisciplinaire Carnot de Bourgogne (France) and Wroclaw Univ. of Science and Technology (Poland); Pierre Béjot, Lab. Interdisciplinaire Carnot de Bourgogne (France); Karol Tarnowski, Wroclaw Univ. of Science and Technology (Poland); Bertrand Kibler, Lab. Interdisciplinaire Carnot de Bourgogne (France) . . . . . [12143-23]

Lunch/Exhibition Break . . . . . Tue 12:30 to 13:50

SESSION 6

LOCATION: SALON 9, NIVEAU/LEVEL 0 . . . . . TUE 13:50 TO 17:10

Nonlinear Material Systems I

Session Chair: **Thibaut Sylvestre,** FEMTO-ST (France)

13:50: **Nonlinear topological photonics** *(Invited Paper)*, Hrvoje Buljan, Univ. of Zagreb (Croatia) . . . . . [12143-24]

14:20: **Time-varying optical nonlinearities near an epsilon-near-zero condition**, Anton Bykov, King's College London (United Kingdom); Guixin Li, Institute for Quantum Science and Engineering, Southern Univ. of Science and Technology (China); Anatoly V. Zayats, King's College London (United Kingdom). . . . . [12143-25]

14:40: **Turbulence control by time-symmetry breaking**, Salim Benadouda Ivars, Muriel Botey, Ramon Herrero, Univ. Politècnica de Catalunya (Spain); Kestutis Staliunas, Univ. Politècnica de Catalunya (Spain) and Institució Catalana de Recerca i Estudis Avançats (Spain) . . . . . [12143-28]

15:00: **All-optical Fredkin gate using silicon nitride microring resonator**, Menglong He, Kambiz Jamshidi, TU Dresden (Germany) . . . . . [12143-29]

15:20: **Second harmonic generation in silicon oxynitride thin films**, Jakub Lukeš, Karel Zidek, Institute of Plasma Physics of the CAS, v.v.i. (Czech Republic). . . . . [12143-70]

Coffee Break. . . . . Tue 16:00 to 16:30

LOCATION: SCHWEITZER AUDITORIUM, NIVEAU/LEVEL 0 . . . . . 16:30 TO 18:05

Hot Topics II

Francis Berghmans, Vrije Univ. Brussel (Belgium)
2022 Symposium Chair

16:30: **Welcome and opening remarks**

16:35: **Enhancing optical contrast for cancer detection and therapy guidance** *(Plenary)*, Brian W. Pogue, Thayer School of Engineering at Dartmouth (USA) . . . . . [12146-500]

17:20: **Cell by lens: arguments and divagations for next visionary challenges in biophotonics and beyond** *(Plenary)*, Pietro Ferraro, Istituto di Scienze Applicate e Sistemi Intelligenti "Eduardo Caianiello" (Italy) . [12144-500]

WEDNESDAY 6 APRIL

SESSION 7

LOCATION: SALON 9, NIVEAU/LEVEL 0 . . . . . WED 8:30 TO 10:20

Nonlinear Material Systems II

Session Chair: **Hrvoje Buljan,** Univ. of Zagreb (Croatia)

8:30: **Parametric phase-sensitive amplification in silicon nitride waveguides** *(Invited Paper)*, Victor Torres-Company, Peter Andrekson, Magnus Karlsson, ping Zhao, Zhichao Ye, Chalmers Univ. of Technology (Sweden) . . . . . [12143-30]

9:00: **Polyvinylcarbazole: a new material for passive optical limiting**, Olivier Muller, Morgane Guerchoux, Silke Braun, Théo Jean, Manon Dandois, Lionel Merlat, Institut Franco-Allemand de Recherches de Saint-Louis (France). [12143-31]

9:20: **Experimental and theoretical study of second and third harmonic generation in amorphous silicon**, Laura Rodríguez-Suné, Univ. Politècnica de Catalunya (Spain); Michael Scalora, U.S. Army Combat Capabilities Development Command (USA); Crina M. Cojocaru, Univ. Politècnica de Catalunya (Spain); Neset Akozbek, US Army (USA); Ramon Vilaseca, Jose F. Trull, Univ. Politècnica de Catalunya (Spain) . . . . . [12143-32]

9:40: **Electric-field poling of silicon nitride waveguides for the linear phase modulation**, Boris Zabelich, Edgars Nitiss, Ecole Polytechnique Fédérale de Lausanne (Switzerland); Anton Stroganov, LIGENTEC SA (Switzerland); Camille-Sophie Brès, Ecole Polytechnique Fédérale de Lausanne (Switzerland) . . . . . [12143-33]

10:00: **Investigation of LBO and BBO subnanosecond optical parametric amplifiers operating in the visible spectrum range**, Julius Vengelis, Gabrielė Stanionytė, Eglė Vėjalytė, Viktorija Tamulienė, Vygandas Jarutis, Vilnius Univ. (Lithuania) . . . . . [12143-34]

Coffee Break. . . . . Wed 10:20 to 10:50

SESSION 8

LOCATION: SALON 9, NIVEAU/LEVEL 0 . . . . . WED 10:50 TO 12:20

Nonlinear Sources and Dynamics

Session Chair: **Victor Torres Company,** Chalmers Univ. of Technology (Sweden)

10:50: **Pulse dynamics in microlasers** *(Invited Paper)*, Soizic Terrien, The Univ. of Auckland (New Zealand). . . . . [12143-35]

11:20: **Polarization symmetry breaking of regenerative pulses in excitable microlasers with delayed optical feedback**, Stefan Ruschel, The Univ. of Auckland (New Zealand); Venkata Anirudh Pammi, Ctr. de Nanosciences et de Nanotechnologies (France); Bernd Krauskopf, Neil G. R. Broderick, The Univ. of Auckland (New Zealand); Sylvain Barbay, Ctr. de Nanosciences et de Nanotechnologies (France) . . . . . [12143-36]

11:40: **Investigation of optical parametric generator pumped by subnanosecond passively Q-switched micro-laser pulses**, Jonas Banys, Justina Savickytė, Ona Balachninaitė, Simona Armalytė, Viktorija Tamulienė, Vygandas Jarutis, Julius Vengelis, Vilnius Univ. (Lithuania) . . . . . [12143-37]

12:00: **Computation of Kerr lensing effect in laser amplifiers**, Christoph Pflaum, Friedrich-Alexander-Univ. Erlangen-Nürnberg (Germany) . . . [12143-38]

Lunch/Exhibition Break . . . . . Wed 12:20 to 13:50

SESSION 9

LOCATION: SALON 9, NIVEAU/LEVEL 0 . . . . . WED 13:50 TO 15:20

Multimode Dynamics II

Session Chair: **Katarzyna Krupa,** Institute of Physical Chemistry PAS (Poland)

13:50: **Multimode effects in nonlinear fibre optics: from telecommunications to high-harmonic generation** *(Invited Paper)*, Peter Horak, Optoelectronics Research Ctr. (United Kingdom) . . . . . [12143-39]

14:20: **Fast nonlinear integration of the nonlinear Schrödinger equation using a neural network**, Lauri Salmela, Tampere Univ. (Finland); Mathilde Hary, Tampere Univ. (Finland) and Institut FEMTO-ST, Univ. Bourgogne Franche-Comté (France); Mehdi Mabed, John M. Dudley, Institut FEMTO-ST, Univ. Bourgogne Franche-Comté (France); Goëry Genty, Tampere Univ. (Finland) . . . . . [12143-40]

14:40: **Light propagation in disordered aperiodic Mathieu lattices generated with two different randomization methods**, Jadranka Vasiljević, Institute of Physics Belgrade (Serbia); Dejan V. Timotijević, Institute for Multidisciplinary Research, Univ. of Belgrade (Serbia); Dragana M. Jović Savić, Institute of Physics Belgrade (Serbia) . . . . . [12143-41]

Light transport and localization in disordered aperiodic Mathieu lattices

J. M. Vasiljevic[1], D. V. Timotijevic[2], and D. M. Jovic Savic[1]

[1] *Institute of Physics, University of Belgrade, P.O. Box 68, 11001 Belgrade, Serbia*

[2] *Institute for Multidisciplinary Research, University of Belgrade, Kneza Višeslava 1, 11030, Belgrade, Serbia*

Complex systems may be governed by just a few simple rules, not unlike highly ordered systems such as periodic, still, they produce patterns that can be compared to random systems. Complex photonic lattices are suitable for the investigation of many physical phenomena from solid-state to atomic physics with easier experimental realization. Light transport in complex optical systems is a rich and fascinating topic of research. From the investigation of light propagation in aperiodic and disordered media plentiful interesting optical phenomena are obtained, such as Anderson localization.

Nondiffracting beams are highly relevant in optics and atom physics, particularly because their transverse intensity distributions propagate unchanged for hundreds of diffraction lengths [1]. They have potential applications in free-space wireless communications, optical interconnections, long-distance laser machining, and surgery. Four different fundamental families of propagation invariant light fields, distinguish in the underlying real space coordinate system, exist: Discrete, Bessel, Mathieu, and Weber nondiffracting beams [2-4], also, suitable for generation of photonic lattices [5-8].

We realized deterministic aperiodic photonic lattices with controllable complexity, using Mathieu beams combined in metastructures and spliced in both transverse dimensions with different offsets [7], and shown that such lattices hinder light diffraction in comparison to periodic lattices [9]. A further step of randomization of these structures allows for an additional level of diffraction control. Also, the propagation of light in such structures is an unexplored topic, hence will be one of the topics of investigation in this paper. The aim is to involve the fundamental concepts of structured dielectric materials, photonic crystals, as promising candidates for advanced information processing with the unique property of light localization as a nonlinear light-mater interaction phenomenon. We focus our research on the generation of randomized aperiodic lattices with gradually controlled disorder degree in various systems with the investigation of the relationship between complexity and randomness.

We present a comprehensive numerical study of the transverse localization of light in disordered aperiodic Mathieu photonic lattices comparing disorder degree differentiation. A disorder-enhanced light transport is observed for all disorder degrees. With increasing disorder strength light transport becomes diffusive-like and with further increase of disorder degree the Anderson localization is observed. Furthermore, the influence of lattice intensity on the localization effects is studied. The difference in light transport is attributed to various levels of lattice intensity managed by disorder degree. Additionally, we show that localization length differs along different directions, due to the crystal and lattice anisotropy.

References:

[1] Z. Bouchal, Czech. J. Phys. 53 537 (2003).
[2] J. Durnin, J. J. Miceli, and J. H. Eberly, Phys. Rev. Lett. 58, 1499 (1987).
[3] J. C. Gutiérrez-Vega, M. D. Iturbe-Castillo, and S. Chávez-Cerda, Opt. Lett. 25, 1493 (2000).
[4] M. A. Bandres, J. C. Gutiérrez-Vega, and S. Chávez-Cerda, Opt. Lett. 29, 44 (2004).
[5] B. Freedman, G. Bartal, M. Segev, R. Lifshitz, D. N. Christodoulides, and J. W. Fleisher, Nature 440, 1166, 2006.
[6] M. Boguslawski, N. M. Lučić, F. Dieble, D, V. Timotijević, C. Denz, and D. M: Jović Savić, Optica 3, 711 (2016).
[7] J. M. Vasiljević, A. Zannotti, D. V. Timotijević, C. Denz, and D. M. Jović Savić, Phys. Rev. A 96, 023840 (2017).
[8]J. M. Vasiljević, A. Zannotti, D. V. Timotijević, C. Denz, and D. M. Jović Savić, Phys. Rev. A 97, 033848 (2018).
[9] J. M. Vasiljević, A. Zannotti, D. V. Timotijević, C. Denz, and D. M. Jović Savić, Appl. Phys. Lett.117, 041102 (2020)

Summary for the program

Light transport and localization in disordered aperiodic Mathieu lattices

J. M. Vasiljevic[1], D. V. Timotijevic[2], and D. M. Jovic Savic[1]

[1] *Institute of Physics, University of Belgrade, P.O. Box 68, 11001 Belgrade, Serbia*

[2] *Institute for Multidisciplinary Research, University of Belgrade, Kneza Višeslava 1, 11030, Belgrade, Serbia*

Complex photonic lattices are suitable for the investigation of many physical phenomena from solid-state to atomic physics with easier experimental realization. Light transport in complex optical systems is a rich and fascinating topic of research. Nondiffracting beams are highly relevant in optics and atom physics, particularly because their transverse intensity distributions propagate unchanged for hundreds of diffraction lengths, moreover, suitable for the generation of photonic lattices. Four different fundamental families of propagation invariant light fields, distinguish in the underlying real space coordinate system, exist: Discrete, Bessel, Mathieu, and Weber nondiffracting beams. We realized deterministic aperiodic photonic lattices with controllable complexity, using Mathieu beams combined in metastructures and spliced in both transverse dimensions with different offsets, and shown that such lattices suppress light diffraction comparing with periodic lattices. A further step of randomization of these structures permits an additional level of diffraction control. The propagation of light in such structures is an unexplored topic, hence it is one topic of investigation in this paper. The aim is to involve the fundamental concepts of structured dielectric materials, photonic crystals, as promising candidates for advanced information processing with the unique property of light localization as a nonlinear light-mater interaction phenomenon. We generate randomized aperiodic lattices with gradually controlled disorder degree in various systems to investigate the relationship between complexity and randomness. We present a comprehensive numerical study of the transverse localization of light in disordered aperiodic Mathieu lattices comparing disorder degree differentiation. A disorder-enhanced light transport is observed for all disorder degrees. With increasing disorder strength light transport becomes diffusive-like and with further increase of disorder degree, the Anderson localization is observed. Furthermore, the influence of lattice intensity on the localization effects is studied. The difference in light transport is attributed to various levels of lattice intensity managed by disorder degree.

ID: 120
TOM 5 Resonant Nanophotonics

Controlling chromaticity by lamellar gratings

Hiroyuki Ichikawa, Naoki Arita, Keigo Shikimi, Ryunosuke Tani
Ehime University, Japan

Fundamental numerical study on controlling chromaticity with the simplest diffractive structure is carried out. Observed various characteristics on transmission/reflection and dielectric/metal will be useful guidelines for practical optimisation of device structures.

ID: 150
TOM 8 Non-linear and Quantum Optics

Light propagation in disordered aperiodic Mathieu photonic lattices

Jadranka M Vasiljević[1], Dejan V Timotijević[2], Dragana M Jović Savić[1]
[1]Institute of Physics, University of Belgrade, Belgrade, Serbia; [2]Institute for Multidisciplinary Research, University of Belgrade, Belgrade, Serbia

We present the numerical modeling of two different randomization methods of photonic lattices. We compare the results of light propagation in disordered aperiodic and disordered periodic lattices. In disordered aperiodic lattice disorder always enhances light transport for both methods, contrary to the disordered periodic lattice. For the highest disorder levels, we detect Anderson localization for both methods and both disordered lattices. More pronounced localization is observed for disordered aperiodic lattice.

ID: 251
TOM 13 Advances and Applications of Optics and Photonics

Chip integrated photonics for ion based quantum computing

Steffen Sauer[1,2], Anastasiia Sorokina[1,2], Carl-Frederik Grimpe[3], Guochun Du[3], Pascal Gehrmann[1,2], Elena Jordan[3,5], Tanja Mehlstäubler[3,4], Stefanie Kroker[1,2,3]
[1]Institut für Halbleitertechnik, Technische Universität Braunschweig, Hans-Sommer-Str. 66, 38106 Braunschweig, Germany; [2]Laboratory for Emerging Nanometrology, Langer Kamp 6a/b, 38106 Braunschweig, Germany; [3]Physikalisch-Technische Bundesanstalt, Bundesallee 100, 38116 Braunschweig, Germany; [4]Institut für Quantenoptik, Leibniz Universität Hannover, Welfengarten 1, 30167 Hannover, Germany; [5]DLR-Institut für Satellitengeodäsie und Inertialsensorik, Leibniz Universität Hannover, Welfengarten 1, 30167 Hannover, Germany

Ion traps are a promising platform for the realisation of high-performance quantum computers. To enable the future scalability of these systems, integrated photonic solutions for guiding and manipulating the laser light at chip level are a major step. Such passive optical components offer the great advantage of providing beam radii in the µm range at the location of the ions without increasing the number of bulk optics. Different wavelengths, from UV to NIR, as well as laser beam properties, such as angle or polarisation, are required for different cooling and readout processes of ions. We present

PROCEEDINGS VOLUME 13004
SPIE PHOTONICS EUROPE | 7-12 APRIL 2024

Nonlinear Optics and its Applications 2024

Editor(s): John M. Dudley (/profile/John.Dudley-20163), Anna C. Peacock, Birgit Stiller, Giovanna Tissoni (/profile/giovanna.tissoni-3754)

Editor Affiliations + ()

IN THIS VOLUME

12 Sessions, 36 Papers, 22 Presentations, 13 Posters

STRUCTURED LIGHT AND MULTIMODE EFFECTS

Dimensionality crossover of radial discrete diffraction in optically induced Mathieu photonic lattices (/conference-proceedings-of-spie/13004/130040J/Dimensionality-crossover-of-radial-discrete-diffraction-in-optically-induced-Mathieu/10.1117/12.3017229.full)

Presentation + Paper

Jadranka M. Vasiljević (/profile/Jadranka.Vasiljević-4097119), Vladimir P. Jovanović (/profile/Vladimir.Jovanovic-5044206), Aleksandar Ž. Tomović (/profile/Aleksandar.Tomovic-5044208), Dejan V. Timotijević, Radomir Žikic, Milivoj R. Belić, Dragana M. Jović Savić

Proceedings Volume Nonlinear Optics and its Applications 2024, 130040J (2024) https://doi.org/10.1117/12.3017229 (https://doi.org/10.1117/12.3017229)

Hide Abstract -

We demonstrate transitional dimensionality crossover of radial discrete diffraction in optically induced radial-elliptical Mathieu photonic lattices. Varying the order, characteristic structure size, and ellipticity of the Mathieu beams used for the photonic lattices generation, we control the shape of discrete diffraction distribution over the combination of the radial direction with the circular or elliptic. We also investigate the transition from one-dimensional to two-dimensional discrete diffraction by varying the input probe beam position. Discrete diffraction is the most pronounced along the crystal anisotropy direction.

QUANTUM NONLINEAR PHOTONICS

Spontaneous parametric down-conversion in ultrathin samples (/conference-proceedings-of-spie/13004/130040K/Spontaneous-parametric-down-conversion-in-ultrathin-samples/10.1117/12.3016302.full) Presentation + Paper

Maria V. Chekhova (/profile/Maria.Chekhova-11511)

Proceedings Volume Nonlinear Optics and its Applications 2024, 130040K (2024) https://doi.org/10.1117/12.3016302 (https://doi.org/10.1117/12.3016302)

Read Abstract +

Quantum correlated twin beams in cascaded optical parametric oscillator (/conference-proceedings-of-spie/13004/130040L/Quantum-correlated-twin-beams-in-cascaded-optical-parametric-oscillator/10.1117/12.3016656.full) Presentation + Paper

Salvatore Castrignano, Iolanda Ricciardi, Pasquale Maddaloni (/profile/Pasquale.Maddaloni-52021), Paolo De Natale (/profile/Paolo.de-Natale-25131), Stefan Wabnitz (/profile/Stefano.Wabnitz-7150), Maurizio De Rosa (/profile/Maurizio.De-Rosa-4261090)

Proceedings Volume Nonlinear Optics and its Applications 2024, 130040L (2024) https://doi.org/10.1117/12.3016656 (https://doi.org/10.1117/12.3016656)

Read Abstract +

Dimensionality crossover of radial discrete diffraction in optically induced Mathieu photonic lattices

Jadranka M. Vasiljević[1], Vladimir P. Jovanović[2], Aleksandar Ž. Tomović[2], Dejan V. Timotijević[2], Radomir Žikic[2], Milivoj R. Belić[3], and Dragana M. Jović Savić[1]

[1] *Institute of Physics, University of Belgrade, P.O. Box 68, 11001 Belgrade, Serbia*
[2] *Institute for Multidisciplinary Research, University of Belgrade, Kneza Višeslava 1, 11030, Belgrade, Serbia*
[3] *Division of Arts and Sciences, Texas A & M University at Qatar, 23874, Doha, Qatar*

Light manipulation in photonic lattice (PL) is a prime area of investigation and application in optics [1]. PLs provide a huge platform for investigating discrete light diffraction effects. Discrete diffraction of light was theoretically and experimentally observed in both one-dimensional (1D) and two-dimensional (2D) structures, as well as in aperiodic or other systems. Truncating periodic PLs cause additional distortion of the periodicity, resulting in the formation of optical surface states akin to electronic surface states in periodic systems [2]. The continuous transition from 1D to 2D PLs is an attractive field of study, with a still open question regarding intermediate states that can occur in such physical systems with dimensionality crossover that do not exist in either 1D or 2D geometries [3].

Nondiffracting beams, propagation-invariant fields over hundreds of diffraction lengths even in the presence of weak nonlinearity [4], are ideal for generating 2D PLs and have diverse applications in free-space wireless communications, optical interconnections, long-distance laser machining, and surgery. There are four fundamental families of such propagation-invariant light fields: Discrete, Bessel, Mathieu, and Weber nondiffracting beams [5-7]. Among these, Mathieu beams are preferred for optical lattice writing, enabling solitons, elliptical vortex solitons, and the creation of various aperiodic and disordered PLs through optical induction in photorefractive crystals, as well as for particle manipulation [8-12].

In this paper, experimentally and theoretically we examine conditions for discrete diffraction occurrence in aperiodic Mathieu PLs. The unique shape of Mathieu beams enables the creation of *naturally truncated aperiodic PLs* with our advanced one-pass experimental realization by optically induction in the photorefractive crystal using a single Mathieu beam [13]. Such photonic structures in elliptical-radial geometries offer diverse shapes, with circular, elliptical, and hyperbolic waveguide paths and radial spikes, raising questions about discrete diffraction dimensionality. Mathieu lattice period and the refractive index modulation are connected via Mathieu beam parameters (the beam order, characteristic structural size, and the ellipticity of the beam). Different local environments within these lattices during propagation create additional variations in discrete diffraction effects.

We study weak nonlinear light propagation in various aperiodic Mathieu PLs and experimentally and numerically demonstrate radial and angular discrete diffraction in them. We are able to control discrete diffraction in the radial direction and shape their distributions in perpendicular directions: circular, elliptic, or hyperbolic, by modifying the Mathieu beam's order, size, and ellipticity. Additionally, we investigate the transition from 1D to 2D discrete diffraction, highlighting the significant role of crystal anisotropy in our medium, with the most prominent 2D discrete diffraction observed along the crystal anisotropy direction. Our findings lay the groundwork for exploiting light propagation in a novel class of optical lattices, extending beyond these specific lattice configurations, and generalized to diverse types of optically induced lattices. Such adaptivity and reconfigurability of light-guiding structures are vital for advancement in modern photonics with a significant step towards innovative wave-guiding applications and light-routing approaches.

References:

[1] F. Lederer, G. I. Stegeman, D. N. Christodoulides, G. Assanto, and M. S. Y. Silberberg, Phys. Rep. 463(1-3), 1–126 (2008).
[2]. S. Suntsov, K. G. Makris, G. A. Siviloglou, R. Iwanow, R. Schiek, D. N. Christodoulides, G. I. Stegeman, R. Morandotti, H. Yang, G. Salamo, M. Volatier, V. Aimez, R. Arès, M. Sorel, Y. Min, W. Sohler, X. Wang, A. Bezryadina, and Z. Chen, J. Nonlinear Optic. Phys. Mat. 16(04), 401–426 (2007).
[3] A. Szameit, Y. V. Kartashov, F. Dreisow, M. Heinrich, T. Pertsch, S. Nolte, A. Tünnermann, V. A. Vysloukh, F. Lederer, and L. Torner, Phys. Rev. Lett. 102(6), 063902 (2009).
[4] A. Zannotti, J. M. Vasiljević, D. V. Timotijević, D. M. J. Savić, and C. Denz, Opt. Lett. 44(7), 1592–1595 (2019).
[5] J. Durnin, J. J. Miceli, and J. H. Eberly, Phys. Rev. Lett. 58(15), 1499–1501 (1987).
[6] J. C. Gutiérrez-Vega, M. D. Iturbe-Castillo, and S. Chávez-Cerda, Opt. Lett. 25(20), 1493–1495 (2000).
[7] M. A. Bandres, J. C. Gutiérrez-Vega, and S. Chávez-Cerda, Opt. Lett. 29(1), 44–46 (2004).
[8] J. M. Vasiljević, A. Zannotti, D. V. Timotijević, C. Denz, and D. M. J. Savić, Appl. Phys. Lett. 117(4), 041102 (2020).
[9] J. M. Vasiljević, A. Zannotti, D. V. Timotijević, C. Denz, and D. M. Jović Savić, Phys. Rev. A 97(3), 033848 (2018).
[19] J. V. Vasiljević, A. Zannotti, D. V. Timotijević, C. Denz, and D. M. J. Savić, Phys. Rev. A 96(2), 023840 (2017).
[11] D. V. Timotijević, J. M. Vasiljević, and D. M. J. Savić, Opt. Express 30(5), 7210–7224 (2022).
[12] K. Dholakia and T. Čižmár, Nat. Photonics 5(6), 335–342 (2011).
[13] J. M. Vasiljević, V. P. Jovanović, A Ž. Tomović, D. V. Timotijević, R. Žikic, M. R. Belić, and D. M. Jović Savić, Opt. Express 31, 28946-28953 (2023).

Summary for the program :

Dimensionality crossover of radial discrete diffraction in optically induced Mathieu photonic lattices

Jadranka M. Vasiljević[1], Vladimir P. Jovanović[2], Aleksandar Ž. Tomović[2], Dejan V. Timotijević[2], Radomir Žikic[2], Milivoj R. Belić[3], and Dragana M. Jović Savić[1]

[1] *Institute of Physics, University of Belgrade, P.O. Box 68, 11001 Belgrade, Serbia*
[2] *Institute for Multidisciplinary Research, University of Belgrade, Kneza Višeslava 1, 11030, Belgrade, Serbia*
[3] *Division of Arts and Sciences, Texas A & M University at Qatar, 23874, Doha, Qatar*

We focus our experimentally and numerical investigation of weak nonlinear light propagation in various aperiodic Mathieu lattices optically induced in the photorefractive medium using our advanced one-pass experimental setup. We demonstrate the transitional dimensionality of discrete diffraction within such radial-elliptical Mathieu photonic lattices. We control the shape of discrete diffraction distribution over the combination of the radial direction with the circular, elliptic, or hyperbolic through adjustments of beam order, characteristic structure size, and ellipticity of the Mathieu beams used for the photonic lattices generation. By varying the input beam position, we investigated the transition from one-dimensional to two-dimensional diffraction, and we observed the most prominent discrete diffraction along the crystal's anisotropic direction.

LPHYS'21

LPHYS'21. PROGRAM:

Seminar 5: Nonlinear Optics & Spectroscopy

Co-chairs:

Yuri Kivshar
Australian National University, Canberra, Australia
ysk@internode.on.net

Olga G. Kosareva
Lomonosov Moscow State University, Moscow, Russia
kosareva@physics.msu.ru

Vladimir A. Makarov
Lomonosov Moscow State University, Moscow, Russia
makarov@ilc.edu.ru

Monday, 19 July, 2021

S5.1 **(16:00 – 17:30)** **Chair**: Sergey Stremoukhov (Russia)

16:00 – 16:20 J M Vasiljević (Institute of Physics, Belgrade, Serbia), A Zannotti (Institute of Applied Physics and Center for Nonlinear Science (CeNoS), Munster, Germany), D V Timotijević (Institute for Multidisciplinary Research, Belgrade, Serbia), C Denz (Institute of Applied Physics and Center for Nonlinear Science (CeNoS), Munster, Germany), D .M Jović Savić (Institute of Physics, Belgrade, Serbia)
Twisted Photonic Lattices Created by Elliptical Mathieu Beams Abstract

16:20 – 16:35 D H G Espinosa (School of Electrical Engineerig and Computer Science, University of Ottawa, Ottawa, Canada), S R Harrigan (Department of Physics, University of Ottawa, Ottawa, Canada), K M Awan (Stewart Blusson Quantum Matter Institute, University of British Columbia, Vancouver, Canada), P Rasekh (School of Electrical Engineerig and Computer

Twisted Photonic Lattices Created by Elliptical Mathieu Beams

J M Vasiljević[1], A Zannotti[2], D V Timotijević[3], C Denz[2], and D .M Jović Savić[1]

[1]*Institute of Physics, 11080, Belgrade, Serbia. Contact Phone: +381113713088*
[2]*Institute of Applied Physics and Center for Nonlinear Science (CeNoS), 48149 , Munster, Germany*
[3]*Institute for Multidisciplinary Research, Belgrade, Serbia*
Contact Email: jadranka@ipb.ac.rs

Nondiffracting beams are highly applicable in optics, photonics, and atom physics, peculiar because their transverse intensity distributions propagate unchanged for hundreds of diffraction lengths and allow the creation 1D and 2D photonic lattices in photosensitive media[1]. Four different fundamental families of propagation invariant light fields exist, distinguish in the underlying real space coordinate system: Discrete, Bessel, Weber, and Mathieu nondiffracting beams [2-5]. *Mathieu beams* are the solution of the Helmholtz equation in elliptic cylindrical coordinates [5-7], therefore they are the best suited to address physical effects in elliptical coordinates. Mathieu beams are classified according to their symmetry properties as even and odd. Their transverse discrete intensity distributions can be shaped by their order and an ellipticity parameter. These real-valued beams are characterized by only discrete spatial phase distributions. By complex superposition of appropriate even and odd Mathieu beams, *elliptical Mathieu beams* are obtained, with remarkable continuously modulated spatial phase distributions that act as orbital angular momenta, related with transverse energy flow [8].

Experimentally and numerically, we investigated linear and nonlinear self-action of elliptical Mathieu beams in a photorefractive SBN crystal [8]. Linear propagation of elliptic Mathieu beams enables a nondiffracting transverse intensity distribution with transverse energy redistribution along elliptic paths compensated in each point. In contrast, their nonlinear self-action in SBN breaks this sensitive equilibrium and leads to the formation of high-intensity filaments, which rotate in the direction determined by the energy flow. We show that such filamentation depends on the strength of the nonlinearity and the structure size of used Mathieu beams. We investigate the nonlinear propagation of such refractive index formations in SBN crystal and show they are convenient as lattice-writing light to optical induction of two-dimensional chiral twisted photonic refractive index structures with tunable ellipticity. This study provides considerably advancing the field of chiral light and photonic structures since we demonstrated that elliptical Mathieu beams are suitable for the fabrication of two-dimensional photonic lattices with elliptic trajectories by optical induction technique.

References

[1] Z Bouchal, Czech. J. Phys. **53**, 537 (2003)

[2] J Durnin, J J Miceli and J H Eberly, J. Opt. Soc. Am. **4**, 651 (1987)

[3] J Durnin, J J Miceli and J H Eberly, Phys. Rev. Lett. **58**, 1499 (1987)

[4] M A Bandres, J C Gutiérrez-Vega and S Chávez-Cerda, Opt. Lett. **29**, 44 (2004)

[5] J C Gutiérrez-Vega, M D Iturbe-Castillo and S Chávez-Cerda, Opt. Lett. **25**, 1493 (2000)

[6] J C Gutiérrez-Vega, M D Iturbe-Castillo, G.A Ramírez, E Tepichín, R M Rodriíguez-Dagnino, S Chávez-Cerda and G H C New, Opt. Commun. **195**, 35 (2001)

[7] J C Gutiérrez-Vega, M A Meneses-Neva and S Chávez-Cerda, Am. J. Phys. **71**, 233 (2003)

[8] A Zannotti, J M Vasiljević, D V Timotijević, D M Jović Savić and C Denz, Adv. Opt. Mater. **6**, 1701355 (2018)

Linkin Science

Exploring & Connecting Science

Proceedings of

3rd Edition of Virtual Online Conference on

Advancements of Laser, Optics & Photonics

September 01-02, 2021

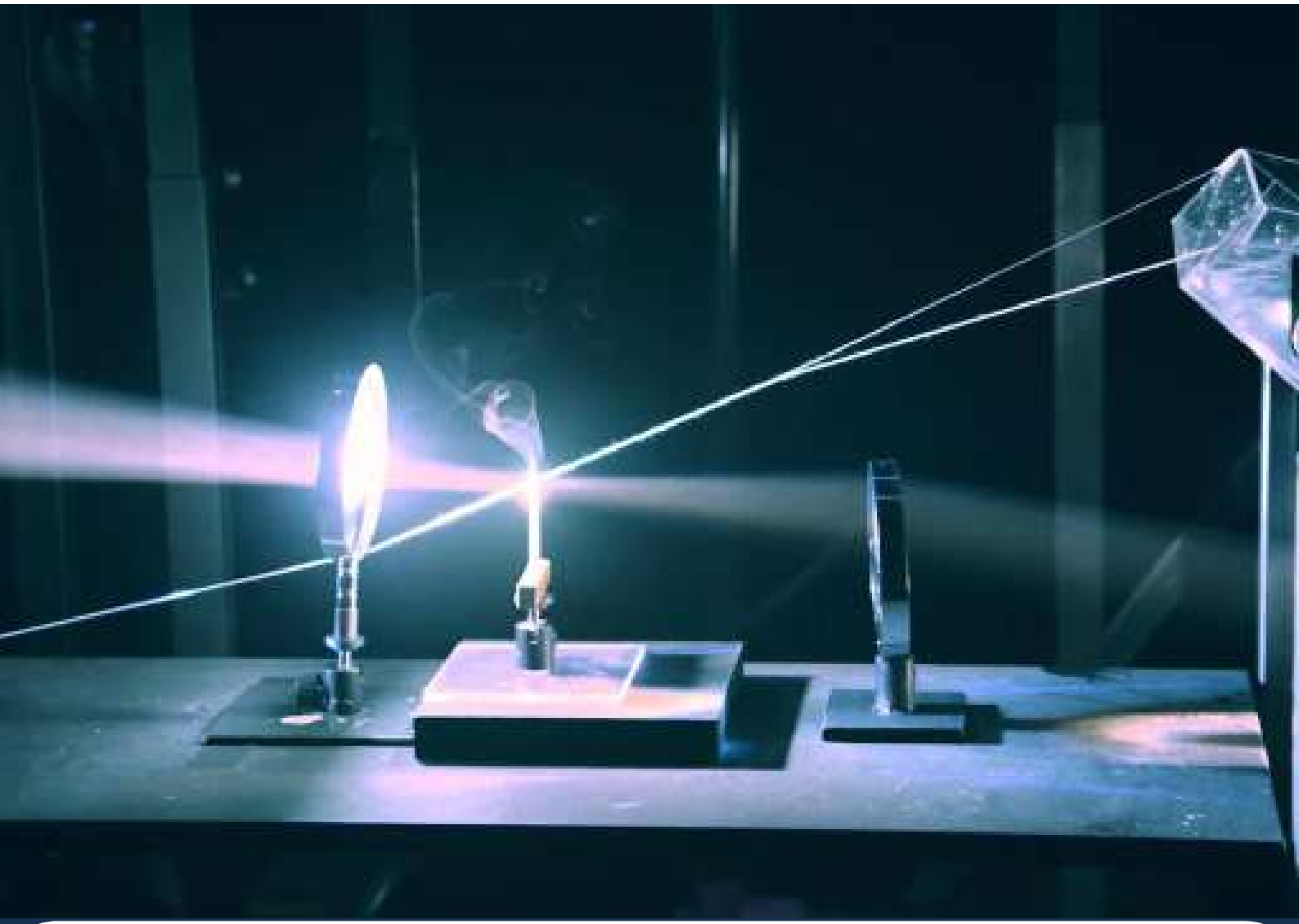

HOSTING ORGANIZATION

Linkin Science Pvt. Ltd

649 Mission St. 5th Floor, San Francisco, CA 94105, USA

Ph: +1 (415) 704-1402 | www.laseroptics.linkinscience.com | laseroptics@linkinscience.com

Experimental realization of chiral photonic lattices

Vasiljević[1*], Alessandro Zannotti[3], D. V. Timotijević[2], Cornelia Denz[3], and D. M. Jović Savić[1]

[1,2]University of Belgrade, Serbia

[3]University of Münster, Germany

Nondiffracting beams find their applications in optics, photonics, and atom physics. Particularly, their transverse intensity distribution propagates unchanged for hundreds of diffraction lengths, consequently allowing the creation of 1D and 2D photonic lattices with nondiffracting beams in photosensitive media. Low diffraction and robustness of nondiffracting beams make them appropriate for deployment in free-space wireless communications, optical interconnections, long-distance laser machining, optical tweezers, biology, surgery, etc. There are four different propagation invariant light fields: Plane waves, Bessel, Weber, and Mathieu nondiffracting beams. Mathieu beams are the solution of the Helmholtz equation in elliptic cylindrical coordinates, therefore being the best suited to address physical effects described in elliptical coordinates. They are classified according to their symmetry properties as even and odd Mathieu beams. Elliptical Mathieu beams are obtained as a complex superposition of appropriate even and odd Mathieu beams, with remarkable continuously-modulated spatial phase distributions that create orbital angular momenta, related with a transverse energy flow. Their transverse intensity distribution can be shaped by their order and the parameter of ellipticity.

We study linear characteristics and nonlinear self-action of elliptical Mathieu beams in a photorefractive crystal experimentally and numerically. Linear propagation of such beams validates a nondiffracting transverse intensity distribution with transverse energy redistribution along elliptic paths compensated in each point. In contrast, their nonlinear self-action breaks this sensitive equilibrium and leads to the formation of high-intensity filaments, which rotate in the direction determined by the energy flow. Our study advances the field of chiral light and photonic structures by pointing to the suitability of Elliptical Mathieu beams as light patterns for optical induction of chirally twisted photonic lattices with elliptic envelopes in the transverse plane. The order of used Elliptical Mathieu beam determines the number of created chiral waveguides, where the waveguides slopes can be manipulated by changing the nonlinearity strength or the structure size of the used beam.

Biography

Dr. Jadranka M. Vasiljević received her Ph.D. degree in 2020 at the Faculty of Physics at Belgrade University, Serbia. Since 2015 she joined the research group of Dr. DraganaJovićSavić at the Institute of Physics, University of Belgrade, Serbia. She is part of the Laboratory for Nonlinear Photonics at the Institute of Physics, University of Belgrade, Serbia. Her research area is Nonlinear Optics and Photonics. Currently, research interests are nondiffracting beams, in particular, based on the family of Mathieu beams. She is studying the realization of two-dimensional dynamical structures in the photorefractive medium by Mathieu beams, aperiodic and complex structures with Mathieu beams, and investigating phenomena correlated with light propagation in Mathieu photonic lattices.

Notes:

Linkin Science

Exploring & Connecting Science

Conference Program

3rd Edition of Virtual Online Conference on Advancements of Lasers, Optics and Photonics

September 01-02, 2021

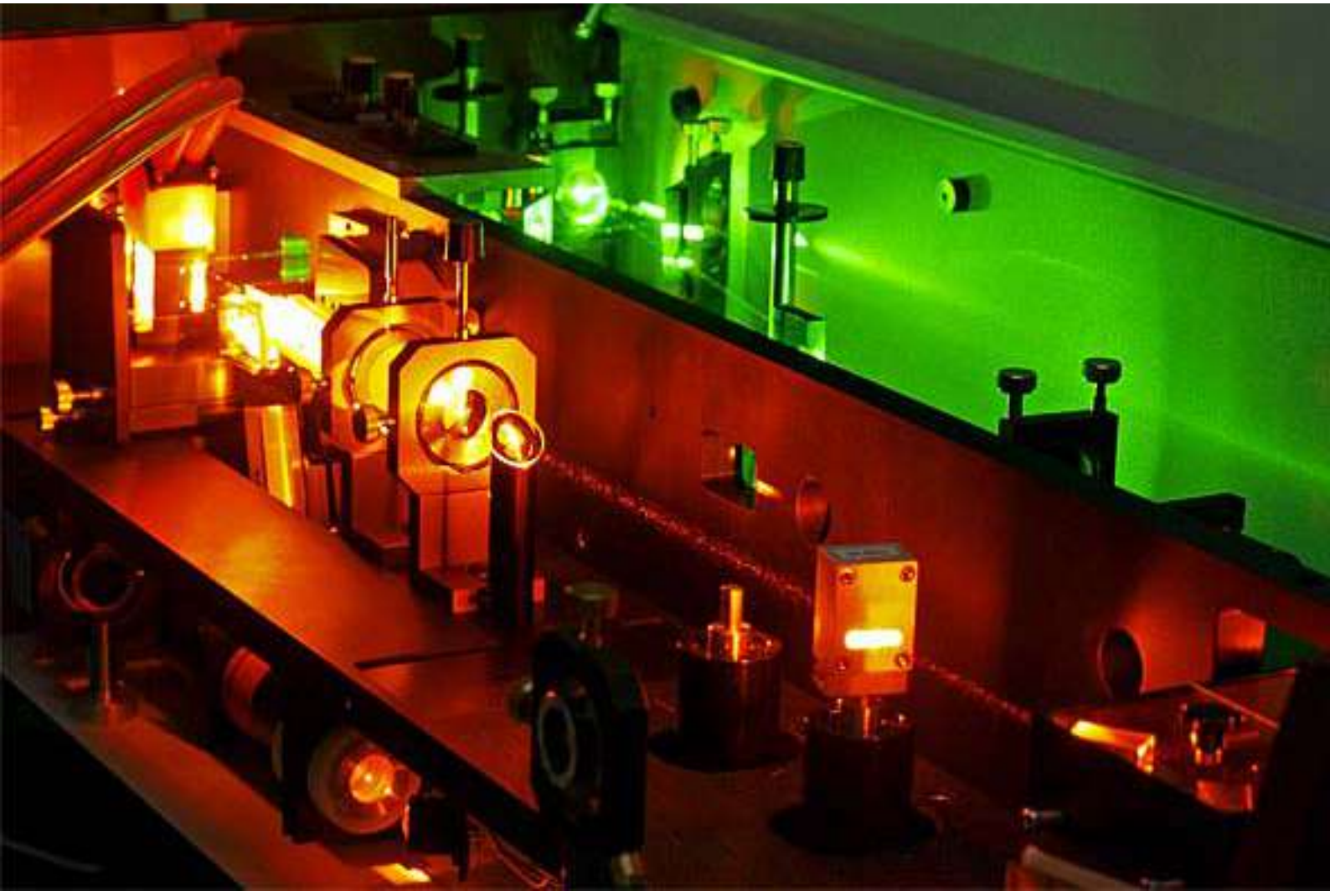

HOSTING ORGANISATION

Linkin Science Pvt. Ltd

649 Mission St. 5th Floor, San Francisco, CA 94105, USA

Ph: +1 (415) 704-1402 | www.laseroptics.linkinscience.com | laseroptics@linkinscience.com |

Conference Program

DAY 1: Wednesday 1st September 2021 EDT Time Zone

09:00-09:30	Opening Session Welcome Address
09:30-10:05 **Keynote**	**Photonics in Radar and LiDAR Systems** Paulo Pereira Monteiro**,** *University of Aveiro, Portugal* (Local Time: 14:30)
10:05-10:40 **Keynote**	**Creating Materials with a desired Refraction Coefficient** Alexander G. Ramm, *Kansas State University, USA* (Local Time: 09:05)
10:40-11:15 **Keynote**	**Cryogenic Laser Technology** David C Brown**,** *Fellow of The Optical Society of America, Advanced Photonic Sciences, USA* (Local Time: 10:40)
11:15-11:35	**Break Out Session/ Networking Lounge 20 mins**
11:35-12:00 **Oral Session**	**Multi-Electron Trojan Wave Packets in the Circularly Polarized and the Magnetic Fields on the Multi-layer Langmuir Type (1) Trajectories in Helium Atoms and Quantum Dots** Matt Kalinski**,** *Utah State University, USA* (Local Time: 09:35)
12:00-12:25 **Oral Session**	**Application of lasers in phosphor material development for solid-state lighting** Hisham Menkara**,** *PhosphorTech Corporation, USA* (Local Time: 12:00)
12:25-12:50 **Oral Session**	**Experimental realization of chiral photonic lattices** Jadranka Vasiljevic**,** *University of Belgrade, Serbia* (Local Time: 18:25)
12:50-13:15 **Oral Session**	**Application of ultra-short pulse lasers in the restauration of historical stained-glass** Luis A Angurel**,** *University of Zaragoza, Spain* (Local Time: 18:50)
13:15-13:35	**Break Out Session/ Networking Lounge 20 mins**
13:35-13:50 **Poster Presentation**	**LED Photobiomodulation therapy combined with biomaterial as a scaffold promotes better bone quality in the dental alveolus in an experimental extraction model** Vanessa Dalapria**,** *UNINOVE- Nove de Julho University, Brazil* (Local Time: 14:35)

Oral

Linkin Science

Exploring & Connecting Science

(649 Mission St. 5th Floor, San Francisco, CA 94105)

Certificate of Recognition

Linkin Science and Scientific Committee of Advancements Of Laser, Optics & Photonics 2021

Wish to thank

Prof/Dr/Ms. Jadranka Vasiljevic

University of Belgrade, Serbia

for phenomenal and worthy Oral presentation on

Experimental realization of chiral photonic lattices

at the 3rd Edition of Virtual Conference On Advancements Of Laser, Optics & Photonics

held during September 01-02, 2021

Laser, Optics & Photonics 2021 Scientific Committee

David C Brown

Advanced Photonic Sciences, USA

Subject **Share your research on | 10-11 Feb, 2023**

From Laser, optics and photonics

Sender Laser, optics and photonics

To Jadranka

Date 17.10.2022 08:28

Dear Dr. Jadranka M Vasiljević,

Wishes from Sciwide webinars.

We extend our immense honor to invite you as a Keynote Speaker for the upcoming webinar on "4th Edition of Laser, Optics and Photonics Virtual", which is scheduled during 10-11 Feb 2023 from GMT 07:00 to 12:00.

This virtual conference holds special promise to discuss the future discoveries. The colossal and enthusiastic presence of young and brilliant researchers, scientists, academicians, opticians, laser experts, healthcare professionals, business delegates and exceptional student communities adds to the excitement of the two-days virtual congress which provides an insight

For more information visit: https://sciwideonline.com/v-laser2023/

We look forward meeting you in Virtually.

Thanks & Regards,
Rama. G |Webinar Secretary
V-LASER2023 | SciWide Webinars

SCIWIDE WEBINARS

Final Program

4Th Edition of Laser, Optics and Photonics Virtual

February 10, 2023

Contact us:

Contact: +91 9440424355

E-mail: v-laser2023@sciwideonline.com

Website: https://sciwideonline.com/v-laser2023/

February 10, 2023 GMT 07:00 – 16:00

Webinar Timings	Speakers Timings	
07:00 – 07:10		Introduction

Keynote Sessions-1

07:10 – 07:45	10:10 – 10:45	Title: Shape Memory Effect and Atomic Scale Aspects of Reversibility in Shape Memory Alloys **Osman Adiguzel, Firat University, Turkey.**
07:45 – 08:20	15:45 – 16:20	Title: Recent advance of laser lipolysis **Bin Chen, Xi'an Jiaotong University, China.**
08:20 – 08:55	17:20 – 17:55	Title: Plasmonics and Plasmonic Metamaterials Using Random Metal Nanostructures for High Efficiency Light-Emitting Devices **Koichi Okamoto, Osaka Metropolitan University, Japan.**
08:55 – 09:30	19:55 – 20:30	Title: Nucleation and Dynamics of Chiral Spin Textures in Topological Materials **Oleg Tretiakov, University of New South Wales, Australia.**
09:30 – 10:05	10:30 – 11:05	Title: Composite photonic structures: generation and light propagation in them **Jadranka Vasiljević, Institute of Physics, Serbia.**
10:05 – 10:40	18:05 – 18:40	Title: Photoalignment and photopatterning based on nanosize azodye layers for new liquid crystal display and photonics devices **Vladimir Chigrinov, Hong Kong University of Science and Technology, Hong Kong.**

Invited Sessions

SCIWIDE WEBINARS

V-LASER2023 wish to thank

Prof/Dr/Mr/Ms. **Jadranka Vasiljević**

Institute of Physics, Serbia

for his/her worthy Keynote presentation at

"4th Edition of Laser, Optics and Photonics Virtual"

held on February 10, 2023

Prof. Bin Chen
Xi'an Jiaotong University, China

Composite photonic structures: generation and light propagation in them

J. M. Vasiljević[1], D. V. Timotijević[2], D. M. Jović Savić[1]

[1]Institute of Physics, University of Belgrade, P.O. Box 68, 11001 Belgrade, Serbia
[2] Institute for Multidisciplinary Research, University of Belgrade, Kneza Višeslava 1, 11030 Belgrade, Serbia

Email: jadranka@ipb.as.rs

Presenter Name: Dr. Jadranka Vasiljević
Email: jadranka@ipb.ac.rs
Phone:
Institute/ Organization: Institute of Physics, Belgrade
Country: Serbia
Presentation Category: Oral Presentation

Abstract: Nondiffracting beams are highly applicable in optics, photonics, and atom physics, because their transverse intensity distributions propagate unchanged for hundreds of diffraction lengths and allow the creation of 1D and 2D photonic lattices in photosensitive media [1]. Depending on coordinate system four fundamental families of propagation invariant light fields exist: Discrete, Bessel, Weber, and Mathieu nondiffracting beams [2-4]. Mathieu beams are the solution of the Helmholtz equation in elliptic cylindrical coordinates [4-6]. According to their symmetry properties they are classified as even and odd. Their order and an ellipticity parameter can shape their transverse discrete intensity distributions.

Deterministic aperiodic or complex photonic structures are at the intersection between periodic and disorder crystal structures. In optics, the properties of such structures have been studied, as appealing structures for the control and manipulation of light. Various aperiodic and quasiperiodic photonic structures are realized artificially and light propagation is investigated in them. We experimentally realized the aperiodic photonic structures with controllable complexity, created by different combinations of Mathieu beams, by splicing them in both transverse dimensions in different offsets [7] and we studied light localization in them. In such lattice, light expansion is hindered in comparison to periodic lattice and nonlinear light localization is demonstrated [8].

Furthermore, we numerically modeled two different randomization methods of photonic lattices [9]. We compare the results of light propagation in disordered aperiodic Mathieu lattices and disordered periodic lattices. In disordered aperiodic lattice disorder always enhances light transport for both methods, contrary to the disordered periodic lattice. For the highest disorder levels, we detect Anderson localization for both methods and both disordered lattices. More pronounced localization is observed for disordered aperiodic lattices.

REFERENCES

[1] Z. Bouchal, Czech. J. Phys. 53 537 (2003)
[2] J. Durnin, J. J. Miceli, and J. H. Eberly, J. Opt. Soc. Am. 4, 651 (1987).
[3] M. A. Bandres, J. C. Gutiérrez-Vega, and S. Chávez-Cerda, Opt. Lett. 29, 44 (2004).
[4] J. C. Gutiérrez-Vega, M. D. Iturbe-Castillo, and S. Chávez-Cerda, Opt. Lett. 25, 1493 (2000).

[5] J. C. Gutiérrez-Vega, M. D. Iturbe-Castillo, G. A. Ramírez, E. Tepichín, R. M. Rodriíguez-Dagnino, S. Chávez-Cerda, and G. H. C. New, Opt. Commun. 195, 35 (2001).
[6] J. C. Gutiérrez-Vega, M. A. Meneses-Neva, and S. Chávez-Cerda, Am. J. Phys. 71, 233 (2003).
[7] J. V. Vasiljević, A. Zannotti, D. V. Timotijević, C. Denz, D. M. Jović Savić, Phys. Rev. A 96, 023840 (2017).
[8] J. V. Vasiljević, A. Zannotti, D. V. Timotijević, C. Denz, D. M. Jović Savić, Appl. Phys. Lett. 117, 041102 (2020).
[9] D. V. Timotijević, J. M. Vasiljević, and D. M. Jović Savić. Opt. Express 30(5), 7210 (2022).

Biography of Presenting Author:

Dr. Jadranka M. Vasiljević received her Ph.D. degree in 2020 at the Faculty of Physics at Belgrade University, Serbia. Since 2015 she joined Laboratory for Nonlinear Photonics at the Institute of Physics, University of Belgrade, Serbia. Since 2022 Jadranka is member of project supported by the Science Fund of the Republic of Serbia, program IDEAS, 7714356 – **CompsLight**. Her research area is Nonlinear Optics and Photonics. She is studying realization of two-dimensional dynamical structures in the photorefractive medium by Mathieu beams; realization of aperiodic and complex structures with Mathieu beams; investigation of phenomena correlated with light propagation in Mathieu photonic lattices.

Recent Photograph: (High Resolution)

Прилог 9

Радови у претходном периоду

ADVANCED OPTICAL MATERIALS
www.advopticalmat.de

Visualizing the Energy Flow of Tailored Light

Alessandro Zannotti, Jadranka M. Vasiljević, Dejan V. Timotijević, Dragana M. Jović Savić, and Cornelia Denz*

Exploiting the energy flow of light fields is an essential key to tailor complex optical multistate spin and orbital angular momentum (OAM) dynamics. With this work, the energy flow is identified and quantified by a novel approach that is based on the symmetry breaking induced by nonlinear light–matter interaction of OAM carrying beams at the example of Mathieu beams, showing transverse invariant intensity distributions. These complex scalar nondiffracting beams exhibit outstanding transverse energy flows on elliptic paths. Although their energy is continuously redistributed during linear propagation in homogeneous media, the beams stay nondiffracting. This approach to visualize the energy flow of light is based on the nonlinear self-action in a nonlinear crystal. By this, the sensitive equilibrium is perturbed and accumulation of rotating high-intensity spots is enabled. Intensity distributions on elliptic, chiral paths are demonstrated as a manifestation of the energy flow. Furthermore, the formation of corresponding refractive index modulations that may be implemented as chiral waveguides, is controlled via the beam power and structure size.

1. Introduction

The energy flow of light is determined by both, its spin angular momentum and its orbital angular momentum (OAM), and is generally described by the Poynting vector.[1] Controlling the spatial polarization and phase structure of light, the combination of binary spin states and multistate orbital angular momentum dynamics is an essential key to further establish modern high-dimensional singular optics. These abilities enabled breakthrough research in the areas of spatial polarization modulation,[2] classical entanglement,[3] high-density signal transmission,[4] or optical micromanipulation.[5,6]

In order to investigate two-dimensional energy flows in the transverse plane, in particular nondiffracting beams with transverse invariant intensity distributions and continuously modulated phase distributions are suited. The class of nondiffracting beams has attracted considerable interest and features not only applications in optics, but also in solid state and atom physics.[7–11] A detailed understanding of their energy flows therefore is of high importance in many communities. However, the energy flow of continuously modulated nondiffracting beams withstands a direct observation because it is hidden for the case of linear propagation in homogeneous media. The transverse intensity distribution stays invariant and the energy flow is continuously redistributed.

Four nondiffracting beam families exist as solutions of the paraxial as well as the nonparaxial Helmholtz equation in different coordinate systems:[12–17] Discrete beams in Cartesian, Bessel beams[8] in spherical, Mathieu beams in elliptic, and Weber beams in parabolic coordinates. Among these diverse families, Mathieu beams[9,10,18,19] may be interpreted as a generalized beam class, capable to interpolate between Cartesian and spherical coordinates. In contrast to parabolic Weber beams, their transverse spatial intensity distributions can form closed paths on ellipses, with spatially structured orbital angular momenta[6,20] showing periodic boundaries.

Mathieu beams are highly appealing to access fundamental physical effects in elliptical coordinates.[21] In several studies, they have been beneficially used for particle manipulation,[5] and served as lattice-writing light,[22–26] featuring the nonlinear propagation of (vortex) solitons in these previously linearly induced elliptic lattices. However, the self-action of Mathieu beams in nonlinear media was not investigated until now.

Scalar even and odd Mathieu beams exhibit only real-valued field distributions. Their transverse Poynting vector therefore vanishes. In contrast, the complex superposition of even and odd Mathieu beams leads to generalized elliptic Mathieu beams, showing outstanding continuously modulated spatial phase distributions, i.e., OAM.[5,6,20] Thus, for these beams a transverse energy flow is present. Until today, only a few works have addressed the energy flow in these complex spatially modulated beams with its unique OAM characteristics, e.g., using the OAM structure of Mathieu beams to transfer orbital angular momentum to particles that start to rotate.[5,6,20]

With this work, we present an approach to visualize the energy flow of light at the example of elliptic Mathieu beams. We demonstrate experimentally and numerically that the

A. Zannotti, Prof. C. Denz
Institute of Applied Physics and Center for Nonlinear Science (CeNoS)
Westfälische Wilhelms-Universität Münster
48149 Münster, Germany
E-mail: a.zannotti@uni-muenster.de
J. M. Vasiljević, Prof. D. V. Timotijević, Prof. D. M. Jović Savić
Institute of Physics
University of Belgrade
P.O. Box 68, 11001 Belgrade, Serbia
Prof. D. V. Timotijević
Science Program
Texas A&M University at Qatar
P.O. Box 23874, Doha, Qatar

DOI: 10.1002/adom.201701355

Applied Physics Letters ARTICLE scitation.org/journal/apl

Light propagation in aperiodic photonic lattices created by synthesized Mathieu–Gauss beams

Cite as: Appl. Phys. Lett. **117**, 041102 (2020); doi: 10.1063/5.0013174
Submitted: 8 May 2020 · Accepted: 14 July 2020 ·
Published Online: 27 July 2020

Jadranka M. Vasiljević,[1,a)] Alessandro Zannotti,[2] Dejan V. Timotijević,[1] Cornelia Denz,[2] and Dragana M. Jović Savić[1]

AFFILIATIONS

[1]Institute of Physics, University of Belgrade, P.O. Box 68, 11001 Belgrade, Serbia
[2]Institute of Applied Physics and Center for Nonlinear Science (CeNoS), University of Muenster, 48149 Muenster, Germany

[a)]Author to whom correspondence should be addressed: jadranka@ipb.ac.rs

ABSTRACT

We investigate light propagation in a two-dimensional aperiodic refractive index lattice realized using the interference of multiple Mathieu–Gauss beams. We demonstrate experimentally and numerically that such a lattice effectively hinders linear light expansion and leads to light localization, compared to periodic photonic lattices in a photorefractive crystal. Most promisingly, we show that such an aperiodic lattice supports the nonlinear confinement of light in the form of soliton-like propagation that is robust with respect to changes in a wide range of intensities.

Diffraction is a fundamental feature of wave dynamics in any branch of physics that involves waves: optics, acoustics, quantum mechanics, etc. However, in many applications, propagation-invariant transverse intensity distributions, referred to as nondiffracting beams, are needed. Nondiffracting beams are exact solutions of the Helmholtz equation, which exist in different coordinate systems:[1] superposition of plane waves in Cartesian, Bessel beams in circular cylindrical,[2] Mathieu beams in elliptic cylindrical,[3] and parabolic beams in parabolic cylindrical coordinates.[4]

The potential of nondiffracting structures is well recognized in modern photonic research.[5–9] Among them, the propagation of light through tailored refractive index modulations optically fabricated in photosensitive media by propagation-invariant intensity profiles became the subject of extensive theoretical and experimental investigations since the resulting refractive index structure represents a pure 2D material.[10–14] This field of linear and nonlinear optics in photonic lattices typically uses simple nondiffracting Cartesian beam configurations, often hexagonal light structures, to modulate the refractive index since this allows mimicking features of 2D graphene,[15] its famous bandgap structure,[16] or its nonlinear light matter interaction, leading to spatial soliton formation.[17] In a few recent studies, solitons, elliptically shaped vortex solitons, or even vortex necklaces are observed in optically induced photonic lattices by nondiffracting Mathieu beams.[12,18–20] Moreover, the superposition of this kind of elliptic nondiffracting beam allows the formation of different aperiodic photonic structures.[21]

Although the physics of periodic photonic systems is of fundamental interest, deviation from periodicity is important as it leads to higher complexity. One such deviation in optics results in the realization of photonic quasicrystals,[8] structures with a reduced degree of order between periodic and disordered ones.

The localization of waves is an intriguing research subject observed in a variety of classical and quantum systems,[22,23] including light waves,[24–27] Bose–Einstein condensates,[28] and sound waves.[29] Although the transverse expansion properties in periodic photonic lattices,[30–33] as well as in disordered ones,[34–36] have been investigated extensively, light localization and transverse expansion in photonic quasicrystals[37,38] is still an open question.

In this paper, we investigate the effects of light propagation in aperiodic photonic structures created by synthesized Mathieu–Gauss (MG) beams in a photorefractive crystal,[21] experimentally and numerically. We investigate how various input beam positions influence the diffraction and compare them with appropriate periodic waveguide arrays. We find that our approach effectively suppresses the beam expansion depending on the refractive index modulation Δn. Most importantly, in the nonlinear regime, we find localized states that are robust with respect to changes in the probing light intensities and propagation distance. Such stable solitary states are, thus, much more appealing for applications than typical spatial solitons, especially gap solitons, which react sensitively on changes in the strength of the nonlinearity.[39]

Optics Letters

Morphing discrete diffraction in nonlinear Mathieu lattices

Alessandro Zannotti,[1,*] Jadranka M. Vasiljević,[2] Dejan V. Timotijević,[2,3] Dragana M. Jović Savić,[2] and Cornelia Denz[1]

[1]Institute of Applied Physics and Center for Nonlinear Science (CeNoS), University of Muenster, 48149 Muenster, Germany
[2]Institute of Physics, University of Belgrade, P.O. Box 68, 11001 Belgrade, Serbia
[3]Science Program, Texas A&M University at Qatar, P.O. Box 23874 Doha, Qatar
*Corresponding author: a.zannotti@uni-muenster.de

Received 14 January 2019; revised 20 February 2019; accepted 22 February 2019; posted 22 February 2019 (Doc. ID 357502); published 20 March 2019

Discrete optical gratings are essential components to customize structured light waves, determined by the band structure of the periodic potential. Beyond fabricating static devices, light-driven diffraction management requires nonlinear materials. Up to now, nonlinear self-action has been limited mainly to discrete spatial solitons. Discrete solitons, however, are restricted to the eigenstates of the photonic lattice. Here, we control light formation by nonlinear discrete diffraction, allowing for versatile output diffraction states. We observe morphing of diffraction structures for discrete Mathieu beams propagating nonlinearly in photosensitive media. The self-action of a zero-order Mathieu beam in a nonlinear medium shows characteristics similar to discrete diffraction in one-dimensional waveguide arrays. Mathieu beams of higher orders show discrete diffraction along curved paths, showing the fingerprint of respective two-dimensional photonic lattices.

https://doi.org/10.1364/OL.44.001592

Manipulating waves by customizing their interaction with functional materials enables a variety of photonic applications, e.g., tailored diffraction at gratings to discretize the waves' spectral components [1,2]. Waves in periodically structured media show dynamics that cannot be realized in homogeneous media, determined by the media's band structure. Propagation of light in dielectric media with a periodically varying refractive index can mimic the spatio–temporal characteristics that are typically encountered in discrete systems, and the underlying field evolution effectively becomes "discretized" [1]. Most importantly, the vision to control light with light is realizable only by exploiting nonlinear materials as mediators [3]. Thus, shaping the periodically varying refractive index structure allows for diffraction management to control in turn the light distribution [4].

Different types of periodic photonic structures, including arrays of evanescently coupled optical waveguides [5], optically induced lattices in photorefractive materials [6], and photonic crystals [7], have been employed to engineer and control fundamental properties of wave propagation. Arrays or lattices of evanescently coupled waveguides are prime examples of structures in which *discrete diffraction* [2,5,8] can be observed. These arrays consist of equally spaced identical waveguide elements or sites, possessing all essential characteristics of a photonic crystal structure (Brillouin zones, band structure, etc.). In such a physical setting, light couples between waveguides through tunneling, showing its diffraction characteristics. When low intensity light is injected into one or a few neighboring waveguides, it couples to more and more waveguides, broadening its spatial distribution. Fundamentally new physics occur in contrast to diffraction in homogeneous media. High-intensity light producing nonlinear responses in the refractive index is capable of forming *discrete spatial solitons* [9]. A renewed interest in nonlinear light–matter interaction goes beyond soliton formation. It is devoted to physical systems with dimensionality morphing, e.g., the continuous transformation of the lattice structure from 1D to 2D [10–12].

Nondiffracting beams, having propagation-invariant intensity distributions, allow creating 1D and 2D photonic lattices in photosensitive media. Particularly in the areas of optics and atom physics, these beams enable novel applications [13–16]. Among the variety of different nondiffracting beams, Mathieu beams [15,17] solve the Helmholtz equation in elliptic cylindrical coordinates [18]. They are used for a new type of optical lattice-writing light [19–23] allowing solitons or even elliptically shaped vortex solitons, and are beneficially used for particle manipulation [24]. However, their elliptical characteristics allow going far beyond soliton investigations and extending applications of nonlinear self-action.

In this Letter, we exploit Mathieu beams as lattice-writing light to fabricate discrete waveguide structures and investigate their nonlinear self-action in these structures, leading to morphing discrete diffraction. We investigate Mathieu beams of different orders in a photorefractive crystal, experimentally and numerically. We link linear discrete diffraction with nonlinear self-effects and demonstrate gradual transition from one to two dimensions. We use the term *morphing diffraction* to describe the nonlinear behavior similar to discrete diffraction.

Elliptical vortex necklaces in Mathieu lattices

Jadranka M. Vasiljević,[1] Alessandro Zannotti,[2] Dejan V. Timotijević,[1,3] Cornelia Denz,[2] and Dragana M. Jović Savić[1]
[1]*Institute of Physics, University of Belgrade, P.O. Box 68, 11001 Belgrade, Serbia*
[2]*Institut für Angewandte Physik and Center for Nonlinear Science, Westfälische Wilhelms-Universität Münster, 48149 Münster, Germany*
[3]*Science Program, Texas A&M University at Qatar, P.O. Box 23874, Doha, Qatar*

(Received 25 December 2017; published 27 March 2018)

We demonstrate unusual kinds of discrete vortex beams, elliptical necklaces, realized by Mathieu photonic lattices. Varying the order of the Mathieu lattices and their ellipticity, we can control the shape and size of such necklaces. Besides stable vortex states, we observe oscillatory dipole states or dynamical instabilities and study their orbital angular momentum. Dynamical instabilities occur for higher beam power and higher-order vortices. Also the decay of higher-order phase singularities and their separation is observed in dependence on the ellipticity.

DOI: 10.1103/PhysRevA.97.033848

I. INTRODUCTION

An optical vortex that possesses a phase singularity and a rotational flow around the singular point in a given direction can be found in physical systems of different nature and scale, ranging from water whirlpools and atmospheric tornadoes to quantized vortices in superfluids and quantized lines of magnetic flux in superconductors [1]. The study of optical vortices and associated localized vortex states is important for both fundamental and applied physics, leading to applications in many areas that include optical data storage, distribution and processing, optical interconnects between electronic chips and boards, and free-space communication links [2–4]. They also have potential uses in optical tweezers [5], optical manipulation and trapping [6,7], microscopy [8], and quantum information processing [9,10].

The evolution of nonlinear excitations in systems whose properties are modulated is especially interesting and in optics can be realized when an intense laser beam propagates in the material with a suitable transverse refractive index modulation that can be fabricated in nonlinear materials including semiconductors, liquid crystals, fused silica, polymers, and photorefractive media [11–18]. The combination of diffractive and nonlinear effects with transverse refractive index modulation in photonic lattices opens the possibility to produce spatially localized states of light [19,20]. To optically induce two-dimensional photonic lattices it is appropriate to use nondiffracting light beams that are exact solutions of the Helmholtz equation in different coordinate systems [21,22]: plane waves in Cartesian, Bessel beams in circular cylindrical [23], Mathieu beams in elliptic cylindrical [24], and parabolic beams in parabolic cylindrical coordinates [25].

In this paper we report on the existence of elliptical necklace beams in photonic lattices optically induced by Mathieu nondiffracting beams, using vortices as a probe beam. These necklace beams show discrete intensity spots on elliptical curves, associated with discrete phase vortices. We investigate the conditions for their existence as well as their properties, both experimentally and theoretically. Changing the lattice ellipticity and choosing Mathieu lattices of appropriate order, we control the shape and the size of an elliptical necklace, as well as the number of the "pearls" in the necklace. We investigate the breakup of higher-order vortices (topological charge $C_T = 2,3,4$) into $C_T = 1$ vortices and their rate of separation during propagation. Phase singularity distances increase with C_T, higher lattice ellipticity, and propagation distance. Further, we study the stability of such elliptic necklaces. Supported by the strong nonlinearity, we show the formation of oscillating dipole states in the intensity distribution for very long propagation distances and discuss our results by investigating additionally the transfer of orbital angular momentum (AM) to the lattice. Finally, a high intensity of the probe beam leads to nonlinear dynamical instabilities observable in the intensity distribution of the necklaces.

II. EXPERIMENTAL METHOD AND MODELING OF VORTEX BEAM PROPAGATION IN MATHIEU LATTICES

Figure 1 shows the experimental setup to realize elliptical necklaces. A frequency-doubled, expanded, and collimated Nd:YVO_4 laser with wavelength $\lambda = 532$ nm is split into two separate beams: an ordinary polarized writing and an extraordinary polarized probe beam. Both are spatially tailored in intensity and phase by a phase-only spatial light modulator Holoeye Pluto VIS. For this purpose, special Fourier filters (FF1 and FF2) are required [26]. The structure beam optically induces refractive index modulations in the 15-mm-long photorefractive Strontium Barium Niobate crystal doped by Cerium (SBN:Ce), thereby addressing the weaker electro-optic coefficient $r_{13} = 47$ pm/V. The birefringent crystal has refractive indices $n_o = 2.325$ and $n_e = 2.358$ and is externally biased with an electric field $E_{\text{ext}} = 1600$ V/cm aligned along the optical $c = x$ axis, perpendicular to the direction of propagation (z axis). Probing the artificial photonic structure is done with the extraordinary polarized probe beam that addresses the stronger electro-optic coefficient $r_{33} = 237$ pm/V. An imaging system consisting of a microscope objective and camera detects transverse intensity distributions at the back of the crystal.

We model our experiment by solving the nonlinear Schrödinger equation for an initial scalar electric field $A(\mathbf{r})$

Creating aperiodic photonic structures by synthesized Mathieu-Gauss beams

Jadranka M. Vasiljević,[1] Alessandro Zannotti,[2] Dejan V. Timotijević,[1,3] Cornelia Denz,[2] and Dragana M. Jović Savić[1]
[1]*Institute of Physics, University of Belgrade, P.O. Box 68, 11001 Belgrade, Serbia*
[2]*Institut für Angewandte Physik and Center for Nonlinear Science (CeNoS), Westfälische Wilhelms-Universität Münster, 48149 Münster, Germany*
[3]*Science Program, Texas A&M University at Qatar, P.O. Box 23874 Doha, Qatar*
(Received 16 May 2017; published 17 August 2017)

We demonstrate a kind of aperiodic photonic structure realized using the interference of multiple Mathieu-Gauss beams. Depending on the beam configurations, their mutual distances, angles of rotation, or phase relations we are able to observe different classes of such aperiodic optically induced refractive index structures. Our experimental approach is based on the optical induction in a single parallel writing process.

DOI: 10.1103/PhysRevA.96.023840

I. INTRODUCTION

Since nondiffracting beams have been introduced in the late 1980s [1,2] as light structures, only recently these structures have drawn considerable attention in various topics such as trapping of colloidal and *in vivo* particles in biophysics [3], atom optics [4], applications of optical lattices in quantum computing [5], as well as quantum optics [6], optical tweezing [7,8], and nonlinear optics [9–11]. Such nondiffracting structures are coming from the well-known classes of simple nondiffracting light beams that are exact solutions of the Helmholtz equation in different coordinate systems [12]: plane waves in Cartesian, Bessel beams in circular cylindrical [2], Mathieu beams in elliptic cylindrical [13], and parabolic beams in parabolic cylindrical coordinates [14].

A simple and robust implementation of optical micromanipulation technologies—optical tweezers—based on nondiffracting beams, has become a standard tool in biological, medical, and physics research laboratories [15]. Another trend in optical manipulation is the use of synthesized optical beams rather than single beams only; such beams enable a much greater freedom in object manipulation than conventional Gaussian beams [16].

The potential of nondiffracting structures is of significant importance for advances in discrete and nonlinear modern photonics [17–21]. Although the physics of periodic photonic systems are of fundamental importance, deviations from periodicity are of importance as they may result in higher complexity. One such deviation in optics results in the realization of photonic quasicrystals [20,22], the structures that lie between periodic and disordered one. They show sharp diffraction patterns that confirm the existence of wave interference resulting from their long-range order. Recently, a new serial approach for the generation of aperiodic deterministic Fibonacci and Vogel spirals as refractive index structures was presented [23,24]. In particular, the Fourier spectra of tailored aperiodic lattices can be customized to range from discrete to continuous [25], thus featuring unique light propagation as well as localization properties in aperiodic photonic lattices. Of particular interest are also flat-band lattices with a dispersionless energy band composed of entirely degenerate states, so that any excitation of these states yields nondiffracting waves. Such flat band systems have been studied in a number of lattice models including quasi-one-, two-, or three-dimensional settings, diamond ladder, Lieb, or kagome lattices [26–28].

In this paper, we demonstrate a powerful approach for the creation of two-dimensional (2D) aperiodic photonic lattices in a single writing process in parallel. It is based on synthesizing two or more nondiffracting Mathieu-Gauss (MG) beams [29]. By coherently superimposing MG beams with different orders, positions, and relative phases we realize transverse invariant propagating intensity distributions capable of optically inducing corresponding refractive index lattices in photosensitive media. Our approach features the fabrication of versatile aperiodic lattices with controllable properties as well as quasi-one-dimensional structures.

II. CHARACTERIZATION OF SYNTHESIZED MATHIEU-GAUSS BEAMS

For the experimental realization of synthesized MG beams we use the experimental setup shown in Fig. 1. We use a frequency-doubled Nd:YVO_4 laser, expand the laser beam, and illuminate as a plane wave a phase-only spatial light modulator "Holoeye Pluto VIS." The reflected light field is modulated in both amplitude and phase. This is possible by addressing a precalculated hologram to the SLM containing the information of the complex light field encoded with an additional blazed grating. By applying an appropriate Fourier filter, the tailored complex light field is realized [30,31]. Additionally, the telescope L1-L2 scales down the SLM size by a factor of 10. This extraordinary polarized "structure beam" is used to optically inscribe refractive index modulations in the 15 mm long photorefractive SBN:Ce crystal which is externally biased with an electric dc field of $E_{\text{ext}} = 2000V\ \text{cm}^{-1}$ aligned along the optical $c = x$ axis, perpendicular to the direction of propagation (z axis).

We simulate the nonlinear light propagation in a photonic structure by numerically solving the nonlinear Schrödinger equation:

$$i\partial_z A(\mathbf{r}) + \tfrac{1}{2}\Delta_\perp A(\mathbf{r}) + \tfrac{1}{2}\Gamma E(|A(\mathbf{r})|^2)A(\mathbf{r}) = 0, \qquad (1)$$

where $\Gamma = k_0^2 w_0^2 n_{o,e}^4 r_{13,33}$, $k_0 = 2\pi/\lambda$ is the wave number and defined by the wavelength $\lambda = 532\,\text{nm}$, $n_o = 2.325$ is the ordinary, $n_e = 2.358$ is the extraordinary bulk refractive index, $r_{13} = 47\,\text{pm/V}$, $r_{33} = 237\,\text{pm/V}$ are the corresponding

Journal of the Optical Society of America B
OPTICAL PHYSICS

Light propagation in quasi-periodic Fibonacci waveguide arrays

N. M. Lučić, D. M. Jović Savić,* A. Piper, D. Ž. Grujić, J. M. Vasiljević, D. V. Pantelić, B. M. Jelenković, and D. V. Timotijević

Institute of Physics, University of Belgrade, P.O. Box 68, 11001 Belgrade, Serbia
**Corresponding author: jovic@ipb.ac.rs*

Received 26 March 2015; revised 19 May 2015; accepted 3 June 2015; posted 5 June 2015 (Doc. ID 236998); published 26 June 2015

We investigate light propagation along one-dimensional quasi-periodic Fibonacci waveguide array optically induced in Fe:$LiNbO_3$ crystal. Two Fibonacci elements, A and B, are used as a separation between waveguides. We demonstrate numerically and experimentally that a beam expansion in such arrays is effectively reduced compared to the periodic ones, without changing beam expansion scaling law. The influence of refractive index variation on the beam expansion in such systems is discussed: more pronounced diffraction suppression is observed for a higher refractive index variation.

OCIS codes: (050.5298) Photonic crystals; (190.5330) Photorefractive optics.

http://dx.doi.org/10.1364/JOSAB.32.001510

1. INTRODUCTION

The discovery of quasi-crystals in condensed matter by Shechtman *et al.* [1] and their theoretical analysis by Levine and Steinhardt [2] has inspired a new field of research in optics and photonics.

Examples in the field of optics are photonic quasi-crystals with dielectric multilayers forming the Fibonacci sequence as proposed by Kohmoto *et al.* [3], and realized in [4–6], as well as other deterministic aperiodic structures with long-range order [7,8]. Photonic quasi-crystals have peculiar optical properties. Namely, they lie between periodic and disordered structures and exhibit unique and rich symmetries in Fourier space that are not possible within periodic lattices. The large variety of aperiodic structures is very important and could provide significant flexibility and richness when engineering the optical response of devices [9].

The localization of waves is a ubiquitous phenomenon observed in a variety of classical and quantum systems [10–12], including light waves [13–16], Bose–Einstein condensates [17,18], and sound waves [19]. Although stated more than 50 years ago [11], Anderson localization is still one of the most appealing approaches in optical wave manipulation. In this regard, a transverse localization of light in waveguide lattices turns out to be a particularly interesting concept [13,14]. As the transverse expansion properties in periodic photonic lattices [20–23], as well as in disordered ones [14,24–26], have been investigated extensively, the quasi-periodic photonic lattices emerged as a further attractive research field. The light localization in the Aubry–André model of a quasi-periodic lattice is observed [27], but the transverse expansion in many other models of photonic quasi-crystals [28] is still an open question.

In this paper, we extend these concepts to the beam expansion in quasi-periodic Fibonacci waveguide arrays, considering light propagation along waveguides. We fabricate the array of identical waveguides (identical refractive index profile). The distance between successive waveguides is modulated in the Fibonacci manner. This means that the sequence of separations consists of two elements, A and B, lined in such a way to make a Fibonacci word. We consider how various input beam positions (incident positions) influence diffraction, and compare them with appropriate periodic waveguide arrays. In general, we find the beam expansion is slowed in quasi-periodic Fibonacci waveguide arrays. Increasing the refractive index variation, the effect is more pronounced.

2. EXPERIMENTAL SETUP AND THEORETICAL BACKGROUND

For the experimental realization of the Fibonacci waveguide array we use $LiNbO_3$ crystal, doped with 0.05% of iron. Dimensions of the crystal are 3 mm × 0.5 mm × 10 mm, with the optical axis along the z direction (10 mm). Waveguides are fabricated using an in-house developed laser writing system with a CW laser at 473 nm and a precise two-axis positioning platform. The platform can move the crystal in the x–z plane. The laser beam propagates along the y axis and it is focused by the 50× microscope objective slightly below the upper surface of the crystal. In this way, the laser makes a controllable local change of the refractive index. By moving the sample along the

Phronesis
RESEARCHERS WORLD..

Certificate of Appreciation

THIS CERTIFICATE IS PRESENTED TO

On behalf of Phronesis LLC, we wish to thank

Dr. Jadranka M. Vasiljević

Institute of Physics, University of Belgrade, Serbia

for his/her phenomenal and worthy oral presentation on

Localization of Light in Mathieu Aperiodic Photonic Lattices

at the

"Webinar on

Lasers, Optics and Photonics"

held during

October 21-22, 2020

Best Regards

iLASERS

Phronesis
RESEARCHERS WORLD..

Webinar on

LASERS, OPTICS & PHOTONICS

October 21-22, 2020

PHRONESIS LLC

5 Great Valley Pkwy, STE 235 | Malvern PA 19355, USA | Tel: +1 (302) 469-7080

E: contact@phronesisonline.com | W: https://phronesisonline.com

Day-2 - October 22, 2020

Keynote Session	
10:00-10-45	Title: Surface Morphology, Optical Properties and Exciton Relaxation Processes in Nanoassemblies Based on Semiconductor Quantum Dots and Porphyrins
	Eduard Zenkevich, Belarussian National Technical University, Belarus
10:45-10:55 Eye Relaxation Break	
Sesions: Quantum Mechanics | Nonlinear Lasers and Nonlinear Optics | Optical Tomography and Optical Metrology	
10:55-11-25	Title: Causa Equat Effectum in Quantum Mechanics
	Peter Enders, Kazakh National Pedagogical Abai University, Kazakhstan
11:25-11-55	Title: Tertiary Quantization of Quantum Electrodynamics Equations as a Method for Solving Secondary Quantized Equations
	Veklenko B.A., Joint Institute for High Temperatures of the Russian Academy of Sciences, Russia
11:55-12:05 Eye Relaxation Break	
12:05-12-35	Title: Localization of Light in Mathieu Aperiodic Photonic Lattices
	Jadranka M. Vasiljević, Institute of Physics, University of Belgrade, Serbia
12:35-13-05	Title:Fringe Pattern Analysis Using the Fast Fourier Transform and the Morlet Wavelet Transforms
	Dahi Ghareab Abdelsalam Ibrahim, National Institute of Standards, Egypt
13:05-13:35	Title: A New Class of Binary Quantum Codes Based on Self-Dual Orientable Embeddings of K4s, 4s
	Avaz Naghipour, University College of Nabi Akram, Iran
Panel Discussions 13:35-13:50	
POSTERS 13:50 ONWARDS (Each Poster for 10 Minutes)	
P-01	Title: The Eigenstates of Photon Creation Operator
	Huai-Yu Wang, Tsinghua University, China
P-02	Title: Properties of Quantised Space as Source of Nonlocality
	Zbigniew Tarnawski, AGH University of Science and Technology, Poland
P-03	Title: Phenomenology of Ultrarelativistic Heavy Ion Collision Using Glauber Model
	Sarfraj Khan, J.P university, India

Localization of Light in Mathieu Aperiodic Photonic Lattices

Jadranka M. Vasiljević
Institute of Physics, University of Belgrade, Serbia

We demonstrate a kind of aperiodic photonic structure realized using the interference of multiple Mathieu beams. Depending on the beam configurations, their mutual distances, angles of rotation, or phase relations we are able to observe different classes of such aperiodic optically induced refractive index structures. Our experimental approach is based on the optical induction in a single parallel writing process.

We study light propagation in a two-dimensional aperiodic photonic lattice realized using the interference of multiple Mathieu beams. We demonstrate experimentally and numerically that such a lattice effectively hinders linear light expansion and leads to light localization. Most promisingly, we show that such an aperiodic lattice supports the nonlinear confinement of light in the form of soliton-like propagation that is robust with respect to changes in a wide range of intensities. The additional level to control the diffraction of light is to add disorder in the aperiodic Mathieu lattice. We realized disordered Mathieu aperiodic lattices and investigate light propagation in them. We observed disorder-enhanced light transport and light localization in disordered aperiodic M.u lattices.

Biography

Dr. Jadranka Vasiljević studied the Faculty of Science at Kragujevac University, Serbia, and graduated as MS in 2014. Since then she joined the research group of Dr. Dragana Jović Savić at the Institute of Physics, University of Belgrade, Serbia. She is part of nonlinear photonics laboratory at the Institute of Physics, University of Belgrade, Serbia. She received her Ph.D. degree in 2020 at the Faculty of Physics at Belgrade University, Serbia. She has published 6 research articles in SCI(E) journals.

SPIE. PHOTONICS EUROPE

International Day of Light
16 May

TECHNICAL PROGRAMME

Photonics Europe 2018

TECHNICAL PROGRAMME

EXHIBITION GUIDE

Conferences and Courses
22–26 April 2018

Exhibition
24–25 April 2018
Strasbourg Convention & Exhibition Centre
Strasbourg, France

www.spie.org/pe

Studies on coupling between guided modes and tamm states in one-dimensional photonic crystals, Sudha Maria Lis S., Shivakiran N. B. Bhaktha, Pratyusha Das, Sakshi Sharma, Indian Institute of Technology Kharagpur (India) . . . . . [10672-124]

Enhanced graphene nonlinear response through geometrical plasmon focusing, José Ramón Martínez Saavedra, ICFO - Institut de Ciències Fotòniques (Spain); F. Javier Garcia de Abajo, ICFO - Institut de Ciències Fotòniques (Spain) and Institució Catalana de Recerca i Estudis Avançats (Spain) . . . . . [10672-125]

Waveguide-integrated narrowband transmission filter consisting of two grooves and a ridge cavity, Evgeni A. Bezus, Leonid L. Doskolovich, Dmitry A. Bykov, Image Processing Systems Institute, Russian Academy of Sciences (Russian Federation). . . . . [10672-126]

Efficient synthesis and optical properties of highly luminescent copper nanoclusters, Maria Jessabel Talite, National Chiao Tung Univ. (Taiwan); Chi-Tsu Yuan, Chung Yuan Christian Univ. (Taiwan); Wu-Ching Chou, National Chiao Tung Univ. (Taiwan) . . . . . [10672-127]

Numerically optimized design for enhanced coupling efficiency of single-photon sources integrated into single-mode waveguides, Theresa Hoehne, Zuse Institute Berlin (Germany); Peter Schnauber, Sven Rodt, Stephan Reitzenstein, Institut für Festkörperphysik, Technische Univ. Berlin (Germany); Sven Burger, Zuse Institute Berlin (Germany) and JCMwave GmbH (Germany) . . . . . [10672-128]

Dielectro-plasmonic tweezers for scalable trapping and hot electrons applications, Alberto Lauri, Emiliano Cortés, Evangelina Pensa, Imperial College London (United Kingdom); Avijit Barik, Univ. of Minnesota (United States); Aliaksandra Rakovich, Imperial College London (United Kingdom); Sang-Hyun Oh, Univ. of Minnesota (United States); Stefan A. Maier, Imperial College London (United Kingdom). . . . . [10672-129]

Surface wave detection of hypersound in single plasmonic nanoantennas, Rodrigo Berte, Imperial College London (United Kingdom); Fabricio Della Picca, Lab. de Electronica Cuantica, Univ. de Buenos Aires (Argentina) and El Instituto de Física de Buenos Aires (Argentina) and Consejo Nacional de Investigaciones Científicas y Técnicas (Argentina); Yi Li, Emiliano Cortés, Imperial College London (United Kingdom); Stefan A. Maier, Imperial College London (United Kingdom) and Ludwig-Maximilians-Univ. München (Germany); Andrea Bragas, Lab. de Electronica Cuantica, Univ. de Buenos Aires (Argentina) . . . . . [10672-130]

Anderson localization of visible light for high-quality on-chip optical cavities, Oliver Trojak, Tom Crane, Luca Sapienza, Univ. of Southampton (United Kingdom) . . . . . [10672-131]

Polarization conversion within ultracompact on-chip all-plasmonic nanocircuits, Martin Thomaschewski, Yuanqing Yang, Sergey I. Bozhevolnyi, Univ. of Southern Denmark (Denmark) . . . . . [10672-132]

Optical sensing with Anderson localized light, Oliver Trojak, Tom Crane, Luca Sapienza, Univ. of Southampton (United Kingdom). . . . . [10672-133]

Plasmon-exciton interaction in the thin film of inhomogeneous ensemble of silver nanoparticles and cyanine J-aggregates, Anton A. Starovoytov, Rezida D. Nabiullina, Igor A. Gladskih, ITMO Univ. (Russian Federation) . . . . . [10672-134]

Planar waveguide coupler based on tilted Bragg gratings and a discrete cladding mode, Mathias Weisen, Matthiew T. Posner, Optoelectronics Research Ctr. (United Kingdom); James C. Gates, Optoelectronics Research Ctr., Univ. of Southampton (United Kingdom); Corin Gawith, Peter G. R. Smith, Peter Horak, Optoelectronics Research Ctr. (United Kingdom) . . . . [10672-135]

Investigation of bimetallic hollow nanoparticles for colorimetric detection of mercury, Sangeeta Yadav, VIT Univ. (India); Saumey Jain, KTH Royal Institute of Technology (Sweden); Jitendra Satija, Ctr. for Nanobiotechnology, VIT Univ. (India). . . . . [10672-136]

Using all dielectric and plasmonic cross grating metasurface for enhancing efficiency of CZTS solar cells, Omar A. M. Abdelraouf, The American Univ. in Cairo (Egypt) and Ain Shams Univ. (Egypt); Ahmed Shaker, Ain Shams Univ. (Egypt); Nageh K. Allam, The American Univ. in Cairo (Egypt) . . . . . [10672-137]

Study of thermo-optical properties of nanofluids of gold and silver nanoparticles funcionalized with polyethylene glycol and sodium dodecyl sulfate in water using thermal lens spectroscopy, Orlando Villegas, Jimmy Castillo, Alberto Fernández, Hector Gutierrez, Univ. Central de Venezuela (Venezuela) . . . . . [10672-138]

One-pot synthesis red emission of photoluminescent silane capped gold nanoclusters, Hsiu-Ying Huang, Chi-Tsu Yuan, Chung Yuan Christian Univ. (Taiwan) . . . . . [10672-139]

Nanofabrication on unconventional platforms: implications for novel opto-electronic functionalities, design, and enhanced performance, Jagdish Anakkavoor Krishnaswamy, Kavita Garg, Sandeep B.S., Kumar M.P., Praveen C. Ramamurthy, Debiprosad Roy Mahapatra, Indian Institute of Science (India) . . . . . [10672-140]

The glutathione-capped gold nanoclusters based on doping zinc ion with aggregation-induced emission enhancement, Kun-Blin Cai, Li-Yun Chang, Chi-Tsu Yuan, Hsiu-Ying Huang, Chung Yuan Christian Univ. (Taiwan) . . . . . [10672-141]

Near-field localization of Au nano-objects: PEEM and group theory description, Sarra Mitiche, Sylvie Marguet, Fabrice Charra, Ludovic Douillard, CEA-Ctr. de SACLAY (France) . . . . . [10672-142]

Nanostructured layer of InP on GaP surface, Tinatin Laperashvili, Orest Kvitsiani, Institute of Cybernetics (Georgia); Davit Lapherashvili, Georgian Technical Univ. (Georgia) . . . . . [10672-143]

Integration of carbon nanotubes in slot photonic crystal cavities, Elena Durán-Valdeiglesias, Ctr. de Nanosciences et de Nanotechnologies (France); Thi Hong Cam Hoang, Ctr. de Nanosciences et de Nanotechnologies (France) and Institute of Materials Science (Viet Nam); Carlos Alonso-Ramos, Samuel Serna, Ctr. de Nanosciences et de Nanotechnologies (France); Weiwei Zhang, Ctr. de Nanosciences et de Nanotechnologies (France) and Univ. of Southampton (United Kingdom); Xavier Le Roux, Ctr. de Nanosciences et de Nanotechnologies (France); Matteo Balestrieri, CEA-Ctr. de SACLAY (France) and Commissariat à l'Énergie Atomique (France) and Nanosciences et Innovation pour les Matériaux, la Biomédecine et l'Énergie (France); Francesco Biccari, Anna Vinattieri, Lab. Europeo di Spettroscopie Non-Lineari, Univ. degli Studi di Firenze (Italy); Delphine Marris-Morini, Ctr. de Nanosciences et de Nanotechnologies (France); Arianna Filoramo, CEA-Ctr. de SACLAY (France) and Commissariat à l'Énergie Atomique (France) and Nanosciences et Innovation pour les Matériaux, la Biomédecine et l'Énergie (France); Massimo Gurioli, Lab. Europeo di Spettroscopie Non-Lineari, Univ. degli Studi di Firenze (Italy); Eric Cassan, Ctr. de Nanosciences et de Nanotechnologies (France) . . . . . [10672-144]

Optical coupling of a Mie-resonant silicon nanoparticle to a waveguide revealed by third harmonic generation spectroscopy, Kirill I. Okhlopkov, Alexander A. Ezhov, Pavel A. Shafirin, M.V. Lomonosov Moscow State Univ. (Russian Federation); Nikolay A. Orlikovskiy, Bauman Moscow State Technical Univ. (Russian Federation); Maxim R. Shcherbakov, M.V. Lomonosov Moscow State Univ. (Russian Federation) and Cornell Univ. (United States); Andrey A. Fedyanin, M.V. Lomonosov Moscow State Univ. (Russian Federation) . . . . . [10672-145]

Distance dependence of carrier transfer via tunneling processes from graphene quantum dots to InGaN quantum well, Tzu-Neng Lin, Svette Reina Merden S. Santiago, Ji-Lin Shen, Chung Yuan Christian Univ. (Taiwan) . . . . . [10672-146]

Propagation of surface helicons in a semiconductor, Valentin A. Tolkachev, Chelyabinsk State Univ. (Russian Federation); Igor V. Bychkov, Dmitry A. Kuzmin, Chelyabinsk State Univ. (Russian Federation) and South Ural State Univ. (Russian Federation); Vladimir G. Shavrov, Kotel'nikov Institute of Radio Engineering and Electronics of Russian Academy of Sciences (Russian Federation); Olga Kharitotnova, Chelyabinsk State Univ. (Russian Federation) . . . . . [10672-147]

Chirality and discrete diffraction in nonlinear Mathieu lattices, Marius Rimmler, Alessandro Zannotti, Westfälische Wilhelms-Univ. Münster (Germany); Jadranka Vasiljevic, Dejan V. Timotijevic, Dragana M. Jović Savić, Univ. of Belgrade (Serbia); Cornelia Denz, Westfälische Wilhelms-Univ. Münster (Germany) . . . . . [10672-148]

Helium Ion beam fabrication of nanofiber Bragg cavitites, Andreas W. Schell, ICFO - Institut de Ciències Fotòniques (Spain); Hideaki Takashima, Hirogona Maruya, Atsushi Fukuda, Kyoto Univ. (Japan). . . . . [10672-149]

Tailored orbital and spin energy flow structures for advanced optical trapping, Eileen Otte, Eric Asché, Ramon Runde, Cornelia Denz V, Westfälische Wilhelms-Univ. Münster (Germany). . . . . [10672-150]

Compact Bloch surface waves devices based on multimode interference effect, Kirill Safronov, Ksenia A. Abrashitova, Dmitry N. Gulkin, Natalia Kokareva, Ilya Antropov, Vladimir O. Bessonov, Andrey A. Fedyanin, M.V. Lomonosov Moscow State Univ. (Russian Federation) . . . . . [10672-151]

Temperature-dependent photoluminescence in nitrogen-doped graphene quantum dots, Svette Reina Merden S. Santiago, Tzu-Neng Lin, Ji-Lin Shen, Chung Yuan Christian Univ. (Taiwan) . . . . . [10672-152]

A software for the simulation of light scattering by many particles in planarly layered media, Amos Egel, Dominik Theobald, Guillaume Gomard, Uli Lemmer, Karlsruher Institut für Technologie (Germany) . . . . . [10672-153]

GaP-on-insulator as a platform for nonlinear photonics, Simon Hönl, Katharina Schneider, IBM Research - Zürich (Switzerland); Pol Welter, IBM Research - Zurich (Switzerland) and ETH Zurich (Switzerland); Yannick Baumgartner, Herwig Hahn, Lukas Czornomaz, IBM Research - Zürich (Switzerland); Dalziel J. Wilson, IBM Research - Zurich (Switzerland) and École Polytechnique Fédérale de Lausanne (Switzerland). . . . . [10672-154]

Microwave surface plasmon-polariton resonances in VO_2 during metal-insulator phase transition, Dmitry A. Kuzmin, Igor V. Bychkov, Chelyabinsk State Univ. (Russian Federation) and South Ural State Univ. (Russian Federation); Alexander P. Kamantsev, Victor V. Koledov, Dmitry S. Kuchin, Alexey V. Mashirov, Vladimir G. Shavrov, Kotel'nikov Institute of Radio Engineering and Electronics of Russian Academy of Sciences (Russian Federation) . . . . . [10672-155]

Chirality and discrete diffraction in nonlinear Mathieu lattices

M. Rimmler[1], A. Zannotti[1], J. M. Vasiljevic[2], D. V. Timotijevic[2,3], D. M. Jovic Savic[2], and C. Denz[1]

[1]*Institute of Applied Physics and Center for Nonlinear Science (CeNoS), University of Münster, 48149 Münster, Germany*

[2]*Institute of Physics, University of Belgrade, P.O. Box 68, 11001 Belgrade, Serbia*

[3]*Science Program, Texas A&M University at Qatar, P.O. Box 23874 Doha, Qatar*

Non-diffracting beams are highly relevant in optics and atom physics, particularly because their transverse intensity distributions propagate unchanged for hundreds of diffraction lengths. Thus, they feature applications in free-space wireless communications, optical interconnections, long-distance laser machining, and surgery. Four different fundamental families of propagation invariant light fields exist. They distinguish in the underlying real space coordinate system: Discrete, Bessel, Weber, and Mathieu non-diffracting beams. Latter ones obey the Helmholtz equation in elliptic cylindrical coordinates and are therefore best suited to address physical effects in elliptical coordinates.

Mathieu beams are classified according to their symmetry properties as even and odd. Their transverse discrete intensity distributions in elliptical or hyperbolical geometries can be shaped by their order and an ellipticity parameter. These real-valued beams have only discrete spatial phase distributions. In contrast, so called elliptical and helical Mathieu beams are obtained as complex superpositions of appropriate even and odd Mathieu beams, thus showing outstanding continuously modulated spatial phase distributions that act as orbital angular momenta, associated with a transverse energy flow.

In our contribution we investigate and control the nonlinear optical induction of photonic Mathieu lattices in photosensitive media. As flexible material we chose a photorefractive SBN crystal, showing a non-local, anisotropic nonlinearity.

Focusing on elliptic Mathieu beams, during linear propagation their transverse energy redistribution along elliptic paths is compensated in each point, enabling for an invariant transverse intensity distribution. However, this energy flow withstands a direct observation. We demonstrate that their nonlinear self-action in SBN breaks this sensitive equilibrium. Consequently, a new type of rotating beam formation arises with high intensity filaments corresponding to the energy flow in an enforced preferential direction. This process is beneficially applied to realize chiral twisted photonic refractive index structures with a tunable ellipticity.

Further, we present our studies on the nonlinear dynamics of discrete Mathieu beams in SBN, showing examples of appropriate fundamental even Mathieu beams in order to realize one- and two-dimensional transverse lattices. The nonlinear optical induction process leads to the formation of discrete refractive index lattices and a self-interaction of the writing Mathieu beams with the realized photonic structure, capable of altering the writing beams' propagation similar to the well-known linear discrete diffraction. Controlling the strength of the nonlinearity allows tailoring the degree of diffraction. Moreover, probing the lattice linearly with Gaussian beams and tunable incident angles reveals the signature of discrete and anomalous diffraction. This allows to control the strength of diffraction, such that under certain tilts, the probing beams may cross the lattice diffractionless.

Our investigations both represent individual contributions towards the realization of advanced complex waveguiding in photorefractive crystals.

Book of abstracts

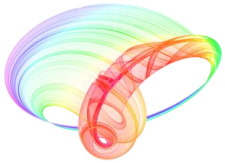

PHOTONICA2019

The Seventh International School and Conference on Photonics, 26 August – 30 August 2019, Belgrade, Serbia

& Machine Learning with Photonics Symposium (ML-Photonica 2019)

& ESUO Regional Workshop

& COST action CA16221

Editors: Milica Matijević, Marko Krstić and Petra Beličev

Belgrade, 2019

2. Nonlinear optics

Waveguiding in Mathieu photonic lattices

J. M. Vasiljević[1], A. Zannotti[2], D. V. Timotijević[1], C. Denz[2] and D. M. Jović Savić[1]
[1]*Institute of Physics, University of Belgrade, P.O. Box 68, 11001 Belgrade, Serbia*
[2]*Institute of Applied Physics and Center for Nonlinear Science (CeNoS), Westfälische Wilhelms-Universität Münster, 48149 Münster, Germany*
e-mail: jadranka@ipb.ac.rs

Nondiffracting beams are highly applicable in optics, photonics and atom physics, peculiar because their transverse intensity distributions propagate unchanged for hundreds of diffraction lengths and allow creating 1D and 2D photonic lattices in photosensitive media [1]. Among the variety of different nondiffracting beams [2-5], Mathieu beams solve the Helmholtz equation in elliptic cylindrical coordinates [4, 6-7]. Mathieu beams are classified according to their symmetry properties as even and odd and their transverse discrete intensity distributions can be shaped by their order and an ellipticity parameter. These real-valued beams are characterized by only discrete spatial phase distributions. By complex superposition of appropriate even and odd Mathieu beams, elliptical Mathieu beams are obtained, showing remarkable continuously modulated spatial phase distributions that possess orbital angular momenta, associated with transverse energy flow.

We exploit Mathieu beams as lattice-writing light to fabricate discrete waveguide structures and investigate their nonlinear self-action in these structures, leading to morphing discrete diffraction. We investigate Mathieu beams of different orders in a photorefractive SBN crystal, experimentally and numerically. We link linear discrete diffraction with nonlinear self-effects and demonstrate a gradual transition from one to two dimensions [8]. The self-action of a zero-order Mathieu beam in a nonlinear medium shows characteristics similar to discrete diffraction in one-dimensional waveguide arrays. Mathieu beams of higher orders show discrete diffraction along curved paths, showing the fingerprint of respective two-dimensional photonic lattices.

Linear propagation of elliptic Mathieu beams enables a nondiffracting transverse intensity distribution with transverse energy redistribution along elliptic paths compensated in each point. In contrast, their nonlinear self-action in SBN breaks this sensitive equilibrium. We demonstrated a new type of rotating beam formation arises with high-intensity filaments corresponding to the energy flow in an enforced preferential direction [9]. This process is beneficially applied to realize chiral twisted photonic refractive index structures with a tunable ellipticity.

REFERENCES

[1] Z. Bouchal, Czech. J. Phys. 53, 537 (2003).
[2] J. Durnin, J. Opt. Soc. Am. A 4, 651 (1987).
[3] J. Durnin, J. J. Miceli, J. H. Eberly, Phys. Rev. Lett. 58, 1499 (1987).
[4] J. C. Gutiérrez-Vega, M. D. Iturbe-Castillo, S. Chávez-Cerda, Opt. Lett. 25, 1493 (2000).
[5] M. A. Bandres, J. C. Gutiérrez-Vega, Chávez-Cerda, Opt. Lett. 29, 44 (2004).
[6] J. C. Gutiérrez-Vega et al., Opt. Commun. 195, 35 (2001).
[7] J. C. Gutiérrez-Vega, R. M. Rodriguez-Dagnino, Am. J. Phys. 71, 233 (2003).
[8] A. Zannotti et al., Adv. Optical Mater. 6, 1701355 (2018).
[9] A. Zannotti et al., Opt. Lett. 44, 1592 (2019).

Book of abstracts

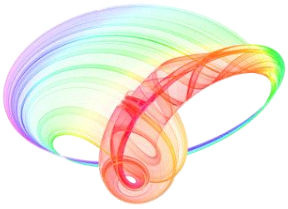

PHOTONICA2017

The Sixth International School and Conference on Photonics

& COST actions: MP1406 and MP1402

MultiscaleSolar

HERALD

&H2020-MSCA-RISE-2015 CARDIALLY workshop

CARDIALLY

28 August – 1 September 2017

Belgrade, Serbia

Editors

Marina Lekić and Aleksandar Krmpot

Institute of Physics Belgrade, Serbia

Belgrade, 2017

2. Nonlinear optics

Realizing aperiodic photonic lattices by synthesized Mathieu-Gauss beams

J. M. Vasiljević[1], Alessandro Zannotti[2], D. V. Timotijević[1,3], Cornelia Denz[2], D. M. Jović Savić[1]
[1]*Institute of Physics,University of Belgrade, P.O. Box 68, 11001 Belgrade, Serbia*
[2] *Institute of Applied Physics and Center for Nonlinear Science (CeNoS), Westfälische Wilhelms-Universität Münster, 48149 Münster, Germany*
[3]*Science Program, Texas A&M University at Qatar, P.O. Box 23874 Doha, Qatar*
e-mail: jadranka@ipb.ac.rs

Over the years, non-diffracting wave configurations have drawn considerable attention, particularly in the areas of optics, atom physics, biophysics, as well as optical tweezing [1], and nonlinear optics [2, 3]. The interest in such optical waves is due to the fact that, their transverse intensity distributions propagate unchanged for hundreds of diffraction lengths. The potential of non-diffracting structures is of significant importance for advances in discrete and nonlinear modern photonics [4, 5]. One prominent class of non-diffracting waves is given by Mathieu beams, which appear as translationally invariant solution of the Helmholtz equation in elliptic cylindrical coordinates.
Synthesizing two or more non-diffracting Mathieu-Gauss (MG) beams, we demonstrate a powerful new approach for the creation of two-dimensional (2D) aperiodic photonic lattices, in a single writing process in parallel. Depending on the beam configurations of coherently superimposed MG beams, their mutual distances, angles of rotation or phase relations we are able to realize transverse invariant propagating intensity distributions capable to optically induce corresponding refractive index lattices in photosensitive media. Our approach features the fabrication of versatile aperiodic lattices with controllable properties as well as quasi one-dimensional structures. Our results and methods enable further investigations of light propagating in such aperiodic photonic lattices, and could find applications in modern optical information processing.

REFERENCES
[1] V. Garcés-Chávez, D. McGloin, H. Melville, W. Sibbett, and K. Dholakia, Nature 419, 145 (2002).
[2] J.W. Fleischer, M. Segev, N. K. Efremidis, and D. N. Christodoulides, Nature 422, 147 (2003).
[3] H. Martin, E. D. Eugenieva, and Z. Chen, Phys. Rev. Lett. 92, 123902 (2004).
[4] F. Diebel, B. M. Bokić, M. Boguslawski, A. Piper, D. V. Timotijević, D. M. Jović, and C. Denz, Phys. Rev. A 90, 033802 (2014).
[5] F. Diebel, B. M. Bokić, D. V. Timotijević, D. M. Jović Savić, and C. Denz, Opt. Express 23, 24351 (2015).

PHOTONICA2015

V International School and Conference on Photonics
& COST actions: MP1204 and BM1205
& the Second international workshop "Control of light and matter waves propagation and localization in photonic lattices“
www.vin.bg.ac.rs/photonica 2015

Book of Abstracts

Editors
Suzana Petrović, Goran Gligorić and Milutin Stepić

Belgrade, 2015.

We have also found a PBG fiber and a gas configuration whose characteristics permit the propagation of such stable solitons. Nevertheless, the linear gain, that is possible because the gas is only confined in the hollow core but not in the cladding holes, brings background instability.

Here, we systematically address the configurations of gases confined in PBG fibers that are more suitable for stable dissipative solitons, studying the dependence of sign and magnitude of the equation parameters with the experimental conditions. Moreover, we will obtain a propagation equation in fourth order which introduces a delayed Raman scattering term. This new term creates a new branch of solutions that exist and are stable in a limited range of the parameter space for which there is linear loss, so that, the background is stable.

REFERENCES

[1] T. Hong, Phys. Rev. Lett. 90, 183901 (2003).
[2] C. Hang, V. V. Konotop, Phys. Rev. A 81, 053849 (2010).
[3] Y. Wu, L. Deng, Phys. Rev. Lett. 93, 143904 (2004).
[4] J. Xu, G. Huang, Opt. Exp. 2, 5149 (2013).
[5] Y. Zhang et al., Phys. Rev. A 82, 053837 (2010).
[6] Z. Wu et al., Opt. Exp. 23, 8430 (2015).
[7] M. Facão et al., Phys. Rev. A 91, 013828 (2015).

Light propagation in deterministic aperiodic Fibonacci waveguide arrays

J. M. Vasiljević, N. M. Lučić, D. V. Timotijević, A. Piper, D. Ž. Grujić,
D. V. Pantelić, B. M. Jelenković and D. M. Jović Savić
Institute of Physics, University of Belgrade, P.O. Box 68, 11001 Belgrade, Serbia
e-mail: jadranka@ipb.ac.rs

During the 1980s quasi-crystallographic structures in solid state physics fundamentally amazed the scientific community [1], and inspired a new field of research in optics and photonics. Owing to the analogy of photonic lattices to solid state systems, the first optical experiments were implemented analyzing aperiodic media [2]. Irregular photonic lattices are of great interest as these structures offer proper band gaps where propagation is forbidden while translation invariance and thus the general scheme of Bloch wave propagation within periodic arrangements are broken. Asking for aperiodic structures rapidly the nomenclature of Fibonacci grating came up for this often is referred to as the embodiment of irregularity [3,4]. Generally spoken, the research field of aperiodic lattices is a fertile topic [5] as these structures offer the possibility of light localization in deterministic disordered structures that are settled between periodic and disordered systems [6]. Light localization in quasi-periodic photonic lattices is observed in Aubry André model and also realized experimentally in AlGaAs substrate [7].

We extend these concepts to quasi-periodic Fibonacci waveguide arrays, considering light propagation along waveguides. We fabricate the array of identical waveguides (identical refractive index profile) in Fe:$LiNbO_3$ crystal. The distance between successive waveguides is modulated in Fibonacci manner. This means that the sequence of separations consists of two elements, A and B, lined in such a way to make Fibonacci word. We have analyzed experimentally and numerically how various incident beam positions influence propagation and localization characteristics and compare it with appropriate periodic waveguide arrays. In general, we find the beam expansion is slowed down in quasi-periodic Fibonacci waveguide arrays, and localization properties in such lattice are closer to a random than periodic lattice. However, with a modification of the refractive index variation, the localization effects are observed for shorter propagation distances by increasing refractive index variation.

REFERENCES
[1] D. Shechtman et al., Phys. Rev. Lett. 53, 1951 (1984).
[2] D. Levine, P. J. Steinhardt, Phys. Rev. Lett. 53, 2477 (1984).
[3] G. Gumbs, M. K. Ali, Phys. Rev. Lett. 60, 1081 (1988).
[4] E. L. Albuquerque, M. G. Cottam, Phys. Rep. 376, 225 (2003).
[5] Z. V. Vardeny, A. Nahata, A. Agrawal, Nat. Photon. 7, 177 (2013).
[6] A. Lagendijk, B. van Tiggelen, D. S. Wiersma, Phys. Today 62, 24 (2009).
[7] Y. Lahini et al., Phys. Rev. Lett 103, 013901 (2009).

Counterpropagating optical solitons in PT symmetric photonic lattices

M. S. Petrović [1,2], A. I. Strinić [2,3] and M. R. Belić [2]
[1] *Institute of Physics, PO Box 57, 11001 Belgrade, Serbia*
[2] *Texas A&M University at Qatar, PO Box 23874, Doha, Qatar*
[3] *Institute of Physics, University of Belgrade, PO Box 68, 11080 Belgrade, Serbia*
e-mail: petrovic@ipb.ac.rs

We construct solitonic solutions for the system of two optical beams propagating in opposite directions [1, 2] in parity-time (PT) symmetric [3, 4] photonic lattices by using modified Petviashvili method [5]. Our system support PT symmetric fundamental solitons, as well as solitary vortices. We propagate them and investigate their basic characteristics. We report power transfer between counterpropagating beams and symmetry breaking (or split-up) transition.

REFERENCES
[1] M. Petrovic et al., Phys. Rev. Lett. 95, 053901 (2005).
[2] M. S. Petrovic et al., Laser Photonics Rev. 5, 214 (2011).
[3] C. M. Bender, S. Boettcher, Phys. Rev. Lett. 80, 5243 (1998).
[4] C. M. Bender, Rep. Prog. Phys. 70, 947 (2007).
[5] V. I. Petviashvili, Fiz. Plazmy 2, 469 (1976) [Sov. J. Plasma Phys. 2, 257 (1976)].

UNIVERSITY OF BELGRADE
FACULTY OF PHYSICS

Jadranka M. Vasiljević

Propagation, localization, and control of light in Mathieu lattices

Doctoral Dissertation

Belgrade, September 2020